THE JOURNAL OF

PHYSICAL CHEMISTRY

Volume 74, Number 14 July 9, 1970

NOTES

COMMUNICATIONS TO THE EDITOR

AUTHOR INDEX

THE JOURNAL OF
PHYSICAL CHEMISTRY

VOLUME 74, NUMBER 14 JULY 9, 1970

Infrared Spectroscopic Investigation of Zeolites and Adsorbed Molecules. VI. Interaction with *n*-Propyl Chloride

by C. L. Angell and Maria V. Howell

Union Carbide Research Institute, Tarrytown Technical Center, Tarrytown, New York 10591 *(Received February 2, 1970)*

A number of different uni-, bi-, and tervalent cation-containing Y zeolites were exposed to *n*-propyl chloride or *n*-propyl bromide at room temperature. It was observed that two OH groups were formed on the zeolite samples. There were very few OH groups formed with NaY but significant reaction occurred on bivalent cation-containing Y zeolites or on AgY. The two bands characteristic of decationized zeolites were formed in each case, but the sizes and relative ratios of the two bands varied greatly with the cations present. This indicates that the reaction of the zeolite with the *n*-propyl chloride mainly depends on the polarizing ability of the cations. An inference that the chloride of the *n*-propyl chloride molecule is associated with the cation is drawn from experiments observing the cation-specific carbon monoxide adsorption. The thermal stability of these newly created OH groups is considerably less than those observed in decationized zeolites, suggesting that the removal of OH groups on heating occurs not by the removing of water but by the removal of an HCl molecule. The possibility of making zeolites that contain both cations and hydroxyl groups by this method is discussed, as well as creation of zeolites in which the proportion of the two hydroxyl groups can be varied.

Introduction

In part I of this series[1] it has been shown that when a fully activated zeolite sample is exposed to dry HCl or DCl gas, a very fast reaction occurs with the formation of the two hydroxyl groups characteristic of decationized zeolites. This observation was now extended to the interaction of a number of different uni-, bi-, and tervalent cation-containing Y zeolites with *n*-propyl chloride or *n*-propyl bromide at room temperature. It was observed that the same two OH groups were formed on the zeolite samples as on exposure to HCl—these were the two bands characteristic of decationized zeolites. The presence or absence of surface cations after propyl chloride treatment was established by observing the cation-specific[2] carbon monoxide adsorption. From these observations it was possible to come to a conclusion about the mechanism of the interaction between zeolites and propyl chloride. This method presents the possibility, besides the partial back-exchange of NH_4 exchanged zeolites, of making zeolites that contain both cations and hydroxyl groups. Actually, this way all the cations present remain in the structure, while in addition surface hydroxyl groups are created.

Experimental Section

The compositions of the zeolite samples used in this work have been given previously (part I, Table I; for LaY see ref 3). The short path length infrared cells, the preparation of the pellets, and the activation techniques have also been described in part I.[1] Activations at 700° were carried out with cells the lower halves of which were made of quartz. Infrared spectra were obtained on a Perkin-Elmer Model 225 double beam grating spectrophotometer. The hydroxyl region in

(1) Part I: C. L. Angell and P. C. Schaffer, *J. Phys. Chem.*, 69, 3463 (1965).

(2) Part II: C. L. Angell and P. C. Schaeffer, *ibid.*, 70, 1413 (1966).

(3) J. A. Rabo, C. L. Angell, and V. Schomaker, presented at the 4th International Congress on Catalysis, Moscow, June 1968.

some cases was also run on a Perkin-Elmer Model 112 single beam spectrometer converted into grating operation. The *n*-propyl chloride and the *n*-propyl bromide were obtained from Fisher. Perdeuterated *n*-propyl bromide was obtained from Mallinckrodt Chemicals and was specified to be of 98% isotopic purity. These compounds were used without any further purification but were degassed by the freeze–pump–thaw technique. Carbon monoxide was obtained in lecture bottle sizes from the Matheson Co. and contained approximately 0.2% carbon dioxide impurity. No attempt was made to remove this impurity; actually its presence was convenient, since when CO gas was added to the zeolite samples to check on the presence of the cation-specific CO band, the cation-specific CO_2 band[4] could also be observed (see Figure 4). The zeolite samples used in the experiments were all flash vacuum activated. The vacuum system was capable of pumping down to approximately 10^{-6} Torr. Deuterium exchange of the decationized Y zeolite has been described previously.[5]

Results

The following samples were exposed to *n*-propyl chloride: NaY, NaX, MgY, CaY, SrY, BaY, CoY, NiY, ZnY, AgY, LaY, and decationized Y;[6] CaY and decationized Y were exposed to *n*-propyl bromide also. When a CaY sample activated under vacuum at 500° and showing very small hydroxyl bands at 3744 and 3640 cm^{-1} was exposed to 100 Torr pressure of *n*-propyl chloride at room temperature, a broad band appeared at 3200 cm^{-1} in addition to the characteristic CH stretching bands of *n*-propyl chloride in the 3000–2800-cm^{-1} region (see Figure 1). On evacuation at room temperature for approximately 2 hr most of the *n*-propyl chloride was removed, as could be seen by the decrease of the CH stretching bands. The 3200-cm^{-1} broad band decreased considerably while at the same time a strong sharp band appeared at 3640 cm^{-1}. In addition to this, a small band appeared at 3540 cm^{-1}. The region near 1640 cm^{-1} where the OH bending frequency of water occurs was carefully observed, but the presence of water could not be detected during any stage of the reaction.

When a NaY sample activated at 500° under vacuum was exposed to 100 Torr of *n*-propyl chloride at room temperature, a very much smaller band appeared at 3200 cm^{-1}, while the CH stretching bands of *n*-propyl chloride were approximately the same size as in the case of CaY, indicating that approximately the same amount of *n*-propyl chloride was adsorbed on the two samples. When the sample was evacuated at room temperature, the formation of an OH band at 3640 cm^{-1} could be observed. However, this band was considerably smaller than the one formed on CaY.

When a sample of silver Y, activated at 500° under vacuum and showing quite small OH bands in the usual positions, was exposed to *n*-propyl chloride at 100 Torr at room temperature, a very large broad band appeared at 3200 cm^{-1} (see Figure 2). On evacuating this sample the OH bands that appeared at 3640 and 3540 cm^{-1} were so large that they completely blanked out the OH region.

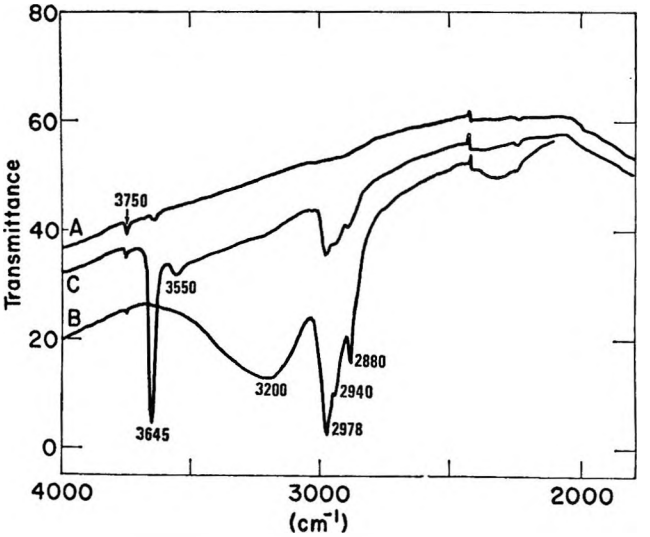

Figure 1. CaY with *n*-propyl chloride: A, zeolite activated at 500°; B, with 100 Torr of *n*-propyl chloride at room temperature; C, evacuated at room temperature for 60 min.

The same set of experiments was carried out on a number of other bivalent cation-containing zeolite samples: MgY, SrY, BaY, CoY, NiY, and ZnY. In each case the formation of two OH bands in the usual positions could be observed after the *n*-propyl chloride was evacuated from the system, but the proportion of the two bands varied with the cation present (see Figure 3). When a LaY sample activated under vacuum at 500° was exposed to *n*-propyl chloride and then the system evacuated at room temperature, there was no observable increase in the size of the two OH bands already present[3] in the sample. In addition, when a LaY sample was activated at 700° to remove all the OH bands, and then exposed to *n*-propyl chloride and evacuated, there were no observable OH groups present in the spectrum.

Another CaY sample was exposed to 100 Torr of *n*-propyl bromide in a similar set of experiments, but there were no significant differences observed in the spectrum from those with the *n*-propyl chloride. The broad band appeared in the same position at 3200 cm^{-1} and the new bands created at 3640 and 3540 cm^{-1} had the same proportions as in the case of CaY exposed to *n*-propyl chloride.

(4) C. L. Angell, *J. Phys. Chem.*, **70**, 2420 (1966).

(5) C. L. Angell and M. V. Howell, *ibid.*, **73**, 2551 (1969).

(6) Throughout this article the type Y zeolite is designated NaY, see U. S. Patent No. 3,130,007. Forms in which sodium has been exchanged with other cations are designated as CaY, etc. The term "decationized Y" will mean NH_4Y which was treated to decompose the NH_4 ions (see U. S. Patent No. 3,130,006).

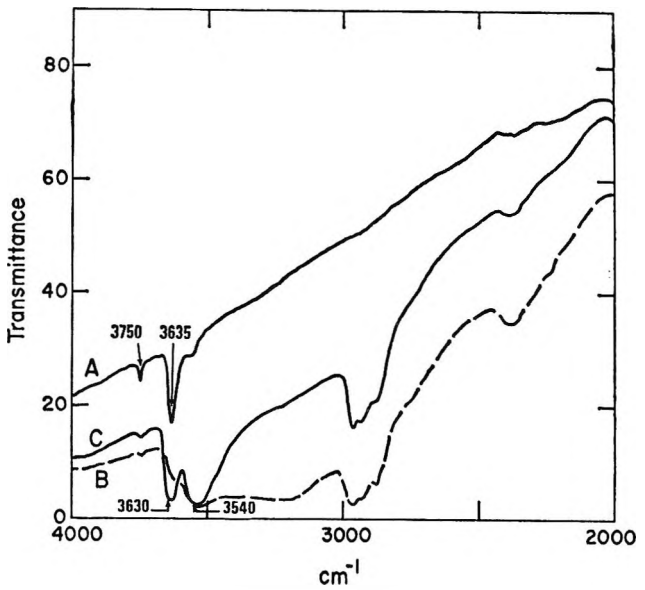

Figure 2. AgY with *n*-propyl chloride: A, zeolite activated at 500°; B, with 100 Torr of *n*-propyl chloride at room temperature; C, evacuated at room temperature for 15 min.

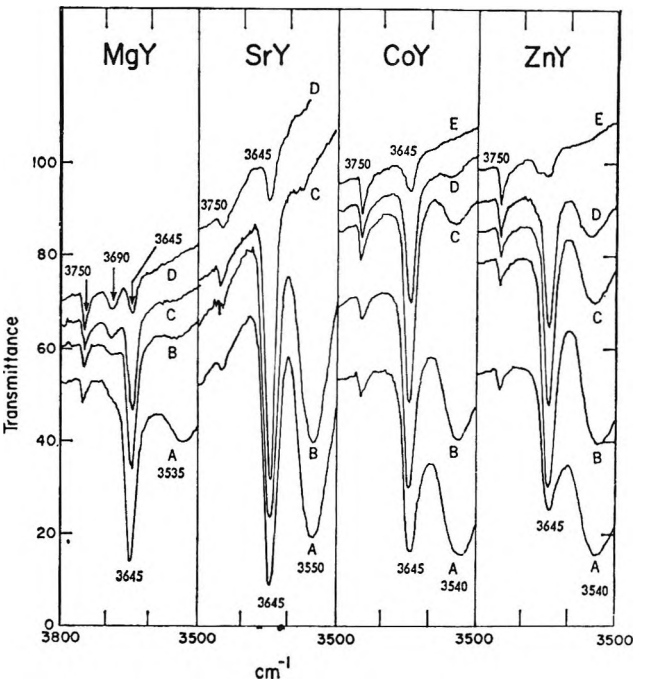

Figure 3. Removal of OH bands generated by *n*-propyl chloride on several zeolites by evacuation. MgY: A, room temperature, 30 min; B, 200°, 1 hr; C, 300°, 1 hr; D, 400°, 1 hr. CoY: room temperature, 30 min; B, 100°, 1 hr; C, 300°, 1 hr; D, 400°, 1 hr; E, 490°, 1 hr. SrY: A, room temperature, 30 min; B, 95°, 1 hr; C, 300°, 1 hr; D, 400°, 1 hr. ZnY: A, 100°, 1 hr; B, 200°, 1 hr; C, 300°, 1 hr; D, 400°, 1 hr; E, 500°, 1 hr.

When a CaY sample was exposed to 100 Torr of perdeuterio-*n*-propyl bromide, the spectrum showed a broad band at about 2380 cm^{-1}. After evacuating the system at room temperature, the spectrum showed the presence of bands at 2682 (strong) and 2615 cm^{-1} (very weak) which are the positions for OD bands that are obtained by deuterium exchanging the usual OH bands that occur on decationized Y zeolite.[5]

When a decationized Y sample, in which all the OH groups were deuterium exchanged, was exposed to 100 Torr of *n*-propyl bromide, a broad band appeared at 2420 cm^{-1}, the 2685-cm^{-1} OD band disappeared completely, but there was no change in the 2615-cm^{-1} OD band.

A sample of CaY was vacuum activated, and the sizes of the 2196-cm^{-1} carbon monoxide band, as well as the 2360-cm^{-1} carbon dioxide band, were observed on the addition of 200 Torr of carbon monoxide. (The carbon dioxide occurred as an impurity in the carbon monoxide; see the Experimental Section, Figure 4B.) After evacuating the carbon monoxide at room temperature, the sample was exposed to 100 Torr of *n*-propyl chloride at room temperature. The sample then was evacuated at 100° for 1 hr. The spectrum showed a strong 3640-cm^{-1} OH band; on the addition of 200 Torr of carbon monoxide, no 2196-cm^{-1} carbon monoxide or 2630-cm^{-1} carbon dioxide bands could be observed. The sample was evacuated at 160° for 2 hr; the OH band did not show any change. Addition of 200 Torr of CO did not produce the characteristic CO or CO_2 bands (Figure 4C). Similarly after evacuating the sample at 210° for 2 hr, the OH band did not change and no CO or CO_2 bands could be observed. When the sample was evacuated at 300° for 1.5 hr, the OH band was still unchanged; no CO band was observed but a very weak CO_2 band could be observed (Figure 4D). The sample then was evacuated at 400° for 1 hr. The OH band now appeared approximately one-quarter the size of the previous band; on the addition of 200 Torr of carbon monoxide the CO and the CO_2 bands appeared nearly the size they were in the original spectrum (Figure 4E). The sample then was evacuated at 450° for 1 hr. The OH band further decreased and now was approximately the same size as on the original untreated sample. On the addition of 200 Torr of CO, the characteristic CO and CO_2 bands were back to exactly the same size as they were on the original untreated sample exposed to carbon monoxide. These experiments indicated that the 3640-cm^{-1} OH band is unaffected by heating at temperatures up to 300°. However, heating at 450° removes this band completely.

Similar thermal stability measurements were carried out on the other bivalent cation-containing zeolite samples treated with *n*-propyl chloride. In most of these cases both the 3640- and 3540-cm^{-1} OH bands could be observed, and it was found that both the proportions and the relative thermal stabilities of the two bands definitely depended on the cation (see Figure 3). In some cases the 3540-cm^{-1} band could be completely removed at 300° while the 3640-cm^{-1} band was not affected at all (*e.g.*, SrY). In other cases the two bands

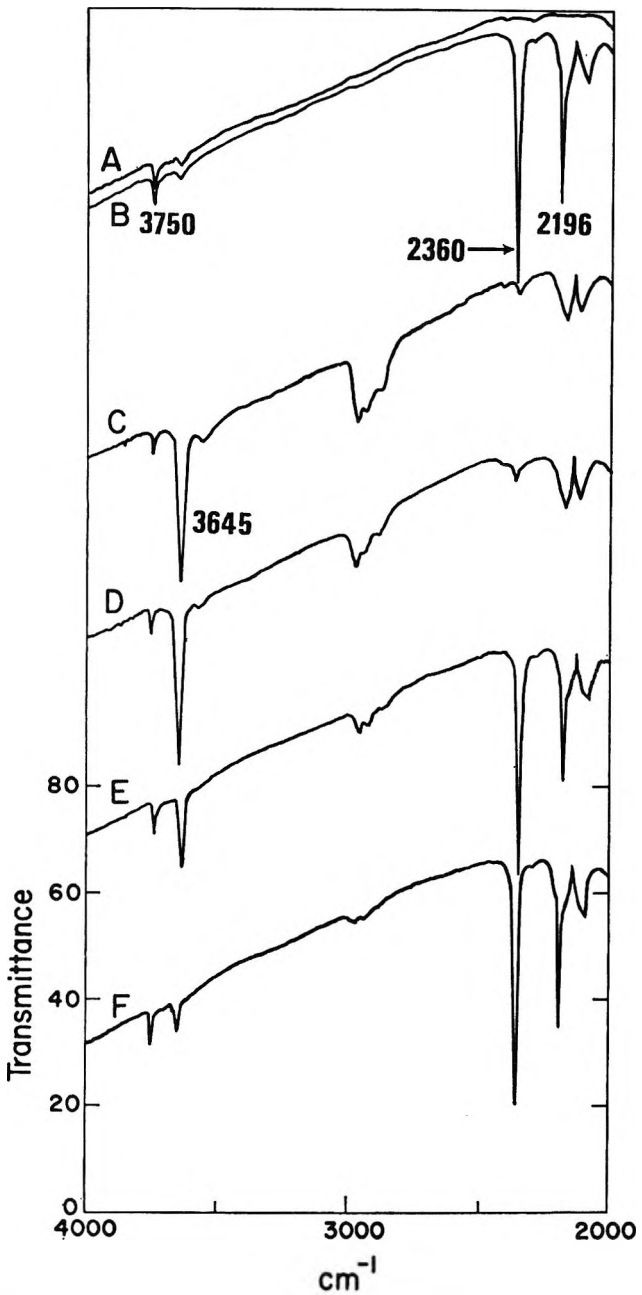

Figure 4. Cation-specific CO and CO_2 bands on *n*-propyl chloride treated CaY zeolite: A, zeolite activated at 500° for 3 hr; B, with 200 Torr of CO at room temperature (for the CO_2 impurity, see Experimental Section); C, exposed to 100 Torr of *n*-propyl chloride, then evacuated at 160° for 2 hr, then with 200 Torr of CO; D, evacuated at 300° for 1.5 hr, then with 200 Torr of CO; E, evacuated at 400° for 1 hr, then with 200 Torr of CO; F, evacuated at 450° for 1 hr, then with 200 Torr of CO. Note: No attempt was made to reproduce the rotational fine structure of the gaseous CO in the 2000–2200-cm^{-1} region clearly discernible in the original spectra.

seemed to decrease at approximately the same rate on gradual heating (*e.g.*, ZnY).

Discussion

In the case of HCl acting on anhydrous zeolite, the highly polar HCl molecule attacks a surface oxygen, the proton attaches itself to the oxygen atom, while the chloride part goes to another part of the framework. Experiments with HCl did not give any clue about the position of the remaining chloride ion. How does the interaction of *n*-propyl chloride with a dehydrated zeolite create OH groups? The absence of water during the experiments is a clear indication that it is indeed the *n*-propyl chloride that creates the OH group. The following reasonable mechanism is suggested. The zeolite dehydrohalogenates the *n*-propyl chloride molecule splitting out HCl and leaving propene. The HCl then *in situ* reacts with a surface oxygen atom creating the OH groups. The cation dependence of this reaction suggests the mechanism of the dehydrohalogenation. It is the strong electrostatic field of the cation which is responsible for this reaction; the electrostatic field polarizes the molecule at the chloride end and splits out the hydrogen chloride molecule. This mechanism is supported by the fact that NaY zeolite produces very few hydroxyl groups with *n*-propyl chloride, since the field due to the sodium ion is much smaller than that due to the bivalent cations; these latter produce large amounts of hydroxyls on interaction with *n*-propyl chloride. LaY, on the other hand, does not create any OH groups with *n*-propyl chloride. This latter finding confirms our previous suggestion[3] that in LaY there are no surface cations in the zeolite cavity at room temperature.

If the proton part of the HCl goes on a surface oxygen creating hydroxyl groups, where does the chloride part go? Our experiments with carbon monoxide provide an answer. It has been shown in part II[2] that carbon monoxide gives characteristic CO stretching bands when adsorbed on different bivalent cation-containing zeolites. The frequency of this CO vibration could be correlated with the size of the cation or with the strength of the electrostatic field due to the cation. This way it was clearly established that the carbon monoxide molecule was attached to the cation. Of course this could occur only with cations in accessible positions on the surface of the cavities (in sites S_{II}). In the present experiments the addition of CO to a sample of CaY, previously exposed to *n*-propyl chloride and with hydroxyl groups created on it, did not give the cation-specific band thus, indicating that there were no surface cations available, although the original sample did show the calcium ion specific carbon monoxide band quite clearly (see Figure 4). Similar results were obtained with the cation-specific carbon dioxide band at 2260 cm^{-1}. This then suggests that the chloride part of the molecule is associated with the surface cation. In the case of the CaY the chloride clearly blocks these cations, and they are no longer available for the adsorption of carbon monoxide. The partial removal of the OH band on heating at 400° and the partial return of the cation specific CO and CO_2 bands seem to indicate that the removal of the OH groups and the liberation of

the cations for surface interaction are one and the same step. On heating at 450° the OH band is completely removed and at the same time the calcium ions are completely liberated as seen by the fully restored cation specific CO and CO_2 bands. This, therefore, suggests that the removal of the OH is accomplished by interaction with the neighboring chloride ion on a cation and actually HCl is removed. We have not carried out experiments to try to detect HCl in the gas, since the zeolite samples used in the infrared measurements were extremely small (about 20 mg).

This interpretation also explains the lower stability of the OH groups compared to the OH bands on a decationized zeolite, which are only partially removed at 500 to 550° and heating to 700° is required to remove them completely.[7] In the case of the OH groups of a decationized zeolite the only method of removal of the OH groups is the splitting out of water molecules from the structure, while in the case of *n*-propyl chloride treated zeolites the removal of the OH groups is accomplished by the abstraction of HCl molecules from the OH groups and the neighboring cations. It is reasonable to assume that it is much easier to remove two atoms attached to the surface in the case of HCl than to pull out oxygen atoms from the structure in the case of the removal of the OH groups as water.

Another interesting observation is the different proportions of the two OH groups on the various cation-containing zeolites created by treatment with *n*-propyl chloride. A lot has been written about the two OH bands appearing on decationized zeolites (for a comprehensive review see ref 8). The significant difference in reactivity with adsorbed molecules and in acidity of the two hydroxyl groups has been pointed out by several authors.[7,9-11] Most writers agree that the two OH bands represent OH groups which differ in the position of the oxygen atoms within the zeolitic framework. However, it is not agreed which of the OH bands represents which oxygen position. The different proportions of the two OH groups on different bivalent cation-containing zeolites observed in our work must indicate that the electrostatic field of the cation in the zeolite is not only responsible for the dehydrohalogenation of the *n*-propyl chloride molecule, but must also have some directive influence on where the proton will be attached to the framework structure. The mechanism of this directive influence is not clear, but it seems reasonable that, if the chloride part of the HCl is attached to the cation, as shown previously, then the proton part would attach itself to an oxygen atom close to the cation. In this case different cation distributions for the different zeolites might be responsible for this directive influence.

The large variation in the proportions of the two OH bands on various cation-containing zeolites treated with propyl chloride makes it unlikely that changes in the extinction coefficients of the OH bands due to the different cations would alone be responsible for this effect. However, it is possible that there is some variation in the extinction coefficients due to the cations, since there is a small variation of the frequencies of the OH bands on various cationic forms of zeolites.

We feel that the significance of the creation of the OH groups by interaction with *n*-propyl chloride lies in the following. It has been demonstrated by several authors that the stability of the zeolite structure strongly depends on the presence of cations. On the other hand, OH groups are necessary for certain catalytic reactions.[3] Previously one could put OH groups into the zeolite only by ammonium ion exchanging the cations and then removing the ammonia by heating.[12] To obtain a good balance between cations and OH groups, back-exchanged zeolites have been prepared and described several times; bivalent and tervalent cations have been used for this purpose. By using our technique it is possible to keep all the cations in the zeolite structure and, in addition, introduce OH groups to the zeolitic surface. Furthermore, it is possible to do this with a large variety of cations, especially with bivalent cation-containing zeolites. This way it is possible to choose a cation which provides the most stable zeolitic structure and then introduce OH groups while maintaining the presence of the cations. It is not quite clear at this stage whether the cations in any way influence the OH groups, especially their acidity or reactivity. The frequencies of the OH groups on all of the bivalent cation zeolites created by the reaction with *n*-propyl chloride seem to be the same, although slight variations in frequency have been noted for the OH bands originally existing on these zeolites.[1,13]

In addition, the method provides a means whereby the proportion of the two OH groups can be varied. There has been quite a bit of speculation on which of the OH groups of the decationized zeolite are really responsible for the catalytic activity. However, if and when definite evidence is obtained that one or the other of these OH groups is responsible for the protonic-type catalytic activity of zeolites, a method will be available to vary the proportion of these two OH groups in various zeolites.

Since we have shown previously[1] that the same OH groups can be created by interaction with anhydrous hydrogen chloride, the question arises: why not use hydrogen chloride? In what way is our proposed method of using *n*-propyl chloride better? We feel that the hydrogen chloride is such an active reagent that it at-

(7) J. W. Ward, *J. Catal.*, 9, 225 (1967).

(8) M. R. Basila, *Appl. Spectr. Rev.*, 1, 307 (1968).

(9) T. H. Hughes and H. M. White, *J. Phys. Chem.*, 71, 2192 (1967).

(10) J. T. Richardson, *J. Catal.*, 9, 182 (1967).

(11) J. B. Uytterhoeven, P. Jacobs, K. Makay, and R. Schoonheydt, *J. Phys. Chem.*, 72, 1768 (1968).

(12) J. A. Rabo, P. E. Pickert, D. N. Stamires, and J. E. Boyle, *Actes Congr. Intern. Catalyse, 2e, Paris*, 2055 (1960).

(13) J. W. Ward, *J. Phys. Chem.*, 72, 4211 (1968).

tacks the external surface immediately on contact. This means that all of the OH groups will be formed on the external surface or very close to the surface of the zeolite crystallites. In the case of interaction with *n*-propyl chloride, we have demonstrated that the reaction occurs only at sites where there are cations present. Therefore, the *n*-propyl chloride actually has to enter the zeolitic cavities before a dehydrohalogenation reaction and formation of hydroxyl groups can occur. In this way a more even distribution of OH groups will be achieved than through interaction with hydrogen chloride. Since it is clear that catalytic reactions occurring on zeolites happen on the internal surfaces of the cavities, an even distribution of the OH groups all over the zeolitic surface is of significance in determining the catalytic properties of the zeolite used.

Acknowledgment. The authors wish to express their thanks to Dr. J. A. Rabo and Professor Verner Schomaker for helpful discussions.

Optical Studies of Thin Films on Surfaces of Fused Quartz

by A. C. Hall

Mobil Research and Development Corporation, Field Research Laboratory, Dallas, Texas 75221
(Received November 12, 1969)

Examination of deposited Langmuir–Blodgett monolayers indicates that fused quartz is a suitable substrate for ellipsometric studies. Thin films of adsorbed water on fused quartz surfaces do not exhibit the highest refractive indices reported for anomalous water condensed in quartz capillaries.

Introduction

The analysis of reflected polarized light is in principle one of the simplest and most versatile techniques for examining surfaces. Given a clean surface it is possible to infer its optical constants from experimental data. If the surface carries a plane, parallel-sided dielectric film, then the experimental data constitute a qualitative and quantitative analysis of the film.[1] That is, its refractive index and thickness are determined provided the nature of the bounding media is known, and subject to assumptions regarding the variation of refractive index between the boundaries of the film. In the Drude approximate formula (below), the film is taken to be an optically uniform layer for the sake of simplicity.

According to Drude,[2] if the substrate is transparent, and if the film thickness, d, is very small compared with λ, the wavelength of light, then for plane polarized light incident at Brewster's angle and at 45° azimuth

$$\rho = \frac{d\pi}{\lambda}\left(\frac{(1 + n^2)^{1/2}}{(1 - n^2)} \times \frac{(\bar{n}^2 - 1)(\bar{n}^2 - n^2)}{\bar{n}^2}\right)$$

where n, $\bar{n}$ are the refractive indices of substrate and film, respectively, and ρ is the so-called ellipticity coefficient. Clearly, ρ is always a small quantity and will be positive, zero, or negative according to whether $\bar{n} < n$, $\bar{n} = n$, or $\bar{n} > n$.[3]

It has been shown by Buff[4] that the given equation is not strictly valid, even as an approximation, and that allowance should be made for the inherent birefringence of the surface film. In practice, however, it is found that results obtained from the Drude equation are accurate. Only in the case of the transition zone at a vapor–liquid interface does film anisotropy appear to have produced considerable errors.[5]

Because ellipsometry applies to specularly reflecting surfaces, it has certain inherent advantages as a tool for the study of adsorption, by contrast with techniques that require high-area adsorbents. But ellipsometry is not always easily applicable, and one of the major difficulties is that uncontaminated surfaces are hard to find. Metals except, perhaps, gold are covered by an oxide layer unless great care is taken in preparation and handling. Dielectrics, although frequently less reactive, pose similar problems.[6,7] Fortunately, fused

(1) E. Passaglia, R. R. Stromberg, and J. Kruger, Ed., "Ellipsometry in the Measurement of Surfaces and Thin Films," National Bureau of Standards, Miscellaneous Publication 256, 1956.

(2) P. Drude, "The Theory of Optics," Longmans, Green and Co., New York, N. Y., 1920, p 292.

(3) R. W. Wood, "Physical Optics," Macmillan, New York, N. Y., 1934, p 360.

(4) F. P. Buff, 1966 Saline Water Conversion Report, U. S. Government Printing Office, Washington, D. C., p 26.

(5) K. Kinosita and H. Yokota, *J. Phys. Soc. Jap.*, **20**, 1086 (1965).

(6) L. Holland, "The Properties of Glass Surfaces," Wiley, New York, N. Y., 1964, p 122.

quartz is well suited to serve as an optical substrate: it is available in high purity, and relatively free from strains, striae, and bubbles. These properties are shared by crystalline quartz which, because of them, was long ago proposed as a reflectance standard.[8]

The potential technological importance of anomalous water has induced a number of laboratories, in this country and abroad, to initiate experimental programs aimed at discovering whether, in fact, it exists. While there is little doubt that the aqueous fluid condensed from water vapor in narrow capillaries of glass or quartz can have physical properties quite different from those of ordinary water, it is at least possible that these originate in causes other than a hitherto unknown structural modification of water. The clearest indication of true allotropy is in recently published[9] vibrational spectra, which are compatible with the existence of polymerized H_2O.

There is evidence that anomolous water, once formed, can persist outside of capillaries[9,10] but, with a single exception,[11] it appears never to have been prepared in other surroundings. For this reason it has not yet been available in quantities large enough to permit definitive characterization. The hypotheses of its formation generally involve an ordering interaction of the hydroxyl groups or oxygen atoms at the silica surface with H_2O adsorbed from the vapor phase.[12] It might be supposed, therefore, that water adsorbed near the silica surface should be at least as anomalous as water held in the capillaries (diameter $\sim$10–50 μ) generally used. Thus, it would be convenient to use ellipsometry to observe whether the refractive index of the adsorbate has anomalous properties. Deryagin, Zorin, and Churaev[13] measured the refractive index of anomalous water contained, as usual, in capillaries. They found values, in white light, between 1.3 (ordinary water) and 1.5, depending upon the degree of "structural modification." Since the refractive index of fused quartz is 1.46 at 5461 Å, reflection from its surface should exhibit positive or negative ellipticity, or no effect, according to whether the surface film refractive index is less than 1.46, greater, or the same.

Experimental Section

Following alignment of the ellipsometer,[14] the procedures followed were essentially those of Rayleigh.[15] The analyzer was set at $\pm 45°$, and fine adjustment made with the polarizer in either quadrant. The quarter-wave compensators were alternately set with fast and slow axes in the plane of incidence.

Two ellipsometers were used. Observations of clean quartz surfaces and of barium stearate monolayers on quartz surfaces were made with a Gaertner L119 ellipsometer. The light source was a University Laboratories Model 240 He–Ne laser, and a specially constructed quarterwave plate was used for the 6238-Å wavelength. The adsorption of water vapor on fused quartz was observed with a Rudolph and Sons, Inc., Model 437-200E ellipsometer, previously described.[16]

All specimens were of Spectrosil A fused quartz furnished by Thermal American Fused Quartz Co. The barium stearate films were deposited from a Langmuir trough on slabs thick enough so that reflections from the front and back could be separated. The water vapor was adsorbed on the hypotenuse of a 90° prism, contained in a Pyrex cell. The arms of the cell were arranged so that the incident and reflected beams should strike the quartz surface at Brewster's angle and the cell windows within 2° of the perpendicular. The cell windows were microscope cover glasses, selected for freedom from birefringence and attached by Torr Seal low-vapor pressure resin, cured at room temperature. Degassed water was contained in a side arm reservoir frozen in liquid nitrogen. The cell was evacuated to 1×10^{-5} Torr, then repeatedly filled with helium and outgassed, during which process the specimen was exposed to gentle glow discharge while shielded from electron bombardment. The relative pressure of water vapor was fixed by maintaining the reservoir at temperatures controlled by a thermostat, the vacuum cell being heavily insulated, and the temperature difference measured by a Hewlett Packard 2801A quartz thermometer. In order to eliminate strains in the windows, the cell was brought to atmospheric pressure by purified He.

Results

On the fused quartz surface as received eight different areas on a given prism gave ρ values between -0.00066 and -0.00026, with a mean of -0.00048. However, large positive ρ were also encountered; *e.g.*, 0.00131, 0.00113, 0.00113 on a given surface. Fused quartz has a low refractive index, and it is plausible that an adventitious layer could have a higher one. This might occur in the polishing process, either by production of a dense surface film or by contamination of the surface with material of high refractive index. The former possibility has been advanced already,[17] and the latter seems

(7) A. Vasicek, *J. Opt. Soc. Amer.*, **37**, 979 (1947).

(8) J. Koenigsberger, *Phys. Z.*, **4**, 494 (1903).

(9) E. R. Lippincott, R. R. Stromberg, W. H. Grant, and G. L. Cessac, *Science*, **164**, 1482 (1969).

(10) B. V. Deryagin, D. S. Lichnikov, K. M. Merzhanov, Ya. I. Rabinovitch, and N. V. Churaev, *Dokl. Akad. Nauk SSSR*, **181**, 823 (1968).

(11) B. V. Deryagin, Z. M. Zorin, and N. V. Churaev, *Kolloid Z.*, **30**, 308 (1968).

(12) R. W. Bolander, J. L. Kassner, and J. T. Zung, *Nature*, **221**, 1233 (1969).

(13) B. V. Deryagin, Z. M. Zorin, and N. V. Churaev, *Dokl. Akad. Nauk* SSSR, **182**, 811 (1968).

(14) F. L. McCrackin, E. Passaglia, R. R. Stromberg, and H. L. Steinberg, *J. Res. Nat. Bur. Stand.*, **67A**, 363 (1963).

(15) Rayleigh, *Phil. Mag.*, **33**, 1 (1892).

(16) A. C. Hall, *J. Phys. Chem.*, **69**, 1654 (1965).

(17) H. Yokota, K. Kinosita, and H. Sakata, *Jap. J. Appl. Phys.*, **3**, 805 (1964).

by no means improbable, since it is known that the specimens at hand were polished with Barnesite, a substance of very high refractive index.[18]

The positive ellipticities are less easily accounted for. The minimum possible thickness of the layer, *i.e.*, assuming $\bar{n} = \sqrt{n}$, is about 7 Å. If we suppose the layer in question to be quartz, but porous, and assign a value found by Vasicek[19] for a layer on glass, $\bar{n} = 1.36$, then a thickness of 11 Å would be sufficient. Whatever their nature, these layers are undesirable, since their optical effect is comparable in magnitude to that expected to be produced by the deposited monolayer.

First efforts to reduce ellipticity by careful cleaning were unsuccessful. Each specimen was treated ultrasonically in boiling ethanol and exposed to vapor degreasing in Baker Analyzed spectrophotometric acetone. Following such treatment small changes in ellipticity were noted, but in no case was it reduced to the level sought. Rayleigh[20] had shown that even in the case of glass it was possible to bring ellipticity to zero by polishing, but such treatment tends to be irreproducible. Etching with HF appears to be a more promising way of removing a surface layer with minimum damage to the optical properties of the substrate. Among the first to advocate this technique were the Rayleighs,[21,22] who used 0.5% "commercial acid," and 8% and 2% "commercial acid," respectively. In these experiments the more concentrated solutions, although faster, seemed to develop more obvious latent scratches which, while not conspicuously harmful to observation, were avoided by using 0.5% solution. In every case the etching solutions were constantly stirred.

Table I shows the trend of ellipticity resulting from continued immersion.

Table I

t, min	$-\rho \times 10^4$	t, min	$-\rho \times 10^4$
0	10	30	7.0
5	8.7	40	7.4
10	7.8	60	6.1
15	7.6	95	4.3
20	7.8	135	1.7

Barium stearate monolayers were deposited by techniques used previously,[16] but is was found that on surfaces of fused quartz supposed to be extremely clean, it was not always possible to deposit a continuous monolayer even near collapse pressure (≃40 dyn/cm).

The results for specimens that were fully covered are given in Table II.

Table II

$-\rho$ Initial	$-\rho$ Final	$-\rho$ Initial	$-\rho$ Final
0.00009	0.00051	0.00017	0.00069
0.00011	0.00070	0.00017	0.00087
0.00012	0.00077	0.00019	0.00082
0.00012	0.00067	0.00021	0.00071
0.00014	0.00071	0.00025	0.00090

Assuming the thickness of the monolayer[23] to be 24.4 Å, it is possible to calculate its mean refractive index *via* Drude's equation. Allowance is made for the initial ellipticity by subtracting it from the final value, an approximation that has been used by Bouhet[24] and Hofmeister.[25] The mean of the calculated indices is between 1.47 and 1.48, with an average value nearer 1.48, considerably lower than might have been expected. Langmuir and Blodgett,[23] using thick, built-up layers of barium stearate, showed the film to be uniaxial with axis perpendicular to the surface, and for $\lambda = 5461$ Å, $n_e = 1.55$, and $n_0 = 1.49$. The monolayer is also birefringent, but the optical effect is so small that, given the accuracy of the measurement, there is nothing to be gained by taking it into account, although the necessary equations are given by Schopper.[26] Both Bouhet and Hofmeister, using ellipsometry, found that condensed monolayers of fatty acids spread on aqueous solutions were characterized by refractive indices lower than the values for bulk material, and Hofmeister attributed this to water molecules intruding into the monolayer. In this case, presumably when the monolayer is transferred from the liquid surface to the solid, the film becomes slightly less coherent. In covering a larger area its density is reduced correspondingly and therefore its refractive index also.

For water vapor condensed on fused quartz the measured ellipticities are given as a function of relative pressure in Figure 1; bars show the limits of instrumental accuracy. Although ellipticity shows a tenfold increase over the range of P/P_0, there is no observable change in polarizing angle or elliptical orientation. It is, therefore, impossible to determine the refractive index of the adsorbate and its thickness. One must instead compute the thickness using assumed values for its refractive index. Isotherms are shown in Figure 2 for $n_{H_2O} = 1.33$, approximately the value for bulk water, and $n_{H_2O} = 1.40$. As required by optical theory, the larger (anomalous) index corresponds to a higher degree of adsorption at a given relative pressure; in this

(18) A. D. Weeks, D. R. Ross, and R. F. Marvin, *Amer. Mineral.*, **48**, 1187 (1963).
(19) A. Vasicek, *J. Opt. Soc. Amer.*, **37**, 145 (1967).
(20) Rayleigh, *Phil. Mag.*, **16**, 444 (1908).
(21) Rayleigh, *Nature*, **64**, 385 (1901).
(22) Rayleigh, *Proc. Roy. Soc., Ser. A*, **160**, 507 (1937).
(23) K. B. Blodgett and I. Langmuir, *Phys. Rev.*, **51**, 964 (1937).
(24) Ch. Bouhet, *Ann. Phys. (Paris)*, **15**, 5 (1931).
(25) E. Hofmeister, *Z. Phys.*, **36**, 137 (1953).
(26) H. Schopper, *ibid.*, **132**, 146 (1952).

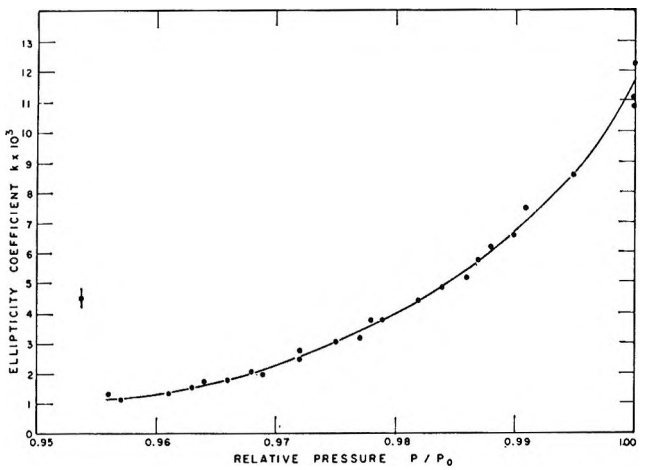

Figure 1.

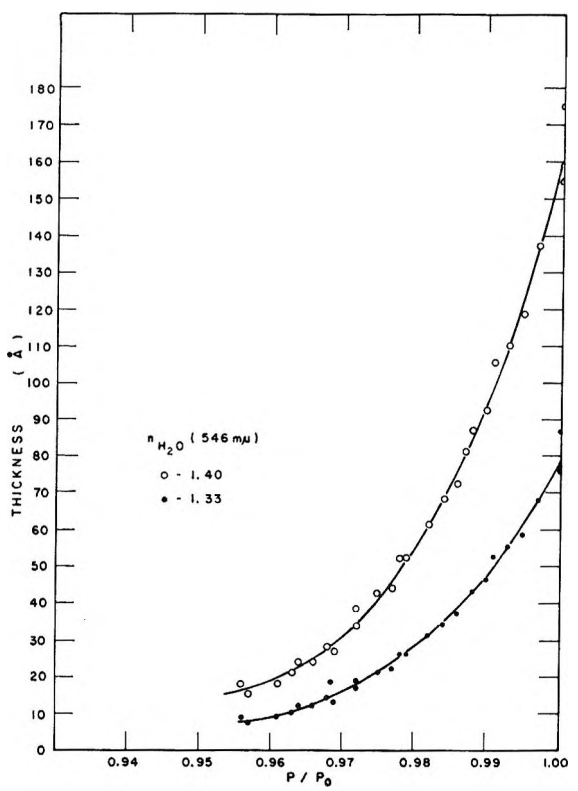

Figure 2.

case, about twice the value derived assuming the bulk index.

Since negative ellipticity was not observed, the water adsorbed at the quartz surface has a refractive index less than the largest values cited by Deryagin, *et al.* Because, as previously mentioned, the film is extremely thin, it is impossible to say more than this. Other evidence on the matter is available in the results of Frazer[27] who, using a sensitive photometric technique of ellipsometry, studied adsorption of water vapor on glass at room temperature. Only positive ellipticities were reported, though this is not so significant as in the case of silica since the refractive index of glass exceeds 1.50. However, taking the refractive index of the adsorbed water film to be the bulk value, Frazer found monolayer adsorption very close to the same relative pressure as determined for fused quartz by gravimetric techniques.[28] It is perhaps worth noting that in 1954–1955, Deryagin and Zorin[29] reported results in a study of the adsorption of water vapor by glass, using the so-called micropolarization technique. In this case the refractive index of the adsorbed film was taken to be that of bulk water, and the resulting isotherm is not greatly different from that given here for fused quartz.

There is an interesting discrepancy between all of these results obtained by an optical method and measurements made by more conventional techniques; namely, the former give much larger thicknesses for the adsorbed film at given relative pressure. Using volumetric and gravimetric methods, Hagymassy, Brunauer, and Mikhail[30] have shown that for both water and nitrogen on a number of substrates, including silica gel and quartz, the statistical number of monolayers at unit relative pressure does not much exceed 6, and at 0.9 relative pressure, the number is less than 4.

Bayh and Pflug[31] used a sensitive ellipsometer to study water vapor adsorption on cleavage faces of alkali halides and found monolayer thickness to be about 3.6 Å. If this value is applied to the optical data here, then according to Figure 2, 6 layers are present at $P/P_0 \simeq 0.97$, and at saturation the number is about 22. Frazer's results for water vapor on glass show about 8 layers at $P/P_0 \simeq 0.92$, and 6 layers at $P/P_0 \simeq 0.86$. Deryagin and Zorin show about 20 layers at saturation and 6 layers near $P/P_0 \simeq 0.97$.

It is generally believed that the Drude equation, if not strictly valid, still provides a fairly accurate measure of thickness in thin film systems. This is substantiated by optical studies of films whose thickness is known from other measurements. There is some uncertainty as to the effective refractive index of a very thin film, which can reasonably be supposed to be different from the bulk value. But, according to the Drude equation, the minimum possible film thickness corresponds to $n = \sqrt{n}$ and amounts to about 58 Å or 16 layers in the case at hand.

Conclusions

1. Fused quartz, unlike most kinds of glass, is a useful substrate for study of very thin dielectric films by ellipsometry. Optical surfaces of very low residual ellipticity can be prepared by treatment with dilute HF.
2. It is possible to detect a monolayer of barium

(27) J. H. Frazer, *Phys. Rev.*, **33**, 97 (1929).

(28) J. W. Whalen, *J. Phys. Chem.*, **65**, 1676 (1961).

(29) B. V. Deryagin and Z. M. Zorin, *Zh. Fiz. Khim.*, **29**, 1755 1955).

(30) J. Hagymassy, S. Brunauer, and R. Sh. Mikhail, *J. Colloid Interface Sci.*, **29**, 485 (1969).

(31) W. Bayh and H. Pflug, *Z. Angew. Phys.*, **25**, 358 (1968).

stearate on fused quartz by measurements at Brewster's angle.

3. In these experiments on silica, and in similar ones on glass, it is clear that the adsorbed water film is not modified to the degree cited by Deryagin and Churaev as maximum. There is, indeed, no indication that it is different from ordinary bulk water despite the fact that the appearance of anomalies should be favored by at least two factors due to the films being extremely thin: (1) the proximity of the substrate; (2) a surface to volume ratio much larger than in the narrowest capillaries used to date.

This by no means proves that anomalous water does not exist. In the first place, whether or not it forms is supposed to depend upon minute details of surface preparation. Moreover, even under favorable conditions its genesis seems to be quite unpredictable.[32] These results serve to narrow the scope of the search for the material.

4. Finally, the results illustrate a discrepancy between adsorption data obtained by ellipsometry and by conventional methods. Since these techniques are applied to optically smooth, planar surfaces, and to small particles, respectively, it may be of interest to discover the reasons for the substantial differences that are found.

Acknowledgment. This paper is published by permission of the management of Mobil Research and Development Corp.

(32) V. I. Anisimova, B. V. Deryagin, I. G. Ershova, D. S. Lichnikov, Ya. I. Rabinovitch, V. Kh. Simonova, and N. V. Churaev, *Russ. J. Phys. Chem.*, **41**, 1282 (1967).

The Reversible Hydration of Formaldehyde. Thermodynamic Parameters

by Andreas A. Zavitsas, Mark Coffiner,[1] Thomas Wiseman,[1] and Lourdes R. Zavitsas

Department of Chemistry, The Brooklyn Center of Long Island University, Brooklyn, New York 11201
(Received January 27, 1970)

The thermodynamic parameters for the reversible hydration of formaldehyde have been evaluated by ultraviolet spectrophotometry, with appropriate corrections for polymerization and for nonspecific absorption contributions; $\Delta H = -8.4 \pm 0.5$ kcal/mol, $\Delta S = -12.6 \pm 1.7$ eu. No significant shift of λ_{max} with temperature was found.

Our investigations of the kinetics and mechanisms of the reactions of formaldehyde with phenol have led us to an examination of formaldehyde equilibria.[2] We found no reliable measurements of the temperature dependence of the equilibrium constant for the hydration of formaldehyde,[3] eq 1. Although the mechanism

$$HCHO + H_2O \rightleftharpoons HOCH_2OH \qquad (1)$$

of the reaction may involve more than one molecule of water, eq 1 is considered adequate for thermodynamic considerations.[3] Spectrophotometric studies of the n–π^* carbonyl absorption near 288 mμ[4] have been hampered by several, occasionally unrecognized, factors: (a) the concentration of the unhydrated species is very small, for equilibrium 1 lies far to the right; (b) the extinction coefficient of the aldehyde is small and it cannot be determined without previous knowledge of the hydration equilibrium constant; (c) high total concentrations of formaldehyde cannot be used with impunity because of extensive reversible polymerization reactions[5] of the type shown in eq 2, which become significant above 1 M total formaldehyde; and (d) concentrated aqueous solutions of formaldehyde exhibit substantial nonspecific absorption well into the region of the n–π^* transition, thus making it difficult to assign a base line for the reading of the specific absorption.

$$n HOCH_2OH \rightleftharpoons HO(CH_2O)_nH + (n-1)H_2O \qquad (2)$$

Calorimetric measurements of ΔH for reaction 1 on dissolving HCHO gas in water are complicated by the simultaneous release of a substantial heat of dilution.[6]

Values for the equilibrium constant[7] are available

(1) Undergraduate research participant.

(2) A. A. Zavitsas, *J. Polymer Sci., Part A-1*, **6**, 2533 (1968); A. A. Zavitsas, R. D. Beaulieu, and J. R. LeBlanc, *ibid.*, **6**, 2541 (1968); A. A. Zavitsas, *J. Chem. Eng. Data*, **12**, 94 (1966).

(3) For a review see: R. P. Bell, *Adv. Phys. Org. Chem.*, **4**, 1 (1966).

(4) D. E. Freeman and D. Klemperer, *J. Chem. Phys.*, **40**, 604 (1964).

(5) Equation 2 is not meant to imply that HCHO is not the species involved in the polymerizations.

(6) A. Iliceto, *Gazz. Chim. Ital.*, **84**, 536 (1954).

(7) Usually the equilibrium constant has been expressed as the ratio of the anhydrous to the hydrated species.

or can be calculated from some existing data at various temperatures and concentrations of formaldehyde in aqueous solutions;[8-10] there is rather poor agreement among the various values of the equilibrium constant and particularly among the slopes of plots of the points from each investigation *vs.* $1/T°K$. An excellent critical review of available data has been published.[3] An apparently reliable value for the equilibrium constant is that of Valenta,[11] obtained by pulse polarography in dilute phosphate buffer of pH 7, reported as $[HCHO]/[HOCH_2OH] = 4.37 \times 10^{-4}$ at 20°; the method is based on the fact that HCHO is reducible whereas the hydrates are not,[12] and on the assumption that dehydration is slow relative to the duration of the polarographic pulse.

To be better applicable to systems containing appreciable amounts of formaldehyde, the equilibrium content should be defined as in eq 3, in which N_{H_2O} indi-

$$K = [HOCH_2OH]/([HCHO]N_{H_2O}) \quad (3)$$

cates molar fraction of free water. Thus defined the polarographic value becomes $K = 2.33 \times 10^3$.

Experimental Section

Reagents. Formaldehyde solutions were prepared by mixing 20 g of paraformaldehyde powder (Mallinckrodt), 100 ml of distilled H_2O and 0.5 g of reagent grade magnesium oxide powder and distilling at a very rapid rate with a short head and a condenser cooled by lukewarm water; the first 25% of the distillate was discarded and the next 50% was collected. The pH of the solutions was usually between 3.8 and 4.6; batches of lower pH were discarded. Magnesium oxide greatly facilitates the solution of paraformaldehyde. The formaldehyde content of the collected distillate was approximately 17%, as HCHO, by the hydroxylamine hydrochloride titration method.[13] Solutions above 22 wt % were found to develop a haze on standing at room temperature. The pH was adjusted with 0.5 *M* sodium hydroxide immediately before use; it was rechecked at the end of the measurements and it was found to have remained unchanged within the accuracy of the pH meter.

Measurements. Uv measurements were obtained on freshly prepared formaldehyde solutions in thermostated cell compartments, either with 10.00-cm cells in a Bausch and Lomb Spectronic 505 operated in the absorbance mode, or with 5.00-cm cells in a Perkin-Elmer 450 operated in the transmittance mode with subsequent conversion of the readings to absorbance. We employed concentrations between 14 and 18 wt % over the pH range of 5.60–8.90. An average of ten observations at various temperatures were taken per sample with the highest temperature reading taken first, the following six readings at progressively lower temperatures, and the last three readings at progressively higher temperatures again. In this manner, any thermally irreversible changes that might have occurred during the measurements would have become apparent; this procedure also verified that the equilibria were established at each temperature.

We found it imperative to limit the time of exposure of the samples to heat and to the uv beam of the instrument. The samples were removed from the thermostated compartments during most of the substantial time required for the attainment of a steady new temperature at the circulating bath; prolonged exposure led to an increase in the nonspecific absorbance (see below) and to the appearance of a new absorption at 326 mμ.

Results

In principle the concentration of $HOCH_2OH$ can be calculated if the polymerization equilibrium constants for each value of n in eq 2 are known; such calculations, using the same value of equilibrium constant for all values of n greater than 2, have been performed with the appropriate computer programs.[14] We employed a different and simpler approximation which describes the polymerization equilibria quite accurately; the generalized eq 2 was found to be equivalent, on the average and over a wide range, to eq 4. The average

$$2.6[HOCH_2OH] \overset{K=26}{\rightleftharpoons} [HO(CH_2O)_{2.6}H] + 1.6[H_2O] \quad (4)$$

values of n and of the pseudoequilibrium constant given in eq 4 were found to give the best fit over the widest range to the available experimental data as shown in Figure 1.[15] We attempted to fit the bisulfite titration data[16] rather than that of the other sources which was obtained by nmr in D_2O solutions with unspecified deuterium isotope effects on the equilibrium constant for polymerization. In the hydration equilibria of higher aldehydes, isotope effects in D_2O are known to amount to over 15%.[10] Cyclic structures such as trioxane amount to less than 1% up to 30 wt % formaldehyde and they can be ignored for our purposes.[14] The per cent of formaldehyde in the form of monomeric hydrate is affected only slightly by temperature and pH and the same approximation, eq 4, can be used over the range of these reaction variables used in our measurements.

(8) R. Bieber and G. Trumpler, *Helv. Chim. Acta*, **30**, 1860 (1947).
(9) J. F. Walker, "Formaldehyde," 3rd ed, Reinhold, New York, N. Y., 1964, p 61.
(10) L. C. Gruen and P. T. McTigue, *J. Chem. Soc.*, 5217 (1963).
(11) P. Valenta, *Collect. Czech. Chem. Commun.*, **25**, 853 (1960).
(12) R. Brdicka, *ibid.*, **20**, 387 (1955); *Chem. Listy*, **48**, 1458 (1954); *Z. Elektrochem.*, **59**, 787 (1955).
(13) See ref 9, p 493.
(14) K. Moedritzer and J. R. Van Wazer, *J. Phys. Chem.*, **70**, 2025 (1966).
(15) For a description of the solution of the empirical equation see the Appendix.
(16) A. Iliceto and S. Bezzi, *Ric. Sci.*, **19**, 999 (1949).

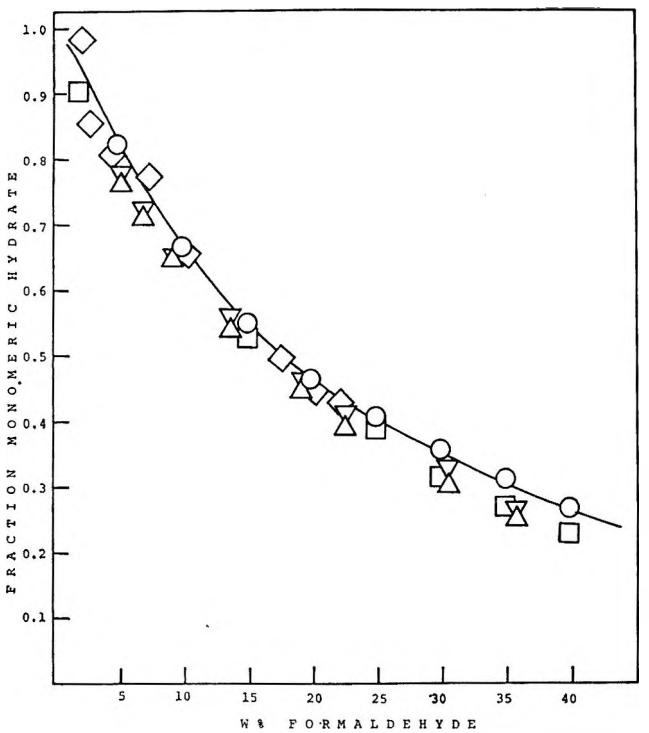

Figure 1. Fraction of formaldehyde in the form of $HOCH_2OH$ *vs.* total weight per cent formaldehyde: ○, by bisulfite titration at 35°, ref 16; △, by nmr in D_2O at 34°, ref 17; ▽, by nmr in D_2O at 60°, ref 17; ◇, by nmr in D_2O at ambient, ref 18; □, calculated for D_2O solution at 30°, ref 14. The line indicates values obtained by solving eq 4.

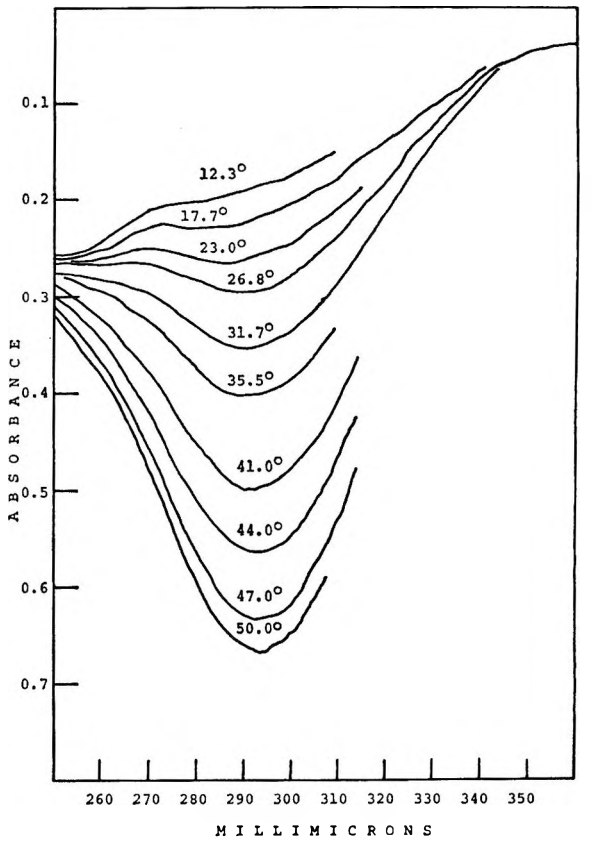

Figure 2. Absorbance *vs.* wavelength for run no. 1 of Table I. The presence of some nonspecific absorbance under λ_{max} is apparent.

The small temperature dependence is evident from the data in Figure 1, and from reported values for the average degree of polymerization, P_n, excluding monomer: at 13.76 wt % formaldehyde in D_2O, P_n = 2.28 at 34°, 2.27 at 60°, and 2.25 at 90°; at 22.61 wt %, P_n = 2.42 at 34°, 2.44 at 60°, and 2.43 at 90°.[17] These concentrations bracket our range. In agreement with the above, the enthalpy change for the polymerization has been reported to be very small.[14,18] The negligible effect of pH has been demonstrated by cryoscopic measurements of the average molecular weight of a 25.52 wt % solution; the value increased by 0.4% in going from a neutral solution to pH 10.7.[19]

The extinction coefficient of the n–π^* absorption of HCHO was assumed to remain constant over our temperature range, by analogy from similar reports on acetone[10] confirmed by us.

Typical uv curves from our work are shown in Figure 2. Since the hydration equilibrium lies far to the right, eq 1, semilog plots of absorbance *vs.* $1/T$°K should be linear. The relation between the equilibrium constant for hydration, K, and the absorbance, A, for this case is given by eq 5. ϵ denotes the extinction

$$\ln K = -\ln A + \ln (\epsilon l[HOCH_2OH]/N_{H_2O}) \quad (5)$$

coefficient, l the length of the solution, and $HOCH_2OH$ the calculated (see Appendix) concentration of methylene glycol.

When absorbance is read as the difference between that at λ_{max} and at 360 mμ, such semilog plots show departures from linearity, as seen in Figure 3. Figure 2 clearly shows that there is an appreciable contribution to the absorbance at λ_{max} from the tail end of the nonspecific absorption; the magnitude of this contribution is not apparent by inspection. This nonspecific absorption has been reported as being temperature independent[20] and we confirmed this finding. We made a computer-aided search for the optimum amount of nonspecific absorbance to be substracted in each experiment by examining the sum of the squares of the residuals, in least-squares fittings of the points to a straight line, as a function of the amount subtracted; the plots were paraboloid with sharp minima.

The curvature indicated by the raw data for run 5 in Figure 3 disappears upon subtraction of 0.453 absorbance unit of nonspecific tail end absorption; the amount subtracted is the optimum value for linearity in this run. The nonspecific absorption varied from sample to sample and it seemed to depend on the aging

(17) Y. Ihashi, K. Sawa, and S. Morita, *J. Chem. Soc. Jap., Ind. Chem. Sec.*, **68**, 1427 (1965).

(18) P. Skell and H. Suhr, *Chem. Ber.*, **94**, 3317 (1961).

(19) A. Iliceto and S. Bezzi, *Chim. Ind.* (Milan), **33**, 212 (1951).

(20) J. F. Walker, ref 9, p 60.

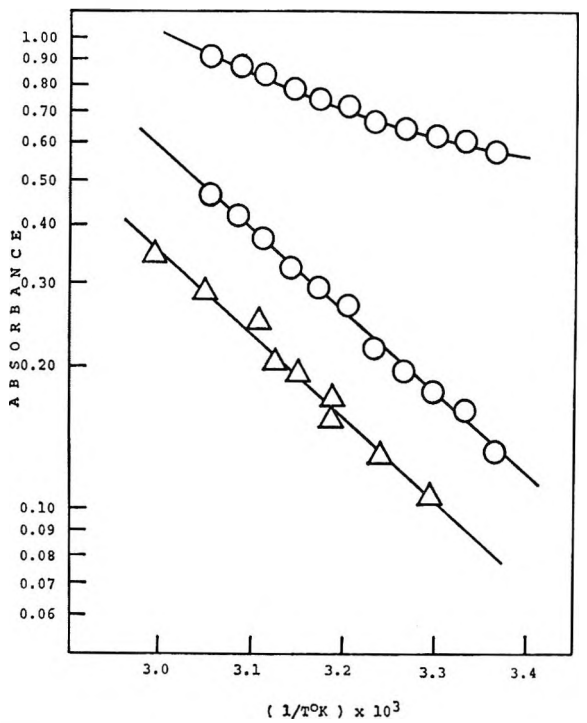

Figure 3. Absorbance *vs.* $1/T$°K: O, run no. 5 of Table I; upper set of points indicates raw data, lower set (joined by straight line) indicate net absorbance after subtraction of the optimum nonspecific absorance; △, run no. 4, net absorance.

of the formaldehyde solutions (see Experimental Section). Run 5 showed the largest amount of nonspecific absorbance; more typical was run 4, Figure 3, which required a little over 0.1 absorbance unit to be subtracted. The optimum amount given by the computer search appeared compatible with the uv curves by inspection; for run 1, Figure 2, for example, the nonspecific absorbance contribution at λ_{max} was evaluated as 0.064. Generally the minima of the "goodness of fit" function were quite sharp, indicating unmistakably the need for an optimum base line correction to be applied to each set of data for best linearity. Table I outlines conditions and data for six experiments. The slopes of plots of the raw absorbance data *vs.* $1/T$°K varied rather widely from sample to sample; after application of the optimum base line correction for best linearity, there was acceptable agreement as shown in Figure 3 and in Table II. It appears that this type of correction procedure has not been used previously in any of the numerous investigations of the hydration of formaldehyde by uv spectrophotometry.

Table I: Experimental Conditions and Extrapolated Net Absorbance Values

Run no.[a]	Total wt % HCHO	pH	A (20°)[b]	t range °C, (points)	[HOCH₂OH], M
1	16.97	5.60	0.140	12.3–50.0 (10)	3.07
2	16.73	6.00	0.144	30.0–61.0 (11)	3.05
3	16.24	7.35	0.0698	29.5–60.7 (9)	2.99
4	15.83	7.48	0.0687	30.3–61.1 (9)	2.96
5	17.21	7.50	0.115	24.0–54.0 (11)	3.09
6	16.64	8.90	0.139	22.0–44.0 (9)	3.04

[a] 1, 2, 5, and 6 with 10.00-cm cells, absorbance measurements; 3 and 4 with 5.00-cm cells, transmittance measurements subsequently converted to absorbance. [b] Net absorbance extrapolated to 20°.

Table II: Derived Values and Calculated Thermodynamic Parameters

Run no.	$-\{dA/d(1/T)\} \times 10^{-4}$	Intercept	ϵ	$-\Delta H$, kcal/mol	$-\Delta S$, eu
1	0.450	13.4	10.0	8.94	15.2
2	0.391	11.2	10.1	7.76	10.8
3	0.455	12.8	10.1	9.04	15.4
4	0.402	11.0	10.1	8.00	12.0
5	0.400	11.5	8.6[a]	7.94	11.4
6	0.448	11.3	10.0	8.91	11.0

[a] This run exhibited by far the largest nonspecific absorbance; even after the appropriate corrections, it cannot be considered as reliable as the others.

Plots of log K, equivalent to log A, *vs.* $1/T$°K have been reported to be curved and attempts were made to obtain improved linearity by the proper choice of extinction coefficient.[10] In view of eq 5, the relation between the value of the extinction coefficient and the linearity of such plots is not evident. The contribution of the nonspecific absorbance at λ_{max} is the cause of curvature in our case.

The values of the thermodynamic parameters were obtained from $\Delta H = R\{dA/d(1/T)\}$ and $\Delta S = -R\{\text{Intercept} - \ln(\epsilon l[HOCH_2OH]/N_{H_2O})\}$. The enthalpy is independent of the extinction coefficient, but the entropy does have a relatively small dependence. The value of the extinction coefficient can be obtained by use of eq 5 from the best available value of K,[3] that of Valenta at 20°,[11] in conjunction with our extrapolated values of net absorbance at the same temperature, Table I. The values of the extinction coefficient resulting from each run and the calculated thermodynamic parameters are given in Table II.

Discussion

It should be noted that the value of approximately 10 obtained in this work for the extinction coefficient of formaldehyde appears low compared to that for similar compounds; we found $\epsilon = 17.5 \pm 0.2$ for acetone in water (constant between 30 and 60°) and for acetaldehyde in water $\epsilon = 17$ has been reported.[21] How-

(21) R. P. Bell and J. C. Clunie, *Trans. Faraday Soc.*, **48**, 439 (1952).

ever, variations in ϵ_{max} with structure for small aldehydes are not uncommon.[22] For formaldehyde ϵ = 12.5 has been assumed previously by extrapolation from higher aldehydes;[8] ϵ = 7 also has been used as a rough estimate.[10]

Our value of $\Delta H = -8.4 \pm 0.5$ kcal/mol can be compared with previous rough estimates of 8–10;[3] it is a reasonable value since the sum of the heats of solution and hydration of gaseous formaldehyde in water is 14.6 kcal/mol[23] and the latent heat of the monomeric gas is 5.57 kcal/mol,[24] setting an upper limit of approximately 9 kcal/mol. A recent statistical analysis of available thermodynamic data for the reactions of formaldehyde with water and with its own polymers gave a "best" value of $\Delta H = -9.3$ as part of an overall consistent set.[25]

The entropy change found, $\Delta S = -12.6 \pm 1.7$ eu, is in the expected direction for this kind of reaction but no meaningful comparisons can be made with other aldehydes since entropy changes for carbonyl hydrations vary rather widely.[3,22,26]

Increasing temperature appears to lead to a small red shift in λ_{max} for formaldehyde, Figure 2. A general property of n–π^* bands is a red shift in going from a polar to a nonpolar medium; the dipole moment decreases in going from the ground to the excited state.[4] In this case it should be noted that the dielectric constant of water decreases substantially with increasing temperature. Such small red shifts for formaldehyde have been reported previously.[20] The shift can be attributed to decreased hydrogen bonding of the ground state at higher temperature. However, we find no comparable shift with acetone in water over the same temperature range. We have concluded that this apparent shift probably is not real; it is the result that would be expected from the algebraic addition of an increasing and broad signal to a steeply sloping base line (the tail-end of the nonspecific absorption).

Acknowledgment. We wish to thank the Brooklyn Center Committee on Research of Long Island University for support of part of this work.

Appendix

Solution of eq 4

$$26 = [HO(CH_2O)_{2.6}H][H_2O]^{1.6}/[HOCH_2OH]^{2.6} \quad (6)$$

or

$$26 = (1/2.6)[F](1 - m)[H_2O]^{1.6}/(m[F])^{2.6} \quad (7)$$

where $[F]$ denotes total formaldehyde concentration in moles per liter as determined titrimetrically, and m denotes the fraction of the total that is in the form of methylene glycol, Figure 1. Also

$$[H_2O] = [H_2O]_{tot} - [HOCH_2OH] - [HO(CH_2O)_{2.6}H] \quad (8)$$

or

$$[H_2O] = [H_2O]_{tot} - m[F] - (1/2.6)(1 - m)[F] \quad (9)$$

where total H_2O is calculated by difference from total weight and the analytical weight per cent formaldehyde, after the appropriate corrections for density.

In principle, eq 7 and 9 can be combined and solved. We solved eq 7 by the Newton–Raphson method, an iterative procedure that requires an initial estimate of m. Equation 9 was updated at every iteration and the method succeeds because H_2O converges fast. A listing of the appropriate computer program in FORTRAN IV is available from the senior author on request.

(22) Y. Pocker and D. G. Dickerson, *J. Phys. Chem.*, **73**, 4005 (1969).

(23) M. W. Hall and E. L. Piret, *Ind. Eng. Chem.*, **41**, 1277 (1949).

(24) See ref 9, p 46.

(25) J. B. Thomson and W. M. D. Bryant, *Polym. Prep. Amer. Chem. Soc., Div. Polym. Chem.*, **11**, 204 (Feb 1970).

(26) As an example of the effect of the extinction coefficient value on the entropy change calculations, we found that ΔS would become less negative by only about 1 eu if an extinction coefficient as high as 16 were to be used.

Determination to 5 kbars of the λ Transition Temperature in Sodium Nitrate

by W. Klement, Jr.[1]

Department of Geophysics and Geochemistry, Australian National University, Canberra, A.C.T., Australia *(Received September 23, 1969)*

Differential thermal analysis signals for the λ transition in sodium nitrate have been obtained in experiments to 5 kbars in hydrostatic apparatus with heating–cooling rates of ~10–30° min^{-1}. If the equilibrium transition temperature is taken as midway between the temperatures of the heating and cooling signals (which differed by ~5°), the best linear fit suggests $dT_\lambda/dp \approx 7.2°$ $kbar^{-1}$; if the curvature, $d^2T_\lambda/dp^2 < 0$, is allowed, the initial slope is ~8° $kbar^{-1}$.

Rapoport[2] suggested that the temperature, T_λ, of the λ transition in sodium nitrate increased with pressure at the rate of 6.3 ± 0.2°[3] $kbar^{-1}$ at zero pressure; this suggestion was based on an investigation over the range of ~5–40 kbars in apparatus using solid pressure-transmitting media with differential thermal analysis (dta) in which, unfortunately, only a weak signal on cooling thru the transition could be detected. By correlating various zero-pressure thermodynamic data, Klement[4] proposed instead that $dT_\lambda/dp \approx 8.6°$ $kbar^{-1}$. This note describes an investigation by dta of the λ transition to 5 kbar in hydrostatic apparatus.

Analar sodium nitrate of "analytical reagent" grade (<0.015% specified impurities) was compacted into pellets 1.50 cm long by 10.7 mm diam under a nominal pressure of 3 kbars. A blind hole of 1.20-mm diameter 1.14 cm deep was drilled into a molybdenum "thermocouple well" of 2.46-mm diameter which was pressed into a hole drilled along the pellet axis. In Paterson's apparatus[5] (which was designed for deformation work), argon is used as the pressure-transmitting medium and the cylindrical sample and adjacent steel end pieces are encased in a 0.25 mm thick annealed copper sheath. Heating is accomplished by passing current through nichrome windings concentric with the specimen. By means of an axial hole, an assembly comprised of three chromel–alumel thermocouples (with sheaths ~0.5-mm diameter) was introduced into the molybdenum well; the junctions were spaced ~9 mm apart and from the end. Pressure is measured by a manganin cell[5] calibrated against a Heise gage and is known to an accuracy of at least ±50 bars.

The molybdenum well represents a compromise between the desired factors: (a) of high thermal conductivity and good thermal contact between specimen and thermocouple and (b) of strength sufficient to prevent extrusion of the sample into the axial hole or collapse about the thermocouple. In one run, a stainless steel well was used but the signals observed were inferior to those obtained with the design herein described.

In order to obtain sufficiently distinct and reproducible dta signals (even after amplification with a dc amplifier), it was necessary to abruptly alter the furnace current so that temperature varied at rates of ~10–30° min^{-1}. The variation in temperature among the thermocouples in the sample was, however, almost always within 1°. Thus all of the useful data were obtained by varying temperature isobarically; some attempts to achieve better precision by isothermally varying pressure were unsuccessful because pumping on–bleeding off the gas caused excessive variations in temperature.

Upon commencing a run, the specimen was pressurized to a few hundred bars and annealed for 5–10 min a few degrees below the transition. Sufficiently distinct and reproducible signals could not be obtained initially at the lowest pressures; it seemed that a number of cycles through the transition, as well as going to slightly higher pressures and temperatures, were necessary. Shown in Figure 1 are the temperatures of the heating and cooling signals accepted for the transition for the several runs, for both increasing and decreasing pressure. The upper pressure here was dictated by the rate at which the pump could maintain the pressure against leakage. The absence of data at the lowest pressures is mostly due to the progressive indistinctness of the signals there. Cooling signals in the range of ~3–4 kbars were difficult to recognize because of the much larger signals due to freezing of small amounts of sodium nitrate which had seeped into the thermocouple well.

The signals were reproducible to ±1° and the uncertainty in the recorder calibration was ±1°. Hence,

(1) Guggenheim Fellow, on leave from School of Engineering and Applied Science, University of California, Los Angeles, Calif. 90024.

(2) E. Rapoport, *J. Phys. Chem. Solids*, **27**, 1349 (1966).

(3) C. W. F. T. Pistorius, E. Rapoport, and J. B. Clark, *Z. Phys. Chem.* (Frankfurt am Main), **59**, 200 (1968).

(4) W. Klement, *J. Phys. Chem.*, **72**, 1294 (1968).

(5) M. S. Paterson, to be published.

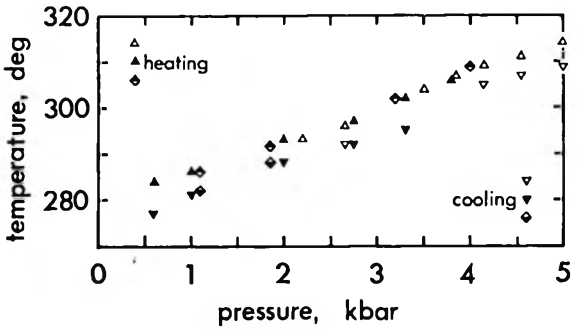

Figure 1. Temperatures of the λ transition obtained on heating and on cooling for various hydrostatic pressures and for various runs (denoted by the different shadings of the symbols) at rates of ~10–30° min^{-1}.

the temperatures plotted in Figure 1 are believed accurate to ±2–3°.

The obvious difference ("hysteresis") in temperatures obtained on heating and on cooling (Figure 1) makes it difficult to precisely specify the equilibrium phase boundary. It is believed that the hysteresis results from the high heating–cooling rates necessary to obtain acceptable dta signals. Ravich and Egorov,[6] working at rates of a few degrees per minute, are somewhat ambiguous about the occurrence of hysteresis although there seems to be ~1° difference between the heating and cooling signals shown in their[6] Figure 6. Rapoport[2] chose not to report the coordinates of his heating signals but a scrutiny of his[2] Figure 2 suggests a hysteresis of a few degrees, at a rate of 4–8° sec^{-1}. The classic dta investigation[7] of Kracek, apparently[8] at rates of 0.15–0.4° min^{-1}, did not seem to show hysteresis but there was a distinct difference in shape between the heating and cooling signals. Measurements[9] by a pulse technique on an oriented single crystal suggest that the thermal diffusivity near T_λ is less than 10^{-3} cm^2 sec^{-1}, which qualitatively can be used to explain the thermal lag although a quantitative correlation cannot be made here for the various geometries.

In the present work (Figure 1), the hysteresis appears to remain about constant (5 ± 2°) over the investigated interval. If one averaged between heating and cooling signals in the attempt to obtain the equilibrium transition temperature at the various pressures, there would result a plausible extrapolation back to zero pressure for a T_λ there of 275–276°, in agreement with most workers. A linear fit of the data (Figure 1) suggests then a slope of ≈7.2° $kbar^{-1}$. The present data are accurate enough to show that Rapoport's suggested[2,3] initial slope of 6.3 ± 0.2° $kbar^{-1}$ is definitely too low, although this value for the slope may be appropriate near 4–5 kbar (Figure 1). If some "curvature" were allowed for the phase boundary—with $d^2T_\lambda/dp^2 < 0$ as is typical,[10] the initial slope would be ~8° $kbar^{-1}$. Possibly the present data below 5 kbars might be considered together with Rapoport's result[2,3] at higher pressures for an estimate of the curvature of the phase boundary, but such a comparison is too difficult to attempt here.

Acknowledgment. Dr. M. S. Paterson is thanked for encouragement and comments.

(6) G. B. Ravich and B. N. Egorov, *Russ. J. Inorg. Chem.*, **5**, 1257 (1960).

(7) F. C. Kracek, *J. Amer. Chem. Soc.*, **53**, 2609 (1931).

(8) F. C. Kracek, *J. Phys. Chem.*, **34**, 225 (1930).

(9) L. Kubicar, *Fyz. Cas.*, **18**, 58 (1968).

(10) W. Klement and A. Jayaraman, *Progr. Solid State Chem.*, **3**, 289 (1966).

A Macroscopic Description for the λ Transition in Sodium Nitrate

by W. Klement, Jr.[1]

School of Engineering and Applied Science, University of California, Los Angeles, California 90024
(Received September 23, 1969)

For extensive intervals of temperature about the λ transition temperature T_λ of sodium nitrate, the thermal expansion $1/V(\partial V/\partial T)_p \approx B|T - T_\lambda|^{-1/3}$ and the specific heat $c_p/T \approx C + D|T - T_\lambda|^{-1/3}$ where, among the constants, B and D are ~2.3 times greater below T_λ than above. These representations are consistent with the experimental results for dT_λ/dp *via* a Pippard relation. Comparison of existing adiabatic elastic moduli allows estimates at various temperatures of the compliances $|s_{13}|$ and $|s_{14}|$, which have neither been measured nor previously estimated. If the order parameter for the transition is approximately identified with the relative volume (which varies as $|T_\lambda - T|^{2/3}$), the present results are unified in a scaling law approach.

The λ transition in crystalline sodium nitrate was one of the first λ transitions discovered[2] in solids and has since been the object of many experiments. There is inadequate agreement as to the microscopic features[3] of the transition, which appears to involve positional and rotational disorder of the NO_3^- ions, and this uncertainty may be the main reason why a comprehensive theoretical analysis is lacking. There is also some disagreement where several sets of measurements exist (*e.g.*, thermal expansion[2,4,5]) and it is likely that the experimental difficulties have not been clearly delineated, especially in the region of rapid variation near the transition temperature T_λ. A recent discussion[6] of the thermodynamics attempted to overlook the differences among T_λ apparent in the various experiments. The present approach is to admit that these differences among T_λ exist but to seek simple yet accurate analytical representations for the temperature variation of the various quantities relative to T_λ, *i.e.*, as functions of $|T - T_\lambda|$, and then to attempt the correlations. This approach, with its minimal assumptions about the microscopic aspects, has led to concise and relatively accurate descriptions for the λ transitions in such complex and diverse substances as quartz[7-9] and liquid sulfur,[10] for which thorough microscopic understanding is also lacking.

The immediate impetus for the present discussion was the publication[11] of some elastic moduli data measured on high-purity crystals over an extensive temperature range, especially very close to T_λ. The fact that these results[11] could be simply and accurately represented then led to the analysis of the other pertinent data, which do not appear to be so nearly definitive.

The Craft–Slutsky data[11] for the adiabatic elastic stiffnesses c_{33} and c_{44} are shown in Figure 1, plotted as inverse stiffness *vs.* $|T - T_\lambda|^{1/3}$ with $T_\lambda = 276.6°$ which is within experimental precision of the cited[11] 276.7°. The inverse stiffnesses are plotted not only for convenience in estimating (below) the adiabatic elastic compliances s_{13} and s_{14} but also because linear relations are obtained over more extensive temperature intervals than if the c_{ij} were plotted directly against the chosen abscissa. The suitability of the function $|T - T_\lambda|^{1/3}$ to "linearize" the temperature variation here is the first clue in the analysis.

The next item is the careful estimate[12] of the fraction of "disordered" NO_3^- ions at various temperatures below T_λ. Sato, *et al.*,[12] fitted the shapes of certain ir peaks (from single crystals) by superpositions of the peak shapes at $T_\lambda \approx 276°$ and at 26° where, respectively, complete disorder and no disorder were assumed; their estimates[12] for the disordered fraction vary linearly with $(T_\lambda - T)^{2/3}$, as shown in Figure 2. The interpretation for such an interpolation is limited in that the disordered fractions so estimated must be unity and zero at the high- and low-temperature ends, respectively, but there is the suggestion that the transition proceeds over a more extensive temperature interval than is usually considered.

Another extensive set of data, including the interval very near T_λ, is from the dilatometry measurements[2] of Kracek. This technique,[2] which apparently[13] involved

(1) Guggenheim Fellow, on leave at Australian National University, Canberra, A.C.T.

(2) F. C. Kracek, *J. Amer. Chem. Soc.*, **53**, 2609 (1931).

(3) See discussions and citations in ref 12, 18, 20.

(4) G. B. Ravich and B. N. Egorov, *Russ. J. Inorg. Chem.*, **5**, 1257 (1960).

(5) J. B. Austin and R. H. H. Pierce, *J. Amer. Chem. Soc.*, **55**, 661 (1933).

(6) W. Klement, *J. Phys. Chem.*, **72**, 1294 (1968).

(7) W. Klement and L. H. Cohen, *J. Geophys. Res.*, **73**, 2249 (1968).

(8) W. Klement, *ibid.*, **73**, 4711 (1968).

(9) W. Klement, *ibid.*, **74**, 3287 (1969).

(10) W. Klement, to be published.

(11) W. L. Craft and L. J. Slutsky, *J. Chem. Phys.*, **49**, 638 (1968).

(12) Y. Sato, K. Gesi, and Y. Takagi, *J. Phys. Soc. Jap.*, **19**, 449 (1964).

(13) It is stated that there was no difference in the results from both polycrystalline and single crystal material but it is not clear what the state of the material was for the individual runs.

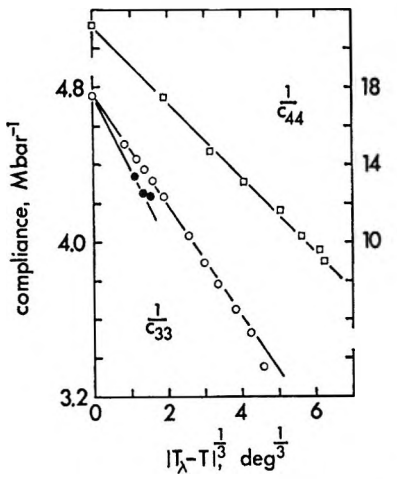

Figure 1. Adiabatic elastic "compliances" $1/c_{33}$ and $1/c_{44}$, from data of Craft and Slutsky, plotted *vs.* $|T_\lambda - T|^{1/3}$ for $T_\lambda = 276.6°$. The $1/c_{44}$ data (squares) are referred to the right-hand ordinate; the $1/c_{33}$ data (circles) to the left-hand ordinate. Open symbols denote data for $T \leq T_\lambda$, filled symbols data for $T > T_\lambda$.

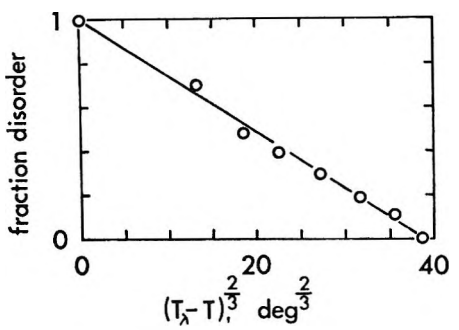

Figure 2. "Disordered" fraction of nitrate ions, from interpolations of Sato, *et al.*, plotted *vs.* $(T_\lambda - T)^{2/3}$ for $T_\lambda \approx 276°$.

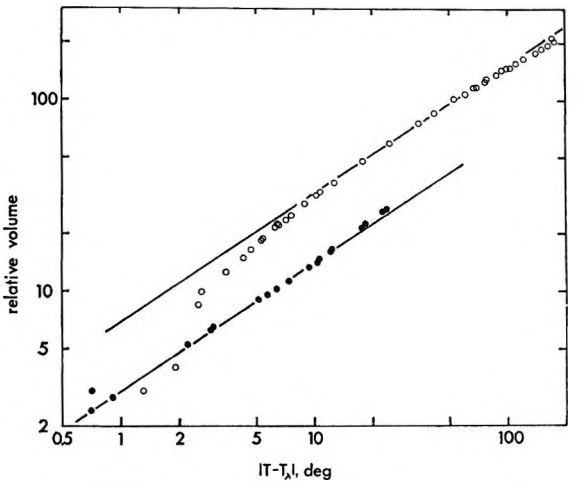

Figure 3. Log–log plot of relative volume $|V_\lambda - V|$, from data of Kracek, *vs.* $|T - T_\lambda|$. Open symbols denote data for $T < T_\lambda$, filled symbols data for $T > T_\lambda$. The ordinate is in relative units of $10^{-4}|V_\lambda - V|$ with $V_\lambda = 1.02600$, as discussed in the text; $T_\lambda = 275.5°$. The drawn lines are of slope $^2/_3$ and correspond to a ratio of A (eq 1) below T_λ to that above of 2.3.

mostly polycrystalline material, probably yields results of high precision but of lesser accuracy since "corrections" (made in an unspecified way) of *ca.* 10% are required; Ravich and Egorov,[4] who obtained somewhat different results for the thermal expansion, have also offered some criticisms of the technique. Presumably because of the long waits for equilibrium, these was no observation[2] of "hysteresis" in the transition—such as occurs for most dynamic experiments. In the log–log plot (Figure 3) of relative volume $|V - V_\lambda|$ *vs.* $|T - T_\lambda|$, there are chosen $T_\lambda = 275.5°$ and V_λ, the volume at T_λ, = 1.02600 (relative to the specific volume at 25° taken[2] as unity), both of which are closely constrained by the extensive data;[2] also the chosen T_λ coincides with that value found in differential thermal analysis (dta) experiments[2] on the same material. To a good approximation (Figure 3) over a decade or so

$$|V - V_\lambda| \approx A|T - T_\lambda|^{2/3} \qquad (1)$$

with deviations very close to T_λ and down to $\approx T_\lambda - 5°$, which of course is where the compressibilities and thermal expansions are quite large and the requisite "corrections" in the technique[2] presumably are most difficult. The ratio of A below T_λ to that above (eq 1) is constrained to the range of 2.0–2.5. Equation 1 infers that the volumetric thermal expansion varies as

$$\frac{1}{V}\left(\frac{\partial V}{\partial T}\right)_p \approx B|T - T_\lambda|^{-1/3} \qquad (2)$$

where the constant B differs accordingly below and above T_λ.

The most recent thermal expansion data,[4] due to Ravich and Egorov, are from experiments with "pure recrystallized" material run at rates of 0.2–6° min^{-1} and reproducible to 0.5°. In the log–log plot of Figure 4, T_λ is chosen as $\approx 272.0°$, which appears to be constrained[4] within $\sim \pm 1°$ and which is in some contrast to the $T_\lambda \sim 275$–$276°$ resulting from their dta studies[4] on the same material. Also shown in Figure 4 are the volumetric thermal expansions calculated from the tabulated linear coefficients from measurements[5] on single crystals. There is a surprising consonance in the two sets[4,5] of data just below T_λ (Figure 4) despite the hysteresis and plastic deformation encountered by Austin and Pierce; T_λ is taken at 277°, as compared to the suggested[5] 278°, for the Austin–Pierce data. The thermal expansions above T_λ, which are far from definitive, are compatible with eq 2, with the ratio of B below T_λ to that above constrained to the range of 1.9–2.4.

The temperature variation of the specific heat may be anticipated since, near T_λ, the Pippard relations are expected to apply. For the several cases in which adequate data have been available for testing, no exceptions have been found for these relations, which are

$$\frac{c_p}{TV}\left(\frac{dT_\lambda}{dp}\right) - \frac{1}{V}\left(\frac{\partial V}{\partial T}\right)_p \approx \text{constant} \qquad (3)$$

and

$$\frac{1}{V}\left(\frac{\partial V}{\partial T}\right)_p\left(\frac{dT_\lambda}{dp}\right) + \frac{1}{V}\left(\frac{\partial V}{\partial p}\right)_T \approx \text{constant} \qquad (4)$$

as $T \rightarrow T_\lambda$. There are no direct determinations for the isothermal compressibility, $-1/V(\partial V/\partial p)_T$, *vs.* temperature so eq 4 cannot be tested. On the other hand, eq 3 suggests (eq 2) that

$$\frac{c_p}{TV} \text{ or } \frac{c_p}{T} \approx C + D|T - T_\lambda|^{-1/3} \qquad (5)$$

where, among the constants, C is the same but D differs below and above T_λ.

Four sets[14-17] of specific heat measurements, near T_λ, are available for polycrystalline material. Mustajoki's measurements[14] are the most extensive and clearly show considerable hysteresis for the samples of 99.9% purity. The most recent work[17] of Reinsborough and Wetmore essentially corroborates the results[16] of Sokolov and Shmidt and hence is not considered further. The data[14-16] are plotted in Figure 5 *vs.* $|T - T_\lambda|^{-1/3}$ to within $\approx T \pm 1.5°$, beyond which there is considerable scatter, some of which may be due to the uncertainty in locating T_λ. For these plots, the transition temperatures have been chosen as 272.0° (Sokolov and Shmidt[16]), 278.0° (Miekk-oja[15] on heating) and 278.0 and 270.0° (Mustajoki,[14] on heating and on cooling, respectively). Linear fits of the data (Figure 5) seem plausible enough up to the melting point and down to ~150° ($(T_\lambda - T)^{-1/3} \approx 0.2$) with $C \approx$ 0.15–0.18 J deg^{-2} fw^{-1} and the ratio of D below T_λ to that above in the range of 2.3–2.6 (eq 5). It is well recognized that crystal imperfections, impurities, etc. tend to broaden and smear out the specific heat cusp for most λ transitions, although the problem is not well understood quantitatively. Kubicar[18] has presented specific heat measurements on a single crystal, which indeed show a sharper cusp near T_λ; unfortunately Kubicar's data[18] are systematically greater than the other, reasonably concordant measurements[14-17] and this is probably to be attributed to the difficulties in calibration for the pulse technique.[18]

By considering the numerical coefficients A, B, and D of the representations of eq 1, 2, and 5 as obtained from the preferred fits to the data of Figures 3, 4, and 5, estimates for dT_λ/dp may be made *via* eq 3. The slopes so estimated range from 7.0 to 8.1° kbar^{-1}, the lower limit coming from the volume data (A and eq 1) and the upper limit from the thermal expansion data (B and eq 2). Because of the uncertainties (discussed above) in the data[2] leading to the estimate for A, the upper limit for the slope is considered to be the superior value; there is good accord with the direct determination[19] for dT_λ/dp.

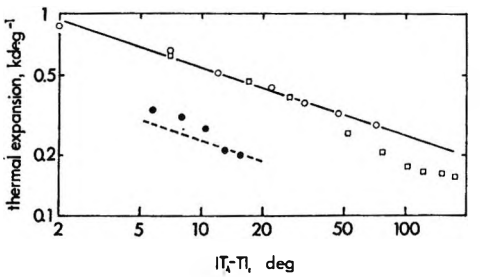

Figure 4. Log–log plot *vs.* $|T_\lambda - T|$ of volumetric thermal expansion coefficients, $1/V(\partial V/\partial T)_p$ from data of Ravich and Egorov (circles) and of Austin and Pierce (squares). Open symbols denote data for $T < T_\lambda$, filled symbols for $T > T_\lambda$; the respective T_λ are discussed in the text. The drawn lines are of slope $-1/3$ and correspond to a ratio of B (eq 2) below T_λ to that above of 2.3.

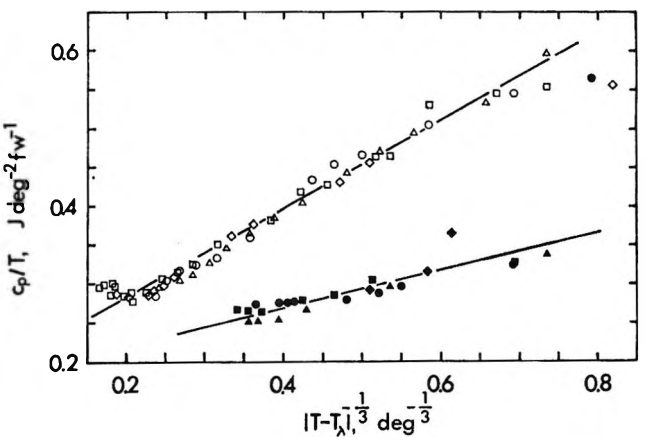

Figure 5. Plot of c_p/T data *vs.* $|T - T_\lambda|^{-1/3}$. Circles denote data of Sokolov and Shmidt, triangles data of Miekk-oja on heating and squares and diamonds heating and cooling data, respectively, of Mustajoki; the respective T_λ are discussed in the text. Open symbols denote data for $T < T_\lambda$, filled symbols data for $T > T_\lambda$. The drawn lines correspond (eq 5) to an intercept $C \approx 0.170$ J deg^{-2} fw^{-1} and to a ratio of D below T_λ to that above of 2.3.

Without getting involved in the controversies over the microscopic aspects of the transition, a representation may be suggested for the data of Andrew, *et al.*, on the temperature variation of the electric quadrupole coupling constant of ^{23}Na nuclei. Andrew, *et al.*,[20] observed the rapid variation with temperature, such as is characteristic of the various thermodynamic quan-

(14) A. Mustajoki, *Ann. Acad. Sci. Fenn., Ser. A6*, 5 (1957).

(15) H. Miekk-oja, *ibid., Ser. A1*, 7 (1941); as cited in ref 14.

(16) V. A. Sokolov and N. E. Shmidt, *Izv. Sektora Fiz.-Khim. Anal. Inst. Obshch. Neorg. Khim. Akad. Nauk SSSR*, 26, 123 (1955), as cited in ref 4.

(17) V. C. Reinsborough and F. E. W. Wetmore, *Aust. J. Chem.*, 20, 1 (1967).

(18) L. Kubicar, *Fyz. Cas.*, 18, 58 (1968).

(19) W. Klement, *J. Phys. Chem.*, 74, 2751 (1970).

(20) E. R. Andrew, R. G. Eades, J. W. Hennel, and D. G. Hughes, *Proc. Phys. Soc.*, 79, 954 (1962); R. G. Eades, J. W. Hennel, and E. R. Andrew, *ibid.*, 71, 1019 (1958).

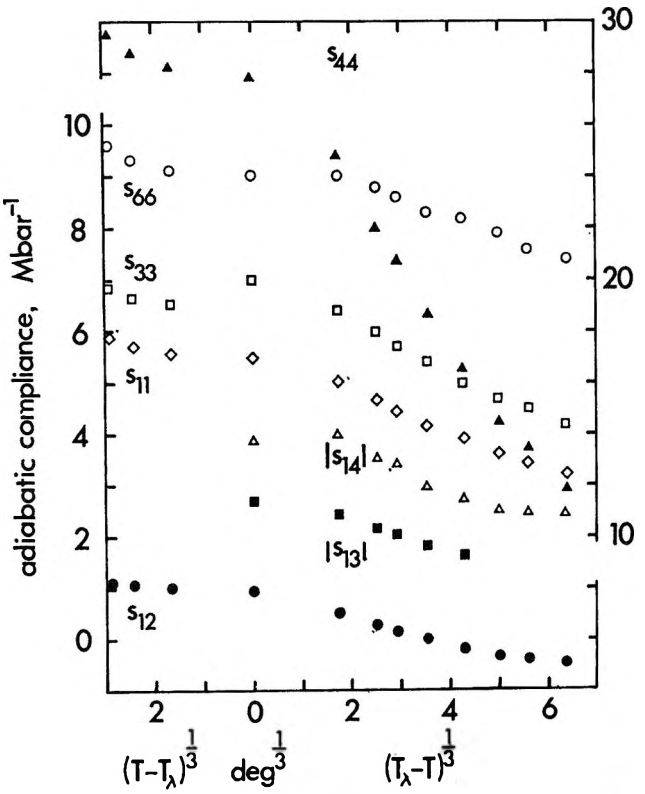

Figure 6. Plot of adiabatic compliance moduli *vs.* $(T - T_\lambda)^{1/3}$ for $T > T_\lambda$ and *vs.* $(T_\lambda - T)^{1/3}$ for $T \leq T_\lambda$; $T_\lambda \approx 275.5°$. Estimates for $|s_{14}|$ (open triangles) and $|s_{13}|$ (filled squares) discussed in the text; all other moduli are from data of Kornfel'd and Chubinov. The right-hand ordinate corresponds to the s_{44} data (filled triangles) only, whereas the left-hand ordinate corresponds to the data for s_{66} (open cicles), s_{33} (open squares), s_{11} (open diamonds), s_{12} (filled circles) as well as $|s_{14}|$ and $|s_{13}|$.

tities discussed above, but could not conclusively define the microscopic mechanism despite extensive calculations. It may be verified, however, that their data[20] for the coupling constant vary linearly with $(T_\lambda - T)^{1/3}$ from just below T_λ down to room temperature.

Returning to the adiabatic elastic moduli, it is necessary that Craft and Slutsky's recent contribution[11] be considered more carefully with respect to the earlier results of Kornfel'd and Chubinov for the adiabatic elastic compliances s_{11}, s_{33}, s_{44}, and s_{12} over the interval 20–300°. Craft and Slutsky[11] claim a discrepancy between their c_{44} and the comparable stiffness they calculated from the Kornfel'd–Chubinov data,[21] which can be verified to be merely $1/s_{44}$. This is erroneous, since, for the crystal symmetry involved, the correct interrelation[22] is

$$\frac{1}{c_{44}} = s_{44} - \frac{s_{14}^2}{s_{66}} \tag{6}$$

Thus, at this stage, there is no evidence for any inconsistency between these two sets of measurements; in fact, if both sets are tentatively accepted, estimates may be made at various temperatures for the adiabatic elastic compliances s_{13} and s_{14}, which have not yet been measured. The procedure is to obtain $1/c_{44}$ and $1/c_{33}$ by interpolation (Figure 1) for those $|T - T_\lambda|$ corresponding to the temperatures at which the Kornfel'd–Chubinov compliances ($T_\lambda \approx 275.5°$) are tabulated and then to calculate $|s_{14}|$ from eq 6 and $|s_{13}|$ from the relation[23]

$$s_{13}^2 = s_{66}\left(s_{33} - \frac{1}{c_{33}}\right) \tag{7}$$

The $|s_{14}|$ and $|s_{13}|$ so estimated are shown in Figure 6 for the $|T - T_\lambda|$ where the two sets of data overlap. It is likely that $s_{13} < 0$ since then the Poisson ratios s_{13}/s_{11} and $-s_{13}/s_{33}$ would be positive (as is usual) but nothing definite can be concluded here for the signs of s_{13} and s_{14}. The adiabatic elastic compliances[21] are plotted *vs.* $|T - T_\lambda|^{1/3}$ in Figure 6 to show that approximately linear relations are obtained over extensive temperature intervals below T_λ. Estimates for the adiabatic compressibility (assuming $s_{13} < 0$) at the various $|T - T_\lambda|$ indicate the same sort of temperature dependence, with about the same sort of scatter as the individual moduli (Figure 6), due perhaps to inadequacies in the Kornfel'd–Chubinov data.[21] One of Garland's relations[6,23] postulates a simple dependence of the individual adiabatic compliances and c_p/T but it is not worthwhile to further[6] pursue that suggestion here since the existing specific heat data disagree enough among each other to make such a correlation fragile. Thus, with only these incomplete data for the elastic moduli, the relative variations with temperature above and below T_λ cannot be delineated any further. However, it was discovered[9] for quartz that the shear compliances s_{44} and $s_{66} = 2(s_{11} - s_{12})$ plotted against each other for various temperatures yielded straight lines above and below the transition temperature. Such also seems to be the case for the less extensive sodium nitrate data,[21] with s_{44} increasing ~4 times as much with s_{66} below T_λ as above.

In the foregoing, the temperature variation of many quantities was well expressed by simple functions of the form $|T - T_\lambda|^i$, where the exponents (or indices) i differed for the various parameters. Since considerable current work[24] is devoted to elucidation of relations among these indices—mostly with transitions much more experimentally and theoretically accessible than the one in sodium nitrate, an attempt may be made to put the present results in the appropriate context of these "scaling laws" (following the procedures and nomenclature of Kadanoff, *et al.*[24]). First, it is neces-

(21) M. I. Kornfel'd and A. A. Chubinov, *Sov. Phys.-JETP*, 6, 26 (1958).

(22) W. G. Cady, "Piezoelectricity," Dover, New York, N. Y., 1964.

(23) C. W. Garland, *J. Chem. Phys.*, 41, 1005 (1964).

(24) L. P. Kadanoff, W. Götze, D. Hamblen, R. Hecht, E. A. S. Lewis, V. V. Palciauskas, M. Rayl, J. Swift, D. Aspnes, and J. Kane, *Rev. Mod. Phys.*, 39, 395 (1967).

sary to choose an "order parameter"; as with the description[8] for the quartz inversion, it is convenient to take $|V_\lambda - V|$ as the approximate order parameter, which then yields the index $\beta \approx {}^2/_3$ (eq 1) and which is microscopically plausible in view of the results[12] of Sato, *et al.* (Figure 2). The temperature variation of the specific heat below and above T_λ (Figure 5; eq 5) yields the indices $-\alpha$ and $-\alpha'$, respectively, $\approx -{}^1/_3$. Requisite knowledge for the isothermal compressibility is lacking; however, since

$$-\frac{1}{V}\left(\frac{\partial V}{\partial p}\right)_T = -\frac{1}{V}\left(\frac{\partial V}{\partial p}\right)_S + \left[\frac{1}{V}\left(\frac{\partial V}{\partial T}\right)_p\right]^2\left[\frac{c_p}{TV}\right]^{-1} \quad (8)$$

and the adiabatic compressibility apparently varies only as strongly as $|T - T_\lambda|^{1/3}$, it may be assumed that the second term on the right-hand side of eq 8 dominates[25] near T_λ and that the indices $-\gamma$ and $-\gamma'$ below and above, respectively, $\sim -{}^1/_3$. Thus the conditions[24] that $\alpha = \alpha'$, $\gamma = \gamma'$ and

$$2 - \alpha = \gamma + 2\beta = \beta(\delta + 1) \quad (9)$$

are completely satisfied if $\delta = {}^3/_2$. The definition here for δ is *via* the relation

$$|V_\lambda - V|^\delta = |p - p_\lambda| \quad (10)$$

at the temperature T_λ corresponding to the λ transition pressure p_λ. There are no data for the equation of state for which eq 10 might be examined. Equation 9 and the scaling law approach,[24] with the numerical values for the indices, then yield explicit predictions for the indices (*e.g.*, η, ν,ν'[24]) which describe the behavior due to fluctuations near the transition; there do not appear to be any data presently available to test such predictions.

These macroscopic theories have very little to say concerning the range of temperatures (and pressures) about T_λ over which the correlations and analytical representations are expected to be valid. Empirically, the c_p/T representations (eq 5) appear to be useful from ~150° up to the melting point (Figure 5). The representations for the thermal expansion may be useful over a similar temperature range but this cannot be inferred yet because the best of the data (of Ravich and Egorov[4]) only extend down to 200° (Figure 4). Similarly, a specification of the temperature ranges for the validity of the representations for the other quantities would seem to require a suitable microscopic model. The macroscopic approach also does not offer any insight into the origin of either the approximate factor 2.3, which is required to "symmetrize" the temperature variation of the several thermodynamic quantities about T_λ, or the approximate exponents ${}^1/_3$, ${}^2/_3$, etc., required to "linearize" the variation; better measurements of course can refine these numerical factors.

Nevertheless, for all of these shortcomings, the present approach to the λ transition in sodium nitrate results in a more quantitative and concise description than hitherto, with avenues suggested for estimates of quantities not yet adequately measured. It is perhaps surprising that such simple representations seem to suffice for a physical situation in which there appears to be positional and vibrational disordering, libration, hindered rotation, etc. of the constituent ions of enough complexity to have frustrated a comprehensive interpretation of so many investigations[3] so far.

(25) Equation 4 is thus satisfied also.

A Reinvestigation of the Crystal Structure of the Zeolite Hydrated NaX

by David H. Olson

Mobil Research and Development Corporation, Central Research Division Laboratories, Princeton, New Jersey 08540
(Received December 11, 1969)

The crystal structure of hydrated NaX has been reinvestigated using single crystal X-ray techniques. Although the basic structural features agree with the earlier powder X-ray study of Broussard and Shoemaker, several, more detailed, features of the structure have been found. The probable space group and lattice parameter of the crystal studied are Fd3 and 25.028 Å, respectively. The space group and the two average tetrahedral atom (Si, Al)–oxygen bond distances, 1.619 (4) and 1.729 (4) Å, indicate that the Si and Al atoms are ordered to a considerable extent. The nonframework atom site occupancies and assignments are as follows: site I, 9 Na^+; site I′, 8 Na^+ and 12 H_2O; near site II′, 26 H_2O; site II, 24 Na^+ and 8 H_2O. In addition, seven low occupancy supercage scattering sites due to H_2O and/or Na were found. The occupancy of site II gives direct evidence for the influence of aluminum content on cation siting in hydrated faujasites; *i.e.*, a supercage six-ring of tetrahedra must contain three Al ions before ion siting is energetically favorable. This rule appears to apply to hydrated mono and polyvalent cation faujasites.

Introduction

Hydrated NaX is the parent material for all zeolite X derivatives, *i.e.*, catalysts, drying agents, etc. The crystal structure of this commercially important zeolite was reported nearly a decade ago by Broussard and Shoemaker,[1] and elucidation of its crystal chemistry (primarily ion-exchange properties) has relied heavily upon the results of their powder diffraction study.

The availability of large crystals of hydrated NaX and our preliminary observation of diffraction symmetry lower than that assumed in the early study prompted us to reinvestigate the structure of the material. The lower diffraction symmetry suggested the possibility of obtaining information on the ordering of Si and Al ions; this information was subsequently obtained. The cation distribution found differs in many respects from that found earlier,[1] although many of the differences found can be attributed to the higher accuracy obtained in our study. Evidence for an effect of Al content on the siting of cations in supercage six-rings also was found.

Experimental Section

The NaX single crystal used in this study was grown by Charnell.[2] The crystal, which was a well-formed octahedron 60 μ on an edge, was mounted in an open capillary tube for X-ray examination. The preliminary diffraction photographs exhibited m3 Laue symmetry, and the extinctions were consistent with the space group Fd3. The lattice parameter, a_0 = 25.028 (5) Å, was determined by double-scanning diffractometry[3] on a Siemens goniometer equipped with a General Electric Eulerian Cradle. The intensity data were collected using the moving-crystal, moving-counter technique with nickel-filtered copper radiation. One-minute background counts were taken at each end of a three-degree, three-minute scan. The intensities of the 1014 unique reflections contained in $^1/_3$ octant (120° 2θ cutoff) were measured. The standard deviations of the structure factors were computed as described earlier.[4] Only those structure factors (694) having values greater than twice their standard deviations were used in solving and refining the structure.

The unit cell composition of the zeolite

$$Na_{88}[Al_{88}Si_{104}O_{384}]\cdot 220H_2O$$

was determined from the relation between the lattice parameter and aluminum content.[5] The sodium content represented by this composition agrees with the value found for the parent preparation, *i.e.*, 15.0 wt % on a dry basis.

Determination and Refinement of the Structure

Least-squares[6] and Fourier techniques were combined with trial faujasite framework parameters and estimated cation parameters to solve the structure. The structure factors were computed using scattering factors for Si^{2+}, Al^+, O^-, and Na^+, based upon the HFS ionic scattering factors of Hanson and Pohler.[7] In the last two least-squares cycles, the scattering factors were adjusted in accordance with the assumption that T1 is a pure Si site, and T2 is a site having 0.08 Si plus 0.92 Al. For this compositional assignment, the average T1–O

(1) L. Broussard and D. P. Shoemaker, *J. Amer. Chem. Soc.*, **82**, 1041 (1960).

(2) J. Charnell, Mobil Research and Development Corp., Paulsboro, N. J. 08066, to be published.

(3) H. W. King and L. F. Vassmillet, "Advances in X-Ray Analysis 5," W. M. Mueller, G. R. Mallett, and M. J. Fox, Ed., Plenum Publishing Co., New York, N. Y., 1961, pp 78–79.

(4) D. H. Olson, *J. Phys. Chem.*, **72**, 4366 (1968).

(5) E. Dempsey, G. H. Kuehl, and D. H. Olson, *ibid.*, **73**, 387 (1969).

(6) W. R. Busing, K. O. Martin, and H. A. Levy, "ORFLS," Oak Ridge National Laboratory, Oak Ridge, Tenn., 1962.

(7) H. P. Hanson and R. F. Pohler, *Acta Crystallogr.*, **21**, 435 (1966).

Table I: Observed and Calculated Structure Factors for Hydrated NaX

H	K	FOBS	FCAL
****L = 0*******			
8	0	665	316
****L = 1*******			
12	0	1739	-1832
16	0	3682	3639
20	0	680	-622
24	0	1490	1935
28	0	534	548
6	2	1833	1752
14	2	1716	-1840
22	2	1261	1244
26	2	511	355
4	4	2445	-2493
8	4	3570	3587
16	4	1439	1380
20	4	983	-838
2	6	954	820
6	6	2654	2688
10	6	649	763
14	6	381	-510
18	6	1561	-1627
22	6	1800	-1800
26	6	822	-805
4	8	3350	3409
8	8	4082	3842
12	8	926	536
20	8	3699	3796
24	8	606	-709
6	10	353	546
10	10	4086	-4106
14	10	971	-991
18	10	553	-531
22	10	2534	2550
8	12	1184	1237
12	12	5301	5425
16	12	745	-645
24	12	1188	-1189
2	14	1746	-1810
10	14	1573	-1661
14	14	881	861
18	14	653	-603
4	16	1007	911
8	16	621	-545
12	16	460	-467
16	16	1034	-984
6	18	1727	-1688
14	18	947	-862
4	20	344	-360
8	20	3633	3466
2	22	1074	1018
6	22	2073	-2135
10	22	2692	2610
8	24	896	-830
12	24	1546	-1514
2	26	847	804
6	26	579	-571

H	K	FOBS	FCAL
10	26	276	176
****L = 1*******			
21	11	1508	1500
23	11	1807	-1797
25	11	910	270
5	13	1295	-1263
7	13	511	428
9	13	1263	-1253
11	13	977	810
13	13	475	-474
15	13	508	434
17	13	770	796
19	13	846	-866
23	13	476	-526
3	15	514	438
5	15	438	467
7	15	657	-563
9	15	708	-620
11	15	412	356
15	15	412	-448
19	15	521	628
5	17	594	-689
9	17	421	-565
11	17	683	-701
13	17	626	713
15	17	318	-251
17	17	668	552
21	17	303	321
3	19	680	-572
9	19	347	-419
7	19	746	737
9	19	1347	1374
13	19	732	-620
19	19	328	484
19	19	321	242
3	21	646	-642
5	21	1171	-1324
11	21	1036	-982
9	21	1395	1394
11	21	318	190
15	21	338	422
17	21	338	296
23	21	477	558
5	23	1002	-994
7	23	360	285
13	23	1047	-1861
13	23	296	-353
3	25	784	761
25	25	352	64
9	25	914	938
5	27	429	-300
7	27	466	585
****L = 2*******			
6	2	1393	-992
8	2	2433	2324

H	K	FOBS	FCAL
8	14	343	-230
10	14	552	-449
12	14	1363	1386
14	14	414	416
16	14	1167	1248
18	14	329	-268
20	14	1020	1118
24	14	526	-740
6	16	694	617
8	16	1065	1131
10	16	394	-506
14	16	816	862
16	16	368	450
18	16	575	-521
20	16	360	-208
4	18	437	399
6	18	554	-514
8	18	1133	-1118
12	18	495	368
16	18	342	-344
20	18	543	391
4	20	478	-375
6	20	1619	-1508
8	20	358	105
10	20	1174	-1147
12	20	476	659
14	20	608	673
18	20	522	479
4	22	965	1000
8	22	638	-591
12	22	393	-356
14	22	590	506
6	24	771	816
10	24	509	503
12	24	293	-125
14	24	832	-861
4	26	683	602
6	26	412	378
****L = 3*******			
5	3	3362	-3555
7	3	1997	-1803
11	3	2301	2147
13	3	1117	1170
15	3	1022	-830
19	3	849	827
21	3	1135	1134
23	3	1598	1569
27	3	975	941
7	5	1218	1293
11	5	441	494
13	5	402	203
15	5	1182	1236
17	5	647	591
19	5	1953	-1982
21	5	449	-301

H	K	FOBS	FCAL
25	5	582	614
5	7	659	748
9	7	548	-612
11	7	340	925
13	7	303	989
15	7	592	776
19	7	322	-787
21	7	321	954
23	7	572	-592
27	7	490	-341
7	9	467	-509
9	9	928	867
11	9	2372	-2965
13	9	757	-773
17	9	1393	-2017
21	9	583	-514
23	9	388	323
25	9	268	71
5	11	530	462
7	11	753	805
9	11	2574	-2807
11	11	810	691
15	11	1535	1611
21	11	744	828
25	11	1461	-1377
5	13	336	151
7	13	1149	1090
9	13	592	-499
13	13	395	303
13	13	1652	1645
15	13	581	565
17	13	503	397
21	13	898	915
23	13	379	-342
5	15	1311	1348
7	15	1119	1125
11	15	1326	1381
15	15	1077	982
17	15	910	-817
19	15	606	-736
23	15	605	-515
7	17	409	-400
9	17	2144	-2159
11	17	356	284
13	17	710	613
15	17	705	-722
19	17	324	355
21	17	325	346
5	19	1809	-1844
7	19	961	-853
11	19	331	-375
13	19	916	-859
19	19	441	360
7	21	660	763
9	21	573	-666

H	K	FOBS	FCAL
11	21	1036	1004
13	21	735	705
17	21	274	305
7	23	504	-549
11	23	370	306
13	23	605	-545
15	23	561	-623
21	23	830	856
5	25	390	-339
9	25	563	518
11	25	1306	-1223
7	27	688	-585
****L = 4*******			
4	4	1124	-921
6	4	583	-147
8	4	1544	1539
12	4	1354	1283
14	4	315	248
16	4	683	-263
18	4	601	548
20	4	1327	-1326
22	4	302	-270
8	6	3644	-3703
8	6	601	-589
****L = 5*******			
5	5	7949	-7765
9	5	834	-900
5	5	286	322
13	5	884	-920
15	5	1272	-1159
17	5	1235	1211
21	5	735	-810
23	5	393	-436
25	5	277	-238
27	5	1112	1064
11	7	1184	1345
11	7	1461	-1340
13	7	1164	1219
17	7	2101	2095
19	7	442	454
23	7	774	836
25	7	429	-360
9	9	566	-728
9	9	1507	1636
11	9	587	502
13	9	1361	-1281
19	9	1549	-1552
21	9	551	-612
25	9	1067	1101
7	11	1352	-1215
11	11	2847	-2932
13	11	378	-474
15	11	533	-514
17	11	1700	-1699
21	11	352	-474

H	K	FOBS	FCAL
7	13	939	1015
9	13	1181	-1246
13	13	373	-390
15	13	1326	1358
17	13	405	-333
19	13	572	-634
21	13	377	-328
23	13	290	172
7	15	363	-100
9	15	1216	-1217
13	15	1154	1145
15	15	736	716
17	15	1065	1007
19	15	427	158
21	15	422	347
23	15	318	380
7	17	2135	2152
9	17	344	69
11	17	2057	-2030
13	17	457	-371
15	17	962	936
17	17	1921	-1890
21	17	249	-65
11	19	396	424
13	19	785	-736
15	19	342	516
17	19	771	-780
19	19	552	-628
7	21	381	194
9	21	690	-676
15	21	419	508
21	21	537	594
9	21	418	-148
11	23	537	476
13	23	312	236
15	23	400	323
9	25	905	945
****L = 6*******			
6	6	4003	4450
8	6	530	304
10	6	563	-710
12	6	985	-954
16	6	4580	4676
18	6	421	295
22	6	1217	1180
24	6	423	382
8	8	701	741
10	8	425	351
12	8	954	930
14	8	2525	-2592
16	8	614	385
20	8	466	-342
22	8	578	458
24	8	338	343

H	K	FOBS	FCAL
26	8	1005	1062
8	10	398	219
10	10	1031	-978
12	10	1895	-1876
16	10	542	-578
20	10	692	-639
24	10	693	658
8	12	671	459
10	12	1937	-1994
12	12	1030	1006
14	12	402	422
18	12	804	918
22	12	774	716
8	14	1976	-1953
14	14	2398	2466
16	14	419	-457
20	14	952	1035
10	16	842	-931
12	16	593	-527
16	16	662	667
18	16	1806	-1892
20	16	452	385
22	16	715	673
24	16	427	-320
12	18	970	958
16	18	1793	-1834
20	18	515	-609
8	20	343	-91
10	20	596	-524
14	20	1241	1330
18	20	523	-553
12	22	680	667
16	22	643	548
8	24	367	304
10	24	761	785
8	26	789	802
****L = 7*******			
9	7	1111	1193
11	7	600	-678
13	7	507	-217
17	7	476	-480
19	7	355	265
23	7	413	429
25	7	745	840
9	9	441	513
11	9	1361	1398
15	9	923	1002
17	9	967	896
19	9	423	-360
21	9	303	287
23	9	309	-309
25	9	493	363
9	11	1048	1021
13	11	668	779

H	K	FOBS	FCAL
15	11	1154	-1262
17	11	913	835
11	13	411	290
13	13	314	220
21	13	492	463
9	15	560	629
11	15	1150	-1146
15	15	335	100
15	15	729	-632
19	15	515	600
7	17	1192	1157
11	17	915	829
15	17	385	120
17	17	1532	-1699
19	19	599	-555
19	19	340	394
19	19	816	757
19	19	928	-1012
9	21	401	-145
21	21	493	323
13	21	306	201
9	23	462	-350
13	23	247	285
9	25	561	469
****L = 8*******			
8	8	2233	2290
10	8	428	531
12	8	2497	2940
16	8	2269	2321
18	8	481	433
8	10	287	-127
8	10	631	-545
10	10	1759	1636
14	10	1315	-1409
10	12	342	-401
12	12	794	-799
24	12	282	240
10	12	305	-74
12	12	824	-869
16	12	825	766
24	12	595	575
10	14	1116	-1146
14	14	648	-613
14	14	324	-394
18	14	378	529
18	14	857	858
14	16	661	702
16	16	478	352
16	16	654	339
12	16	442	562
16	16	610	-557
18	16	562	-526
22	16	882	709

H	K	FOBS	FCAL
18	18	543	-673
20	18	469	-391
12	20	354	-464
16	20	580	-484
18	20	259	-211
22	20	797	-732
24	20	729	855
24	24	374	333
****L = 9*******			
9	9	1337	1485
9	11	1157	1269
13	11	1540	-1594
19	11	1189	-1165
21	11	667	-574
23	11	1169	-1192
25	11	634	639
13	13	1050	-1087
15	13	562	578
17	13	617	-295
19	13	344	-257
25	13	725	-698
13	15	634	597
15	15	339	317
17	15	659	606
19	15	512	-532
11	15	336	313
15	15	736	755
15	17	451	409
21	15	415	422
11	17	607	-664
13	17	647	646
15	17	470	360
17	17	497	-577
11	19	472	-442
19	19	699	-624
21	19	346	-242
13	21	484	538
15	21	494	385
11	23	450	-264
****L = 10******			
13	13	1527	-1468
17	13	1061	-1087
19	13	311	373
21	13	624	-654
15	15	277	-187
17	15	607	-495
19	15	283	323
15	17	351	-323
15	19	481	408
****L = 11******			
16	14	1182	-1233
18	14	349	334
18	16	682	727
16	18	481	485
****L = 12******			
16	16	1962	-1914

H	K	FOBS	FCAL
20	16	345	319
12	18	350	33
14	18	419	-114
14	20	996	1024
12	22	1530	-1495
14	22	271	-36
****L = 11******			
11	11	4764	5065
13	11	848	-755
17	11	498	390
19	11	284	-44
21	11	1372	-1445
23	11	1361	-1420
15	13	440	-391
17	13	593	560
19	13	640	654
21	13	342	-96
13	15	360	-287
15	15	518	-403
17	15	760	867
19	15	906	905
21	15	352	-149
15	17	628	573
19	17	261	-335
15	19	819	811
17	19	397	-399
15	21	300	243
****L = 12******			
12	12	2611	-2601
16	12	830	793
18	12	307	194
20	12	315	101
22	12	336	203
14	14	1577	-1497
20	14	294	65
14	16	629	585
18	16	478	-452
****L = 13******			
13	13	1527	-1468
17	13	1061	-1087
19	13	311	373
21	13	624	-654
15	15	277	-187
17	15	607	-495
19	15	283	323
15	17	351	-323
15	19	481	408
****L = 14******			
16	14	1182	-1233
18	14	349	334
18	16	682	727
16	18	481	485
****L = 15******			
16	16	1962	-1914

Five Reflections Not Included In The Refinement

h	k	ℓ	FOBS	FCAL
2	2	0	1951	2722
1	1	1	3596	6237
3	1	1	1297	1389
5	1	1	1072	1254
3	3	1	1951	2361

and T2–O distances obtained, 1.619 (4) and 1.729 (4) Å, respectively, fall within 0.010 Å of Smith and Bailey's curve[8] relating average T–O distances and Al content. Our average T–O distances fit Smith and Bailey's curve exactly for T1 (0.93 Si, 0.07 Al) and T2 (0.15 Si, 0.85

(8) J. V. Smith and S. W. Bailey, *Acta Chrystallogr.*, **16**, 801 (1963).

Table II: Fractional Coordinates[a] and Esd's

Atom	Set	P	No./unit cell	X	Y	Z
T1	g	1.00	96.0	−0.05291 (9)	0.12457 (12)	0.03509 (9)
T2	g	1.00	96.0	−0.05352 (9)	0.03671 (9)	0.12309 (12)
O1	g	1.00	96.0	−0.1099 (3)	0.0002 (3)	0.1054 (3)
O2	g	1.00	96.0	−0.0025 (3)	−0.0041 (3)	0.1445 (3)
O3	g	1.00	96.0	−0.0321 (3)	0.0730 (3)	0.0680 (3)
O4	g	1.00	96.0	−0.0706 (3)	0.0772 (3)	0.1761 (3)
Na1	c	0.56 (4)	9.0 (6)	0.0	0.0	0.0
Na2	e	0.25 (4)[b]	8.0 (13)	0.060 (2)[b]	0.060 (2)[b]	0.060 (2)[b]
Na3A	e	0.38 (4)[b]	12.2 (13)	0.230 (2)[b]	0.230 (2)[b]	0.230 (2)[b]
Na3B	e	0.37 (4)[b]	11.8 (13)	0.238 (2)[b]	0.238 (2)[b]	0.238 (2)[b]
OW1	e	0.36 (5)[b]	11.5 (16)	0.074 (2)[b]	0.074 (2)[b]	0.074 (2)[b]
OW2	g	0.27 (2)	25.9 (19)	0.093 (2)	0.086 (2)	0.176 (2)
OW3	e	0.25 (4)[b]	8.0 (13)	0.245 (2)[b]	0.245 (2)[b]	0.245 (2)[b]
OW4	g	0.13 (1)	12.5 (10)	0.281 (2)[b]	0.298 (2)[b]	0.275 (2)[b]
OW5	g	0.31 (3)	29.8 (29)	0.353 (2)	0.345 (2)	0.186 (2)
OW6	g	0.29 (3)	27.8 (29)	0.239 (2)	0.240 (2)	0.392 (2)
OW7	g	0.18 (2)	17.3 (19)	0.174 (2)	0.204 (2)	0.422 (2)
OW8	g	0.17 (2)	16.3 (19)	0.212 (3)	0.387 (3)	0.288 (3)
OW9	g	0.10 (2)	9.6 (19)	0.312 (4)	0.381 (4)	0.200 (4)
OW10	g	0.14 (2)	13.4 (19)	0.258 (3)	0.412 (3)	0.204 (3)

[a] Fd3 origin at $\bar{3}$. [b] Not refined, error estimated.

Table III: Vibration Tensor Components and Esd's (Å²)

Atom	U_{11}	U_{22}	U_{33}	U_{12}	U_{13}	U_{23}
T1	0.0155 (13)	0.0149 (12)	0.0136 (12)	−0.0027 (12)	0.0019 (10)	−0.0031 (13)
T2	0.0155 (13)	0.0122 (12)	0.0117 (12)	0.0017 (10)	−0.0018 (13)	−0.0032 (13)
O1	0.026 (4)	0.029 (4)	0.029 (4)	−0.006 (3)	0.004 (3)	−0.004 (3)
O2	0.025 (4)	0.024 (4)	0.018 (4)	0.011 (3)	−0.003 (3)	−0.005 (3)
O3	0.033 (4)	0.023 (4)	0.027 (4)	0.001 (3)	−0.003 (4)	0.002 (3)
O4	0.027 (4)	0.031 (4)	0.022 (4)	−0.004 (3)	−0.002 (3)	0.016 (3)
Na1	0.032 (6)	0.032 (6)	0.032 (6)	0.018 (4)	0.018 (4)	0.018 (4)
Na2	0.019 (8)[a,b]					
Na3A	0.019 (8)[a,b]					
Na3B	0.019 (8)[a,b]					
OW1	0.023 (10)[a,b]					
OW2	0.063 (13)[a]					
OW3	0.033 (10)[a,b]					
OW4	0.036 (14)[a]					
OW5	0.136 (17)[a]					
OW6	0.136 (16)[a]					
OW7	0.059 (14)[a]					
OW8	0.107 (20)[a]					
OW9	0.073 (26)[a]					
OW10	0.092 (20)[a]					

[a] Isotropic U. [b] Not refined, error estimated.

Al), suggesting some mixing of Al in the T1 site. However, we are inclined to believe that this indication of mixing of Al in the T1 site is a consequence of crystal imperfections rather than actual substitutional disorder (Si and Al ion mixing) in both sites. Earlier single crystal studies[9] of synthetic zeolite X crystals revealed m3m rather than the m3 diffraction symmetry found here for hydrated NaX. Other cationic forms prepared from the NaX of this study also show m3 symmetry, which clearly indicates that the lower symmetry is a result of Si and Al ordering and is not peculiar to the hydrated sodium form. The external morphological features of the crystals used in the earlier studies were less perfect than those of the NaX crystal examined here. It is conceivable that lattice imperfections give rise to volume elements with Si and Al ordered in the opposite

(9) Referred to in D. H. Olson, *J. Phys. Chem.*, **72**, 1400 (1968).

sense with respect to adjacent volume elements, to produce apparent substitutional disorder in the T1 site, and even m3m diffraction symmetry.

Difference maps revealed seven scattering sites in the supercage, which result from partial occupancy by Na^+ ions and water molecules. The occupancy factors of these sites were refined using oxygen scattering factors. The maps also showed that the scattering matter in sites I′ and II probably results from two and three slightly displaced species, respectively.[10] The positional and occupancy parameters for these species were adjusted by examination of a series of difference maps. On the basis of interatomic distances, the scattering matter in site I′ was assigned to Na^+ ion and water oxygen. For site II, it was assigned to two Na^+ ions and a water oxygen, again on the basis of interatomic distances. Having two Na^+ ion positions in the II site is consistent with the low occupancy for the water molecule coordinated to these ions: *i.e.*, only about one-half of the Na^+ ions are coordinated to supercage water (W4), and these form weaker (and longer) bonds to the framework oxygens (O2's)[11] than do the Na^+ ions not coordinated to water.

Because of the strong interaction between population parameters and temperature factors, these were refined in alternate least-squares cycles. All of the weak reflections omitted from the refinement had calculated structure factors within 2.3 standard deviations of their observed values. Five low-order reflections appeared to be affected by extinction and were not included in the refinement. A structure factor listing is given in Table I. The final R value was 0.088.[12] Final positional and thermal parameters are given in Tables II and III. Interatomic distances and angles were computed using ORFFE[13] and are given in Tables IV, V, and VI.

Table IV: Framework Interatomic Distances (Å) and Angles (deg)[a]

Distances	Tetrahedron 1	Tetrahedron 2
T–O1	1.626 (7)	1.738 (7)
T–O2	1.622 (7)	1.719 (7)
T–O3	1.616 (7)	1.737 (8)
T–O4	1.612 (7)	1.723 (7)
	Av 1.619 (4)[b]	Av 1.729 (4)[b]
O1–O2	2.681 (10)	2.862 (10)
O1–O3	2.672 (10)	2.828 (10)
O1–O4	2.585 (10)	2.794 (10)
O2–O3	2.608 (10)	2.817 (10)
O2–O4	2.634 (10)	2.768 (10)
O3–O4	2.681 (10)	2.875 (10)
	Av 2.643 (4)[b]	Av 2.824 (4)[b]
T1–T2 (across O1)	3.078 (3)	
T1–T2 (across O2)	3.154 (3)	
T1–T2 (across O3)	3.112 (4)	
T1–T2 (across O4)	3.196 (4)	
	Av 3.135 (2)[b]	

Angles	Tetrahedron 1	Tetrahedron 2
O1–T–O2	111.3 (4)	111.7 (4)
O1–T–O3	111.0 (4)	108.9 (4)
O1–T–O4	105.9 (4)	107.6 (4)
O2–T–O3	107.3 (4)	109.2 (3)
O2–T–O4	109.1 (4)	107.1 (4)
O3–T–O4	112.3 (4)	112.3 (4)
	Av 109.5 (2)[b]	Av 109.5 (2)[b]
T1–O1–T2	132.4 (4)	
T1–O2–T2	141.5 (5)	
T1–O3–T2	136.3 (4)	
T1–O4–T2	146.8 (5)	
	Av 139.2 (2)[b]	

[a] Estimated standard deviations are in parentheses. [b] Standard deviation computed using $\sigma = 1/n\left[\sum_{i=1}^{n} \sigma_i^2\right]^{1/2}$.

Discussion

The rule forbidding adjacent Al tetrahedra in zeolites requires perfect ordering of Si and Al ions in a Si/Al = 1 zeolite X structure. Arguments favoring retention of the initial ordering scheme in X zeolites with Si:Al ratios up to 1.4 have been presented by Dempsey,[14] and indirect experimental evidence supporting this has been found.[5]

The average T–O distances found for this hydrated NaX crystal indicate that the Si and Al ions are ordered, to a considerable extent. Although the average T1–O distance of 1.619 Å indicates as much as 7% Al in the T1 site, this is believed to be an artifact, produced by crystal imperfections, such as out-of-step ordered domains, rather than evidence for substitutional disorder. The average T–O distances found are taken to indicate that our crystal is near perfect, and that a perfect crystal would yield average T–O distances consistent with a pure Si site (T1) and a site containing both Si and Al ions (T2). This interpretation is consistent with Dempsey's ordered model,[14] although it is certainly not as detailed (his ordered zeolite X model for Si/Al = 1.18 contains 24 unique Si and Al atom sites per unit cell).

(10) Sites I lie at centers of hexagonal prisms. Sites II lie on six-ring faces of sodalite units, on the large cavity side. Sites I′ and II′ lie on the other sides of the respective six-rings of the unprimed sites, within the sodalite cages. With the exception of the I sites, the sites are not defined by unique coordinates.

(11) The framework oxygen atoms are numbered as follows: O1 is the bridging oxygen atom of the double six-membered ring (hexagonal prism), O2 is the oxygen atom that is in both the hexagonal prism six-ring and the supercage six-ring, O3 is the second oxygen atom of the hexagonal prism six-ring, and O4 is the second oxygen atom of the supercage six-ring (a threefold symmetry axis passing through the six-rings generates the remaining four oxygen atoms of each six-ring).

(12) $R = (\Sigma||F_o| - |F_c||)/\Sigma|F_o|$.

(13) W. R. Busing, K. O. Martin, and H. A. Levy, ORFFE, Oak Ridge National Laboratory, Oak Ridge, Tenn., 1964.

(14) E. Dempsey in "Molecular Sieves," Society of Chemical Industry, London, 1968, p 293.

Table V: Interatomic Distances and Angles Involving Nonframework Atoms in and about the Small Pore System

	Distances,[a] Å		
Na1–O3	2.623 (7)	OW2–OW2′[e]	2.53 (8)
Na1–O2	3.618 (6)	OW2–OW2′[f]	2.75 (8)
Na2–O3	2.35 (2)[b]	OW2–OW2′[g]	2.93 (8)
Na2–O2	3.09 (2)[b]	Na3A–O2	2.29 (3)[b]
Na2–OW2	2.51 (7)[b]	Na3A–O4	3.00 (3)[b]
OW1–O3	2.65 (5)[b]	Na3B–O2	2.40 (3)[b]
OW1–O2	3.19 (5)[b]	Na3B–O4	3.06 (3)[b]
OW1–OW2	2.64 (8)[b]	OW3–O2	2.5 (2)[b]
OW2–O2	2.96 (5)	OW3–O4	3.2 (2)
OW2′[c]–O2	3.14 (6)	Na3B–OW4	2.1 (2)[b]
OW2′[d]–O2	3.38 (4)		
	Angles,[a] deg		
O3–Na1–O3′[c]	87.7 (2)	O3–OW1–OW2	99.0 (4)[b]
O3–Na1–O3′[h]	92.3 (2)	O2–OW2–O2′	78.4 (8)
O3–Na2–O3′[c]	101.6 (2)[b]	O2–Na3A–O2′	114.0 (1)[b]
O3–Na2–OW2	98.0 (2)[b]	O2–Na3B–O2′	107.0 (1)[b]
O3–OW1–O3′[c]	87.0 (2)[b]	O2–OW3–O2′	99.0 (2)[b]

[a] Unless noted to the contrary, the value in parentheses is the estimated standard deviation. [b] Some parameters not refined by least squares, error estimated. [c] Related to unprimed by yzx. [d] Related to unprimed by zxy. [e] Related to unprimed by $^1/_4 - x, ^1/_4 - y, z$. [f] Related to unprimed by $z, ^1/_4 - x, ^1/_4 - y$. [g] Related to unprimed by $^1/_4 - y, z, ^1/_4 - x$. [h] Related to unprimed by $\bar{z}\bar{x}y$.

Table VI: Possible Interatomic Distances (Å) Involving Nonframework Atoms in the Supercage[a]

OW4–Na3B	2.1 (2)[b]	OW7–O1′[l]	2.60 (5)
OW4–OW6′[c]	2.7 (2)[b]	OW7–O4′[j]	2.65 (5)
OW4–OW8	2.8 (2)[b]	OW7–OW9′[f]	2.97 (11)
OW4–OW9	2.9 (2)[b]	OW7–OW8′[f]	2.99 (9)
OW4–OW5	3.1 (2)[b]	OW7–OW10′[m]	3.15 (10)
OW4–OW8′[c]	3.1 (2)[b]	OW7–OW7′[k]	3.14 (6)
OW5–OW7′	2.19 (7)	OW8–OW9′[n]	2.40 (13)
OW5–OW7′[d]	2.84 (7)	OW8–OW10	2.49 (10)
OW5–OW10	2.94 (9)	OW8–OW10′[o]	2.39 (10)
OW5–OW8′[e]	3.00 (9)	OW8–O1′[a]	2.91 (7)
OW5–OW6′[f]	3.13 (8)	OW8–OW10′[n]	2.93 (10)
OW5–O1′[g]	3.14 (5)	OW8–OW9′[f]	2.99 (13)
OW6–OW7	2.01 (8)	OW9–O1′[p]	2.82 (10)
OW6–OW7′[h]	2.35 (8)	OW9–OW9′[q]	3.14 (19)
OW6–OW10′[i]	2.50 (9)	OW10–O1′[p]	2.75 (8)
OW6–O4′[j]	2.93 (5)	OW10–OW10′[r]	2.85 (15)
OW6–OW7′[k]	3.12 (8)	OW10–O4′[s]	3.14 (8)

[a] Because all of these nonframework species have fractional occupancy factors (0.10–0.31) the distances listed represent possible, not definite, interactions in the range 2.00–3.20 Å. Unless otherwise stated, the value in parentheses is the estimated standard deviation. [b] Some parameters not refined by least squares, error estimated. The following are transformations applied to the unprimed atom. [c] yzx. [d] $^1/_2 - x, ^1/_4 + y, -^1/_4 + z$. [e] $^3/_4 - y, ^3/_4 - z, x$. [f] zxy. [g] $^1/_4 - x, ^1/_4 - y, z$. [h] $^1/_2 - y, -^1/_4 + z, ^1/_4 + x$. [i] $^1/_2 - x, -^1/_2 + y, ^1/_4 + z$. [j] $^1/_4 - y, z, ^1/_4 - x$. [k] $-^1/_4 + z, ^1/_2 - x, ^1/_4 + y$. [l] $\bar{x}, ^1/_4 + y, ^1/_4 + z$. [m] $-^1/_4 + y, ^1/_2 - z, ^1/_4 + x$. [n] $z, ^3/_4 - x, ^3/_4 - y$. [o] $-^1/_4 + y, ^1/_4 + z, ^1/_2 - x$. [p] $^1/_4 + y, ^1/_4 + z, \bar{x}$. [q] $^3/_4 - x, ^3/_4 - y, z$. [r] $^1/_2 - z, ^1/_4 + x, -^1/_4 + y$. [s] $z, ^1/_4 - x, ^1/_4 - y$.

Table VII: Nonframework Atom Distribution in Hydrated NaX

Site	B and S	This study
I	$16Na^+$	$9Na^+$ (Na1)
I′	O	$8Na^+ + 12H_2O$ (Na2 + OW1)
II′	O	$26H_2O$ (OW2)
II	$32Na'$	$24Na^+ + 8H_2O$ (Na3 + OW3)
Additional supercage sites	None located	$127H_2O$ (and Na) (OW4–1O)

The nonframework atom distribution found in this study is strikingly different from that reported by Broussard and Shoemaker (B and S,[1]) (see Table VII); our results are in better agreement with the general comments made by Baur[15] following reevaluation of Broussard and Shoemaker's data. Baur found that a model with partial occupancies of Na^+ ion in I, I′, and II, and oxygen (water molecule) in II′, gave a better fit than the B and S model.

We find that the Na^+ ions in the small pore system are distributed between sites I and I′, with site occupancies of 9 and 8 Na^+ ions per unit cell, respectively. The total number of Na^+ ions in those two sites, 17.0 (14), is within experimental error of 16, the number normally assumed to be within the small pore system of synthetic X and Y zeolites. This value agrees with Sherry's ion-exchange work, which clearly indicates that there are 16 equivalents of Na^+ ion per unit cell in the small pore system of both X and Y zeolites.[16–18]

Consideration of the sites I and I′ occupancies given in Table VII suggests the following idealized occupancies: 8 Na^+ ions in both I and I′ sites and 8 water molecules also in I′ sites. These values are within three standard deviations of the values of Table VII, and only the differences in the values for the water approach this limit. The reasoning behind these idealized occupancies is based upon the following assumptions.

(a) The chemical composition and center of symmetry requirement leads to the conclusion that in each unit cell there are 12 hexagonal prisms with six aluminum ions (Al_6 prisms), and four prisms with four aluminum ions (Al_4 prisms). Only Al_6 prisms will have Na^+ ions in their I or I′ sites.

(b) Although the energy differences may be small, the Na^+ ion prefers site I′ to site I because of the more favorable coordination to oxygens (see Table V).

(c) Repulsive forces between Na^+ ions limit site I′ occupancy to one per sodalite cage. These three assumptions and the idealized occupancies suggest the

(15) W. H. Baur, *Amer. Mineral.*, **49**, 697 (1964).
(16) H. S. Sherry, *J. Phys. Chem.*, **70**, 1158 (1966).
(17) H. S. Sherry, *ibid.*, **72**, 4086 (1968).
(18) H. S. Sherry, *J. Colloid Interface Sci.*, **28**, 288 (1968).

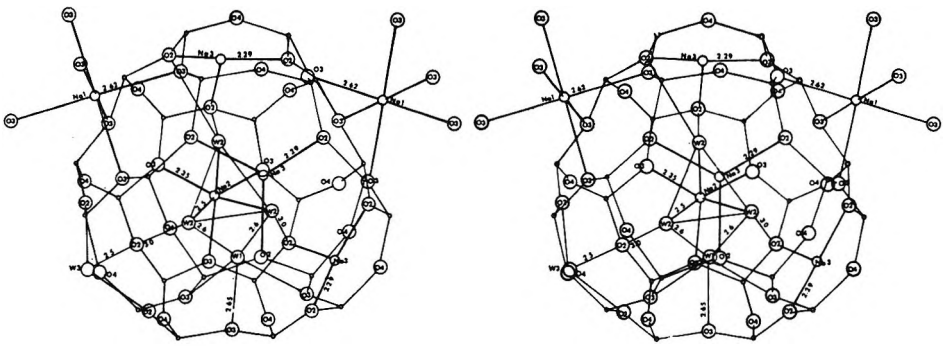

Figure 1. Stereoscopic view of the sodalite cage showing a hypothetical arrangement of nonframework atoms consistent with the observed occupancy factors. The smallest circles are Si and Al sites. Na1's are in I sites, Na2's and W1's are in I′ sites, W2's are near II′ sites and Na3's and W3's are in II sites.

following hypothetical model for the distribution of the Na^+ ions and water molecules about the 16 hexagonal prisms: 8 Al_6 prisms having Na^+ ions in site I, 4 Al_6 prisms having Na^+ ions in both I′ sites, and the 4 Al_4 prisms having water molecules in both I′ sites.

A sodium ion in the I site is octahedrally coordinated by six O3 oxygen ions at a distance of 2.62 Å. Each Na^+ ion in site I′ is coordinated to three framework oxygens (D(Na2–O3) = 2.35 Å) and three water oxygens located near the II′ sites (D(Na2–OW2) = 2.5 Å) (see Figure 1 and the data of Table V). The water molecule in site I′ can hydrogen bond to any of the three O3 framework oxygens (D(OW1–O3) = 2.65 Å) and to two of the three water molecules in site II′. The water molecules in this latter site are disordered about the threefold axes and partially occupy 12 equivalent positions of each sodalite cage (although, strictly speaking, they do not occupy II′ sites, for the sake of simplicity these are referred to as site II′ water molecules). In addition to their coordination to the Na^+ ion in site I′, the site II′ water molecules can hydrogen bond to each other (D(OW2–OW2′) = 2.5–2.9), to a framework oxygen (D(OW2–O2) = 2.96 Å), and/or to the water molecule in site I′, as mentioned above. The disordered OW2's have distances of 2.10, 2.33, and 2.64 Å from OW1. Since the first two distances are unreasonably short, the site occupancies must be such that these distances do not actually occur. As can be seen from the hypothetical model of Figure 1, only two OW2's per sodalite cage hydrogen bond to OW1. Clearly the number of Na^+ ions in site I′ determines the number of water molecules in II′. Both overcrowding and limited hydrogen bonding possibilities may be important factors in controlling the number of water molecules in I′.

In the II sites we find, on a unit cell basis, 24 Na^+ ions and 8 water molecules with Na3A–O2, Na3B–O2, and OW3–O2 distances (threefold) of 2.29, 2.40, and 2.5 Å, respectively. The number of Na^+ ions in II sites agrees exactly with the number of site II six-rings that contain three Al ions (assuming there are no six-rings with one or zero Al ions). This is taken as direct evidence for the influence of the aluminum content of a six-ring on the siting of supercage cations and suggests the rule that three Al ions per six-ring (Al_3 six-rings) are required to make partial dehydration and ion siting energetically favorable. Table VIII[19–22] shows the effect of Al content on ion siting in hydrated faujasite-type zeolites. In the zeolites that contain Al_3 six-rings, ion siting occurs, whereas in those with no Al_3 six-rings, there is no supercage ion siting. Furthermore, the rule appears to apply to mono-, di-, and trivalent cation systems. It is also consistent with Sherry's ion-exchange results, which he has interpreted in terms of partial ion siting of cations in the supercages of X zeolites and no corresponding ion siting in Y zeolites.[16–18] It seems probable that the rule will apply to all zeolites that are sufficiently open to provide a choice between

Table VIII: Effect of Al Content on the Siting of Cations in the Six-Rings of Hydrated Faujasites

	Av. no. of Al (6-ring)	No. of Al_3 6-ring (u.c.)[a]	No. of cations in site II (u.c.)[a]	Ref
NaX	2.75	24	24	This work
BaX	2.66	21	22	16
SrX	2.66	21	15	17
LaX	2.66	21	17	18
Faujasite (Ca, Mg, Na)	1.83	0	0	12
Ca faujasite	1.83	0	0	19
Ce faujasite	1.83	0	0	18
La faujasite	1.83	0	0	19

[a] Unit cell.

(19) D. H. Olson, unpublished research.

(20) D. H. Olson and H. S. Sherry, *J. Phys. Chem.*, 72, 4095 (1968).

(21) D. H. Olson, G. T. Kokotailo, and J. F. Charnell, *J. Colloid Interface Sci.*, 28, 305 (1968).

(22) (a) J. V. Smith and J. M. Bennett, Abstract No. LL5, "American Crystallographic Association Meeting," Buffalo, Aug 1968; (b) J. M. Bennett and J. V. Smith, *Mat. Res. Bull.*, 3, 633 (1968).

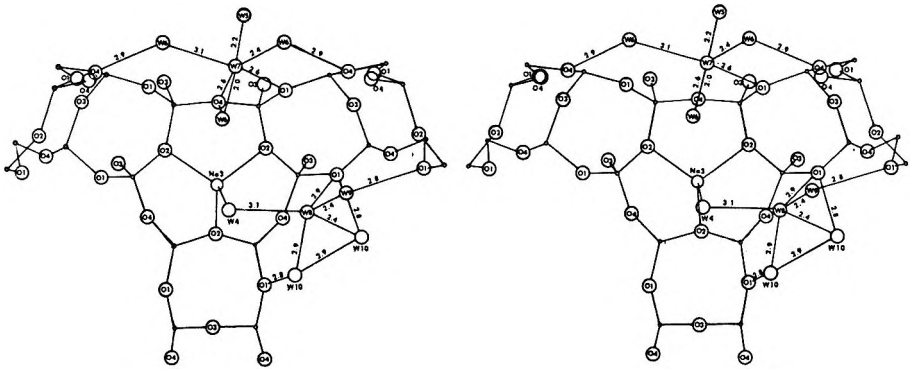

Figure 2. Stereoscopic view of nonframework atoms in the supercage. Possible Na^+ ion sites are labeled W7 and W8. The supercage extends toward the viewer from Na3 which is in site II.

siting of partially dehydrated ions and nonlocalization of fully hydrated cations. Zeolite A is such a structure: in Linde 4A and 5A, where all six-rings have three Al ions, B and S[1] have found that all six-rings contain sited cations. From the above rule, we would predict that in a ZK-4 material (high-silica A-type zeolite) with Si/Al $\geq$ 2, there will be no ion siting in the hydrated zeolite. There are no experimental data to confirm or refute this.

In the case of sodium ions, the equilibrium appears to be overwhelmingly in favor of ion siting in Al_3 six-rings. This implies that for all hydrated sodium faujasites with Si/Al between 1 and 2, the number of Na^+ ions per unit cell not sited in six-rings has the constant value 48, and that for materials with Si/Al greater than 2, this number is simply 16 less than the total Na^+ ion content.

Although seven scattering sites (in addition to the occupied sites II) were found in the supercage, their low occupancy factors, 0.10–0.31, imply that at 25° the water–Na^+ ion mixture is not highly ordered. This is not an unexpected result. Baur points out several experimental results that indicate that the mobility of the cation–water mixture in the supercages of faujasites approaches that in salt solutions.[15] This is consistent with nmr data of Lechert, *et al.*,[23,24] which reveals high mobility of Na ions and H_2O molecules at full water loading. Lechert, *et al.*, find further that the mobility of both species decreases with decreasing water content and that there is a sharp decrease in Na^+ ion mobility at about one-half loading, a point at which the water-to-mobile Na^+ ion ratio drops below four. Although the situation has not been studied exhaustively, no completely satisfactory combination of occupancies of the seven scattering sites was found. Table VI gives the possible interactions of these scattering sites in the interatomic distance range 2.0–3.2 Å. OW4 is 2.1(2) Å from the Na^+ ion in site II, and its occupancy factor implies that, on a time-average basis, about 50% of these Na^+ ions coordinate to supercage water molecules. Equally favorable water structures, that do not involve bonding to Na^+ ions in site II, must also exist.

It should be noted that OW7 has relatively short-range interactions with framework oxygens O1 and O4, 2.60 and 2.65 Å, respectively, and three possible short-range interactions with species OW5 and OW6 (twice). This suggest that OW7 is a partially dehydrated Na^+ ion. Similarly, OW8 has three short-range interactions with species OW9, OW10, and OW10′, suggesting that OW8 may also be an Na^+ ion; however, this is less certain than the assignment of OW7 as an Na^+ ion. The location of these species in the supercage is shown in Figure 2. Species OW5, OW6, OW9, and OW10 are probably water molecules.

Acknowledgments. The many helpful discussions with E. Dempsey and the careful experimental assistance of N. H. Goeke are gratefully acknowledged.

(23) H. Lechert, W. Gunsser, and A. Knappwost, *Ber. Bunsenges. Phys. Chem.*, **72**, 84 (1968).

(24) A. Knappwost, H. Lechert, and W. Gunsser, *Z. Phys. Chem. (Frankfurt am Main)*, **58**, 278 (1968).

Carbon-13 Nuclear Magnetic Resonance Spectra of Some Monosubstituted Thiophenes

by Kensuke Takahashi,

Department of Industrial Chemistry, Nagoya Institute of Technology, Gokiso-cho, Showa-ku, Nagoya, Japan

Tyo Sone,

Department of Applied Chemistry, Yamagata University, Jonan, Yonezawa, Japan

and Kunimi Fujieda

Naka Works, Hitachi, Ltd., Ichige-cho, Katsuta, Ibaraki, Japan *(Received December 10, 1969)*

Carbon-13 resonances for twelve monosubstituted thiophenes have been observed at 15.085 MHz. In 2-substituted thiophenes, the C_4 shifts fall into a narrow range of 5.2 ppm, while the C_5 shifts are spread over a range of 21.1 ppm. This narrow range of shifts is also observed in the C_5 shifts of 3-substituted thiophenes. These results indicate that the C_4 in 2-substituted thiophenes and the C_5 in 3-substituted thiophenes correspond to the *meta* position in substituted benzenes and that one of the principal causes of chemical shifts in these compounds is the resonance effect of the substituents. The coupling constants between carbon-13 and protons through one, two, and three bonds are also reported.

Carbon-13 nmr spectra have been obtained for several aromatic compounds, and the effects of substituents have been discussed.[1-7] In this article we consider the carbon-13nmr spectra of six 2- and six 3-monosubstituted thiophenes.

Experimental Section

Spectral measurements were carried out with a Hitachi R-20A spectrometer, whose center frequency is 15.085 MHz. Most procedures used are similar to those described previously.[8] Chemical shifts were measured by directly counting the resonance frequencies, simultaneously using a proton wide-band decoupler, Hitachi R-208 PWD. The power and band width of this decoupler are easily changed, and the output is applied to the samples by a coil crossed at right angles to both detection and sweep coils. The shifts counted on the decoupled spectra are coincident with those counted on the nondecoupled spectra within the experimental error of less than 0.2 ppm. Sensitivity enhancement is attained by accumulating absorption signals with a 1600-channel signal averaging analyzer, using a spinning 8-mm o.d. sample tube. Chemical shift values are determined by taking the carbonyl resonance of carbon-13 enriched acetic acid as an external reference. These chemical shift values are corrected to the values with carbon disulfide as a reference by adding 15.7 ppm. The samples used in this study were prepared by usual methods and their physical properties coincide with the literature values.

Results and Discussion

(A) Carbon-13 Spectra and Assignment. Typical observed spectra are those of 2-thiophenealdehyde which are shown in Figure 1a, b, c, and d. For convenience, we use the notation C_2, C_3, C_4, and C_5 for the 2-, 3-, 4-, and 5-positioned carbons, and C_x for the carbon adjacent to the substituent. Assignment of signals was done largely on the basis of the observed values of $^1J_{CH}$. As we noted in our previous paper,[9] $^1J_{CH}$ values in the proton spectra are clearly different for the two positions α and β. Therefore, for 2-substituted thiophenes, C_2 and C_5 resonances can be assigned easily, but doubt still remains in the assignment of the C_3 and C_4 resonances. This question can probably be resolved by considering the chemical shift values, kinds of substituents, and other data of long-range coupling constants. A similar difficulty arises for 3-substituted thiophenes. In this case, the assignment of C_2 and C_5 is a little uncertain. As an example, for 2-thiophenealdehyde the chemical shift values of the aromatic carbons were determined to be 49.1, 56.1, 57.9, and 64.4 ppm, measured in the proton decoupled spectrum, as shown in Figure 1a. As is seen from the nonde-

(1) H. Spiesecke and W. G. Schneider, *J. Chem. Phys.*, **35**, 731 (1961).

(2) P. C. Lauterbur, *J. Amer. Chem. Soc.*, **83**, 1838, 1846 (1961).

(3) P. C. Lauterbur, *J. Chem. Phys.*, **38**, 1406, 1415, 1432 (1963).

(4) G. B. Savitsky, *J. Phys. Chem.*, **67**, 2723 (1963).

(5) G. E. Maciel and J. J. Naterstad, *J. Chem. Phys.*, **42**, 2427 (1965).

(6) H. L. Retcofsky and R. A. Friedel, *J. Phys. Chem.*, **71**, 3592 (1967); **72**, 290, 2619 (1968).

(7) T. F. Page, Jr., T. Alger, and D. M. Grant, *J. Amer. Chem. Soc.*, **87**, 5333 (1965).

(8) G. Miyajima, Y. Utsumi, and K. Takahashi, *J. Phys. Chem.*, **73**, 1370 (1969).

(9) K. Takahashi, T. Sone, Y. Matsuki, and G. Hazato, *Bull. Chem. Soc. Jap.*, **38**, 1041 (1965).

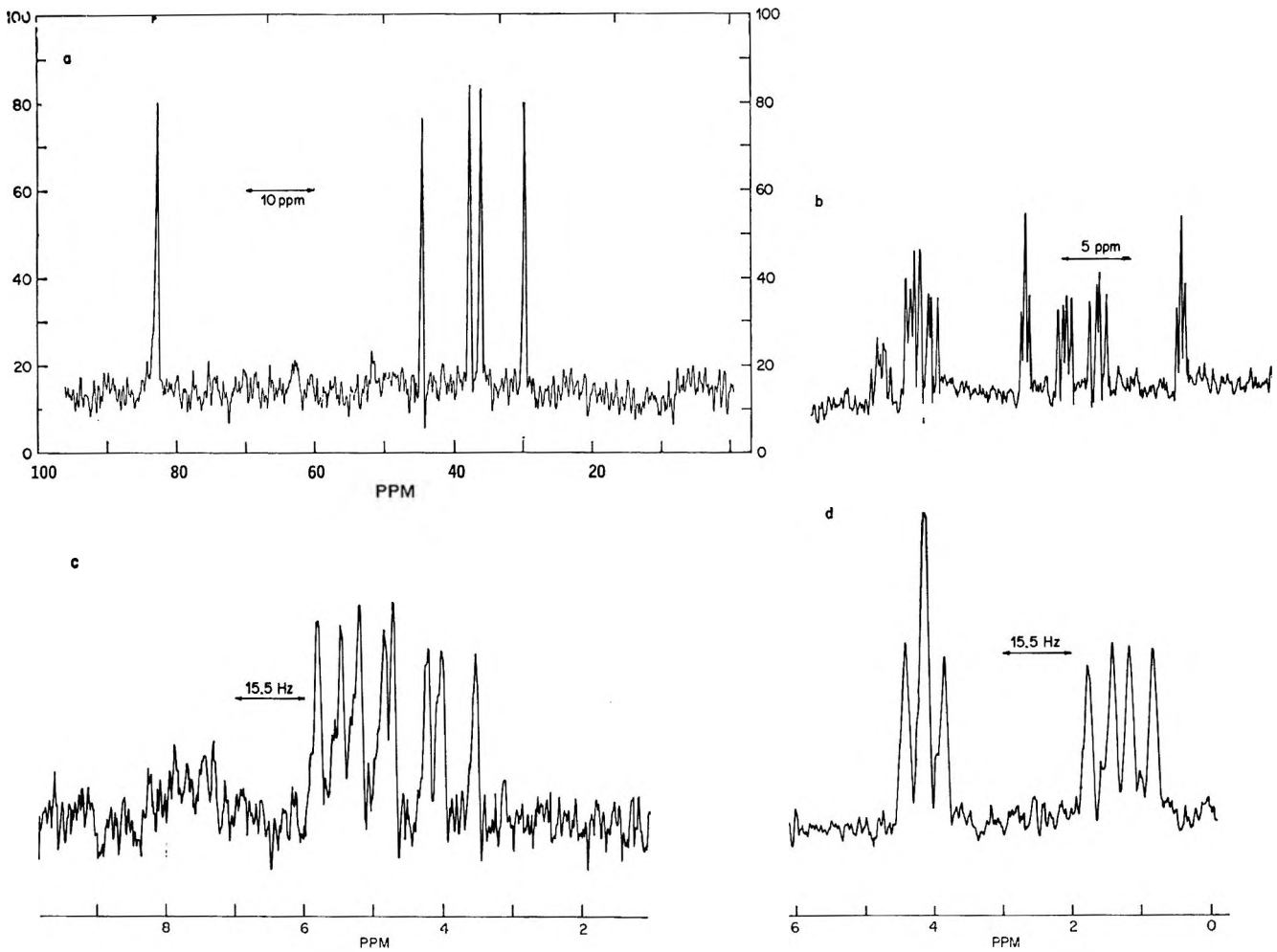

Figure 1. Carbon-13 nmr spectra of 2-thiophenealdehyde; applied frequency increases from right to left at a constant magnetic field: (a) proton-decoubled spectrum of aromatic and carbonyl carbons with a total sweep width of 100 ppm, signal averaged for 16 scans; (b) proton-nondecoupled spectrum of aromatic carbons, signal averaged for 625 scans; (c) expanded spectrum of the higher frequency part of (b), signal averaged for 389 scans; (d) expanded spectrum of the center frequency part of (b), signal averaged for 1024 scans. Sweep time for a single scan is 64 sec in (a) and (b) and 32 sec in (c) and (d).

coupled spectrum in Figure 1b, the signals at 56.1, 57.9, and 64.4 ppm show splittings of 167.5, 187.3, and 172.9 Hz. Consequently, the signal at 57.9 ppm is determined to be that of the C_5. In addition to these large splittings due to $^1J_{CH}$, further small splittings are observed in some expanded spectra, as shown in Figures 1c and d. The fine structures of the signals at 56.1 and 64.4 ppm are recognized as a quartet and a triplet, respectively. The long-range proton-carbon-13 coupling constants are thus determined to be 5.0 and 9.0 Hz for the first of these two signals and 4.5 and 4.5 Hz for the second. These values are to be compared with those observed previously for 2-bromothiophene,[10] 2-methylthiophene, and thiophene.[11] In the present paper, we assume that the long-range coupling constants are mainly determined by the geometrical arrangement of the atoms in these compounds. If the long-range coupling constants and expected substitution effects for the chemical shift values are taken into consideration, the signals at 56.1 and 64.4 ppm may be assigned to those of C_3 and C_4, respectively.

(B) Carbon-13 Chemical Shifts. Carbon-13 chemical shift values are tabulated in Table I. As seen in this table, large chemical shift deviations are observed for the C_x of iodo- and methoxythiophenes. The chemical shift deviation from the unsubstituted compound is usually larger for the C_x atoms of 2-substituted compounds than for those of the corresponding 3-substituted ones, as shown in line II in Figure 2. These shifts are also to be compared with those observed in benzene derivatives.[1,5] The effects of substituents on the chemical shifts of C_x in these three series of compounds are not the same in magnitude but roughly similar in ratio, as shown in lines I, II, and III in Figure

(10) G. Govil, *J. Chem. Soc., A*, 1420 (1967).

(11) F. J. Weigert and J. D. Roberts, *J. Amer. Chem. Soc.*, **90**, 3543 (1968).

Table I: Carbon-13 Chemical Shifts of Monosubstituted Thiophenes in ppm Relative to Carbon Disulfide[a]

Substituent	^{13}C position 2	3	4	5	Others
...	68.1	66.3	66.3	68.1	
2-Br	79.9	62.5	64.8	65.4	
2-I	117.7	54.8	62.8	60.2	
2-CHO	49.1	56.1	64.4	57.9	9.7 (CO)
2-$COOCH_3$	59.3	59.7	65.4	60.6	30.7 (CO)
2-CH_3	53.5	67.8	66.1	69.9	
2-OCH_3	25.8	88.9	68.0	81.1	
3-Br	65.6	82.1	62.4	69.5	
3-I	64.4	113.8	57.3	63.3	
3-CHO	55.4	49.9	67.6	65.2	7.8 (CO)
3-$COOCH_3$	60.6	59.6	65.4	67.1	30.6 (CO)
3-CH_3	72.4	55.7	63.7	67.8	
3-OCH_3	95.8	33.6	73.3	68.0	

[a] Errors are estimated to be ±0.2 ppm.

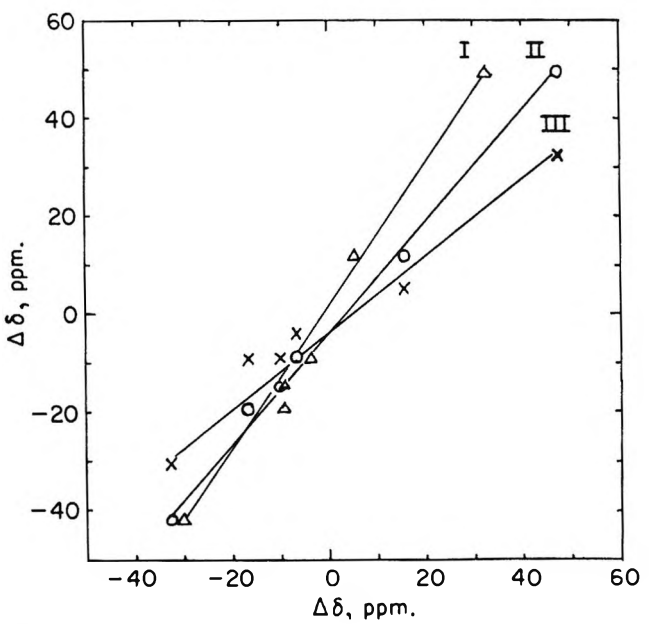

Figure 2. Correlations between changes of chemical shifts of C_x resonances: I, 2-substituted thiophenes (ordinate) *vs.* corresponding benzene derivatives (abscissa): II, 2-substituted thiophenes (ordinate) *vs.* 3-substituted thiophenes (abscissa). III, benzene derivatives *vs.* 3-substituted thiophenes. The Δδ is measured relative to the unsubstituted compound.

2, in which the deviations of the shifts of the C_x for the same substituent become larger in the order benzenes, 3-substituted, and 2-substituted thiophenes. This may be partly due to the mutual interaction between the sulfur atom and the substituents. The shifts of the C_x move from higher to lower field in the order CH_3O, CHO, CH_3, CO_2CH_3, Br, and I for both 2- and 3-substituted thiophenes. The observed range of the chemical shifts due to the positions of the carbons in question becomes narrower in the order C_x, C_3, C_5, and C_4 for 2-substituted thiophenes and in the order C_x, C_2, C_4, and C_5 for 3-substituted thiophenes. The shifts of the C_4 in 2-substituted thiophenes fall into a narrow range of 5.2 ppm, even compared with those of the C_5 (with a range of 21.1 ppm). A similar narrow range of 6.2 ppm is also observed in the shifts of the C_5 in 3-substituted thiophenes. Therefore it was concluded that the shifts of the C_4 in 2-substituted thiophenes and the C_5 in 3-substituted thiophenes are most insensitive to the nature of the substituents (a similar situation was reported some ten years earlier regarding benzene derivatives[1]). This conclusion is in accord with Imoto's observation, based on reactivities of the thiophene derivatives, that both the C_4 in 2-substituted thiophenes and the C_5 in 3-substituted thiophenes correspond to the *meta* position in substituted benzenes.[12] The insensitivity of the chemical shifts of 2- or 3-substituted thiophenes to the substituents at C_4 or C_5, respectively, may be ascribed to the resonance effects of the substituents, as shown below, in which no structure contributes charge delocalization at these positions.

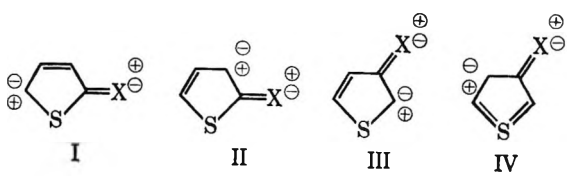

In the above resonance structures, IV has been assumed to have low weight because of the C=S double bond and the appearance of a decuplet around the sulfur, breaking the octet rule.[13] Therefore the shifts of the C_3 and C_5 in 2-substituted thiophenes and those of the C_2 in 3-substituted thiophenes can be presumed to be caused by contributions of the resonance structures I, II, and III. As seen in Figure 3, the shifts of C_3 in 2-substituted thiophenes and those of C_2 in the corresponding 3-substituted thiophenes relative to the unsubstituted compounds are proportional to each other except for iodine, where the former is smaller in magnitude than the latter. Figure 4 shows a rough linearity between the effects of substituents in the shifts of C_3 and C_5 in 2-substituted thiophenes but an absence of such a proportional relation between the shifts of C_4 and C_2 in 3-substituted thiophenes. This behavior may be ascribed to the relative weights of the four resonance structures mentioned above. The correlation of the shifts between the 5-proton and the C_5 in 2-substituted thiophenes is shown by a straight line in Figure 5.[14a] The ratio of the carbon shifts to the proton shifts is about eighteen, as estimated from the slope of the straight line in Figure 5. In some typical aromatic compounds, a unit charge effect on the shift is considered to be about 10 ppm for a proton and 160 ppm for carbon.[14b]

(12) Y. Otsuji, T. Kimura, Y. Sugimoto, E. Imoto, Y. Omori, and T. Okawara, *Nippon Kagaku Zasshi*, **80**, 1021 (1959).

(13) L. Maelander, *Ark. Kemi*, **11**, 397 (1957).

(14) (a) S. Gronowitz and R. A. Hoffman, *ibid.*, **16**, 539 (1960); (b) H. Spiesecke and W. G. Schneider, *Tetrahedron Lett.*, 468 (1961).

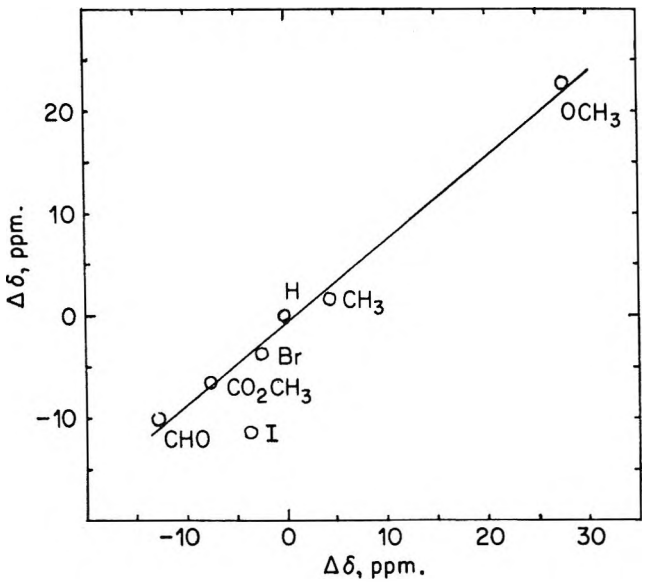

Figure 3. Changes of chemical shifts of C_2 resonances for 3-substituted thiophenes (ordinate) *vs.* those of C_3 resonances for corresponding 2-substituted thiophenes (abscissa).

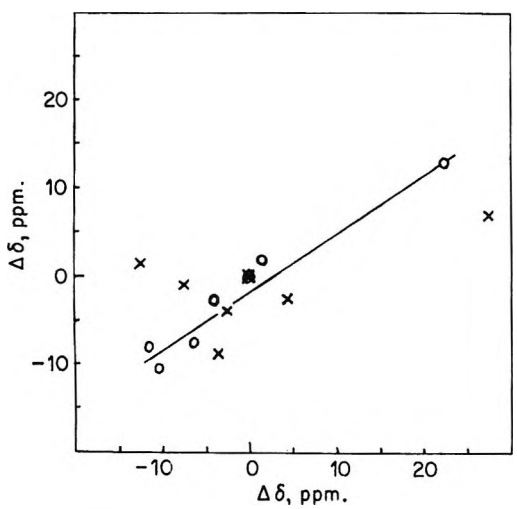

Figure 4. Relation between chemical shift changes of C_5 (ordinate) and C_3 (abscissa) for 2-substituted thiophenes (○), and between shift changes of C_4 (ordinate) and C_2 (abscissa) for 3-substituted thiophenes (×).

Their ratio is about sixteen. This is almost coincident with the slope of the line in Figure 5. Only a rough correlation can be considered to exist between the C_5 shifts and σ_p Hammett constants of substituents but a decisive conclusion should await more data. Work in this area is now in progress.

(C) Coupling Constants between Carbon-13 and Protons. The observed values of $^1J_{CH}$ are shown in Table II. It was shown previously that in bromosubstituted thiophenes $^1J_{CH}$ is larger at the α position than at the β position by about 15 Hz.[9] This seems to hold for all the monosubstituted thiophenes. The observed values of $^1J_{CH}$ at the α position in twelve monosubstituted

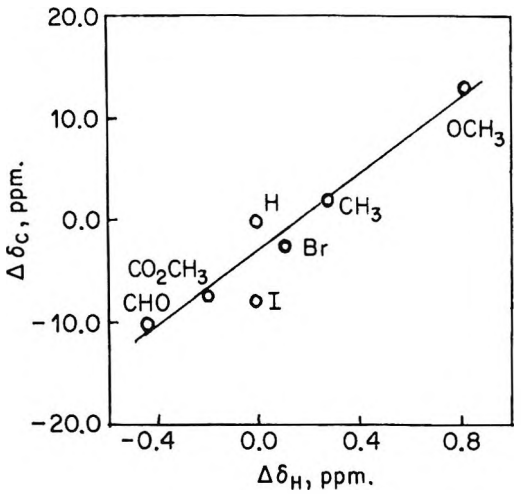

Figure 5. Relation between chemical shift changes of C_5 (ordinate) and H_5 (abscissa)[14a] in 2-substituted thiophenes.

Table II: The Coupling Constants between Carbon-13 and Directly Bonded Protons in Monosubstituted Thiophenes in Hz[a]

Substituent	$^1J_{C_2H_2}$	$^1J_{C_3H_3}$	$^1J_{C_4H_4}$	$^1J_{C_5H_5}$
2-Br	...	171.0	169.6	189.7
2-I	...	171.5	170.0	186.9
2-CHO	...	167.5	172.9	187.3
2-$COOCH_3$	...	171.6	170.8	186.9
2-CH_3	...	161.7	164.6	184.8
2-OCH_3	...	166.5	168.1	189.6
3-Br	188.0	...	175.8	187.5
3-I	183.0	...	171.0	190.0
3-CHO	190.0	...	175.0	190.0
3-$COOCH_3$	188.4	...	172.4	186.9
3-CH_3	182.8	...	166.8	185.9
3-OCH_3	183.5	...	167.2	187.3

[a] Errors are estimated to be ±1.5Hz.

thiophenes fall into a range from 182.8 to 190.0 Hz and those at the β position vary from 161.7 to 175.8 Hz. Therefore they are clearly divided into two ranges. The observed values for thiophene itself also fall into these ranges.[7,15] Some discussion of $^1J_{CH}$ has been given in our previous report.[9] In this study many long-range coupling constants between carbon-13 and protons have been observed and are shown in Table III. Govil has reported values for 2-bromothiophene and his values are larger than ours by about 0.5 ~ 1.0 Hz.[10] This discrepancy is difficult to understand but is possibly due to the experimental procedures taken. The assignments of these long-range coupling constants were made on the assumption that they are similar in magnitude to those of 2-bromothiophene observed by Govil.[10] Therefore the coupling constants observed in the same carbon resonance in each compound are not uniquely assigned; for example, $^2J_{C_3H_4}$ and $^3J_{C_3H_5}$ in 2-substi-

(15) K. Tori and T. Nakagawa, *J. Phys. Chem.*, 68, 3163 (1964).

Table III: The Long-Range Coupling Constants between Carbon-13 and Protons in Monosubstituted Thiophenes in Hz[a]

Substituent	$^2J_{C_2H_4}$	$^3J_{C_5H_5}$	$^3J_{C_4H_3}$	$^2J_{C_4H_5}$	$^3J_{C_5H_3}$	$^2J_{C_5H_4}$
2-Br	6.1	8.5	4.0	4.0	10.1	6.6
2-I	6.1	8.9	3.8	3.8	10.4	6.9
2-$COOCH_3$	5.0	9.0	4.5	4.5	10.5	7.5
2-CHO	5.0	9.0	4.5	4.5	10.5	7.5
2-OCH_3	5.9	7.5	3.1	3.1	10.7	5.6
2-CH_3	5.8[b]	8.2[b]	5.55[b]	3.8[b]	6.8[b]	9.8[b]
Substituent	$^3J_{C_2H_4}$	$^3J_{C_2H_5}$	$^3J_{C_4H_2}$	$^2J_{C_4H_5}$	$^3J_{C_5H_2}$	$^2J_{C_5H_4}$
3-Br	7.3	4.7	7.0	5.7	5.8	5.8
3-I	7.3	5.1	9.0	5.0	6.6	6.6
3-$COOCH_3$	8.3	5.3	8.4	4.7	6.7	6.7
3-CHO	8.2	5.1	8.9	4.5	6.3	6.3
3-OCH_3	6.5	3.4	7.3	4.6	5.9	5.9
3-CH_3	8.95[b]	4.3[b]	7.2[b]	5.5[b]	5.9	7.5

[a] Errors are estimated to be within 0.3 Hz. [b] The values are cited from ref 11.

tuted thiophenes might well be exchanged. The signals of C_x in 2- and 3-substituted thiophenes are too complex in their fine structures to assign with the data now available. The long-range coupling constants in methylthiophenes cannot be determined because they show complex fine multiplet structures caused by the couplings with methyl protons, except $^3C_5H_2$ and $^2J_{C_5H_4}$ in 3-methylthiophene. The values in Table III were obtained from first-order considerations. The observed values of the long-range coupling constants demonstrate that they depend largely on the geometrical positions of interacting nuclei and only partly on the nature of the substituents. One fact of interest is that the coupling constants through three bonds ($^3J_{CH}$) are larger in magnitude than those through two bonds ($^2J_{CH}$) in 2-substituted thiophenes, but this tendency is not observed for 3-substituted thiophenes. One of the exceptions to this is 2-methylthiophene.[11] It is unclear why the magnitudes of $^3J_{C_5H_3}$ and $^2J_{C_5H_4}$ in 2-methylthiophene (6.8 and 9.8 Hz) are the reverse of those of the parent compound (10.0 and 7.35 Hz) given by Weigert and Roberts.[11] Another exception is observed in $^3J_{C_5H_2}$ and $^2J_{C_5H_4}$ in the parent compound.[11] This may be caused by the characteristic nature of $^3J_{C_5H_2}$, in which the path of the coupling contains a hetero atom. Such a path also appears for the $^3J_{C_2H_5}$ in 3-substituted thiophenes, which are smaller than the $^3J_{C_2H_4}$, although both have the same number of intervening bonds between the coupling nuclei. A study of the effect of the substituents on these long-range coupling constants is now being undertaken in substituted benzenes.

Acknowledgments. The authors wish to express their gratitude to Professors Yasuo Matsuki, Genjiro Hazato, and Tsuneo Ikenoue for their continuous encouragement and valuable advice and to Mr. Y. Utsumi and G. Miyajima for their help in measuring the spectra.

Isothermal Diffusion in the System Water–Magnesium Chloride–Sodium Chloride As Studied with the Rotating Diaphragm Cell[1]

by Richard P. Wendt and Mohammed Shamim[2]

Department of Chemistry, Loyola University, New Orleans, Louisiana 70118 *(Received January 19, 1970)*

The set of four diffusion coefficients sufficient for a complete description of isothermal diffusion has been measured at 25° for the system H_2O–$MgCl_2$–NaCl at three compositions. A modified version of the Stokes diaphragm cell was used for the measurements, which resulted in an accuracy of $\pm 0.03 \times 10^{-5}$ cm²/sec in each diffusion coefficient. The diffusion data were combined with activity coefficient data in the literature to calculate the phenomenological transport coefficients and test the Onsager relation at each composition. Measured values for the diffusion and phenomenological coefficients were compared with values predicted by an approximate Nernst-type theory. It was found that the relatively large cross-term diffusion coefficients were well predicted by the approximate theory.

Introduction

Since 1955 when Dunlop and Gosting[3] first measured the set of four diffusion coefficients sufficient for a complete description of isothermal diffusion in a ternary system, several other workers[4] have published results for a number of ternary systems containing electrolytes and nonelectrolytes. Of the electrolyte systems, only one,[5] namely, H_2O–Na_2SO_4–H_2SO_4, contained divalent ions, and none contained the solute $MgCl_2$. The work described here for the system H_2O–$MgCl_2$–NaCl helps fill this data void of special interest to scientists working with systems similar to sea water, provides measured values for diffusion coefficients that can be compared with values predicted from Nernst-type equations[6] for multiion systems containing a divalent ion, and introduces an inexpensive method of moderate accuracy for determining diffusion coefficients.

Theory

Diffusion in Ternary Systems. In this work we use the formalism developed by Hooyman[7] to describe reference frames, diffusion coefficients, and phenomenological coefficients that are consistent with Onsager's theory of irreversible thermodynamics.[8]

According to this theory, for ternary systems the flows $(J_i)_0$ of each solute i, measured with respect to a local reference frame moving with the velocity of the solvent 0, are linearly related to gradients of chemical potentials, $\partial\mu_j/\partial x$, thereby defining the solvent-fixed phenomenological coefficients, $(L_{ij})_0$

$$(J_i)_0 = -\sum_{j=1}^{2} (L_{ij})_0 \frac{\partial \mu_j}{\partial x} \qquad i = 1, 2 \qquad (1)$$

The Onsager relation is

$$(L_{12})_0 = (L_{21})_0 \qquad (2)$$

Solvent-fixed diffusion coefficients $(D_{ij})_0$ are defined by the equations

$$(J_i)_0 = -\sum_{j=1}^{2} (D_{ij})_0 \frac{\partial c_j}{\partial x} \qquad i = 1, 2 \qquad (3)$$

where $\partial c_j/\partial x$ is the concentration gradient (in one dimension, x) of solute j.

Finally, volume-fixed diffusion coefficients D_{ij} are defined by[9]

$$J_i = -\sum_{j=1}^{2} D_{ij} \frac{\partial c_j}{\partial x} \qquad i = 1, 2 \qquad (4)$$

Hooyman, *et al.*,[10] have shown that for systems in which partial molal volumes $\bar{V}_i$ are independent of concentration, and in which one surface of the solution is constrained to have zero velocity, then the volume-fixed reference frame becomes identical with the cell-fixed (or apparatus-fixed) reference frame with respect to which the solute flows are measured in the actual diffusion experiments. Since those conditions approximately prevail in our experiments, where the concentration differences were never greater than *ca.* 0.5 *M* and

(1) This work was supported by Grant No. 14-01-0001-1303 from the Office of Saline Water, U. S. Department of the Interior, Washington, D. C.

(2) Institute of Chemistry, University of Islamabad, Rawalpindi, Pakistan.

(3) P. J. Dunlop and L. J. Gosting, *J. Amer. Chem. Soc.*, **77**, 5238 (1955).

(4) For summaries of diffusion data for ternary systems see: D. G. Miller, *J. Phys. Chem.*, **71**, 616 (1967); E. L. Cussler, Jr., and P. J. Dunlop, *ibid.*, **70**, 1880 (1966); H. Kim, *ibid.*, **70**, 563 (1966).

(5) R. P. Wendt, *ibid.*, **66**, 1279 (1962).

(6) R. P. Wendt, *ibid.*, **69**, 1227 (1965).

(7) G. J. Hooyman, *Physica*, **22**, 751 (1956).

(8) L. Onsager, *Phys. Rev.*, **37**, 405 (1931); **38**, 2265 (1931).

(9) We omit the subscript, V, for convenience.

(10) G. J. Hooyman, *et al.*, *Physica*, **19**, 1095 (1953); S. R. deGroot and P. Mazur, "Non-Equilibrium Thermodynamics," Interscience, New York, N. Y., 1962, p 256.

bulk flow was insignificant, we used volume-fixed flow equations to define the diffusion coefficients.

To calculate the solvent-fixed diffusion and phenomenological coefficients and test the Onsager relation we used transformation equations adapted by Dunlop and Gosting[11] from Hooyman's theory. For these calculations we must know (a) the four diffusion coefficients D_{ij}, (b) the variation of the mean ionic activity coefficient of each solute with respect to the concentration of each solute, and (c) the partial molal volume of each component.

Diaphragm Cell Method. Probably the simplest and most inexpensive (but not necessarily fastest nor accurate) method for studying isothermal diffusion is the diaphragm cell method, described in great detail by Gordon[12] and more recently by Robinson and Stokes.[13]

For binary systems the diaphragm cell equation is

$$\bar{D} = \frac{1}{\beta t} \ln \left(\frac{\Delta C^\circ}{\Delta C} \right) \tag{5}$$

Here t is the time at the end of the experiment; $\Delta C^\circ = C^B - C^A$ at time $t = 0$, *i.e.*, the initial concentration difference between the solution B in the bottom compartment of the cell and solution A in the top compartment; ΔC is the concentration difference at the end of the experiment; β is the cell constant; and $\bar{D}$ is the integral diffusion coefficient, a complicated function of the differential diffusion coefficient, D.

For ternary systems the assumptions used to obtain explicit expressions for the time dependence of the two solute concentration differences are the same as for binary systems, *i.e.*, the pseudo-steady state is assumed for each solute flux density, and the solutions in each compartment are assumed to be uniform. Because of their complexity we present only the general form of the equations; the details of the derivation are given in the literature.[14] The expressions found for the solute concentration differences, ΔC_1 and ΔC_2, at time t are

$$\Delta C_1 = P_1 e^{-\beta \sigma_1 t} + Q_1 e^{-\beta \sigma_2 t} \tag{6}$$

$$\Delta C_2 = P_2 e^{-\beta \sigma_1 t} + Q_2 e^{-\beta \sigma_2 t} \tag{7}$$

In these equations P_1, P_2, Q_1, and Q_2 are nonlinear functions of the diffusion coefficients D_{ij} and the initial concentration differences ΔC_i°, σ_1 and σ_2 are functions of D_{ij} only, and the cell constant β is the same as defined for binary systems. Equations 6 and 7 cannot be solved explicitly for the D_{ij}, but values for D_{ij} can be calculated from measured values for ΔC_i°, ΔC_i, β, and t by using (a) an iteration method[15,16] or (b) approximate methods[17] which require restrictive assumptions about the experimental conditions and relative magnitudes of the D_{ij}. The former method places no restrictions on the experiments or on the magnitude of the D_{ij}, and this method was adapted with some modification for our work.

Special Theory for Ternary Systems. Instead of analyzing for each solute to find each ΔC_i and then calculate the D_{ij} by using the iteration method, we decided to determine overall physical properties of the solutions A and B at the end of the diffusion experiment and use a least-squares iteration method on one equation formed by combining eq 6 and 7.

This procedure is quite similar to that used by Cussler and Dunlop,[15] differing only in the detail that we used values of ΔC_i° determined directly by preparation of the initial solutions instead of determining overall physical properties of the initial solutions. Cussler and Dunlop compared the measured values for D_{ij} from their diaphragm cell experiments with D_{ij} measured for the system H_2O–sucrose–KCl with the Gouy diffusiometer. Agreement within experimental error of the two methods established confidence in the diaphragm cell method in general and in their special procedure in particular.

Each overall physical property measured according to this procedure is a differential property, z, between solutions A and B which must vary linearly with the solute concentration differences, ΔC_1 and ΔC_2

$$z = W_1 \Delta C_1 + W_2 \Delta C_2 \tag{8}$$

In this work we measured Δn, the refractive index difference between solutions A and B, and the specific conductance difference, ΔK, between the same two solutions. Equations for these properties with the form of eq 8 are

$$\Delta n = R_1 \Delta C_1 + R_2 \Delta C_2 \tag{9}$$

$$\Delta K = K_1 \Delta C_1 + K_2 \Delta C_2 \tag{10}$$

R_1 and R_2 are called refractive index increments, and K_1 and K_2 are called conductometric increments. Linearity of these equations and values for the increments W_i were determined for this work by using solutions with known values for ΔC_i.

The working equation for determining the D_{ij} is formed by multiplying both sides of eq 6 by $W_1/(\Delta C_1^\circ$

(11) P. J. Dunlop and L. J. Gosting, *J. Phys. Chem.*, **63**, 86 (1959).

(12) A. R. Gordon, *Ann. N. Y. Acad. Sci.*, **46**, 285 (1945).

(13) R. A. Robinson and R. H. Stokes, "Electrolyte Solutions," Academic Press, New York, N. Y., 1959, Chapter 10; see also J. L. Richardson, *et al.*, OSW Research and Development Report, No. 211, Sept 1966.

(14) E. R. Gilliland, R. F. Baddour, and D. J. Goldstein, *Can. J. Chem. Eng.*, **35**, 10 (1957); E. N. Lightfoot and E. L. Cussler, Jr., *Chem. Eng. Progr. Symp. Sci.*, **61**, 66 (1965); H. Kim, *J. Phys. Chem.*, **70**, 1880 (1966).

(15) E. L. Cussler, Jr., and P. J. Dunlop, *ibid.*, **70**, 1880 (1966).

(16) P. R. Patel, E. C. Moreno, and T. M. Gregory, *J. Res. Nat. Bur. Stand., Sect. A*, **73**, 43 (1969).

(17) F. J. Kelly and R. H. Stokes, "Electrolytes," B. Pesce, Ed., Pergamon Press, Oxford, 1962, pp 96–100; J. K. Burchard and H. L. Toor, *J. Phys. Chem.*, **66**, 2015 (1962).

$+ \Delta C_2^\circ$) and both sides of eq 7 by $W_2/(\Delta C_1^\circ + \Delta C_2^\circ)$, and then adding the two resultant equations

$$y = e^{-\beta\sigma_1 t}[W_1(1 - S)X/2 + W_2B_2(1 - X) + W_2(1 + S)(1 - X)/2 - W_2B_1X] + e^{-\beta\sigma_2 t}[W_1(1 + S)X/2 - W_1B_2(1 - X) + W_2B_1X + W_2(1 - S)(1 - X)/2] \quad (11)$$

Here $y = z/(\Delta C_1^\circ + \Delta C_2^\circ)$, $X = \Delta C_1^\circ/(\Delta C_1^\circ + \Delta C_2^\circ)$, $S = \sqrt{1 + 4B_1B_2}$, and the four parameters σ_1, σ_2, B_1, and B_2 are functions of the four diffusion coefficients D_{ij} $(i, j = 1, 2)$ only. A Newton–Rhapson least-squares iteration method is used to calculate the four parameters from the experimental data; the calculation of the D_{ij} is then straightforward, since the D_{ij} are related to the parameters by

$$D_{21} = B_1(\sigma_2 - \sigma_1)$$

$$D_{12} = B_2(\sigma_1 - \sigma_2)$$

$$D_{22} = {}^1/_2(\sigma_1 + \sigma_2) + {}^1/_2\sqrt{(\sigma_1 + \sigma_2)^2 - 4(\sigma_1\sigma_2 + D_{12}D_{21})} \quad (12)$$

$$D_{11} = \sigma_1 + \sigma_2 - D_{22}$$

At least four different data points are required to calculate the four diffusion coefficients. Each data point consists of values for the initial concentration differences ΔC_1° and ΔC_2°; the differential increments W_1 and W_2 for the particular differential property measured; the cell constant β; the time t; and the differential physical property, z, measured for solutions A and B at time t.

We did not develop a rigorous procedure for calculating probable errors in the diffusion coefficients calculated according to this method, primarily because of the extreme complexity of the least-squares iteration program derived from eq 11. A rigorous error analysis based on a least-squares treatment of eq 6 and 7 has been accomplished by Patel, Moreno, and Gregory,[16] but their analysis was not directly applicable to our procedure.

Theories for Predicting Diffusion Coefficients. One of the purposes of this work was to obtain measured values for the D_{ij} in eq 4 for comparison with theoretically predicted values. The most successful theory for predicting diffusion coefficients for ternary systems was derived by Miller.[18] He combined a rigorous application of irreversible thermodynamics with judicious methods of estimating ternary transport coefficients and activity coefficient derivatives from binary data and he obtained predictions of diffusion coefficients for several ternary systems containing 1–1 electrolytes that agreed with measured values within the experimental error of the diffusion measurements. It would be very interesting to test his theory against data from the system studied in this work containing a divalent ion, but unfortunately (and surprisingly) there are no precise data for transference numbers and diffusion coefficients for the binary system H_2O–$MgCl_2$ in the literature. Instead of testing Miller's theory we must turn to the author's (RPW) theory[6] which is an extension of Gosting's approximate theory.[19] This method was shown to predict the coefficients L_{ij} and D_{ij} within about 10–20% for several strong electrolyte systems, even though it contained the rather drastic assumption that the individual ion mobilities were the same at appreciable concentrations as they were at infinite dilution.

According to this relatively inexact theory, the phenomenological coefficients $(L_{ij})_0$ $(i, j = 1, 2)$ in eq 1 can be estimated for the system under discussion, H_2O–$MgCl_2$–NaCl, by using the equations[20]

$$L_{11} = L_{33}(L_{44} + L_{55})/(4\bar{S})$$

$$L_{12} = L_{21} = -L_{33}L_{44}/(2\bar{S})$$

$$L_{22} = L_{41}(4L_{33} + L_{55})/(4\bar{S})$$

$$\bar{S} = L_{33} + {}^1/_4L_{44} + {}^1/_4L_{55}$$

$$L_{ii} = \lambda_i^0 c_i/(|z_i|F^2 10^7) \qquad i = 3, 4, 5 \quad (13)$$

In these equations, and in all subsequent equations in this paper, the subscript 1 designates $MgCl_2$, 2 is NaCl, 3 is Mg^{2+}, 4 is Na^+, and 5 is Cl^-; λ_i° is the limiting equivalent conductivity of ion i, in cm²/(ohm equiv); c_i is the concentration of ion i, in mol/cc; $|z_i|$ is the absolute value of the valence of ion i; and F is the Faraday constant with dimensions C/equiv.

From the estimates of L_{ij}, estimated values for the $(D_{ij})_0$ are then calculated using the equations[7] defining D_{ij}

$$D_{ij} \cong (D_{ij})_0 = \sum_{k=1}^{2} L_{ik}\mu_{kj} \quad (14)$$

$$\mu_{kj} = (\partial\mu_k/\partial c_j)_{T,P} \qquad i, j = 1, 2 \quad (15)$$

where μ_k is the chemical potential of neutral solute k.

If the partial molal volumes $\bar{V}_i$ were known for the ternary system, then the measured diffusion coefficients D_{ij} could be calculated from estimates of $(D_{ij})_0$ by solving eq 2, ref 11; but since the differences between D_{ij} and $(D_{ij})_0$ are only 1 or 2% in solutions of *ca.* 0.5 *M* total solute concentration, the transformation is hardly worthwhile compared with the overall error introduced by the assumptions of the theory. Note that according to this approximate theory the activity data needed to calculate the chemical potential derivatives are used to help estimate the D_{ij}. If such data are not available, assumptions must be made concerning the variation of the activity coefficients with solute concentra-

(18) D. G. Miller, *J. Phys. Chem.*, **71**, 616 (1967).

(19) L. J. Gosting, *Advan. Protein Chem.*, **11**, 535 (1956).

(20) Equations 27–30, ref 6.

tions. If one assumes that the activity coefficients are independent of both solute concentrations, then the approximate theory described above reduces to the simplified theory presented by Gosting.[19]

Experimental Procedures

The Rotating Diaphragm Cell. To avoid the stirring bar problem inherent in the Stokes diaphragm cell[13] and to permit precision machining of a cell with a relatively large cell constant, we have developed a self-stirring rotating diaphragm cell constructed primarily of Lucite. The opened cell is shown in Figure 1. A stainless steel shaft is screwed into the top of cap A, which also contains a leveling tube filled with light oil and an air bubble. A Nylon taper pin is screwed into the bottom of the cap and permanently affixed with Epoxy cement (Techkits, Demerest, N. J., A-12 Rigid Bond Epoxy). The pin fits into a tapered hole in the top of compartment A to form an air-tight seal between the solution placed in the compartment and the water bath into which the cell is eventually placed. A 20-mm fine porosity fritted glass disk is cemented onto a shoulder in compartment A; an O-ring immediately around the porous disk separates compartment A from

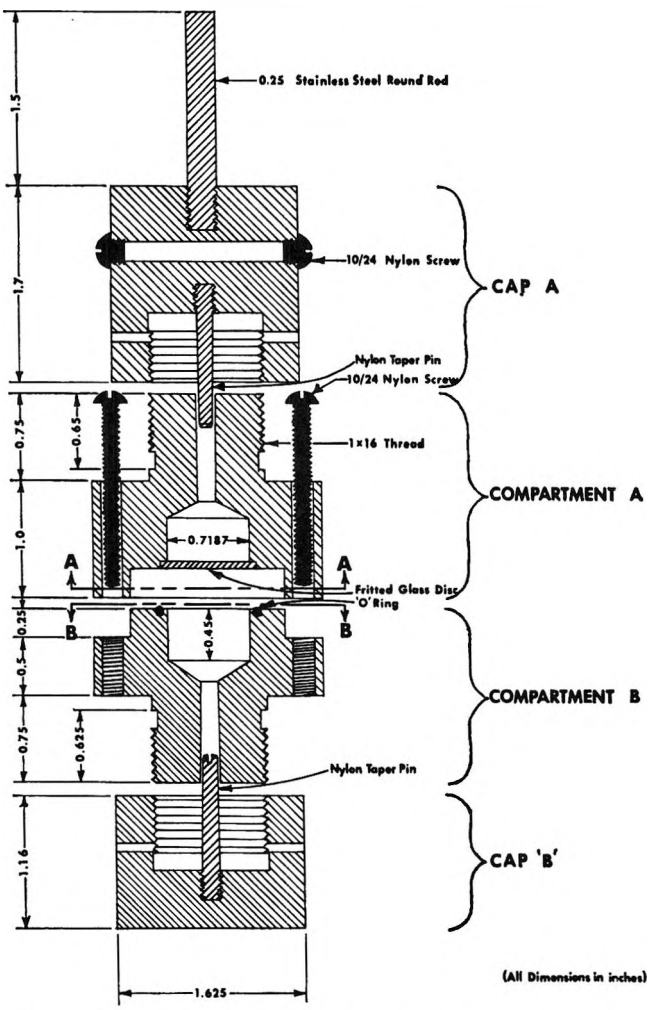

Figure 1. Rotating diffusion cell (vertical cross section).

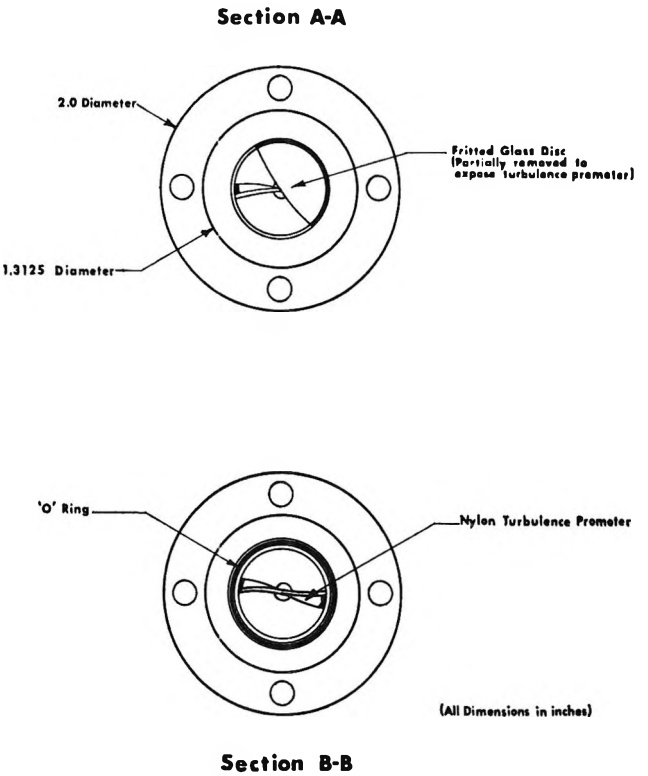

Figure 2. Solution compartments in diffusion cell (horizontal cross section).

B and seals off both compartments from surroundings. The two compartments are clamped together with Nylon screws which are never removed once the cell constant is determined. A Nylon taper pin in cap B fits into the tapered hole in compartment B, and, to provide some volume relief in case of volume changes during diffusion, a small hole is drilled into the end of the taper pin. Each compartment holds *ca.* 3.5 cc of solution;[21] because of the taper pin arrangements the closed system is highly reproducible in volume and the cell constant should not change with time unless the Lucite itself changes dimensions. Small immovable Nylon propellers are inserted into slots above and below the porous disk to help promote turbulence (Figure 2).

In Figure 3 the cell is shown loaded with solution in compartments A and B. The shaft at the top is clamped in the chuck on a low-speed motor, placed in a thermostated water bath, and leveled with the aid of the leveling bubble unit built into the cell. The motor we use is a Sargent Cone-Drive stirring motor (without the cone), Cat. No. S-76445. The motor is plugged into a Variac which controls its speed, and the Variac is connected to the 110 V ac line in series with a relay

(21) The solution volumes, V^A and V^B, and the porous frit volume, V^P, were: for cell NC, V^A = 2.90 cc, V^B = 3.45 cc, and V^P = 0.30 cc; for cell OC, V^A = 2.86 cc, V^B = 3.34 cc, and V^P = 0.30 cc. Although the cell constants were relatively large, these volumes only introduced errors of less than 0.1% in the diaphragm cell equation for binary systems (eq 6, ref 12) and in the equation relating $\bar{D}$ to D (*cf.* eq 23 and Table 3, ref 12).

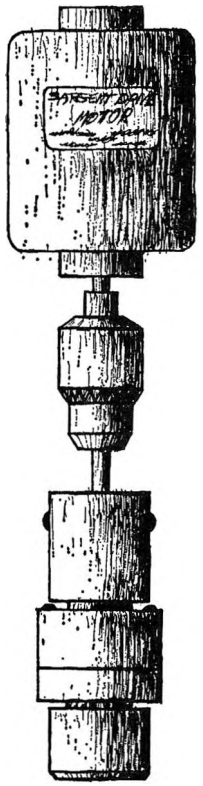

Figure 3. Diffusion cell mounted on a motor.

which intermittently turns the Variac on and off. The relay is actuated by an eccentric cam attached to the shaft of a Bodine synchronous gear motor. In operation the cell accelerates from 0 to about 80 rpm in 5 sec, then coasts to an almost complete stop for 5 sec. The 5-sec on–5-sec off cycle continues throughout the diffusion experiment, which lasted about 16–24 hr for our diffusion cells with cell constants of *ca.* 0.7 cm^{-2}. The acceleration–deceleration cycles induced turbulence within solutions A and B (which were completely confined with no free surface in the diffusion cell), so that the diffusive boundary layers above and below the porous disk were effectively eliminated. Our results with known binary systems were reproducible and consistent with literature values within about 0.4%. Thus, we lose some precision as compared with the Stokes cell, but the ease of construction, lack of any moving parts, and large cell constant for our rotating diaphragm cell make it an attractive diffusion instrument of moderate accuracy.

Calibration of the Diffusion Cell. Two rotating diaphragm cells, designated OC and NC, were used for all experiments. Nominal values for the on–off times and the maximum rotational velocity during the on times were not arrived at by precise quantitative calculations, nor by calibrations at a variety of values for those variables. Instead, the effectiveness of stirring was first estimated visually by injecting a thin layer of $KMnO_4$ solution directly over the porous disk and under the distilled water in compartment A of the cell (compartment B was also filled with water to prevent drainage of solution A into B). The cell was carefully mounted on the motor and rotated at the selected velocity and on–off frequency. We found by this method that a 5-sec on period, a Variac setting such that the cell reached a velocity of 80 rpm during this on period, and 5-sec off period during which time the cell coasted to an almost complete stop, provided very effective stirring of the $KMnO_4$ solution as evidenced by uniformity of the solution in compartment A after only two or three on–off cycles.

The effectiveness of the stirring was tested quantitatively by determining the cell constant, β, for two known binary systems (H_2O–NaCl and H_2O–KCl) at several compositions. The results of these experiments are shown in Table I. Cell constants β were calculated from values for t, ΔC°, and ΔC (determined by refractometric and conductometric measurements at the beginning and end of the experiments) and calculated values[22] for $\bar{D}$.

Methodology for Diffusion Experiments. Solutions A and B for the diffusion experiments were first brought to thermal equilibrium with the water bath at 25°. Compartment B of the diffusion cell was then rinsed three times with a few cubic centimeters of solution B, the compartment was filled completely with solution B, and the solution was forced with air pressure produced by a rubber bulb through the disk into compartment A. This process was repeated three times. Then the compartment was completely filled with solution B, and cap B slowly was screwed into place, the tapered pin in the cap allowing liquid to flow out as the pin advanced to form a tight seal. Compartment A was rinsed several times with solution A and filled completely with that solution; cap A with a taper pin was screwed into place to completely isolate solution A from the outside water bath.

The filled cell was placed in the water bath and the shaft on cap A fastened into the chuck on the stirring motor. The leveling bulk built into cap A was used as the indicator for adjustment of the motor in its clamps until the shaft was perfectly (within *ca.* 1°) vertical; the porous disk was then assumed to be horizontal. The motor was turned on and the intermittent on–off cycles commenced. After *ca.* 1 hr the cell was removed from the motor and bath; we assumed by this time a pseudo-steady state had been reached[23] between solutions A and B in the cell and the porous disk now contained a non-uniform solution instead of uniform solution B initially in the disk.

(22) $\bar{D}$ for H_2O–KCl was calculated using revised data given by L. A. Woolf and J. F. Tilley, *J. Phys. Chem.*, 71, 1962 (1967). To find $\bar{D}$ for H_2O–NaCl we graphically integrated diffusion data of Robinson and Stokes (ref 13, Appendix 11.2).

(23) A rule to estimate a safe time to reach the steady state is given in ref 12, p 286; $t \geq 1.2L^2/D$, where L is the effective length of the diffusion path. For our porous disk we estimate $L = 0.2$ cm; using $D = 1.2 \times 10^{-5}$ cm^2/sec, we find $t \geq 4000$ sec.

Table I:[a] Calibration of Diffusion Cells

Cell	Solute	$(C^B)^\circ$	$(C^A)^\circ$	Time, hr	No. of experiments	β mean value	Av dev from mean, %
NC	NaCl	0.50	0.00	16	5	0.6945	0.30
NC	NaCl	0.50	0.00	24	3	0.6939	0.30
NC	KCl	0.65	0.35	16	7	0.6866	0.44
OC	NaCl	0.50	0.00	16	4	0.7405	0.27
OC	NaCl	0.50	0.00	24	4	0.7430	0.37
OC	KCl	0.65	0.35	16	5	0.7420	0.43

Accepted values: Cell NC, $\beta = 0.6904$ cm^{-1}; cell OC, $\beta = 0.7419$ cm^{-1}

[a] Units for C, mol/l.

After the cell was removed from the water bath cap B was unscrewed. Cap A was still screwed tightly in place with the taper pin forming a tight seal, so that when cap B was unscrewed there was no flow of solution from A into B that might destroy the concentration gradient inside the disk. The solution in B was removed with a syringe, the compartment was rinsed several times with fresh solution B, and cap B was screwed back in place. Cap A was then unscrewed, compartment A was rinsed out several times with fresh solution A, and finally that compartment was completely filled with solution A and the cap was screwed in place. This point in time was taken to be $t = 0$, the beginning of the diffusion experiment. The cell was replaced in the water bath, and the intermittent rotation cycles were commenced.

After the desired diffusion time had elapsed the cell was removed from the water bath. Cap B was unscrewed and solution B was removed. This point in time was taken to be $t = t$, the time at which diffusion ceased. With the cell in the upright position cap A was removed and a few tenths of a cubic centimeter of solution A was allowed to drain back through the disk, in case any solution in the disk was pulled into compartment A when it was opened. Solutions A and B were then analyzed conductometrically and refractometrically as described later.

All filling and emptying procedures were made using disposable 10-cc syringes. The water bath temperature was held constant within ±0.03° of 25.00°. Experiments were occasionally discarded because bubbles were observed in one or both of the compartments in the diffusion cell, but in general, the thermal equilibrium of solutions used in the experiments seemed to be sufficient for preventing bubble formation due to evolution of dissolved air.

Ternary Diffusion Experiments. At each mean composition $\bar{C}_1$, $\bar{C}_2$, several experiments were performed with values of $X = \Delta C_1^\circ/(\Delta C_1^\circ + \Delta C_2^\circ)$ ranging from 0.0 to 1.0. Actually only two experiments were required, since we measured both Δn and ΔR for each experiment, thereby providing four data points to determine the four diffusion coefficients; but the extra experiments increased the precision both of the determination of D_{ij} and the coefficients R_i and K_i, since the latter were determined from initial values of ΔC_i^0 for the diffusion experiments. Experimental times t were generally about 16 hr, a time which gave approximately optimal changes in Δn and ΔR. A few experiments were run for 24 hr to check for any effect of length of time on calculated values for the D_{ij}.

Materials. Conductance grade water was obtained by passing tap water through Continental Water Co. charcoal and ion-exchange units. The water had a specific conductance less than 10^{-6} (ohm cm)$^{-1}$.

KCl, used to determine the diffusion cell constant and to calibrate the refractometer, was prepared by crystallization of analytical reagent KCl dissolved at 100° in conductance water. After three crystallizations the salt was dried at 100° and stored in a desiccator.

Analytical reagent grade NaCl was recrystallized by passing HCl gas through a saturated solution of the salt in conductance water at room temperature. The precipitation was repeated three times. Crystals were collected and washed with cold conductance water, dried at 100°, and stored in a desiccator.

$MgCl_2 \cdot 6H_2O$, analytical reagent grade, was dissolved in hot conductance water and crystallized by cooling. After three crystallizations the collected crystals were dissolved in conductance water to form approximately 10% $MgCl_2$ stock solution. The stock solution was analyzed for weight per cent of $MgCl_2$ according to a magnesium pyrosphosphate gravimetric method described by Kolthoff and Sandell.[24] Analyses were reproducible within 0.1%. During the 12-month period in which $MgCl_2$ was used we prepared four stock solutions, each stored in a 2-l. volumetric flask. Analyses at the beginning and end of storage showed no significant change in composition, and we have confidence that the stock solutions compositions were known with relative accuracies of 0.1%.

Solutions and Density Measurements. Solutions for diffusion experiments were prepared by weighing

(24) I. M. Kolthoff and C. B. Sandell, "Textbook on Quantitative Inorganic Analysis," Macmillan, New York, N. Y., 1965, pp 360, 361.

solute (or stock solution, in the case of $MgCl_2$) into a 100-ml volumetric flask and filling the flask almost to the fiducial mark with conductance water. The flasks were then suspended in a water bath at 25.00°, allowed to thermally equilibrate, and filled with water to the fiducial mark with the aid of a magnifying eyepiece. The volume of each flask had been determined this way by weighing water required to fill to the mark, and reproducibilities of about ±0.02% in the volume were obtained for each flask. We could therefore determine solution densities to within about 0.0002 g/cc by weighing the solutions after they had been prepared to volume. All weights were corrected to vacuum in the usual way. The density information was used to calculate concentration in moles per liter for each solute and to determine with moderate accuracy solution properties such as partial molal volumes.

Conductometry. Conductance measurements were made with a Beckman Instruments, Inc., Model RC-18 conductivity bridge operated at 3 kc in the resistance mode. The conductance cell, a Beckman Instruments, Inc., Model CEL-G100Y184J, had a cell constant of approximately 100 cm^{-1}, held about 0.1 cc of solution, and had a glass jacket through which transformer oil from a thermostated bath was circulated. The temperature of the circulating oil immediately at the outflow of the cell jacket was measured within 0.01° by a short-range mercury thermometer. For some conductance measurements the temperature slowly fluctuated by as much as ±0.05° around the desired temperature, 25°, but the bridge was balanced as the temperature rose and fell past 25° to obtain best values for the resistance that were reproducible within about 0.1%.

To try and determine J_c, the conductance cell constant, the resistance was measured for three solutions of NaCl in water, with concentrations C = 0.5, 0.3, and 0.13 M. Using literature values[25] for the equivalent conductance of each solution, we found significantly different values for J_c: at C = 0.5, J_c = 105.86 cm^{-1}; at C = 0.3m, J_c = 103.52; and at C = 0.13, J_c = 98.78. The design of the cell, being severely restricted by requirements of small solution volume and high cell constant, apparently resulted in this anomalous behavior which prohibits the use of this particular cell for absolute determinations of solution conductances. However, for our analytical needs the cell was adequate when calibrated over the range of concentrations expected for either the binary or ternary solutions used in the diffusion experiments.

For the binary systems KCl in water and NaCl in water the conductance cell was calibrated by measuring the resistance of several solutions of KCl in water and NaCl in water and then preparing deviation graphs similar to those used in ref 25.

For the ternary systems nominal values for the specific conductance, K, were calculated by using J_c = 100. As indicated by eq 10, we expected ΔK, the difference between K for solution B and K for solution A, to be linearly dependent on ΔC_1 and ΔC_2 over the small values used for the ΔC_i. The sum of $\Delta C_1^\circ + \Delta C_2^\circ$ (the known initial concentration differences) was held constant for each set of calibration experiments and the data were fit by the method of least squares to determine K_1 and K_2 in eq 10.

Refractometry. For each set of solutions the refractive index difference, Δn, was measured with a Brice-Phoenix Differential Refractometer, Model BP-2000-V. The green line (546 mμ) from a type AH-3 mercury vapor lamp illuminated the object slit of the apparatus. Oil from a thermostated oil bath passed through the jacket surrounding the quartz cell in the refractometer, and all measurements were made at 25 ± 0.05°. The cell constant was determined by calibration with several KCl–water and NaCl–water solutions, using literature data[26] for accurate values of Δn. A single value for the cell constant, 0.92565×10^{-3}, was found to reproduce Δn within about $\pm 3 \times 10^{-6}$ refractive index units for several values of ΔC, thereby giving us confidence in the accuracy of our refractometric data.

For the ternary systems the refractometric increments R_1 and R_2 were determined from solutions of known ΔC_1° and ΔC_2° by applying the method of least squares to eq 9.

Calculations

The Iteration Process. For each composition point the following data were fed into the computer, according to the iterative least-squares program used to calculate the diffusion coefficients: (a) M, the number of experiments; (b) the first guesses for the parameters S_1, S_2, B_1, and B_2, which are functions only of four initial guessed values for the D_{ij}; (c) the initial solute concentration differences, ΔC_1° and ΔC_2°; (d) the differential increments R_1 and R_2 (for the case of refractometric data points) or K_1 and K_2 (for the case of conductometric data points); (e) the differential physical property Δn (for refractometric data points) or ΔK (for conductometric data points) measured at time t; and (f) the product βt of the cell constant and the diffusion time.

Item b, the initial estimates of the parameters, caused some difficulty. In general, the problem of convergence of iteration procedures such as the Newton–Rhapson method we used cannot be rigorously stated in terms of how close the initial guesses must be. We simply performed computer experiments with our program, using data for item e listed above generated by assuming some model values for D_{ij} (and hence the

(25) J. F. Chambers, J. M. Stokes, and R. H. Stokes, *J. Phys. Chem.*, **60**, 985 (1956).

(26) Tables 1 and 2, Manual BP-2000-V, Phoenix Precision Instrument Co. [their data taken from A. Kruis, *Z. Phys. Chem.* (Leipzig), **343**, 13 (1936)].

parameters S_i and B_i) and values for ΔC_i° and βt which were roughly those expected to be used in the actual diffusion experiments. Convergence was achieved for values of S_i and B_i that differed from the model values by as much as 50%, thereby giving us what turned out to be false optimism about the convergence expected for actual diffusion experiments, for which the Δn or ΔK values contained some scatter due to experimental error.

We found that for actual experiments the first guesses for S_1 and S_2 had to be within approximately 20% or better to obtain convergence, although first guesses for B_1 and B_2 (which were proportional to the cross-term coefficients D_{21} and D_{12}, respectively) could be off by a factor of 2 or 3. The most probable cause of this difficulty was experimental error in the differential quantities Δn and ΔR, which in general were reproducible within about 0.3% for duplicate experiments but which occasionally showed deviations of about 1%. To obtain better first guesses we had to use equations similar to those suggested by Patel, *et al.*,[16] for estimating D_{ij} from experimental values for ΔC_i° and ΔC_i

$$D_{ii} \cong \frac{1}{\beta t} \ln\left(\frac{\Delta C_i^\circ}{\Delta C_i}\right), \Delta C_j^\circ = 0, i \neq j \qquad (16)$$

$$D_{ij} \cong \Delta C_i/(\overline{\Delta C}_j \beta t), \Delta C_i^\circ = 0, i \neq j \qquad (17)$$

Here the $\overline{\Delta C}_j$ are averages defined by $(\Delta C_j^\circ + \Delta C_j)/2$. The concentration differences at time t must be calculated from values for Δn, ΔK, R_i, and K_i. One experiment at $\Delta C_1^\circ = 0$ is sufficient, for example, to estimate D_{22} and D_{12}, since two linear equations in Δn and ΔK (eq 9 and 10) can be solved for the unknowns ΔC_1 and ΔC_2. In this way we estimated initial guesses for the four D_{ij}, calculated S_i and B_i from eq 12 (solved for S_i and B_i), and obtained good convergence of the iteration process for all three systems studied.

We resorted to computer experiments to find approximate uncertainties in the diffusion coefficients caused by the following realistic estimates of absolute and relative errors in the input data

$$\delta\Delta C_i^\circ = 0.1\%, \delta R_i = 0.3\%, \delta K_i = 0.5\%$$

$$\delta\Delta n = 3 \times 10^{-6}, \delta\Delta K = 0.5\%, \delta\beta = 0.4\%, \delta t = 0.01\%$$

Calculated values for the D_{ij} were found to have percentage uncertainties almost directly proportional to the small percentage uncertainty in β, thereby giving us confidence that even for cell NC which showed some anomalous behavior of its cell constant as measured with different solute concentrations (Table I), errors in the D_{ij} caused by errors in β were no more than about 1%. The cross-term coefficients D_{12} and D_{21} were found to be quite sensitive to the increments R_i and K_i. This effect is understandable if one considers the iterative program first to calculate ΔC_1 and ΔC_2 from values for the differential properties z and the increments W_i, and then to compute the D_{ij} according to eq 6 and 7. Near $X = 0$, for example, where the initial value for ΔC_1° is approximately zero, a value for D_{12} is obtained by using Δn, ΔK, R_i, and K_i for that experiment to calculate ΔC_1 and ΔC_2. A small error in R_i or K_i would cause a large relative error in ΔC_1 and hence a large relative error in D_{12} (*cf.* eq 17 for estimating the D_{ij} from experimental data). By using perturbed values for the accepted values for R_i and K_i listed in Table VI we estimate absolute errors of $\pm 0.02 \times 10^{-5}$ in each D_{ij} from this source. Errors in β, Δn, and ΔK were found to cause an additional absolute error of $\pm 0.01 \times 10^{-5}$ in each D_{ij}, so that our estimates amount to absolute errors of about $\pm 0.03 \times 10^{-5}$ in each D_{ij}.

Phenomenological Coefficients. The quantities $(D_{ij})_0$ and μ_{ij} are needed to calculate the $(L_{ij})_0$. To calculate each $(D_{ij})_0$ from measured values for the diffusion coefficients D_{ij}, the partial molal volumes $\bar{V}_i$ of each component must be known, according to eq 2, ref 11; and to calculate the chemical potential derivatives with respect to solute molarity, μ_{ij} in eq 15, the derivatives A_{ik} and B_{kj} must be known.

$$\mu_{ij} = \sum_{k=1}^{2} A_{ik} B_{kj} \qquad (18)$$

$$A_{ik} = (\partial\mu_i/\partial m_k)_{T,P} \qquad (19)$$

$$B_{kj} = (\partial m_k/\partial C_j)_{T,P} \qquad (20)$$

Here m_k is the molality of component k. The required gravimetric quantities $\bar{V}_i$ and B_{kj} are easily calculated if the ternary solution densities vary linearly with the solute concentrations near the particular composition points of interest, $\bar{C}_1$, $\bar{C}_2$. For the solutions used in the diffusion experiments, the densities d were found to follow this simple linear relation within the experimental error (0.02%) of the density measurements

$$d = d^0 + H_1(C_1 - \bar{C}_1) + H_2(C_2 - \bar{C}_2) \qquad (21)$$

The coefficients H_i are used to calculate $\bar{V}_i$ and B_{jk} according to eq 3 and 8, ref 11. We used molecular weights of 18.016 for H_2O, 95.234 for $MgCl_2$, and 58.454 for NaCl for all calculations.

Chemical potential derivatives on a molal scale, A_{ik}, are related to the mean ionic solute activity coefficients, g_i, for the system studied here by[27]

$$A_{11}/(RT) = (1/m_1) + 4/(2m_1 + m_2) + 3\Gamma_{11}$$

$$A_{12}/(RT) = A_{21}/(RT) = 2/(2m_1 + m_2) + 3\Gamma_{12}$$

$$A_{22}/(RT) = (1/m_2) + 1/(2m_1 + m_2) + 2\Gamma_{22} \qquad (22)$$

Here $\Gamma_{ij} = \partial \ln g_i/\partial m_j$. Thus to calculate A_{ik} and hence μ_{ij}, the activity coefficient derivatives Γ_{ij} are needed. We obtained these derivatives by analytical differentiation of expressions given by Wu, Rush, and

(27) Equation 31a, ref 6, with $c_i = m_i$ and $(\gamma_\pm)_i = g_i$, was differentiated with respect to each m_i.

Table II:[a,b] Initial Data from Ternary Diffusion Experiments

Expt no.	C_1^B	C_2^B	C_1^A	C_2^A	$\Delta C_1°$	$\Delta C_2°$	$\Delta n° \times 10^3$	K^B	K^A	$\Delta K°$
					Composition I					
51	0.232059	0.350308	0.232174	0.150444	−0.000115	0.199864	1.925	0.065125	0.049801	0.015324
53	0.232059	0.350308	0.232174	0.150444	−0.000115	0.199864	1.925	0.065091	0.049811	0.015280
55	0.259838	0.319972	0.204179	0.180208	0.055659	0.139764	2.627	0.066287	0.048598	0.017689
57	0.259838	0.319972	0.204179	0.180208	0.055659	0.139764	2.631	0.066295	0.048643	0.017652
56	0.296922	0.280155	0.167064	0.219975	0.129858	0.060180	3.553	0.067709	0.046867	0.020842
58	0.296922	0.280155	0.167064	0.219975	0.129858	0.060180	3.556	0.067760	0.046882	0.020878
52	0.325010	0.250195	0.139176	0.250030	0.185834	0.000165	4.254	0.068413	0.045463	0.022950
54	0.325010	0.250195	0.139176	0.250030	0.185834	0.000165	4.253	0.068587	0.045566	0.023021
					Composition II					
41	0.150164	0.400115	0.150197	0.200269	−0.000033	0.199846	1.942	0.05863	0.04286	0.01577*
43	0.150164	0.400115	0.150197	0.200269	−0.000033	0.199846	1.942	0.05880	0.04276	0.01604
49	0.150164	0.400115	0.150197	0.200269	−0.000033	0.199846	1.941	0.05877	0.04279	0.01598
45	0.180095	0.370021	0.120013	0.230465	0.060082	0.139556	2.759	0.06032	0.04111	0.01921
47	0.180095	0.370021	0.120013	0.230465	0.060082	0.139556	2.755	0.06032	0.04111	0.01921
46	0.200058	0.350219	0.100088	0.250574	0.099970	0.099645	3.243	0.06101	0.04004	0.02097
48	0.200058	0.350219	0.100088	0.250574	0.099970	0.099645	3.256	0.06109	0.04008	0.02101
42	0.250297	0.300519	0.050021	0.299953	0.200276	0.000566	4.602	0.06335	0.03728	0.02607*
44	0.250297	0.300519	0.050021	0.299953	0.200276	0.000566	4.601	0.06344	0.03721	0.02623
50	0.250297	0.300519	0.050021	0.299953	0.200276	0.000566	4.598	0.06345	0.03719	0.02626
					Composition III					
67	0.092889	0.540748	0.092692	0.390228	0.000197	0.150520	1.460	0.062779	0.050813	0.011966
68	0.092889	0.540748	0.092692	0.390228	0.000197	0.150520	1.461	0.062802	0.050834	0.011968
63	0.111358	0.489787	0.074238	0.429874	0.037120	0.059913	1.420	0.061162	0.051578	0.009584
65	0.111358	0.489787	0.074238	0.429874	0.037120	0.059913	1.416	0.061184	0.051661	0.009523
64	0.120609	0.480073	0.064967	0.440123	0.055642	0.039950	1.664	0.061565	0.051156	0.010409
66	0.120609	0.480073	0.064967	0.440123	0.055642	0.039950	1.665	0.061618	0.051159	0.010459
60	0.139285	0.460293	0.046388	0.459925	0.092897	0.000368	2.150	0.062356	0.050284	0.012072
62	0.139285	0.460293	0.046388	0.459925	0.092897	0.000368	2.150	0.062391	0.050312	0.012079
					Composition IB					
1	0.250377	0.400370	0.250427	0.100121	−0.000050	0.300249	2.916	0.07094	0.04813	0.02281
3	0.250377	0.400370	0.250427	0.100121	−0.000050	0.300249	2.923	0.07109	0.04819	0.02290
19	0.250170	0.400020	0.250170	0.100370	0.000000	0.299650	2.895	0.07040	0.04788	0.02262
21	0.250170	0.400020	0.250170	0.100370	0.000000	0.299650	2.901	0.07070	0.04796	0.02274
2	0.400242	0.250044	0.100050	0.250019	0.300192	0.000025	6.833	0.07680	0.04005	0.03675
4	0.400242	0.250044	0.100050	0.250019	0.300192	0.000025	6.836	0.07705	0.04018	0.03687
20	0.400310	0.250030	0.100030	0.250860	0.300280	−0.000830	6.825	0.07644	0.04014	0.03630
22	0.400310	0.250030	0.100030	0.250860	0.300280	−0.000830	6.829	0.07625	0.03993	0.03632
23	0.250170	0.400020	0.250170	0.100370	0.000000	0.299650	2.901	0.07061	0.04803	0.02258
24	0.400310	0.250030	0.100030	0.250860	0.300280	−0.000830	6.814	0.07661	0.04009	0.03652

[a] Subscripts in this and all subsequent tables: 0 = H_2O, 1 = $MgCl_2$, 2 = NaCl. [b] Units: C_i, mol/l.; n, R.I. units; K, ohm^{-1} cm^{-1}.

Scatchard[28] for ln g_1 and ln g_2 for this system. The resulting equations are cumbersome but permit explicit calculation of the Γ_{ij} as functions of m_1 and m_2. Other authors[29] have reported activity data for the system studied here and have tested the data for consistency with simple linear and quadratic expressions such as Harned's rule and its modifications, which if obeyed, would permit simple calculation of the required derivatives. But the activity data do not follow a simple linear or quadratic rule, and hence the aforementioned data and the complicated but precise equations of Wu, *et al.*, were used in our calculations. In eq 22 we let $R = 8.3144 \times 10^7$ ergs/(mol deg) and $T = 298.15°$K.

The derivatives discussed above were used with measured values for the diffusion coefficients to calculate the phenomenological coefficients according to eq 2 and 1d–1h, ref 11.

Results

Diffusion Coefficients for the Ternary System. In Table II are shown the initial data for four compositions: composition I, $\bar{C}_1 = 0.25$, $\bar{C}_2 = 0.25$, and $\Delta C_1° + \Delta C_2° = 0.20$; composition Ib, $\bar{C}_1 = 0.25$, $\bar{C}_2 = 0.25$, and $\Delta C_1° + \Delta C_2° = 0.30$; composition II, $\bar{C}_1 = 0.15$,

(28) Y. C. Wu, R. M. Rush, and G. Scatchard, *J. Phys. Chem.*, **72**, 4048 (1968).

(29) J. N. Butler and R. Huston, *ibid.*, **71**, 4479 (1967); R. D. Lanier, *ibid.*, **69**, 3992 (1965); R. F. Platford, *ibid.*, **72**, 4063 (1968).

Table III:[a] Data at End of Ternary Diffusion Experiments

Expt no.	Cell	βt	$\Delta n \times 10^3$	K^B	K^A	ΔK
			Composition I			
51	OC	45,278	0.985	0.061259	0.053118	0.008141
53	OC	45,645	0.987	0.060957	0.053121	0.007836*
55	NC	42,549	1.543	0.063044	0.052770	0.010274
57	NC	41,666	1.549	0.063044	0.052604	0.010440
56	OC	45,712	2.160	0.063271	0.050974	0.012297
58	OC	44,829	2.184	0.063347	0.050878	0.012469
52	NC	42,121	2.754	0.064914	0.050533	0.014381
54	NC	42,439	2.747	0.065066	0.050533	0.014533
			Composition II			
41	NC	39,612	1.077	0.05566	0.04663	0.00903
43	NC	42,856	1.028	0.05543	0.04678	0.00865
45	NC	41,662	1.638	0.05654	0.04551	0.01103
47	NC	42,574	1.605	0.05665	0.04565	0.01100
46	OC	44,677	1.955	0.05638	0.04410	0.01228
48	OC	45,731	1.935	0.05626	0.04424	0.01202
42	OC	42,489	2.986	0.05832	0.04198	0.01634
44	OC	45,319	2.876	0.05793	0.04217	0.01576
			Composition III			
67	OC	37,967	0.834	0.060107	0.053160	0.006947
68	NC	35,486	0.867	0.060617	0.053442	0.007175
63	NC	42,525	0.860	0.059294	0.053781	0.005513
65	NC	42,670	0.846*	0.059294	0.053818	0.005476
64	OC	45,660	1.004	0.059182	0.053149	0.006033*
66	OC	45,908	0.997	0.059126	0.053265	0.005861
60	NC	40,440	1.416	0.060361	0.052740	0.007621
62	NC	40,475	1.411	0.060372	0.052804	0.007568
			Composition IB			
1	NC	41,928	1.557	0.06629	0.05381	0.01248
3	NC	41,931	1.562	0.06639	0.05388	0.01251
19	NC	40,513	1.583	0.06624	0.05340	0.01284
21	NC	39,436	1.601	0.06616	0.05332	0.01284
2	OC	45,219	4.290	0.06976	0.04724	0.02252
4	OC	45,226	4.294	0.06980	0.04738	0.02242
20	OC	43,624	4.354	0.06975	0.04696	0.02279
22	OC	42,325	4.408	0.06965	0.04674	0.02291
23**	NC	59,046	1.193	0.06494	0.05515	0.00979
24**	OC	63,414	3.567	0.06767	0.04903	0.01864

[a] Units for βt: sec/cm.

$\bar{C}_2 = 0.30$, and $\Delta C_1^\circ + \Delta C_2^\circ = 0.20$; composition III, $\bar{C}_1 = 0.10$, $\bar{C}_2 = 0.46$, and $\Delta C_{10} + \Delta C_{20} = 0.13$. More significant figures are used in the concentration data that can be justified by the accuracy of the density data used to help calculate each C_i, or by the accuracy of the analysis of the $MgCl_2$ stock solution; we include redundant numbers to avoid rounding off errors in subsequent calculations. Duplicate experiments, performed under conditions of similar values for ΔC_i° and time t indicate the reproducibilities of Δn° and ΔK° (Table II), and of Δn and ΔK (Table III). Numbers with asterisks in Table II were not used in the least-squares procedure for calculating K_1 and K_2 (Table VI) and numbers similarly indicated in Table III and the data from experiments 23 and 24 for compositions Ib were not used to calculate the diffusion coefficients.

Diffusion coefficients calculated for compositions I, II, and III are shown in Table IV. The estimated uncertainty of $\pm 0.03 \times 10^{-5}$ in each D_{ij} is significantly smaller than the variation of D_{ij} with average initial composition $\bar{C}_1$, $\bar{C}_2$. It should be emphasized that these are integral diffusion coefficients obtained from experiments with finite concentration differences, and any strong concentration dependences might be manifested by variations in D_{ij} with ΔC_i° at constant $\bar{C}_1$, $\bar{C}_2$.

The D_{ij} in Table IV for composition Ib and I indicate some effect of the sum of concentration differences, sum ΔC_i°, on values for the integral diffusion coefficients. However, except for D_{22} the variation of D_{ij} with sum ΔC_i° is approximately within the experimental error in D_{ij}. Since the integral values presumably approach the true differential values for D_{ij} as sum

Table IV:[a] Diffusion Coefficients and Differential Increments for the System H_2O–$MgCl_2$–NaCl at 25°

Composition	$\bar{C}_1$	$\bar{C}_2$	Sum ΔC_i°	$D_{11} \times 10^5$	$D_{12} \times 10^5$	$D_{21} \times 10^5$	$D_{22} \times 10^5$	R_1	R_2	K_1	K_2
IA	0.25	0.25	0.13	...	...	...	...	0.02284	0.009619	0.1225	0.07575
I	0.25	0.25	0.20	0.892	0.105	0.348	1.203	0.02289	0.009662	0.1241	0.07690
IB	0.25	0.25	0.30	0.915	0.078	0.300	1.293	0.02276	0.009696	0.1219	0.07580
II	0.15	0.30	0.20	0.842	0.045	0.476	1.362	0.02294	0.009741	0.1308	0.08037
III	0.10	0.46	0.13	0.787	0.014	0.634	1.426	0.02305	0.009590	0.1298	0.07937

[a] Units: D_{ij}, cm²/sec, for solute flows in mol/(cm² sec); R_i, (ref. index units) (l.)/mol; K_i, l./(ohm cm mol).

ΔC_i^0 gets smaller, we consider the D_{ij} for composition I and also for compositions II and III, where the sums of ΔC_i° were comparably small, to be identical with differential coefficients within experimental error.

A variance with sum ΔC_i° of the refractometric and conductometric increments, R_i and K_i, would contribute somewhat to any observed dependence of D_{ij} on sum ΔC_i°. Values for these increments shown in Table IV for compositions Ia, I, and Ib indicate small but significant variations with sum ΔC_i°, and values for D_{ij} calculated for composition I using R_i and K_i from compositions Ia and I showed changes in D_{ij} that were somewhat greater than the estimated error. Since the values at time t for ΔC_i of composition I are closer to the relatively small sum ΔC_i° of composition Ia than they are to the larger sum ΔC_i° of composition I, it might be argued that the R_i and K_i for composition Ia should be used to calculate D_{ij}, for composition I. However, the accuracy of R_i and K_i is somewhat less for composition Ia than for composition I because of the larger values for Δn° and ΔK° for the latter composition; furthermore, any errors in preparation of the solutions for composition I would be minimized to some extent by using values for R_i and K_i determined from Δn° and ΔK° for those same solutions. We therefore used R_i and K_i at time t for each composition that were determined from the initial data (Table II) for that system.

Almost all of the experiments lasted about 16 hr, but a few experiments were run for 24 hr to test the effect of time on values calculated for the D_{ij}. A comparison of calculated D_{ij} is given in Table V for composition Ib. Only for coefficient D_{21} do the results at the shorter time differ from results at the longer time by more than the estimated experimental error. We consider this difference to be not significant, partly because of the considerably fewer experiments used to calculate D_{ij} at the longer time, and partly because the cell constant had been shown by a few experiments at 24 hr for binary systems to be the same within experimental error as its value determined at 16 hr (Table I). Time dependence could result either from poor stirring, which may have a cumulative effect, or from appreciable dependence of the D_{ij} on concentration. The latter cause would seem the most likely for our ternary experiments since the integral coefficients obtained in those experiments were not corrected for concentration dependence as were those for the binary systems used to determine β.

Table V: Apparent Time Dependence of Diffusion Coefficients for Composition IB

Av βt	$D_{11} \times 10^5$	$D_{12} \times 10^5$	$D_{21} \times 10^5$	$D_{22} \times 10^5$
42,525	0.915	0.078	0.300	1.293
61,230	0.950	0.090	0.202	1.264

In Table VI we present calculated and observed values for the refractive index differences (Refr.) and conductance differences (Cond.) between solutions A and B in the diffusion cell at the end of the experiment, time t. Values for z(calcd) were calculated from eq 11 using D_{ij} obtained by the least-squares procedure operating on the observed refractive index and conductance differences, z(obsd). Results for this system were typical of those for the other systems: per cent deviations between observed and calculated values for z averaged about 0.3%, a figure which corresponds closely with the estimated reproducibilities in Δn and ΔK at time t. The small summary below Table VI indicates no appreciable dependence of the average per cent deviations on the cell used (NC or OC) or on the physical property measured.

Phenomenological Coefficients and Tests of the Onsager Relation. Densities in Table VII were used to calculate the gravimetric quantities in Table VIII which were in turn used to help calculate the coefficients $(D_{ij})_0$ from values from D_{ij}. They were also needed to calculate the chemical potential derivatives μ_{ij} on a molar scale from literature values for activity coefficient derivatives Γ_{ij} on a molal scale (Table IX). The number of significant figures in C_i and d, Table VII, is about one more than would be estimated from the reproducibility of the data. Percentage uncertainties in the gravimetric quantities, Table VIII, are estimated to be δd°, 0.02%; δH_1, 3%; δH_2, 5%; $\delta \bar{V}_1$, 10%; $\delta \bar{V}_2$, 18%; $\delta \bar{V}_0$, 0.1%; δC_0, 0.02%; δm_1 and δm_2, 0.1%; δB_{11}, 0.1%; δB_{12}, 20%; δB_{21}, 10%; and δB_{22}, 0.05%.

Table VI: Deviations in z for Composition II

Expt	Cell	$\Delta C_1°$	$\Delta C_2°$	z(obsd) × 10^8	z(calcd) × 10^8	Dev, %
67, Refr.	OC	0.00	0.15	0.834	0.832	0.24
67, Cond.	OC	0.00	0.15	6.947	6.906	0.59
68, Refr.	NC	0.00	0.15	0.867	0.862	0.58
68, Cond.	NC	0.00	0.15	7.175	7.159	0.22
63, Refr.	NC	0.04	0.06	0.860	0.861	0.12
63, Cond.	NC	0.04	0.06	5.513	5.519	0.11
65, Cond.	NC	0.04	0.06	5.476	5.509	0.60
64, Refr.	OC	0.06	0.04	1.004	0.999	0.50
66, Refr.	OC	0.06	0.04	0.997	0.996	0.10
66, Cond.	OC	0.06	0.04	5.861	5.889	0.48
60, Refr.	NC	0.09	0.00	1.416	1.414	0.14
60, Cond.	NC	0.09	0.00	7.621	7.580	0.54
62, Refr.	NC	0.09	0.00	1.411	1.413	0.14
62, Cond.	NC	0.09	0.00	7.568	7.577	0.12

Sample	Av dev, %
All cell NC	0.29
All cell OC	0.38
All conductance	0.38
All refractive index	0.26
All experiments	0.32

Table VII:[a] Density Data

Composition I			Composition II			Composition III		
C_1	C_2	d	C_1	C_2	d	C_1	C_2	d
0.232174	0.150444	1.02052	0.150197	0.200269	1.01659	0.092889	0.540748	1.02560
0.232059	0.350308	1.02935	0.150164	0.400115	1.02519	0.092692	0.390228	1.01955
0.204179	0.180208	1.01976	0.120013	0.230465	1.01553	0.046388	0.459925	1.01916
0.259838	0.319972	1.02933	0.180095	0.370021	1.02480	0.139285	0.460293	1.02539
0.167064	0.219975	1.01864	0.100088	0.250574	0.01498	0.074238	0.429874	1.02008
0.296922	0.280155	1.03025	0.200058	0.350219	1.02600	0.111358	0.489787	1.02509
0.139176	0.250030	1.01756	0.050021	0.299953	1.01298	0.064967	0.440123	1.01987
0.325010	0.250195	1.03187				0.120609	0.480073	1.02521

[a] Units for d: g/cc.

Table VIII:[a] Gravimetric Quantities from Density Data

Composition	I	II	III
$\bar{C}_2$	0.25	0.15	0.10
$\bar{C}_2$	0.25	0.30	0.46
$d°$	1.02599	1.02043	1.02292
H_1	0.074218	0.071234	0.67283
H_2	0.041779	0.040814	0.040321
$\bar{V}_1$	21.0788	24.0600	28.0163
$\bar{V}_2$	16.7250	17.6838	18.1757
$\bar{V}_0$	18.0704	18.0611	18.0585
$\bar{C}_0$	54.8159	54.8740	54.7574
m_1	0.25315	0.15173	0.10137
m_2	0.25315	0.30346	0.46629
B_{11}	1.01798	1.01521	1.01655
B_{12}	0.00427	0.00271	0.00186
B_{21}	0.00539	0.00737	0.01321
B_{22}	1.01687	1.01694	1.02225

[a] Units: $\bar{C}_i$, mol/l.; $d°$, g/cc; H_i, 10^{-3} g/mol; $\bar{V}_i$, cc/mol; m_i, molality; B_{ij}, cc/g.

Table IX:[a] Activity Coefficient and Chemical Potential Derivatives

Composition	I	II	III
$\bar{C}_1$	0.25	0.15	0.10
$\bar{C}_2$	0.25	0.30	0.46
Γ_{11}	−0.03043	−0.23414	−0.21586
Γ_{12}	−0.01330	−0.05626	−0.04746
Γ_{21}	0.01995	−0.08438	−0.07119
Γ_{22}	−0.03877	−0.07632	−0.07048
$\mu_{11} \times 10^{-11}$	2.3065	3.1462	3.8386
$\mu_{12} \times 10^{-11}$	0.6836	0.7966	0.7285
$\mu_{21} \times 10^{-11}$	0.6816	0.7956	0.7289
$\mu_{22} \times 10^{-11}$	1.3109	1.2097	0.8878

[a] Units: Γ_{ij}, (molality)$^{-1}$; μ_{ij}, l. ergs/mol^2.

The rather large percentage errors in $\bar{V}_1$ and $\bar{V}_2$ cause no appreciable errors in $(D_{ij})_0$ since the solvent frame transformation eq 2, ref 11, is a second-order correction

Table X:[a,b] Solvent-Fixed Diffusion and Phenomenological Coefficients

Composition	I			II			III		
	Obsd	Error	Predicted	Obsd	Error	Predicted	Obsd	Error	Predicted
$(D_{11})_0 \times 10^5$	0.898	0.030	1.064	0.846	0.030	0.934	0.790	0.030	0.842
$(D_{12})_0 \times 10^5$	0.111	0.030	0.110	0.049	0.030	0.068	0.017	0.030	0.043
$(D_{21})_0 \times 10^5$	0.354	0.030	0.371	0.485	0.030	0.507	0.650	0.030	0.710
$(D_{22})_0 \times 10^5$	1.209	0.030	1.407	1.370	0.030	1.437	1.438	0.030	1.481
$(L_{11})_0 \times 10^{19}$	0.431	0.017	0.516	0.311	0.014	0.339	0.240	0.012	0.249
$(L_{12})_0 \times 10^{19}$	−0.140	0.028	−0.185	−0.164	0.031	−0.167	−0.178	0.041	−0.156
$(L_{21})_0 \times 10^{19}$	−0.141	0.026	−0.185	−0.159	0.014	−0.167	−0.164	0.012	−0.156
$(L_{22})_0 \times 10^{19}$	0.995	0.028	1.170	1.237	0.030	1.298	1.754	0.041	1.796
RR	0.993	0.272	1.000	1.031	0.211	1.000	1.085	0.249	1.000

[a] Units: $(D_{ij})_0$, cm²/sec; $(L_{ij})_0$, mol/(erg cm sec). [b] *RR* (last line) = $(L_{12})_0/(L_{21})_0$.

for dilute solutions. Uncertainties in $(D_{ij})_0$, Table X, are therefore about the same as for D_{ij}, namely, 0.03×10^{-5} cm²/sec. Uncertainties in the chemical potential derivatives μ_{ij} are analogously almost affected by the estimated 0.1% errors in the activity coefficient derivatives Γ_{ij}, since the Γ_{ij} contribute at most about 5% to the values calculated for μ_{ij} (Table IX). Estimated uncertainties in μ_{ij} are about 0.1%, due almost entirely to uncertainties in the molalities m_i.

Values for the phenomenological coefficients $(L_{ij})_0$ in Table II have probable errors shown in Table X. These errors were calculated according to the simplified formulas

$$\delta(L_{ii})_0 = 0.03 \times 10^{-5}(\mu_{jj}^2 + \mu_{ji}^2)^{1/2}/(1000S)$$

$$\delta(L_{ij})_0 = 0.03 \times 10^{-5}(\mu_{ii}^2 + \mu_{ij}^2)^{1/2}/(1000S) \quad (23)$$

$$S = \mu_{11}\mu_{22} - \mu_{12}\mu_{21}$$

Here 0.03×10^{-5}, the uncertainty in each D_{ij}, appears outside the square root radical because that uncertainty is approximately the same for all D_{ij}. Errors in μ_{ij} were considered negligibly small in comparison with errors in D_{ij} and do not appear in eq 23.

The ratio $RR = (L_{12})_0/(L_{21})_0$ should equal unity if the Onsager relation holds. The probable error in *RR* is given in Table X and is to be compared with the absolute value of the difference between 1.00 and the observed ratio *RR*. Within experimental error the Onsager relation is seen to be confirmed for each composition studied here, a result which does not necessarily prove that our diffusion data are accurate, but does give the data some additional credence.

Approximate Theory for Predicting D_{ij} and $(L_{ij})_0$. Values for $(D_{ij})_0$ and $(L_{ij})_0$ from the approximate theory discussed earlier are shown in Table X and are to be compared with observed values in that table. The $(L_{ij})_0$ predicted were calculated according to eq 13 by using the following values[30] for ionic limiting equivalent conductivities: $\lambda_3°(Mg^{2+})$, 53.05 cm/(ohm equiv); $\lambda_4°(Na^+)$, 50.10; and $\lambda_5°(Cl^-)$, 76.35. We used 96,493 C/equiv for the Faraday constant. Predicted values for $(D_{ij})_0$, which are equal to D_{ij} for all practical purposes, were calculated according to eq 14 using predicted $(L_{ij})_0$ and μ_{ij} calculated from data in the literature as discussed previously.

Agreement between predicted and observed values of $(L_{ij})_0$ is remarkably good in most cases, especially for the cross-term coefficients $(L_{12})_0$ and $(L_{21})_0$. Differences between predicted and observed values for the main-term coefficients $(L_{11})_0$ and $(L_{22})_0$ probably result from the drastic assumption that the limiting equivalent conductivities are the same at infinite dilution as they are at finite concentrations; the assumption that the interaction coefficients between the ions are zero probably does not cause much trouble, as has been shown by Miller[18] in his precise analysis of theories for predicting coefficients for several dilute ternary electrolyte systems.

Agreement between predicted and measured values for the D_{ij} is fairly good and the cross-term coefficients D_{12} and D_{21} are predicted almost within experimental error for every system. Trends such as variation of D_{ij} with concentration are predicted qualitatively in all cases. We can conclude that for these solutions of $MgCl_2$ and NaCl in water the approximate theory does a fairly good job on the cross-term coefficients, but at higher concentrations one can expect appreciably larger inaccuracies in the predictions. It should be noted that the predictions of $(L_{ij})_0$ require no thermodynamic activity data for the system, but the D_{ij} do require such data. However, in the concentration ranges studied here it can be shown from data in Table IX that the approximation $\Gamma_{ij} = 0.0$ for all values of $i, j, = 1, 2$ would only make small corrections in the derivatives μ_{ij} used to help calculate the predicted D_{ij}. The theory derived by Gosting[19] would therefore be as approximately accurate as that of Wendt[6] in making the estimates for these D_{ij}.

Summary

Diffusion Experiments. The rotating diaphragm diffusion cell developed for this work seems to us to be

(30) Appendix 6.2, p 465, in Robinson and Stokes, ref 17.

the simplest method yet devised for measuring diffusion coefficients with moderate accuracy. Although it requires calibration, it requires no maintenance or recalibration owing to wear on moving parts. As with all diaphragm cells, the solution concentrations used must be somewhat greater than $C = 0.05\ M$ to avoid solute–porous glass disk interactions, and of course, since our cell is made of plastic it cannot be used with nonaqueous sytems.

For ternary systems studied here we chose to use physical methods of solution analysis instead of chemical methods primarily because of the speed of the former methods. Our particular requirement of linearity between the observed physical difference property z and the solute concentration differences turned out to be somewhat more restrictive than we had anticipated and contained its own built-in limits of accuracy. To obtain high precision in the measurement of Δn, for example, we needed large concentration differences, ΔC_i; but the diffusion coefficients D_{ij} and the increments W_i, such as R_1 and R_2 for the case of refractive index measurements, showed a moderate dependence on ΔC_i (Table IV). Hence the more accurately we measured the difference $z = \Delta n$ (in this example), the less certain we could be that the D_{ij} and R_i were true differential properties instead of some integrated average that depended on ΔC_i. To obtain maximum accuracy in this method for determining D_{ij} the solutions should be analyzed chemically or physically for *each* solute, at the perhaps insurmountable cost of a great number of lengthy analyses. Our entire procedure, therefore, represented somewhat of a compromise with high accuracy to obtain interesting and useful results.

Diffusion Coefficients. The large cross-term coefficients D_{12} and D_{21} measured for each of the H_2O–$MgCl_2$–NaCl compositions studied in this work emphasizes again the magnitude of errors that may be introduced by assuming electrolyte solutes in multicomponent systems diffuse independently. For example, consider a system with average concentrations corresponding to those of composition I and with equal concentration gradients of each solute. Using our results for that composition, we calculate from eq 4 that 89% of the flow of solute 1, J_1, is due to its own concentration gradient and 11% due to the concentration gradient of solute 2. For solute 2 in the same system, 65% of J_2 would be caused by its own concentration gradient and 35% by the equivalent concentration gradient of solute 1. If we ignored the existence of cross-term diffusion coefficients and used a diffusion coefficient for each solute with the same value it had in the corresponding binary systems,[31] namely 1.1×10^{-5} cm^2/sec for $MgCl_2$ and 1.48×10^{-5} for NaCl, the observed flow J_1 would be 10% lower than that predicted from the binary data, and J_2 would be 20% higher than predicted. In lieu of diffusion data for ternary systems, values for D_{ij} predicted from the approximate theory tested here could be readily calculated, but except for very dilute solutions the estimates of all four D_{ij} may introduce more error than the use of Fick's law for each solute.

Acknowledgments. We wish to thank Mr. Clarence W. Schuler and Mr. Joseph C. McPherson of the Physics Department Machine Shop, Louisiana State University (New Orleans), for their assistance in the design and construction of the rotating diaphragm cell. We also thank Dr. C. J. Hebert of the Loyola University Chemistry Department for loaning us his program LRS, a Fortran matrix-inversion subroutine which we included in our iteration program for calculating D_{ij}.

(31) D for $MgCl_2$ is from J. L. Richardson, *et al.*, ref 13; D for NaCl is from Robinson and Stokes, ref 13, Appendix 11.2.

Diffusion Coefficients of Paraffin-Chain Salts and the Formation Energetics of Micelles

by S. P. Wasik and Nina Matheny Roscher

National Bureau of Standards, Washington, D.C. 20234 *(Received January 14, 1970)*

The diffusion coefficients of the colloidal electrolytes decyl, dodecyl, and t tradecyltrimethylammonium bromide have been measured as a function of concentration in aqueous solutions at 25°. These values compared favorably with values obtained from the theoretical expression derived by Hartley. A method is presented for determining the standard Gibbs free energy change of micelle formation from diffusion coefficient *vs.* concentration plots.

In aqueous solutions of paraffin-chain salts there is a tendency for grouping of molecules to take place in which like is associated with like. The nonpolar paraffin chains tend to associate together in some form of fluid arrangement while the polar groups associate with the polar water molecules. These aggregates of molecules, called micelles, fluctuate under the influence of thermal motion and are in equilibrium with neighboring nonaggregated molecules.

A simple form of micelle proposed by Hartley[1] consists of a nearly spherical aggregation of paraffin-chain ions with the hydrophobic part of the ion in the center and the polar part of the outside, the electrical charge of the aggregate being partially neutralized by a number of oppositely charged ions adhering electrostatically to the primary groups. Below the critical micelle concentration, cmc, the paraffin-chain salt essentially behaves as a strong electrolyte.

Experimental methods for investigating this phenomenon have varied widely; conductivity, solubilization, light scattering, viscosity, and other physical properties have been reported. Many of these measurements involve application of an external force, or an additive to the paraffin-chain salt solution. Such application of an external agent is liable to vitiate the results as far as calculations of size, shape, and structure of the micelles are concerned.

Diffusion measurements by a free-boundary method provide a sensitive and accurate means of investigating the properties of micellar solutions without extraneous additives and without the limitations imposed by the use of glass disks or porous plates. Although little work has been reported[2,3] using this technique it appears to be a good method for studying the physical properties of micellar solution.

Hartley derived an expression for the diffusion of an aggregating electrolyte in the transition range from simple to colloidal solution[4] which predicted that the diffusion coefficient should go through a very low minimum in the region where the paraffin-chain salt goes from the simple to the colloidal form. Hartley lacked detailed knowledge of his compounds to treat his results adequately. Since then light scattering techniques have been developed for measuring the aggregation number and effective charge of the micelle, and it is now possible to evaluate the Hartley diffusion expression explicitly.

In this report are presented diffusion measurements on aqueous solutions of the decyltrimethylammonium bromide, $C_{10}Br$, dodecyltrimethylammonium bromide, $C_{12}Br$, and tetradecyltrimethylammonium bromide, $C_{14}Br$, by a free-boundary method. Hartley's expressions for the diffusion coefficient concentration relationship is shown to explain adequately the experimental data. A method is presented for calculating the standard free-energy change from these measurements.

Experimental Section

The alkyl bromides, obtained from the Fisher Scientific Co., were fractionally distilled through a Piras-Glover spinning-band column, 60 cm in length. The center cuts having the same refractive index were used for the preparations. The *n*-alkyltrimethylammonium bromides were prepared by refluxing an excess (10%) of freshly distilled trimethylamine with the alkyl bromide in methyl alcohol for several hours. The excess alcohol and trimethylamine were removed by distillation at room temperature under reduced pressure. The quaternary ammonium bromides were then recrystallized four or five times from different solvents. Analyses for bromide content agree with the theoretical amount within experimental precision.

(1) G. S. Hartley, "Aqueous Solutions of Paraffin-Chain Salts," Hermann, Paris, 1936.

(2) N. Bindney and L. Saunders, *J. Pharm. Pharmacol.*, **7**, 1012 (1955).

(3) R. Parker and S. Wasik, *J. Phys. Chem.*, **63**, 1921 (1959).

(4) G. S. Hartley, *Trans. Faraday Soc.*, **35**, 1109 (1939).

The cell used for the diffusion experiments and the experimental technique have been described in detail by Longsworth.[5] A sharp, plane, horizontal boundary between two solutions of different concentrations was formed in a rectangular cell. The subsequent concentration distribution at the boundary was observed with a Rayleigh interference optical system. The temperature of the water bath in which the cell was immersed during the measurements was controlled at 25 ± 0.005°. Photographs of the interference patterns were taken on glass plates. About forty measurements of the refractive index of the solution as a function of distance in the cell were made for each pattern with a two-dimensional comparator. The relation between the refractive index and the concentration of the solution was determined with a differential refractometer using dextrose (National Bureau of Standards Standard Sample No. 41) as the standard. From these data the concentration distribution was calculated.

The calibration of the interferometer was checked by measuring the diffusion coefficient of dextrose in aqueous solution at 25°. The experimental technique and calculation procedure were those used by Longsworth.[6] The diffusion coefficient of dextrose in a solution of concentration 0.380 g/100 cm³ obtained in six separate measurements was (6.729 ± 0.006) × 10^{-6} cm²/sec compared with the value of (6.728 ± 0.006) × 10^{-6} cm²/sec measured by Longsworth.[6] The zero-time correction in these experiments was less than ±10 sec.

The diffusion coefficients for the paraffin-chain salts were calculated from the general differential equation for a unidirected diffusion process

$$\frac{\partial C}{\partial t} = \frac{\partial}{\partial x}\left(D\frac{\partial C}{\partial x}\right) \tag{1}$$

where C = concentration, t = time, x = distance in the direction of diffusion, D = diffusion coefficient. If diffusion is studied at a liquid junction between two solutions of different concentrations, the boundary conditions which are imposed upon the solution of the diffusion equation are that at $t = 0$, for $x < 0$, $C = C_1$, and for $x > 0$, $C = C_2$ where $C_1 < C_2$. It is assumed that the concentrations at large values of x in the diffusion cell are unaltered during an experiment. With these restrictions, no general solution for eq 1 has been obtained. However, if it is assumed that $x/\sqrt{t} = \sigma$, where σ is a function of C only, eq 1 can be transformed and integrated at constant t to give

$$D = -\left(2t\frac{\partial C}{\partial x}\right)^{-1}\int_{C_1}^{C} x\,dC \tag{2}$$

D in this case is a differential diffusion coefficient corresponding to the definite concentration C rather than an integral coefficient appropriate to the range of concentration, C_1 to C. This calculation is valid only if $(x\sqrt{t_C})$ is constant during the experiment.[3]

The evaluation of the diffusion coefficient from eq 2 requires a simultaneous determination of C, x, and dC/dx at time t. This was done by measuring two of the quantities and calculating the third. Data for C as a function of x were differentiated to obtain dC/dx as a function of C and x. The integral $\int_{C_1}^{C} x\,dC$ in eq 2 was evaluated graphically for each of the experimental points. Since the free boundary experiments do not begin at zero time but effectively at a greater time, there is an error of about 1% in the calculated values of D.

Discussion and Results

To describe the diffusion of an aggregating electrolyte in the transitional range from simple to colloidal solution, Hartley[4] derived the following expression

$$\frac{DF^2}{RT} = \lambda_-^0 - \frac{dC_M}{dC}\left(\lambda_+^0 - \frac{\lambda_M^0}{Z}\right) + \frac{\lambda_-^0 + \lambda_+^0 - \frac{dC_M}{dC}\left(\lambda_-^0 + \theta\lambda_+^0 - \lambda_M^0 + \frac{\theta\lambda_M^0}{Z}\right) \times \left[\left(1 - \frac{C_M}{C}\right)\lambda_+^0 + \frac{C_M}{C}\lambda_M^0\right]}{\lambda_-^0 + \lambda_+^0 - \frac{C_M}{C}(\lambda_-^0 + \theta\lambda_-^0 + \lambda_+^0 - \theta\lambda_M^0)} \tag{3}$$

where λ_-^0, λ_+^0, and λ_M^0 are the equivalent conductance of the counterion, the paraffin-chain ion, and the micelle, respectively; $1 - \theta$ is the fraction of the charge of each micelle neutralized by the association of gegenions. Z is the charge of the micelle, F is the Faraday charge, C is the concentration of the whole electrolyte in equivalents per unit volume calculated without regard to association.

The micelle concentration, C_M, is expressed as

$$C_M = C - C_1$$

where C_1 is the univalent concentration of the unassociated paraffin ion. This equation was derived on classical lines without introducing any thermodynamic or mobility corrections. It is valid only for dilute solutions.

The quantities of dC_M/dC and C_M/C were calculated from the expression for the equilibrium between single ions and micelles

$$C_M K_M = (C - C_M)^m\left(C - \frac{m - p}{m}C_M\right)^{m-p} \tag{4}$$

where K_M is the equilibrium constant, m is the number of paraffin-chain ions per micelle, and p is the effective

(5) L. G. Longsworth, *J. Amer. Chem. Soc.*, **74**, 4155 (1952).
(6) L. G. Longsworth, *J. Phys. Chem.*, **58**, 770 (1954).

charge. Phillips[7] justified using concentration instead of activities in eq 4 by substituting an effective charge for the real charge.

The effective charge, p, may be calculated from the limiting slope of the HC/τ *vs.* C plot, H being the Einstein constant, τ the turbidity and C the micelle concentration.[8] Since p can be explained in terms of the Donnon concept and the fluctuation theory, it is not the real charge, Z, but rather an equivalent ideal charge. It may be interpreted as an activity coefficient. With this implication the double-layer interaction of a micelle ion of actual valence Z is equivalent in behavior to an ideal ion of valence p.

Calculations of C_M/C and dC_M/dC may be simplified by defining a concentration C_0 by the following relation

$$K_M = C_0^{2m-p-1}$$

and the dimensionless quantities $S = (C_M/C)$, $\bar{C} = C/C_0$. Substituting S and $\bar{C}$ into eq 4

$$\bar{C}^{2m-p-1} = S/(1-S)^m\left(1 - \frac{m-p}{m}S\right)^{m-p} \quad (5)$$

Thus $\bar{C}$ may be calculated for given values of S, m, and p. Since

$$C = \bar{C}C_0$$

and

$$C_M = S\bar{C}C_0$$

$$\bar{C}\frac{dS}{d\bar{C}} = \left(\frac{dC_M}{dC} - S\right) \quad (6)$$

From eq 5

$$\frac{dS}{d\bar{C}} = \frac{2m-p-1}{\bar{C}\left[\frac{1}{S} + \frac{m}{1-S} + \frac{(m-p)^2}{m-(m-p)S}\right]} \quad (7)$$

Combining eq 6 and 7 and rearranging terms

$$\frac{dC_M}{dC} = \frac{2m-p-1}{\frac{1}{S} + \frac{m}{1-S} + \frac{(m-p)^2}{m-(m-p)S}} + S \quad (8)$$

The quantity dC_M/dC was calculated for different values of S using values of m and p reported by Debye[8] and Wasik and Hubbard[9] from light scattering measurements on decyltrimethylammonium bromide, dodecyltrimethylammonium bromide, and tetradecyltrimethylammonium bromide solutions.

The equivalent conductance of the paraffin-chain ion, λ_+^0, was calculated from limiting conductance values reported by Scott and Tartar[10] using a value of 78.2 (mol ohm cm)$^{-1}$ for the ion conductance of the bromide ion.

Values for the micelle conductance were calculated from the electrophoretic mobility measurements of

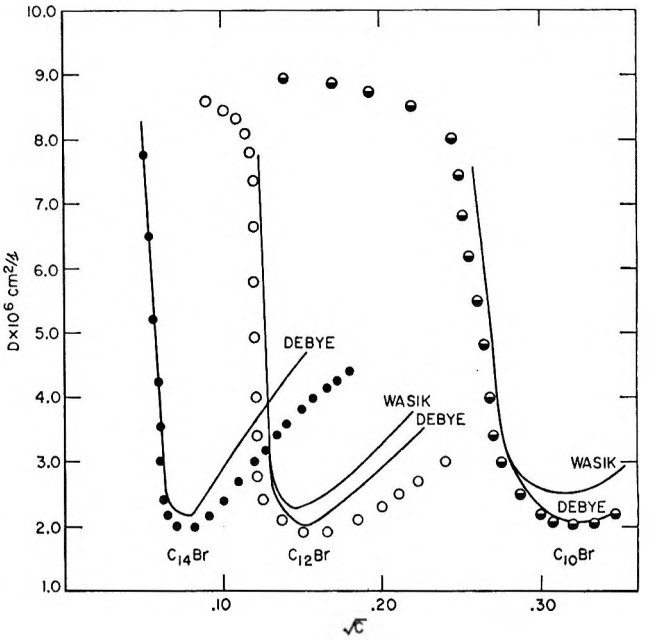

Figure 1. Experimental plots of diffusion coefficient against concentration for decyltrimethylammonium bromide, $C_{10}Br$, dodecyltrimethylammonium bromide, $C_{12}Br$, and tetradecyltrimethylammonium bromide, $C_{14}Br$, and the theoretical plots from eq 3 using Debye's and Wasik and Hubbard's data.

decyl-, dodecyl- and tetradecylamine hydrochloride micelles by Hoyer and Greenfield.[11] These authors state that micelles of paraffin-chain salts of the same carbon chain have essentially the same mobility *vs.* concentration behavior. Although values for the mobility of the $C_{10}Br$, $C_{12}Br$, and $C_{14}Br$ micelles obtained by this method are only an approximation, they do not seriously affect the shape of the theoretical diffusion–concentration plots.

From eq 3 and 8 the theoretical diffusion coefficient was calculated as a function of $\sqrt{C}$. In order to compare the theoretical with experimental plots, a value for C_0 had to be estimated by assigning values of C_0 until the two curves gave a good fit. The value for C_0 in all cases was close to the concentration where $dD/d\sqrt{C}$ was a maximum. In Figure 1 are shown the experimental plots for $C_{10}Br$, $C_{12}Br$, and $C_{14}Br$ along with the theoretical plots from the data given in Table I. The theoretical curves calculated from Debye's[8] values for m and p gave better agreement than those of Wasik and Hubbard[9] because apparently Debye's values for p are the correct values. The minima of the theoretical curves were very sensitive to p and fairly insensitive to m.

(7) J. N. Phillips, *Trans. Faraday Soc.*, **51**, 561 (1955).

(8) P. Debye, *Ann. N. Y. Acad. Sci.*, **51**, 575 (1949).

(9) S. Wasik and W. Hubbard, *J. Res. Nat. Bur. Stand.*, **68A**, 539 (1964).

(10) A. B. Scott and H. V. Tartar, *J. Amer. Chem. Soc.*, **65**, 692 (1943).

(11) W. H. Hoyer and A. Greenfield, *J. Phys. Chem.*, **61**, 735 (1957).

Table I: The Standard Gibbs Free Energy Change, $\Delta G°$, per Molecule Associated with Micelle Formation for the Paraffin Salts Decyltrimethylammonium Bromide, $C_{10}Br$, Dodecyltrimethylammonium Bromide, $C_{12}Br$, and Tetradecyltrimethylammonium Bromide, $C_{14}Br$, Calculated from Eq 9 and 10 for Debye's and Wasik, and Hubbard's Values, for the Number of Paraffin-Chain Ions per Micelle, m, and the Effective Charge, p

Salt	m^a	p^a	m^b	p^b	$\frac{-\Delta G°}{kT}$ [c]	$\frac{-\Delta G°}{kT}$ [d]	$\frac{-\Delta G°}{kT}$ [e]	C_0, mol cm^{-3}
$C_{10}Br$	36	9	31	6.6	11.3	11.4	11.5	0.0767
$C_{12}Br$	50	10.5	55	13.5	14.3	14.3	14.1	0.0164
$C_{14}Br$	75	10.5			17.9	17.8		0.0036

[a] Debye.[8] [b] Wasik and Hubbard.[9] [c] Equation 10, Debye's data. [d] Equation 9, Debye's data. [e] Equation 9, Wasik and Hubbard's data.

The "valley" in the diffusion coefficient–concentration plots results from the fact that dC_M/dC increases much faster than C_M/C. Since λ_+^0 is much bigger than λ_M^0/Z, an increase in dC_M/dC will cause a decrease in the second term of eq 3. In the transition region the third term at first decreases when aggregation begins and subsequently increases. The overall effect is that in general the diffusion coefficient should decrease followed by a rise at higher concentration. A mimimum in the D *vs.* $\sqrt{C}$ plots for associated colloids has previously been reported for sodium dodecyl sulfate[2] and dodecyltrimethylammonium chloride.[3]

Standard Free Energy Change

The standard Gibbs free energy change, $\Delta G°$, per molecule associated with micelle formation may be calculated from the expression

$$\Delta G° = \frac{kT}{m}(2m - p - 1) \ln C_0 \qquad (9)$$

The value of $\Delta G°$ depends on the standard states chosen. If the concentrations are expressed in mole fraction then $\Delta G°$ would be with reference to a state of mole fraction unity.

In Table I are given $\Delta G°$ values calculated from eq 9 using values for C_0 obtained from the diffusion experiments and values of m and p obtained by Debye[8] and Wasik and Hubbard.[9]

Phillips[7] has derived the following expression for the Gibbs free energy change

$$\frac{\Delta G°}{kT} = \frac{\ln 3 + 2 \ln m}{m} + \frac{2m - p - 1}{m} \ln \text{cmc} \qquad (10)$$

where cmc is the critical micelle concentration. This equation was derived by defining the cmc as the point corresponding to the maximum change in gradient in an ideal property-concentration (ϕ against C) relationship, being given by

$$\left(\frac{d^3\phi}{dC^3}\right)_{C=\text{cmc}} = 0$$

Phillips assumed that there exists an equilibrium between the single ions and the micelles and that the micelles are effectively monodispersed. In Table I are given $\Delta G°$ values for $C_{10}Br$, $C_{12}Br$, and $C_{14}Br$ calculated by Phillips from light scattering data of Debye.[8]

The close agreement between the $\Delta G°$ values calculated from Phillip's expression and those obtained from eq 9 lend further support to Hartley's model of the micelle. Both expressions were derived from the assumption that there exists an equilibrium between the single ions and the micelle and that the micelles are effectively monodispersed. The method presented in this report for calculating $\Delta G°$ requires no knowledge of how the cmc should be defined. This is an advantage since the cmc is probably a range of concentration.

The experimental measurements of D and theoretical values derived from light scattering and conductivity data agree well up to the concentration for the minimum value of D (see Figure 1). Above this value the agreement is poor. The likely explanation is a change in the character of the aggregates. Micelles are statistical in character; they are constantly being formed and broken up by thermal motion. They cannot be thought of as persistent entities having well defined geometrical shapes. Hartley's[1] model for the micelle as a spherical aggregate of amphiphilic molecules with the polar groups on its surface and the hydrocarbon chains forming a fluid core is probably valid at low concentrations. At higher concentrations it is replaced by more extended micellar forms. Equation 3 is valid for the diffusion of an aggregating electrolyte in the transition range from simple ion to a Hartley-like micelle. It does not take into consideration a more extended micellar form. This may be partly the reason why the agreement between the theoretical and experimental curves in Figure 1 is not as good at higher concentrations as it is at concentrations near the cmc.

Acknowledgment. We wish to thank Dr. Frederick Mies for his suggestions and his help with the mathematics in this paper.

The Temperature Dependence of the Transmission Coefficient (T_S) for Carbon Dioxide Transport across A Series of Long-Chain Alcohol Monolayers

by J. G. Hawke[1] and I. White

Physical Chemistry Laboratories, Department of Pharmaceutical Chemistry, University of Sydney, Sydney, Australia
(Received June 9, 1969)

The temperature dependence of the transmission coefficients (T_s) for carbon dioxide gas across a series of long-chain alcohols from C_{16} to C_{22} has been measured. Radioactive carbon-14 labeled CO_2 was used to follow the loss of gas from the unstirred aqueous solutions. Monolayers were spread on the gas–liquid interface to their equilibrium spreading pressures (π_s). The diffusion curves were analyzed according to the mathematical model proposed by Hawke and Parts. The transmission coefficients were of the same order as those found by other workers for CO_2 through similar compounds. However, La Mer found values for water to be about 40 times greater reflecting the smaller size of the water molecule. The nonlinear decrease in permeability with increase in chain length would not be expected if Fickean type diffusion was involved. The activation energies found here (*ca.* 12 kcal/mol) are comparable with those found by La Mer for water transport and support the energy barrier theory which equates the activation energy with the energy to form a hole in the monolayer. The increment of E per CH_2 group of 320 cal/mol also agrees with the water tr nspo t work and the value of 400 cal/mol predicted from considering the Loudon–van der Waals dispersion forces between parallel hydrocarbon chains. The energy barrier theory again would predict an increased barrier height accompanying an increase in monolayer thickness. The data presented here are therefore consistent with the transportation of the CO_2 molecule, through the monolayer in a single-step process, rather than a series of jumps, as required by the Fickean diffusion mechanism.

Introduction

The influence of monolayers at the gas–liquid interface on the loss of various gases from their aqueous solution has been studied extensively in this group. This paper deals with the effect of temperature on the permeability of a homologous series of long-chain alcohols to CO_2 gas. La Mer and coworkers[2-5] in a series of papers have examined the permeability of a series of long-chain fatty acids and alcohols to water, following the classical work of Langmuir and Schaefer.[6] These authors report considerably lower permeabilities for monolayers in their close-packed configuration compared with the expanded state. They have also measured the temperature dependence of the permeability to water. Following Glasstone, Laidler, and Eyring's[7] reasoning, the overall activation energy for each methylene group, terminal methyl group, and residual polar head group has been calculated. Barnes and La Mer[3] suggest the data support Langmuir's energy barrier model consisting of a single-step permeation process. We have applied similar reasoning to the results obtained here for the permeation of monolayers by CO_2 gas. Blank[8] criticizes certain aspects of the energy barrier theory such as its inability to account for the high permeability of expanded monolayers and suggests a fluctuating density model might account for these difficulties. Hawke and coworkers[9-12] have examined the permeability of monolayers to CO_2 and H_2S gases at constant temperature and find in common with the results for water permeability that a close-packed configuration is necessary to achieve a high resistance to gas permeation. Values for the permeability in the CO_2 case we expressed as the transmission coefficient were about 40 times smaller than those found for water vapor. Here the transmission coefficient (T_s) is defined as the surface emissivity in grams of gas per second per square centimeter of sur-

(1) Department of Chemistry, Macquarie University, Sydney, Australia, 2113; to whom communications should be addressed.

(2) (a) R. J. Archer and V. K. La Mer, *J. Phys. Chem.*, 59, 200 (1955); (b) H. L. Rosano and V. K. La Mer, *ibid.*, 60, 348 (1956).

(3) G. T. Barnes and V. K. La Mer in "Retardation of Evaporation by Monolayers," V. K. La Mer, Ed., Academic Press, New York, N. Y., 1962, p 9.

(4) M. Blank and V. K. La Mer, ref 3, p 59.

(5) V. K. La Mer, T. W. Healy, and L. A. G. Aylmore, *J. Colloid Sci.*, 19, 448 (1964).

(6) I. Langmuir and I. J. Schaefer, *J. Franklin Inst.*, 235, 119 (1943).

(7) S. Glasstone, K. J. Laidler, and H. Eyring, "The Theory of Rate Processes," McGraw-Hill, New York, N. Y., 1941, pp 8, 195, and 510 ff.

(8) M. J. Blank, *J. Phys. Chem.*, 68, 2793 (1964).

(9) J. G. Hawke, *Aust. At. Energy Symp. Proc., Sydney, 198*, 634 (1958).

(10) J. G. Hawke, Ph.D. Thesis, University of Sydney, 1959.

(11) J. G. Hawke and A. E. Alexander, ref 3, p 67.

(12) J. G. Hawke and A. G. Parts, *J. Colloid Sci.*, 20, 253 (1964).

face area when the gas concentration at the surface is 1 g cm^{-3}. Hawke and Wright,[13] and also Princen and Mason[14] using soap bubbles, find the expanded positively charged long-chain quaternary ammonium compounds offer measurable resistance to CO_2 and O_2 transfer, respectively. However, it is probably not very meaningful to extrapolate linearly from the soap film results to those from insoluble monolayers. In these films having the chains well separated the activation energy calculated from the temperature dependence of the transmission coefficients (T_s) may be compared with the contribution of the head group in uncharged systems. Hawke and White[15] have recently reported an activation energy for the diffusion of CO_2 through the C_{18} alcohol. This value was in close agreement with the value for water transport measured in the late La Mer's laboratory,[4] although Blank[16] has found a much smaller activation energy for the penetration of 1-octadecanol by CO_2 from the gas phase. In this paper we report an extension of this investigation to a homologous series of long-chain alcohols.

Experimental Section

The construction of the apparatus used for the diffusion experiments has been described in detail by White[17] and is illustrated in the line diagram labeled Figure 1. The gold-plated diffusion cell (c) has a depth of 0.400 cm and is thermostated by circulating methanol from a Calora KT, 10K refrigerated apparatus through the cavity D. The temperature of the cell measured by means of an iron–constantan thermocouple was found to vary by not more than $\pm 0.1°$. The whole apparatus was placed inside a glove box and surrounded by a CO_2-free atmosphere whose temperature did not vary by more than $\pm 2°$ during a run. The stock solutions used to fill the cell were kept inside the glove box.

The Diaphragm. The diaphragm B consisted of self-indicating soda-lime powder, stuck onto thin polythene sheet, to absorb the CO_2. The rate of uptake of CO_2 by the absorber was tested by introducing CO_2 below the diaphragm. The count rate from the G.M. counter, A, rose to a new level within the time constant of the rate meter (5 sec). The irreversibility of absorption was tested by passing nitrogen gas over the radioactive diaphragm for 30 min and carbon dioxide gas for 60 hr. In both cases the count rate from the previously absorbed CO_2 remained constant. The capacity of the diaphragm to absorb further CO_2 was checked at the end of a diffusion run and found to be satisfactory.

CO_2 Concentration. The solution was prepared by adding dilute HCl to 0.44612 g of barium carbonate containing 0.775% of carbon-14 labeled barium carbonate (Amersham specific activity 37.8 mCi/mmol) and passing the liberated CO_2 into 1 l. of 0.01 N HCl solution. If this process was 100% efficient, the concentration would then be 10^{-3} M in CO_2. However,

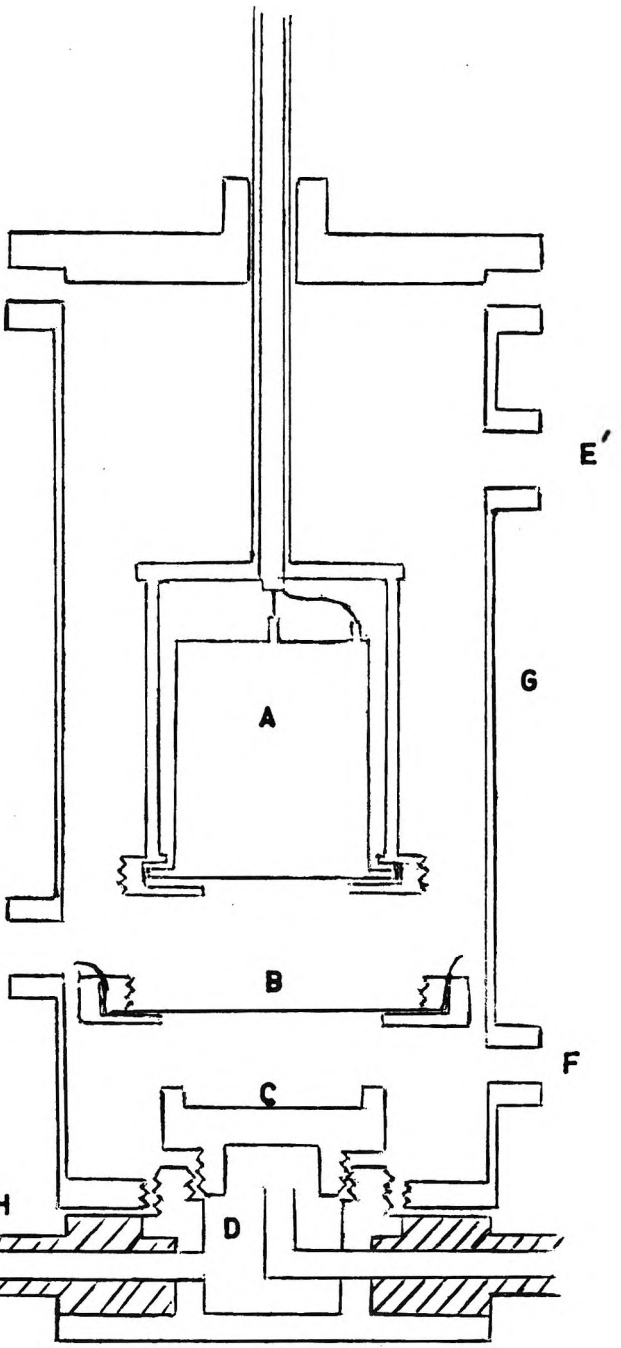

Figure 1. Line diagram of diffusion apparatus.

the concentration falls as the dead space increases in the flask. The concentration of CO_2 was measured by the method of Harlan[18] using a Packard Tri-carb liquid scintillation spectrometer, series 3003, and found to be $(1 \pm 0.5) \times 10^{-4}$ M.

No-Film Experiments. Diffusion experiments were carried out without monolayers to determine the appli-

(13) J. G. Hawke and H. J. D. Wright, *Nature*, 212, 810(1966).
(14) H. W. Princen and S. G. Mason, *J. Colloid Sci.*, 20, 353 (1965).
(15) J. G. Hawke and I. White, *J. Phys. Chem.*, 70, 3369 (1966).
(16) M. Blank, ref 3, p 75.
(17) I. White, MSc. Thesis, University of Sydney, 1966.
(18) J. W. Harlan, *Atomlight*, 19, 8 (1961).

cability of the mathematical model proposed by Hawke and Parts[12] to this system. Since Harvey and Smith[19] have shown that a clean water surface offers no measurable resistance to CO_2 absorption into unstirred solutions, these experiments were compared with the $N = \infty$ curve calculated from the theory. The curves for various temperatures can be made to fit by adjusting the value for the diffusion coefficient of CO_2 in water. Table I gives the results obtained compared with the best data available which have been reviewed by Himmelblau.[20] In this paper we have used the adjusted diffusion coefficients owing to the close fit obtained between the experimental curves and the theoretical. Considerable variation is apparent in the reported values for the diffusion coefficient of CO_2 in water. These variations are presently being investigated.

Table I: Comparison of "Fitted" Diffusion Coefficients and Those Given in the Literature

	Temp, °C			
	0.1	5.1	10.0	15.0
Literature values of diffusion coefficient, $cm^2\ sec^{-1} \times 10^5$	0.96 ±0.1	1.00 ±0.1	1.28 ±0.15	1.45 ±0.18
"Fitted" diffusion coefficient ($cm^2\ sec^{-1} \times 10^5$)	0.99 ±0.1	0.98 ±0.1	1.46 ±0.1	1.87 ±0.2

Table II: Result of Agar–Agar Gel Experiment Compared with "No-Film" Experiment at 0.1° and Theoretical Values for $N = \infty$, $D = 0.993 \times 10^{-5}\ cm^2\ sec^{-1}$, $a = 0.254$ cm

D_t/a^2	M_t/M_∞ (Agar gel) ±0.01	M_t/M_∞ ("no film") ±0.007	M_t/M_∞ (theoret)
0.009	0.063	0.055	0.062
0.018	0.121	0.120	0.117
0.027	0.155	0.155	0.155
0.036	0.190	0.200	0.200
0.045	0.218	0.235	0.228
0.054	0.247	0 260	0 252
0 063	0.264	0.282	0.280
0.072	0.287	0.297	0.300
0.080	0.305	0.314	0.319
0.089	0.322	0.335	0.336
0.107	0.356	0.370	0.366
0.134	0.408	0.419	0.408
0.161	0.433	0.462	0.450
0.179	0.471	0.483	0.471
0.197	0.500	0.513	0.508
0.224	0.534	0.549	0.540
0.250	0.575	0.575	0.565
0.268	0.598	0.594	0.588
0.286	0.615	0.616	0.603
0.313	0.645	0.644	0.628
0.340	0.661	0.665	0.654
0.358	0.678	0.685	0.672
0.402	0.713	0.715	0.707
0.447	0.741	0.750	0.738
0.492	0.764	0.776	0.764
0.536	0.793	0.805	0.787
0.626	0.839	0.840	0.830
0.715	0.862	0.870	0.862
0.805	0.885	0.900	0.889

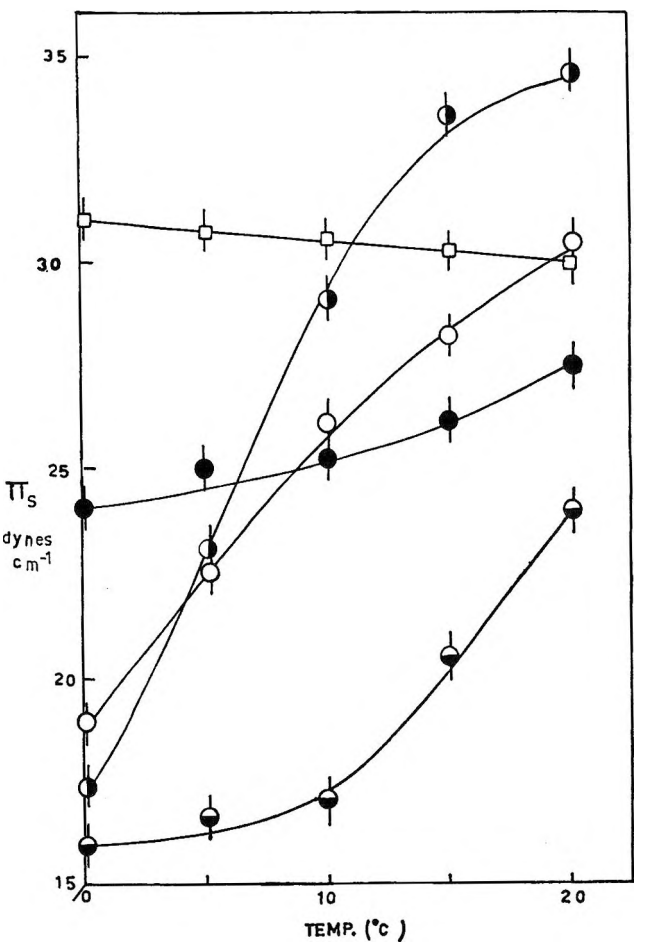

Figure 2. Dependence of spreading pressure (π_s) on temperature: hexadecanol, ◑; octadecanol, ○; N-eicosanol, ●; N-docosanol, ◒; oleic acid, □.

Convection. Evidence for the absence of convection in this system is provided by no-film runs using 0.8% agar–agar gel. The solution was introducted into the cell as a viscous liquid which set rapidly to a gel. The results are listed in full in Table II together with the corresponding results for both a no-film run and values calculated from the $N = \infty$ curve. The agreement is satisfactory within experimental error. The principal error in the gel experiments was introduced by the uncertainty of the depth measurements.

Monolayer Experiments. Materials. The hexadecanol and octadecanol were purchased from the Applied Science Laboratories Inc., State College, Pa., the eicosanol from K & K Laboratories, New York, N. Y., and the docosanol from Koch Light Laboratories, Bucks, England. The C_{16}, C_{18}, and C_{20} compounds were

(19) E. A. Harvey and W. Smith, *Chem. Eng. Sci.*, **10**, 274 (1959).
(20) D. M. Himmelblau, *Chem. Rev.*, **64**, 527 (1964).

shown to be greater than 99.5% pure and the C_{22} compound better than 98% by vapor phase chromatography, no other peaks being observed. The laboratory distilled water was redistilled over alkaline $KMnO_4$ and then double-distilled in quartz. The water then had a conductance at 25° of $2.1 \pm 0.1 \times 10^{-6}$ cm^{-1} and was found to contain less than 10 ppm of organic impurities from radiation dosimetry experiments using ceric sulfate. The nitrogen gas was purified by passing through a liquid air trap, followed by a Linde 5A molecular sieve trap.

Spreading of Monolayers. All compounds were spread by injecting 7×10^{-3} ml of a 1 mg/ml solution in petroleum (bp 40–50°) ether. This quantity was sufficient to cover the surface of the cell with a monolayer *ca.* 1.5 times. The equilibrium spreading pressure (π_s) was reached in all cases 0.5 sec after injection. The completeness of spreading of the monolayer was demonstrated by successive additions of a solution of the compound in petroleum ether to a surface balance. The π/A curve so obtained gave a close-packed area of 19.5 Å^2 molecule^{-1}. Any excess compound present must therefore exist in negligibly small islands. To determine the dependence of the equilibrium surface pressure on temperature, measurements were carried out for each compound in the diffusion cell itself using a vertical platinum plate and torsion balance. The results are shown in Figure 2.

Results

Transmission Coefficients for the Alcohol Monolayers. Values of the transmission coefficient (T_s) are shown in Table III for the temperature range 0.1–15°. These results were then plotted according to the Arrhenius equation as shown in Figure 3. Least-squares calculations from these points gave the values shown in Table IV for the slopes and intercepts for each chain length. Barnes and La Mer[3] give an equation which is the two-dimensional analog of Glasstone, Laidler, and Eyring's[7] equation for the transition state for reactions in the gas phase. These authors have applied this theory extensively to permeability for water through these monolayers and have expressed the permeability P as

$$P = C \exp[\Delta S^{\pm}/R - (\pi_s N_0 A^{\pm}/RT) - (E^{\pm}/RT)]$$

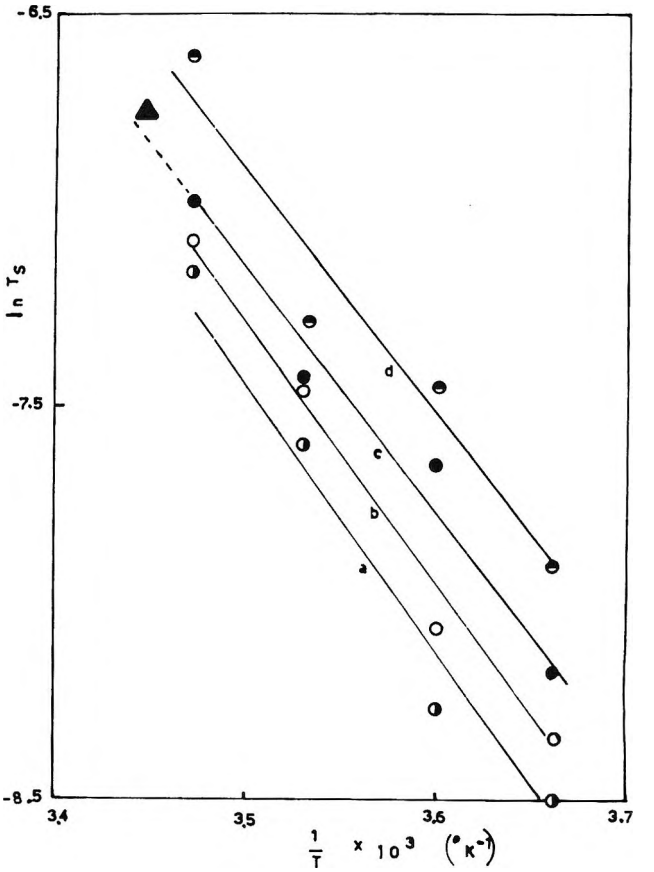

Figure 3. Arrhenius plot of transmission coefficients of alcohol monolayers to carbon dioxide: C_{22} alcohol, ◑; C_{20} alcohol, ○; C_{18} alcohol, ●; C_{16} alcohol, ◓. Value obtained by Blank (1962) for C_{18} alcohol (diffusion from gas to liquid), ▲.

Table III: The Transmission Coefficients of the Monolayers of the C_{16}, C_{18}, C_{20} and C_{22} Alcohols to CO_2

Alcohol	Transmission coefficient, ($10^4 \times$ cm sec^{-1}) 0.1°	5.1°	10.0°	15.0°
C_{16}	3.7	5.9	7.0	13.6
C_{18}	2.8	4.8	5.9	9.3
C_{20}	2.4	3.0	5.8	8.5
C_{22}	2.0	2.6	4.9	7.8

Table IV: Values of $-(\pi_s N_0 A^{\pm} + E^{\pm})$ and $C \exp(\Delta S^{\pm}/R)$ for the Alcohol Monolayers Calculated from the Slopes and Intercepts listed

Alcohol	C_{16}	C_{18}	C_{20}	C_{22}
Slope ($\times 10^3$)	6.0	6.3	6.7	6.8
Intercept	14.9	13.6	16.9	18.2
$-(\pi_s N_0 A^{\pm} + E^{\pm})$, kcal/mol	12.0	12.6	13.3	13.7
$C \exp(\Delta S^{\pm}/R)$, cm/sec	3×10^6	1×10^6	2×10^7	8×10^7

The slopes in Table IV were equated to the term $[-(\pi_s N_0 A^{\pm}/R) - (E^{\pm}/R)]$ and the intercepts to the term $C \exp(\Delta S^{\pm}/R)$. Here $\Delta S^{\pm}$ and $E^{\pm}$ are the entropy and energy of activation, respectively, $N_0 A^{\pm}$ is the area of activation per mole or the increase in area per mole of activated states caused by the formation of free sites, π_s is the surface pressure, and C is the constant which Moore and Eyring[21] suggest depends only on the cross-sectional area of the permeant.

Since the experiments were not done at constant π_s a mean value was chosen and the value of $A = 25$ Å^2

(21) W. J. Moore and H. Eyring, *J. Chem. Phys.*, 6, 381 (1938).

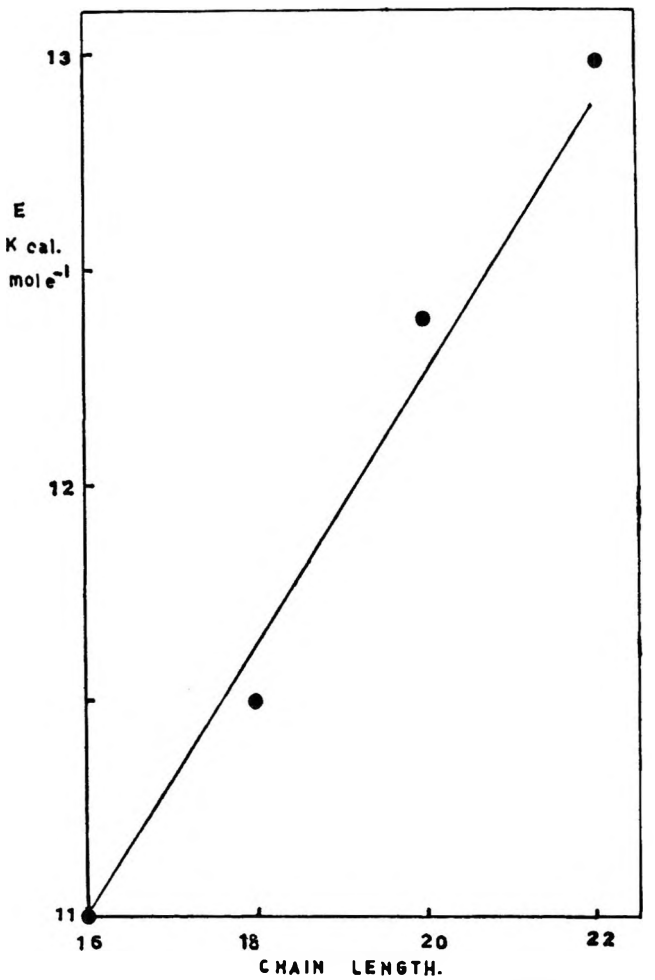

Figure 4. The increase in activation energy for CO_2 diffusion through a series of long-chain alcohol monolayers.

used was that found by Princen and Mason[14] and Hawke[10] for CO_2 permeability through monolayers. Also E, the experimental activation energy, was assumed to be equal to $E^{\ddagger}$. The activation energy per methylene group was then calculated from a plot of E against the number of carbon atoms in the alcohol. This is shown in Figure 4 and gave a value of 320 cal/mol. The residual energy calculated from this value is 6.5 kcal/mol and is in excellent agreement with Barnes and La Mer's determination, namely 6.46 kcal/mol, for the permeability of the C_{16} and C_{18} alcohols to water.

Discussion

Transmission Coefficients. The transmission coefficients found in this work are of the same order of magnitude[16,22] as those found by other workers for CO_2 through similar compounds after correcting for concentration differences. Values found for water in La Mer's laboratory were about 40 times greater and reflect the smaller size of the water molecule and its greater solubility in the monolayer.

The nonlinear decrease in permeability with increase in chain length supports the energy-barrier theory rather than the alternative Fickean diffusion.

Entropy of Activation. If, as Moore and Eyring[21] suggest, the constant C only depends on the cross-sectional area of the permeant, the entropies of activation for various monolayers can be compared by using the same permeant. The preexponential terms listed in Table IV indicate an entropy of activation an order of magnitude lower than that found for water transport and may reflect the greater degree of organization of water in the latter case, and perhaps the greater steric requirements of the activated state in the case of the linear CO_2 molecule.

Activation Energies. The activation energies for the transport of CO_2 through monolayers of hexadecanol and octadecanol are similar to the values obtained by Barnes and La Mer[3] for water transport through the same monolayers. So it appears that the energy barrier theory is correct in its assumption that the activation energy for the penetration process is simply the energy required to form a hole in the monolayer and is not dependent on the size of the permeant. The increment of activation energy per methylene group of about 320 cal/mol is also in good agreement with the water transport work and the value of about 400 cal/mol predicted from considering the London–van der Waals dispersion forces between parallel hydrocarbon chains.[23] If it can be assumed as in the energy-barrier theory that permeating gas molecules must form a hole in the monolayer by collisions of sufficient kinetic energy, then it is not surprising that an increase in the thickness of the monolayer causes an increase in the height of the energy barrier.

Since the activation energy is equal to the energy required to create a lattice vacancy in the monolayer, it should be equal to the energy required for the desorption of a monolayer molecule from the surface. Posner[24] and coworkers have found from a study of the desorption of a series of alcohols from the water surface to the gas phase that the energy required to separate the polar OH group from the water surface was about 5.2 kcal/mol and the increment in energy per CH_2 group was about 520 cal/mol. Jones and Ottewill[25] in similar studies on the adsorption of hydrocarbons have found a value for the increment in energy per CH_2 group of ~420 cal/mol. The agreement between these values and the present work is significant. The value of 6.5 kcal/mol found in this work for the residual energy or the sum of the interaction energies between head groups and terminal methyl groups is also in

(22) E. Sada and D. M. Himmelblau, *J. Amer. Inst. Ch. E.*, 13, 860 (1967).

(23) L. Salem, *Can. J. Biochem. Physiol.*, 40, 1287 (1962).

(24) A. M. Posner, J. R. Anderson, and A. E. Alexander, *J. Colloid Sci.*, 1, 623 (1952).

(25) D. C. Jones and R. H. J. Ottewill, *J. Chem. Soc.*, 4076 (1955).

agreement with Posner's value for the interaction of the OH group. The activation energy for positively charged head groups of the trimethylammonium type are comparable with the residual energy found here. This is surprising in view of the gaseous-like character of these monolayers. However, it may be due to a soft "icelike" structure at the water surface formed by the orientation of the water molecules around the charged head groups leading to a small value of the free surface area. Thus the results presented here are consistent with the transportation of the CO_2 molecules through the monolayer in a single-step process, rather than a series of jumps as required by the Fickean diffusion mechanism.

Acknowledgment. This project has been supported and financed, in part, by the Federal Water Pollution Control Administration, U. S. Department of the Interior, pursuant to the Federal Water Pollution Control Act.

Pyrolysis of Nitromethane-d_3

by C. G. Crawforth and D. J. Waddington

Department of Chemistry, University of York, York YO1 5DD, England *(Received February 12, 1970)*

The pyrolysis of nitromethane-d_3 between 300 and 400° has been studied and results are compared with the pyrolysis of nitromethane. It is shown that there is a deuterium isotope effect which may be ascribed to the reactions: $CD_3\cdot + CD_3NO_2 \rightarrow \cdot CD_2NO_2 + CD_4$ (3a), $CD_3O\cdot + CD_3NO_2 \rightarrow \cdot CD_2NO_2 + CD_3OD$ (7a).

Introduction

Although there is considerable evidence that the initiation reaction in the pyrolysis of nitromethane involves fission of the C–N bond[1-3]

$$CH_3NO_2 \longrightarrow CH_3\cdot + NO_2 \qquad (1)$$

it is not clear what part nitrogen dioxide plays in subsequent reactions, for at these temperatures it is able not only to react with radicals such as methyl,[4] but it may also abstract hydrogen from saturated aliphatic molecules,[5] for example, nitromethane to form nitromethyl.[2a]

$$CH_3NO_2 + NO_2 \longrightarrow \cdot CH_2NO_2 + HNO_2 \qquad (2)$$

This paper is concerned with the pyrolysis of nitromethane-d_3, both in the presence of added nitrogen dioxide and alone, in order to elucidate whether reaction 2 is important in the pyrolysis of nitromethane.

Experimental Section

Materials. Nitromethane (BDH Ltd.) was purified by fractional distillation using a spinning band column (Büchi). It and nitromethane-d_3 (Merck) were over 99% pure as determined by gas chromatography and by pmr (Perkin-Elmer R60). Methyl cyanide and methanol (BDH Ltd.) were also purified by fractional distillation. Methane, ethylene, carbon dioxide, nitrous oxide, nitrogen dioxide (Cambrian Chemicals Ltd.) and methane-d_4 (Merck Sharp and Dohme of Canada Ltd.) were stated to be over 99% pure, and hydrogen and nitrogen (British Oxygen Co. Ltd.) over 99.5% pure, and were used without further purification, impurities not being detectable by gas chromatography. Methyl nitrite[6] and methyl nitrate[7] were prepared from methanol.

Apparatus. A static vacuum apparatus was used. The reactants were introduced into a cylindrical borosilicate glass reaction vessel (250-ml capacity, surface: volume ratio 0.95 cm^{-1}), suspended in an electrical furnace, maintained at a temperature to within ±0.2°. Pressure measurements were made with a transducer (Consolidated Electrodynamics) linked to a recorder (Goertz RE 511).

(1) (a) C. Frejacques, *C. R. Acad. Sci.*, **231**, 1061 (1950); (b) T. L. Cottrell and T. J. Reid, *J. Chem. Phys.*, **18**, 1306 (1950); (c) T. L. Cottrell, T. E. Graham, and T. J. Reid, *Trans. Faraday Soc.*, **47**, 584 (1951).

(2) (a) L. J. Hillenbrand and M. L. Kilpatrick, *J. Chem. Phys.*, **19**, 381 (1951); **21**, 525 (1953); (b) P. Gray, A. D. Yoffe, and L. C. Roselaar, *Trans. Faraday Soc.*, **51**, 1489 (1955).

(3) C. G. Crawforth and D. J. Waddington, *Trans. Faraday Soc.*, **65**, 1334 (1969).

(4) L. Phillips and R. Shaw, "Tenth Symposium on Combustion," Cambridge, England, 1965, p 453.

(5) J. H. Thomas, *Oxid. Combust. Rev.*, **1**, 137 (1965).

(6) J. I. McGarvey and W. D. McGrath, *Trans. Faraday Soc.*, **60**, 2196 (1964).

(7) A. H. Blatt, Ed., Organic Syntheses, Vol. II, J. Wiley, New York, N. Y., 1943, p 412.

Analysis. Nitromethane and its decomposition products were determined by gas chromatography. Injections of gas samples were made using heated glass sampling tubes (20 ml capacity), equipped with a bypass. Pye 104 Model chromatographs were used, with flame ionization and with thermal conductivity detectors. Columns of molecular sieve 5A, 60–85 mesh (methane), Porapak Q, 100–120 mesh (carbon dioxide, ethylene, and nitrous oxide),[8] and Celite (AW), 100–120 mesh 10% Carbowax 1000 (methanol, methyl cyanide, methyl nitrite, methyl nitrate, nitromethane) were used. The chromatograph was linked to an AEI MS 12 mass spectrometer and was used to identify the peaks. Concentrations of reactant and products were obtained from a knowledge of the response of standard amounts, following a series of experiments to ensure that there was no interaction between products during sampling and analysis.

Results and Discussion

Nitromethane-d_3 was allowed to decompose under similar conditions to nitromethane.[3] While the overall pressure increase is similar, the rate of decomposition of nitromethane-d_3, as determined by analysis, and the rate of formation of methane-d_4 are reduced (Figure 1). As in the decomposition of nitromethane,[3] the concentration of methane-d_4 can be used as a measure of the rate of decomposition, for the fraction of methane formed, in the early stages of reaction, is a constant function of the amount of nitroalkane decomposed (Figure 2), and for at least the first 20% of the reaction the yields of methane and methane-d_4 from the two nitroalkanes are similar. This yield, as would be expected, is lower than that obtained at 424° from nitromethane.[3] Figure 2 also shows that the change in pressure is a true reflection of the decomposition of the nitroalkanes.

The reaction order for the decomposition of nitromethane-d_3 varies with pressure, being first order above *ca.* 100 mm pressure (Figure 3). On lowering the pressure, the rate constant decreases. At 50 mm initial pressure, the order of reaction for nitromethane-d_3, as determined by the rate of formation of methane-d_4, is 1.3 (Figure 4), the results being similar to those found for nitromethane.[3] Under these conditions the energy of activation is 49.3 ± 0.5 and 53.7 ± 0.5 kcal/mol for nitromethane[3] and nitromethane-d_3, respectively.

The principal source of methane appears to be from reaction of methyl with the nitroalkane[2,3]

$$CH_3\cdot + CH_3NO_2 \longrightarrow CH_4 + \cdot CH_2NO_2 \quad (3)$$

$$CD_3\cdot + CD_3NO_2 \longrightarrow CD_4 + \cdot CD_2NO_2 \quad (3a)$$

To investigate the role of reaction 2, nitrogen dioxide was added to the reaction vessel and allowed to decompose to equilibrium

$$NO_2 \rightleftharpoons NO + {}^1/_2O_2 \quad (4)$$

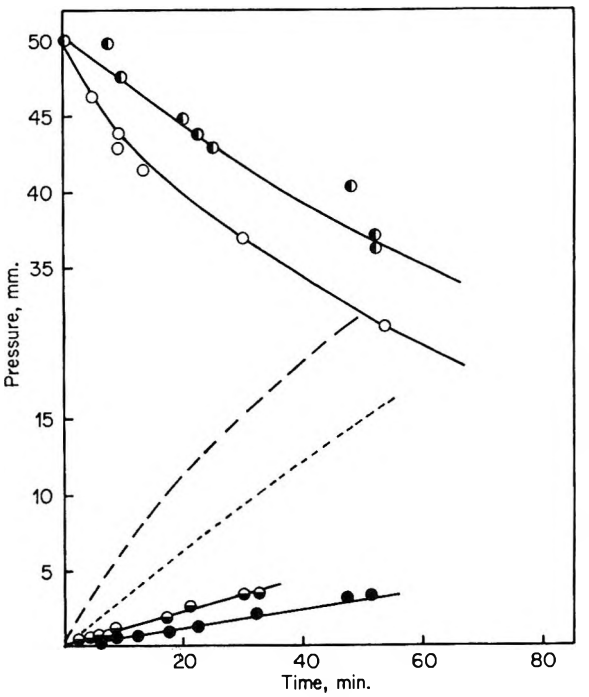

Figure 1. Pyrolysis of nitromethane and nitromethane-d_3; consumption of reactants and formation of methane at 365°; initial pressure, 50 mm; ◒, methane; ●, methane-d_4; ○, nitromethane; ◐, nitromethane-d_3; – – – –, pressure change (nitromethane); · · · ·, pressure change (nitromethane-d_3).

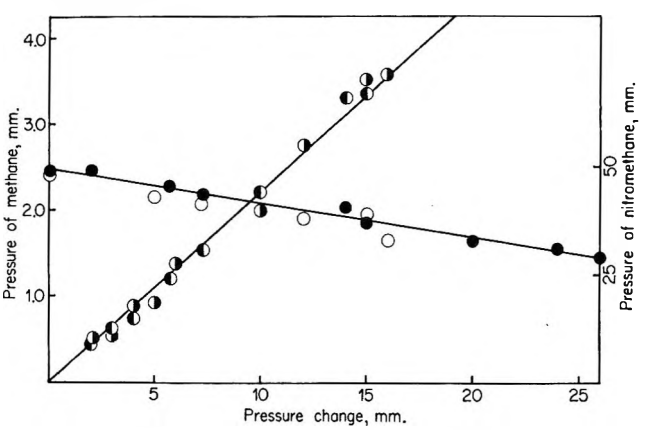

Figure 2. Pyrolysis of nitromethane and nitromethane-d_3; consumption of reactants and formation of methane as a function of pressure change at 365°; initial pressure, 50 mm: ◐, methane; ◑, methane-d_4; ○, nitromethane; ●, nitromethane-d_4.

Under the conditions of these experiments, it can be calculated[9] that 27.5 mm of the 50 mm of nitrogen dioxide added decomposes ($K_{4\ (365)} = 0.16$ atm$^{1/2}$), the calculation being confirmed by experiment, the pressure change being 14.0 mm. The equilibrium mixture retards the consumption of both nitromethane and nitromethane-d_3, the results in Figure 5 being

(8) C. G. Crawforth and D. J. Waddington, *J. Gas Chromatogr.*, **6**, 103 (1968).

(9) "Selected Values of Chemical Thermodynamic Properties," National Bureau of Standards, Technical Note 270-1, 1965.

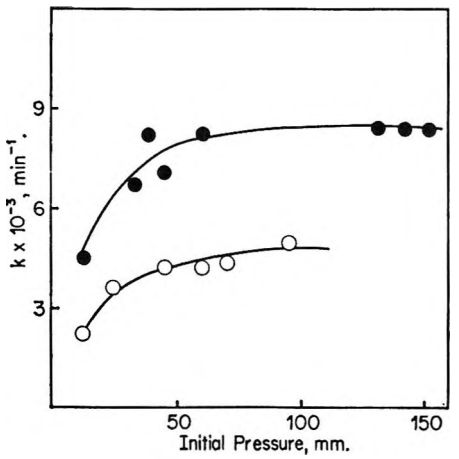

Figure 3. Pyrolysis of nitromethane and nitromethane-d_3; variation of rate constant with initial pressure of reactant at 365°: ●, nitromethane; ○, nitromethane-d_3.

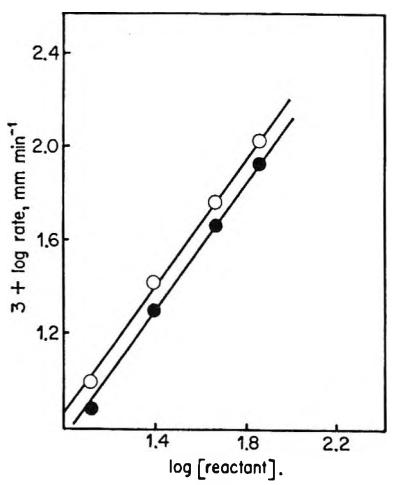

Figure 4. Pyrolysis of nitromethane and nitromethane-d_3; rate of formation of methane as a function of pressure of reactant at 365°; initial pressure, 50 mm: ○, methane; ●, methane-d_4.

obtained by analysis of residual nitromethane and nitromethane-d_3. Separate experiments show that nitric oxide does not retard the consumption of nitromethane, the oxide reacting with methyl to form nitrosomethane which subsequently reacts further with nitric oxide to regenerate methyl, while forming nitrogen.[3,10] Nor does oxygen retard the early stages of reaction,[10] the nitrogen dioxide formed by reaction 1 reacting preferentially with methyl. Only in the later stages of reaction when the concentration of nitrogen dioxide is very low does oxygen play a significant part. Thus the observed retardation of nitromethane and nitromethane-d_3, under the conditions of the experiments discussed in this paper, in the presence of the equilibrium mixture of oxides of nitrogen and oxygen, is due to nitrogen dioxide.

It has been shown that the addition of nitrogen dioxide to nitromethane reduces the concentrations of methyl nitrite, methanol, and methyl cyanide, while

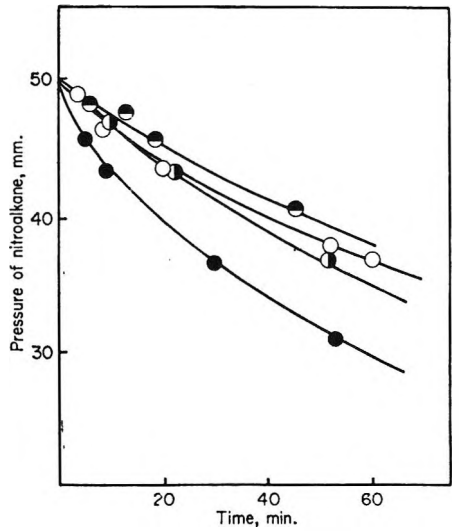

Figure 5. Pyrolysis of nitromethane and nitromethane-d_3; rate of consumption of reactant as determined by analysis in presence of added nitrogen dioxide at 365°: ●, nitromethane, 50 mm; ◑, nitromethane-d_3, 50 mm; ○, nitromethane, 50 mm; nitrogen dioxide, 50 mm; ◒, nitromethane-d_3, 50 mm; nitrogen dioxide, 50 mm.

methane, a major product in the absence of added nitrogen dioxide, is not detectable.[3] Similarly, for nitromethane-d_3, chromatography peaks (confirmed by mass spectrometric analyses) corresponding to methyl nitrite-d_3, methanol-d_4, and methyl cyanide-d_3 are much reduced, in the presence of nitrogen dioxide, while methane-d_4 is not detectable.

As the addition of nitrogen dioxide decreases the rate of decomposition of nitromethane and nitromethane-d_3, it appears that reaction 2 does not play a significant role under these conditions. The reduction in rate is presumably due to reaction between radicals, formed during the decomposition of the nitroalkanes and nitrogen dioxide, for example

$$CH_3\cdot + NO_2\ (+M) \longrightarrow CH_3NO_2\ (+M) \quad (5)$$

$$CD_3\cdot + NO_2\ (+M) \longrightarrow CD_3NO_2\ (+M) \quad (5a)$$

and the rate of secondary attack by methyl on nitromethane (reactions 3 and 3a) is reduced. This is confirmed by analysis for methane, which is not detected in presence of nitrogen dioxide. If methane had been formed it would have been found on analysis as it is stable under the conditions of these experiments.[11,12]

In the presence of nitrogen dioxide, methyl reacts not only as in reactions 3 and 3a to form nitromethane but also to yield methoxyl[3,4]

$$CH_3\cdot + NO_2 \longrightarrow CH_3O\cdot + NO \quad (6)$$

$$CD_3\cdot + NO_2 \longrightarrow CD_3O\cdot + NO \quad (6a)$$

(10) C. G. Crawforth and D. J. Waddington, to be published.

(11) For example, A. B. Gagarina and N. M. Emanuel, *Russ. J. Phys. Chem.*, **33**, 90, 197 (1959).

(12) C. G. Crawforth, Ph.D. Thesis, University of York, 1968.

Methanol and methanol-d_4 formed early in the decomposition are produced by disproportionation reactions of methoxyl[13] or by hydrogen abstraction.

$$CH_3O\cdot + CH_3NO_2 \longrightarrow CH_3OH + \cdot CH_2NO_2 \quad (7)$$

$$CD_3O\cdot + CD_3NO_2 \longrightarrow CD_3OD + \cdot CD_2NO_2 \quad (7a)$$

Methanol is not detectable in larger quantities for it is rapidly oxidized by nitrogen dioxide under these conditions.[14] Moreover, reactions 7 and 7a will have to compete with reactions 8 and 8a, respectively, particularly when excess nitrogen dioxide is added.[15]

$$CH_3O\cdot + NO_2 \longrightarrow CH_3ONO_2 \quad (8)$$

$$CD_3O\cdot + NO_2 \longrightarrow CD_3ONO_2 \quad (8a)$$

The stabilization of radicals by reactions 5, 5a, 8 and 8a accounts for the reduction in rate of decomposition of the nitroalkanes in the presence of added nitrogen dioxide and for the reduced yield of methanol and of methyl nitrite, also formed from methoxyl.

If there is no interaction between methyl and nitrogen dioxide

$$k_{CH_3NO_2}/k_1 = 2$$

This ratio will decrease if reaction 5 plays an important part in the reaction. Thus, in order to show that reaction 5 occurs to a significant extent, the ratio of $k_{CH_3NO_2}:k_{CH_3NO_2+NO_2}$ should tend to 2. In fact, the ratio, as calculated from Figure 5 is almost $2(k_{CH_3NO_2} = 1.1 \times 10^{-2}$ min^{-1}; $k_{CH_3NO_2+NO_2} = 5.6 \times 10^{-3}$ min^{-1}).

The addition of a similar amount of nitrogen dioxide only reduces the rate constant for the decomposition of nitromethane-d_3 by a factor of 1.3 ($k_{CD_3NO_2} = 6.2 \times 10^{-3}$ min^{-1}; $k_{CD_3NO_2+NO_2} = 4.7 \times 10^{-3}$ min^{-1}) implying abstraction reactions 3a and 7a are slower than the corresponding reactions 3 and 7. The difference in activation energy for the pyrolysis of nitromethane and nitromethane-d_3 can thus be explained in terms of attack by methyl and methoxyl radicals on the parent nitroalkane. Although the role of nitrogen dioxide in the system is to reduce the rate of attack by methyl, reactions 5 and 5a must still be occurring, for even when excess nitrogen dioxide is added, the rate of consumption of nitromethane-d_3 is still slower than that of nitromethane.

Acknowledgments. Our thanks are due to Shell Research Limited for financial assistance for apparatus and to the Kingston upon Hull Education Department for a studentship (C. G. C.). Our thanks are also due to Miss M. A. Warriss for technical assistance, to Dr. C. B. Thomas for mass spectrometric analyses, and to Dr. D. M. Goodall for helpful discussions.

(13) For example, P. Gray, R. Shaw, and J. C. J. Thynne, *Progr. React. Kinet.*, **4**, 63 (1967).

(14) R. Silverwood and J. H. Thomas, *Trans. Faraday Soc.*, **63**, 2476 (1967).

(15) G. Baker and R. Shaw, *J. Chem. Soc.*, 6965 (1965).

The Kinetics of the Uranium-(III)Uranium(VI) and the Neptunium(III)-Neptunium(VI) Reactions in Aqueous Perchlorate Solutions[1]

by T. W. Newton and R. B. Fulton[2]

University of California, Los Alamos Scientific Laboratory, Los Alamos, New Mexico 87544 *(Received February 10, 1970)*

The kinetics of the reactions $M^{3+} + MO_2^{2+} = M^{4+} + MO_2^{+}$, where M = uranium or M = neptunium, were studied in aqueous perchlorate solutions. For both reactions the hydrogen ion dependence is not significant and the rate law is $-d[M^{3+}]/dt = k[M^{3+}][MO_2^{2+}]$. At 25° in 0.1 *M* $HClO_4$, $k_U = 1.1 \times 10^4\ M^{-1}\ sec^{-1}$ and $k_{Np} = 2.2 \times 10^4\ M^{-1}\ sec^{-1}$. Temperature dependence data lead to $\Delta H_U^* = 4.15 \pm 0.07$ kcal/mol and $\Delta H_{Np}^* = 0.96 \pm 0.11$ kcal/mol. The ionic strength dependence for the uranium reaction was studied between 0.05 and 1.0 *M* and found to be in accord with the extended Debye–Hückel equation.

Introduction

The kinetics of the rapid reactions 1 and 2 have been studied for comparison with the analogous plutonium[3]

$$U^{3+} + UO_2^{2+} = U^{4+} + UO_2^{+} \quad (1)$$

$$Np^{3+} + NpO_2^{2+} = Np^{4+} + NpO_2^{+} \quad (2)$$

reactions and with other actinide(III)–actinide(VI) reactions.[4] In this connection these reactions are particularly interesting because of their large negative $\Delta F°$ values, −16 kcal/mol and −22.6 kcal/mol, respectively.[5]

Previous work on uranium ion–uranium ion reactions has been concerned with the disproportionation of U(V)[6] and with the U(IV)–U(VI) exchange reaction.[7] In the neptunium system, reaction 2 appears to be the only such reaction not previously studied by Hindman and his coworkers.[8]

Although the rates of reactions 1 and 2 are quite high, with second-order rate constants greater than $10^4\ M^{-1}\ sec^{-1}$ at 25°, dilute solutions can be studied in stirred absorption cells with satisfactory precision. Reaction 1 is complicated by the additional rapid reaction 3. However, in acid concentrations greater than about 0.05

$$U^{3+} + UO_2^{+} + 4H^{+} = 2U^{4+} + 2H_2O \quad (3)$$

M this reaction is enough faster than (1) so that its rate need not be known with high precision. Conversely, in solutions of low acidity reaction 4 complicates the study of reaction 2.

$$Np^{4+} + NpO_2^{2+} + 2H_2O = 2NpO_2^{+} + 4H^{+} \quad (4)$$

Experimental Section

Reagents. A stock solution of U(VI) perchlorate was prepared by the dissolution of pure U_3O_8 in fuming $HClO_4$ followed by two recrystallizations from water. It was analyzed by reduction to U(IV) and titration with standard Ce(IV) sulfate. A solution prepared by dissolving a sample of UO_2 in HNO_3 and fuming nearly to dryness with $HClO_4$ gave the same kinetic results within the experimental error. Solutions of U(III) were prepared by reduction of U(VI) on zinc amalgam and were kept in contact with the amalgam until used. The Zn(II) and possible traces of Cl^- were found to be without effect on the measured rates. The concentrations of the various U(III) solutions were determined spectrophotometrically at 3500 Å where the extinction coefficient was found to be 1620 $M^{-1}\ cm^{-1}$ in solutions ranging from 0.10 to 1.0 *M* $HClO_4$ and from 1 to 25°. The extinction coefficient determinations were made in 10-cm cells and the solutions were analyzed using a spectrophotometric titration with standardized Fe(III) perchlorate at 3500 Å. U(III) is a powerful reducing agent but can readily be handled in acidic solutions in the absence of oxygen.[9] Solutions of U(V) were prepared by the reduction of U(VI) with Eu(II) as previously described.[6b]

Stock solutions of Np(VI) and Np(III) were prepared and analyzed as previously described.[4] Very dilute ($\sim 2 \times 10^{-4}\ M$) Np(III) stock solutions for the rate runs were prepared by diluting more concentrated solutions with $HClO_4$ which had been treated with Zn–Hg and storing the solution under argon on the amalgam until use. These solutions were analyzed as before.[4] Stock solutions of $HClO_4$ and $LiClO_4$ were prepared and

(1) Work supported by the U. S. Atomic Energy Commission.

(2) Los Alamos Scientific Laboratory Postdoctoral Fellow.

(3) S. W. Rabideau and R. J. Kline, *J. Phys. Chem.*, **62**, 617 (1958).

(4) R. B. Fulton and T. W. Newton, *ibid.*, **74**, 1661 (1970).

(5) J. J. Katz and G. T. Seaborg, "The Chemistry of the Actinide Elements," Methuen and Co., Ltd., London, 1957, p 428.

(6) (a) D. T. Pence and G. L. Booman, *Anal. Chem.*, **38**, 1112 (1966); (b) T. W. Newton and F. B. Baker, *Inorg. Chem.*, **4**, 1166 (1965) and the references cited.

(7) (a) B. J. Masters and L. L. Schwartz, *J. Amer. Chem. Soc.*, **83**, 2620 (1961); (b) E. Rona, *ibid.*, **72**, 4339 (1950).

(8) J. C. Hindman, "Proceedings Second UN Geneva Conference," Vol. 28, Session C-10, 1958, p 941; or T. W. Newton and F. B. Baker, Advances in Chemistry Series, No. 71, American Chemical Society, Washington, D. C., 1967, p 268.

(9) (a) J. H. Espenson and R. T. Wang, *Chem. Commun.*, 207 (1970); (b) A. Sato, *Bull. Chem. Soc. Jap.*, **40**, 2107 (1967).

analyzed as before.[4] The concentration units used in this paper are moles per liter (M) at 23°.

Procedure. Reaction rates were determined spectrophotometrically in stirred absorption cells as previously described.[10] Appropriate amounts of $HClO_4$, $LiClO_4$, and water were put into a cell which was then swept with purified argon and brought to temperature in the thermostat in the light beam of the Cary Model 14 spectrophotometer. Temperatures were determined with a calibrated thermometer in the thermostat. Correction was made for the small (~0.1°) difference between the cell and the thermostat. The necessary quantity of one of the reactant solutions was then injected into the cell and when steady readings were obtained the other reactant was injected. The timing was by means of the recorder which traveled at 8.00 in./min. For runs at the lowest concentrations the 0–0.1 slide wire was used. All of the reactant solutions were thoroughly deaerated with purified argon and were maintained at temperatures close to the desired run temperature.

The U(III) reactions were followed at 3500 Å where the extinction coefficients of all species other than U(III) are negligibly small. The initial concentrations of U(III) were calculated from the initial absorbance values and the extinction coefficient. The initial concentrations of the other reactant, U(VI) or U(V), were determined from the total absorbance change in runs for which U(III) was in excess.

The Np(III) runs were made at 2650 Å where the extinction coefficients of Np(III) and Np(VI) are about 1590 M^{-1} cm^{-1} and 870 M^{-1} cm^{-1}, respectively. For the reaction products, Np(IV) and Np(V), the extinction coefficients are much smaller, 40 M^{-1} cm^{-1} and 100 M^{-1} cm^{-1}, respectively.[11] Initial reactant concentrations were calculated from the volumes of the stock solutions injected into the reaction cells.

Stoichiometry. Spectrophotometric titrations of U(III) with U(VI) at 3500 Å gave linear plots of absorbance *vs.* milliliters of U(VI) solution added (corrected for the small volume changes) and the end points indicated that in the presence of excess U(III), 1.98 ± 0.02 mol of U(III) are consumed for each mole of U(VI) added. These observations show that reaction 1 is followed by reaction 3. The stoichiometry in the presence of excess U(VI) depends on the relative rates of the two reactions. The rate of reaction 3 was therefore measured under various conditions and calculation shows that, for example, 1.23 mol of U(IV) are formed per mole of U(III) reacted, even when the initial [U(VI)]/[U(III)] ratio is as high as 4.

The stoichiometry of the Np(III)–Np(VI) reaction in 1 M $HClO_4$ was found to be in accord with equation 2 by means of spectrophotometric titrations at 2670 Å. Known amounts of 3×10^{-5} M Np(VI) were titrated with Np(III). The average Np(III) concentration from three such titrations was 1.96×10^{-4} M, with a range of 1.6%. The value determined by titration with standard Ce(IV) agreed within the experimental error; it was 0.8% lower. The reaction between Np(III) and Np(V) is too slow to affect the observed stoichiometry and it can be shown that reaction 4 is relatively unimportant except at low acid concentrations and higher temperatures. The rate law for (4) was found[12] to be $-d[Np(IV)]/dt = k_4[Np^{4+}][NpO_2^{2+}]\cdot[H^+]^{-2}$ and average values of the rate constant ranged from 3.44 to 2.69 M sec^{-1} between $\mu = 0.55$ and 2.0 M at 25°. Extrapolation gives 0.07 M sec^{-1} and 1.0 M sec^{-1} for $\mu = 0.1$ M at 25° and 45°, respectively. In 0.1 M acid the rate constants are small enough to be ignored since the rate constants for reaction 2 are near 2.4×10^4 M^{-1} sec^{-1} at both temperatures. In 0.01 M acid ($\mu = 0.1$ M), however, the second-order rate constants for (4) are about 700 and 10^4 M^{-1} sec^{-1} at 25 and 45°; thus an appreciable effect is to be expected at the higher temperature. Calculations for 45°, 0.01 M $[H^+]$ and $[Np(VI)]_0/[Np(III)]_0 = 2$ show that when 10% of the Np(III) is left, 1.43 mol of Np(VI) are consumed for each mole of Np(VI) oxidized.

Calculations. Concentration *vs.* time data for the U(III)–U(V) reaction (3) were found to be in good agreement with the expected second-order rate law

$$-d[U(V)]/dt = k_3[U(III)][U(V)] \qquad (5)$$

Values for k_3 were determined using the integrated form of eq 5 by a least-squares procedure.

When the U(III)–U(VI) reaction (1) is studied, reaction 3 occurs also. By making the approximation that (3) is much faster than (1), runs with excess U(III) were found to be in agreement with

$$-d[U(VI)]/dt = k_1[U(III)][U(VI)] \qquad (6)$$

Thus reactions 1 and 3 were treated as competitive, consecutive second-order reactions. The resulting simultaneous differential equations were treated numerically and values for k_1 which best reproduced the observed absorbance *vs.* time data were determined by least squares as previously described.[13] The calculated values for k_1 were found to be relatively insensitive to the values of k_3 assumed in the calculations.

The data for the Np(III)–Np(VI) reaction (2) in 0.1 M $HClO_4$ are in good agreement with a second-order rate law analogous to eq 5. In some of the runs with excess Np(III) a small decrease in absorbance with time was observed after the Np(VI) was consumed. This is attributed to the reaction of Np-

(10) T. W. Newton and F. B. Baker, *J. Phys. Chem.*, **67**, 1425 (1963).

(11) R. Sjoblom and J. C. Hindman, *J. Amer. Chem. Soc.*, **73**, 1744 (1951).

(12) J. C. Hindman, J. C. Sullivan, and D. Cohen, *ibid.*, **76**, 3278 (1954).

(13) T. W. Newton, G. E. McCrary, and W. G. Clark, *J. Phys. Chem.*, **72**, 4333 (1968).

(III) with traces of oxygen, and the necessary small corrections were applied to the determination of k_2. In solutions only 0.01 M in $HClO_4$ (μ = 0.1 M) with excess Np(VI), decreases in absorbance with time were observed after the Np(III) was consumed. This is attributed to reaction 4. Reactions 2 and 4 were treated as competitive, consecutive second-order reactions, as above.

Results

The U(III)–U(V) Reaction (3). The rate of this reaction is close to the limit of our stirred absorption cell apparatus, but k_3 was determined with sufficient precision for the calculation of k_1. The initial concentrations of U(III) and U(V) were varied in the ranges (0.2–2.0) × 10^{-5} M and (0.2–1.24) × 10^{-5} M, respectively. For eight experiments at 25° in 0.1 M $HClO_4$, $10^{-4}k_3$ averaged 5.0 and ranged from 4.7 to 5.5 M^{-1} sec^{-1} with no apparent pattern. These reactant concentrations were low enough so that the disproportionation of U(V) was much too slow to compete with reaction 3. The effects of temperature, hydrogen ion concentration, and ionic strength are shown in Table I. The appropriate data were extrapolated to μ = 0.2 M and it was found that the hydrogen ion dependence at that ionic strength and 25.1° is given by k_3 = 5.5 × 10^4 + (1.3 × 10^5) $[H^+]$ M^{-1} sec^{-1}. The apparent activation energies, based on the two temperatures, are essentially the same at 0.06, 0.10, and 0.17, M H^+; they are 2.5, 2.6, and 2.2 kcal/mol, respectively.

Table I: Effect of Temperature, Acid Concentration, and Ionic Strength on k_3

$[HClO_4]$, M	Ionic strength, M[a]	No. of detn	$10^{-4}k_3$, M^{-1} sec^{-1} Av	$10^{-4}k_3$, M^{-1} sec^{-1} Mean dev[b]
		25.1°		
0.06	0.06	5	3.8	0.1
0.10	0.10	8	5.0	0.2
0.04	0.21	4	6.0	0.3
0.10	0.20	1	6.8	...
0.17	0.17	3	7.2	0.2
		0.8°		
0.06	0.06	4	2.6	0.1
0.10	0.10	1	3.4	...
0.06	0.22	4	4.6	0.1
0.17	0.17	4	5.2	0.2

[a] Made up with $LiClO_4$. [b] Mean deviation from the mean.

Values of k_3 at ionic strengths greater than 0.2 M were obtained by extrapolation using the extended Debye–Hückel equation with $\mathring{a}$, the distance of closest approach set at 8.8 Å. For unit ionic strength the estimated k_3 values are 1.1 × 10^5 and 5.6 × 10^5 M^{-1} sec^{-1} for 0.04 and 1.0 M $HClO_4$, respectively. The value 8.8 Å was chosen to lie in the range found for reactions of U(VI).[14,15] If 7 Å is chosen, the effect on k_1 is an increase of 14% in the least favorable case, μ = 1.00, $[H^+]$ = 0.04 M and excess U(VI).

The U(III)–U(VI) Reaction (1). A number of runs were made at 25.1° in 0.10 M $HClO_4$ to confirm the applicability of eq 5 to reaction 1. The initial concentrations of U(III) and U(VI) were varied in the ranges (0.25–4.6) × 10^{-5} M and (0.70–5.1) × $10^{-5}M$, respectively. Values for k_1 were calculated from the data under the assumption that k_3 = 5 × 10^4 M^{-1} sec^{-1} as determined previously. Twenty five runs at 25.1° in 0.10 M $HClO_4$ gave an average for $10^{-4}k_1$ of 1.20 M^{-1} sec^{-1} with a mean deviation of 0.04; the range was from 1.12 to 1.32 M^{-1} sec^{-1}. A small but probably insignificant trend appears in the data. The observed values were treated by least squares and found to be given by the equation: k_1 = (1.34 ± 0.08) × 10^4 − (4.62 ± 3.17) × 10^7 [U(III)] − (5.33 ± 4.24) × 10^7[U(VI)] + (1.43 ± 1.22) × 10^{12}[U(III)][U(VI)] M^{-1} sec^{-1}. The indicated uncertainties are the standard deviations, which are large enough to show that the apparent reactant dependences are not significant. Additional runs were made which show that neither Zn(II) from the amalgam nor the product U(IV) affect the rate constants.

The hydrogen ion dependence of k_1 was studied in $HClO_4$–$LiClO_4$ solutions at ionic strengths close to 0.6 M. The data, summarized in Table II, show an insignificant dependence at both 0.8 and 25.1°.

Table II: Hydrogen Ion Dependence of k_1 in Solutions with Ionic Strength 0.6 M[a]

$[HClO_4]$, M	No. of detn	$10^{-4}k_1$, M^{-1} sec^{-1} Av	$10^{-4}k_1$, M^{-1} sec^{-1} Mean dev[b]
	0.8°		
0.05	4	1.87	0.02
0.24	4	1.82	0.06
0.43	4	1.78	0.06
0.61	4	1.81	0.09
	25.1°		
0.04	7	3.82	0.14
0.22	6	3.60	0.22
0.40	4	3.75	0.20
0.60	5	3.85	0.24

[a] Made up with $LiClO_4$; the actual ionic strengths ranged from 0.58 to 0.63 M; k_1 values were corrected to 0.6 M using the parameters in Table VI. [b] Mean deviation from the mean.

The ionic strength dependence was studied in $HClO_4$–$LiClO_4$ solutions at 0.8 and 25.1°; the results are summarized in Table III. Since the hydrogen ion

(14) T. W. Newton and F. B. Baker, *J. Phys. Chem.*, **69**, 176 (1965); 8.33 Å for V(II).

(15) T. W. Newton, *J. Phys. Chem.*, **74**, 1655 (1970); 8.94 Å for Np(III).

Table III: Ionic Strength Dependence of k_1 for the U(III)–U(VI) Reaction[a]

	25.1°				0.8°			
	No. of	$10^{-4}k_1$, M^{-1} sec^{-1}			No. of	$10^{-4}k_1$, M^{-1} sec^{-1}		
μ, M[b]	detn	Av	Mean dev[c]	Calcd[d]	detn	Av	Mean dev	Calcd
0.053	...	...	...	...	12	0.382	0.007	0.384
0.100	11	1.17	0.03	1.16	19	0.568	0.008	0.563
0.125	9	1.32	0.05	1.33	...	...	...	...
0.225	12	1.96	0.08	1.93	8	0.937	0.015	0.943
0.580	12	3.69	0.17	3.62	...	...	...	...
0.610	10	3.73	0.21	3.76	16	1.84	0.07	1.83
0.750	4	4.47	0.38	4.37	3	2.13	0.03	2.13
1.00	6	5.51	0.14	5.47	9	2.64	0.09	2.63

[a] Variable acid concentrations. [b] Made up with $LiClO_4$. [c] Mean deviation from the mean. [d] Calculated using: $\log k_1 = \log k^0 + (A\Delta z^2\mu^{1/2})/(1 + B\mathring{a}\mu^{1/2}) + C\mu$; the values of the various parameters are as follows. For 0.8°: $A^e = 0.4889$; $B^e = 0.3242$; $k^0 = 580 \pm 12^f$ M^{-1} sec^{-1}, $\mathring{a} = 8.84 \pm 0.19^f$ Å, $C = 0.139 \pm 0.020^f$ M^{-1}; and for 25.1°: $A^e = 0.5092$; $B^e = 0.3286$; $k^0 = 1178 \pm 76$ M^{-1} sec^{-1}; $\mathring{a} = 9.41 \pm 0.55$ Å; $C = 0.173 \pm 0.048$ M^{-1}. [e] From R. A. Robinson and R. H. Stokes, "Electrolyte Solutions," Butterworths, London, 1955, p 491. [f] Standard deviations calculated by the least-squares program.

dependence was shown to be negligible, the data at various hydrogen ion concentrations were pooled and found to be in accord with the extended form of the Debye–Hückel equation: $\log k_1 = \log k^0 + (A\Delta z^2 \cdot \mu^{1/2})/(1 + B\mathring{a}\mu^{1/2}) + C\mu$. The values of the three adjustable parameters which best reproduce the experimental data at the two temperatures are listed in Table III.

The temperature dependence of k_1 was studied between 0.8 and 36.5° in 0.10 M $HClO_4$ solutions. The results are summarized in Table IV. The activation parameters, determined using the Eyring equation, are $\Delta F^* = 11.92$ kcal/mol, $\Delta H^* = 4.15 \pm 0.07$ kcal/mol, and $\Delta S^* = -26.06 \pm 0.25$ cal/mol deg in 0.10 M $HClO_4$ at 25°. These parameters fit the observed k_1 values with a root-mean square deviation of 3.5% and a maximum deviation of 6.4%. For the data at $\mu = 1.0$ M, the activation parameters are $\Delta F^* = 10.99$ kcal/mol, $\Delta H^* = 4.33 \pm 0.18$ kcal/mol, and $\Delta S^* = -22.3 \pm 0.6$ cal/mol deg. The uncertainties listed here are the standard deviations, so the observed small effect of μ on ΔH^* is probably not significant.

Table IV: Effect of Temperature on k_1, for the U(III)–U(VI) Reaction[a]

Temp,	$10^{-4}k_1$, M^{-1} sec^{-1}		
°C	Av[b]	Mean dev[c]	Calcd[d]
0.8	0.570	0.009	0.568
25.1	1.14	0.040	1.15
36.5	1.57	0.050	1.55

[a] Mean 0.10 M $HClO_4$. [b] Mean of 10 determinations. [c] Mean deviation from the mean. [d] Calculated using $\Delta H^* = 4.146$ kcal/mol and $\Delta S^* = -26.06$ cal/mol deg in the Eyring equation.

The Np(III)–Np(VI) Reaction (2). Rate runs at 25.1° in 0.1 M $HClO_4$ showed that the apparent second-order rate constant, k_2, is independent of the initial reactant concentrations. The concentration ranges were (1.5–12.5) $\times 10^{-6}$ M Np(III) and (1.6–12.4) $\times 10^{-6}M$ Np(VI). The sixteen observed rate constants ranged from 2.17×10^4 to 2.32×10^4 M^{-1} sec^{-1} with no apparent pattern.

The hydrogen ion dependence was found to be quite small in a short series of experiments at 36.5 and 45.0°. Rate constants were determined in 0.10 M $HClO_4$ and in 0.01 M $HClO_4$–0.09 M $LiClO_4$ solutions. The effect of reaction 4 is quite significant in the latter solutions, so the results are not as accurate as those for 0.10 M $HClO_4$. The rate constants for $[H^+] = 0.01$ were (9 ± 5)% greater at 36.5° and (35 ± 12)% greater at 45.0° than the corresponding values for $[H^+] = 0.1$ M.

The temperature dependence was studied in 0.10 M $HClO_4$ at temperatures ranging between 1.0 and 45.0°; the results are summarized in Table V. These data lead to the following activation parameters at 25°: $\Delta F^* = 11.53$ kcal/mol, $\Delta H^* = 0.99 \pm 0.10$ kcal/mol, and $\Delta S^* = -35.4 \pm 0.3$ cal/mol deg. These parameters were determined by least squares and reproduce

Table V: Effect of Temperature on k_2, for the Np(III)–Np(VI) Reaction[a]

Temp,	No. of	$10^{-4}k_2$, M^{-1} sec^{-1}		
°C	detn	Av	Mean dev[b]	Calcd[c]
1.0	3	1.68	0.05	1.73
12.8	3	1.93	0.02	1.95
25.1	16	2.24	0.06	2.19
36.4	3	2.42	0.02	2.41
44.8	4	2.48	0.03	2.58

[a] In 0.1 M $HClO_4$. [b] Mean deviation from the mean. [c] Calculated using $\Delta H^* = 0.99$ kcal/mol and $\Delta S^* = -35.4$ cal/mol deg in the Eyring equation.

the observed rate constants with a root-mean square deviation of 3.8% and a maximum deviation of 8.9%. The uncertainties are the standard deviations calculated by the least-squares program. If the small $[H^+]$ dependence mentioned above is assumed to have the form $k_2 = k_2' + k_2''[H^+]^{-1}$, the same data lead to slightly different values of the activation parameters: $\Delta F^* = 11.54$ kcal/mol, $\Delta H^* = 0.90 \pm 0.11$ kcal/mol, and $\Delta S^* = -35.7 \pm 0.4$ cal/mol deg.

Reaction 2 was studied at $\mu = 0.1$ *M* only; however, it is reasonable to assume that the ionic strength dependence of this reaction will parallel that observed for the U(III)–U(VI) reaction (1). On this basis we estimate the following parameters for $\mu = 1.0$ *M*: $\Delta F^* = 10.62$ kcal/mol, $\Delta H^* = 1$ kcal/mol, and $\Delta S^* = -32$ cal/mol deg.

Table VI: Thermodynamic and Activation Parameters for $M^{3+} + MO_2^{2+} = M^{4+} + MO_2^+$ Reactions[a]

	M = U	M = Np
$\Delta F°$, kcal/mol	−16	−22.6
$\Delta H°$, kcal/mol	−26.8	−36
$\Delta S°$, cal/mol deg	−33.8	−38
k, 10^{-4} M^{-1} sec^{-1} [b]	1.14	2.18
ΔF^*, kcal/mol[b]	11.92	11.55
ΔH^*, kcal/mol[b]	4.15 ± 0.07	0.96 ± 0.11
ΔS^*, cal/mol, deg[b]	−26.1 ± 0.25	−35.5 ± 0.4

[a] 25° and 1 *M* $HClO_4$ except as indicated. [b] 0.1 *M* $HClO_4$.

Discussion

The thermodynamic and activation parameters for the two reactions described in this paper are summarized in Table VI. All of the reactions of this type which have been studied so far are discussed in connection with Table VIII in ref 4.

The most interesting features brought out by the present investigation are (a) the close similarity in the rates in spite of the rather large difference in the $\Delta F°$ values and (b) the surprisingly large difference in the ΔS^* values for two apparently similar reactions.

Reactions of Trifluoromethyl Radicals in the Photolysis of Hexafluoroacetone and Hexafluoroazomethane

by Shuang-Ling Chong and Sidney Toby

School of Chemistry, Rutgers, The State University, New Brunswick, New Jersey 08903 *(Received September 3, 1969)*

The photolysis of hexafluoroacetone (HFA) at 3130 Å, and of hexafluoroazomethane (HFZ) at 3660 Å was studied in the range 0.1–8 Torr and 30–200°. Conditions were chosen such that $\Phi(CO)$ or $\Phi(N_2)$ was near unity so that primary deactivation was negligible. Addition reactions of CF_3 to HFA were not important but, in agreement with previous work, CF_3 readily added to HFZ with $k(\text{addition})/[k(\text{combination})]^{1/2} = 260e^{-3900/RT}$ $l.^{1/2}$ $mol^{-1/2}$ $sec^{-1/2}$. Carbon dioxide was an important product at higher temperatures and low-incident intensities and the mechanism for the heterogeneous formation of this product is considered. The effects of added gases in the photolysis of HFZ were investigated. No third-body effects in the combination of CF_3 radicals were seen but the rate of formation of carbon dioxide was found to increase in the presence of added carbon monoxide.

Introduction

The photolysis of hexafluoroacetone (HFA) and of hexafluoroazomethane (HFZ) are frequently used sources of trifluoromethyl radicals. The primary photolytic processes for HFA[1-3] and HFZ[4] have received considerable attention recently and the basic features of the secondary processes have been established for

(1) W. R. Ware and M. L. Dutton, *J. Chem. Phys.*, **47**, 4670 (1967).

(2) J. S. McIntosh and G. B. Porter, *ibid.*, **48**, 5475 (1968).

(3) A. Gandini, D. A. Whytock, and K. O. Kutschke, *Proc. Roy. Soc., Ser. A*, **306**, 503, 511, 529, 541 (1968).

(4) E. C. Wu and O. K. Rice, *J. Phys. Chem.*, **72**, 542 (1968).

both HFA[5-7] and HFZ.[8-11] However, interesting areas of uncertainty remain. The production of carbon dioxide, presumably from the heterogeneous reaction between CF_3 and the silica reaction cell, was noted in the photolysis of HFZ[10] above 150°, and HFA[5] at 300°. Carbon dioxide was also found as a product in other systems containing CF_3 radicals[12,13] but not in a study of the photolysis of trifluoroacetone[14] nor in another study of the photolysis of HFA[7], both at temperatures up to 350°. The predominant use of silica photolysis cells in photochemistry made this feature worth investigating. Further, a comparison of the addition of CF_3 radicals to HFA and to the isoelectronic HFZ was made. Finally, the effect of pressure of added gases was studied to learn if deactivation of vibrationally excited C_2F_6 was of importance.

Experimental Section

A conventional high-vacuum apparatus, with greaseless valves in the photolysis and product fractionation sections, was used. The cylindrical quartz photolysis cell, volume 0.524 l., was mounted in a modified convection oven with cell dead-space of about 1% and temperature control to within ±0.3 at 200°.

The beam from an Osram HBO-75-W high-pressure mercury arc was filtered with the combination described by Calvert and Pitts[15] for 3130 Å. A combination of Corning O-52 and 7-60 was used for the 3660 region and was found to give greater intensity than the suggested filter[15] with similar monochromaticity. Incident intensity was varied with neutral density filters and monitored with an RCA 935 phototube.

HFA was purchased from General Chemical Division, Allied Chemical, Inc., HFZ from Merck Sharp and Dohme, Montreal, and both compounds were distilled several times before use and their purity was checked by gas chromatography. Helium and carbon monoxide were research grade materials from Matheson Co. and were used directly. Products were partially separated with a low-temperature still and chromatographed with a silica gel column. In the case of HFZ runs with added gases, we were unable to measure the nitrogen formed because of the large amount of noncondensable gas added. Nitrogen formation was therefore estimated from the phototube reading and the amount formed when HFZ at the same pressure was photolyzed alone.

Results

HFA was photolyzed at 3130 Å and HFZ at 3660 Å except where noted. A dark run with HFZ at 200° for 70 hr showed less than 0.6% decomposition, as expected.[16] Reactant pressures were kept sufficiently low to avoid primary deactivation so that it could be assumed that $\Phi(CO)$ and $\Phi(N_2)$ were unity in the photolysis of HFA[5] and HFZ,[4,9] respectively. This point will be discussed further below.

The results of runs using HFA are shown in Tables I and II. CF_4 was never found in the products and CO_2 appeared at 200° but not at 100°. The HFZ data are given in Table III with the first five runs at each temperature done at constant incident intensity. CO_2 did not appear at 31°, was formed somewhat erratically at 100°, and showed clear trends at 200°.

Tables IV and V show data from runs in which HFZ

Table I: Photolysis of HFA at 3130 Å, 100° and Constant Incident Intensity. Effect of Variation of Pressure

P_{HFA}, Torr	Time, sec × 10^{-4}	R_{CO}, M sec^{-1} × 10^{10}	$\Phi(C_2F_6)$
1.91	0.555	15.5	1.02
1.63	0.720	13.2	1.01
1.37	0.800	10.3	0.98
1.10	1.08	8.35	1.05
0.72	1.72	6.4	1.02
0.22	6.19	0.79	1.1

Table II: Photolysis of HFA at 3130 Å, 7.5 Torr and 200°. Effect of Variation of Incident Intensity

P_{HFA}, Torr	Time, sec × 10^{-4}	R_{CO}, M sec^{-1} × 10^{10}	$\Phi(C_2F_6)$	$\Phi(CO_2)$
7.47	1.20	1.08	0.936	0.22
7.52	2.74	0.54	1.04	0.11
7.57	3.97	0.28	0.91	0.41
7.50	6.64	0.19	0.79	0.25
7.54	16.0	0.095	0.74	0.74
7.55	33.7	0.040	0.27	1.1

(5) P. S. Ayscough and E. W. R. Steacie, *Proc. Roy. Soc., Ser. A*, **234**, 476 (1956).

(6) J. S. McIntosh and G. B. Porter, *Trans. Faraday Soc.*, **64**, 119 (1968).

(7) A. S. Gordon, *J. Chem. Phys.*, **36**, 1330 (1962).

(8) G. O. Pritchard, H. O. Pritchard, and A. F. Trotman-Dickenson, *Chem. Ind. London*, 564 (1955).

(9) J. R. Dacey and D. M. Young, *J. Chem. Phys.*, **23**, 1302 (1955).

(10) G. O. Pritchard, H. O. Pritchard, H. I. Schiff, and A. F. Trotman-Dickenson, *Trans. Faraday Soc.*, **52**, 849 (1956).

(11) J. R. Dacey, R. F. Mann, and G. O. Pritchard, *Can. J. Chem.*, **43**, 3215 (1965).

(12) R. M. Smith and J. G. Calvert, *J. Amer. Chem. Soc.*, **78**, 2345 (1956).

(13) G. O. Pritchard and E. W. R. Steacie, *Can. J. Chem.*, **35**, 1216 (1957).

(14) R. A. Sieger and J. G. Calvert, *J. Amer. Chem. Soc.*, **76**, 5197 (1954).

(15) J. G. Calvert and J. N. Pitts, Jr., "Photochemistry," Wiley, New York, N. Y., 1966.

(16) E. Leventhal, C. R. Simonds, and C. Steel, *Can. J. Chem.*, **40**, 930 (1962).

Table III: Photolysis of HFZ. Effects of Variation of Temperature, Pressure, and Incident Intensity

P_{HFZ}, Torr	Time, sec × 10^{-4}	R_{N_2}, M sec^{-1} × 10^{10}	$\Phi(C_2F_6)$	$\Phi(CO_2)$
		31.5°		
1.90	0.872	2.89	0.215	0
1.00	1.28	2.17	0.277	0
0.50	2.67	0.58	0.41	0
0.23	5.53	0.24	0.56	0
0.12	15.9	0.083	0.69	0
1.00	2.29	1.11	0.238	0
1.01	3.36	0.67	0.17	0
0.98	6.29	0.17	0.12	0
0.99	26.9	0.075	0.076	0
		100.4°		
1.88	2.24	5.63	0.064	0.083
1.44	0.900	5.13	0.056	0.21
1.06	1.25	2.84	0.10	Trace
0.50	2.46	2.66	0.075	0
0.14	7.89	0.136	0.41	...
1.02	2.41	1.52	0.043	0.1
1.02	3.98	0.503	0.024	0
1.00	5.99	0.304	0.019	0.009
1.01	10.3	0.182	0.0036	0.091
		200.9°		
2.09	0.827	2.98	0.0133	0.12
1.03	1.31	1.33	0.0219	0.075
0.59	3.23	0.70	0.067	0.025
0.28	5.39	0.31	0.13	0.044
0.07	17.3	0.04	0.48	0
1.05	2.67	0.77	0.018	0.070
1.00	6.27	0.27	0	0.25
1.04	10.8	0.19	0	0.37
2.05[a]	7.90[a]	0.060[a]	0.019[a]	1.39[a]
2.02[a]	32.7[a]	0.022[a]	0.028[a]	2.0[a]

[a] 3130 Å; all other runs at 3660 Å.

Table IV: Photolysis of 0.2 Torr of HFZ at 200° and 3660 Å. Effect of Added Helium

P_{HFZ}, Torr	P_{He}, Torr	Time, sec × 10^{-4}	R_{N_2},[a] M sec^{-1} × 10^{10}	$\Phi(C_2F_6)$	$\Phi(CO_2)$	$R_{CO_2}/R_{C_2F_6}^{1/2}$, $M^{1/2}$ sec$^{-1/2}$ × 10^6
0.20	0	3.40	0.50	0.21	0.17	2.6
0.21	12.3	6.24	0.32	0.061	0.038	0.9
0.20	24.9	6.46	0.32	0.14	...	...
0.19	50.6	6.41	0.32	0.16	0.19	2.7
0.21	74.2	6.26	0.50	0.19	0.12	2.0
0.19	74.3	2.37	0.50	0.23	0.19	2.8
0.21	105	6.35	0.32	0.20	0.14	1.8
0.19	252	6.16	0.32	0.18	0.064	0.9

[a] $\Phi(N_2)$ assumed to be unity.

Table V: Photolysis of 0.2 Torr of HFZ at 3660 Å. Effect of Added CO

P_{HFZ}, Torr	P_{CO}, Torr	Time, sec × 10^{-4}	R_{N_2}[a] All in M sec^{-1} × 10^{10}	$R_{C_2F_6}$	R_{CO_2}[b]	$R_{CO_2}/R_{C_2F_6}^{1/2}$, $M^{1/2}$ sec$^{-1/2}$ × 10^6
			31.2°			
0.21	0	2.65	0.52	0.318	0	
0.20	35.5	2.52	0.51	0.255	0.12	
0.20	56.5	2.63	0.51	0.233	0	
0.20	101	2.62	0.53	0.182	0	
0.19	149	2.60	0.51	0.169	0.05	
0.20	194	2.61	0.51	0.147	0	
0.21	250	2.66	0.51	0.133	0	
			102°			
0.20	0	2.58	0.54	0.104	0.06	2.0
0.21	18.3	3.19	0.56	0.121	0.13	3.7
0.20	40.2	3.21	0.56	0.100	0.19	6.0
0.20	79.8	2.95	0.52	0.087	0.32	11
0.20	133	2.66	0.54	0.077	0.42	15
0.21	198	2.86	0.51	0.065	0.38	15
			200°			
0.20	0	6.29	0.45	0.079	0.081	2.9
0.20	39.5	6.26	0.43	0.073	0.22	8.2
0.19	80.4	6.29	0.43	0.065	0.24	9.4
0.21	99.1	6.20	0.38	0.050	0.35	16
0.19	149	6.35	0.43	0.051	0.35	16
0.19	200	6.16	0.41	0.046	0.40	18
0.20	250	6.14	0.41	0.041	0.42	21

[a] Estimated from photocell when CO present. [b] Corrected for 0.012% CO_2 impurity in CO.

was photolyzed in the presence of helium and carbon monoxide.

Discussion

Addition Reactions. In the photolysis of HFA no evidence for an addition reaction was found and the results may be accounted for by the simple sequence

$$(CF_3)_2CO + h\nu \longrightarrow 2CF_3 + CO \quad (0)$$

$$2CF_3 \longrightarrow C_2F_6 \quad (1)$$

$$CF_3 + SiO_2 \longrightarrow CO_2 + SiF_3 \quad (2)$$

The SiF_3 may then react to give SiF_4, which was found by Ayscough and Steacie[5] but which would not have been found under our conditions of analysis. At 100° we found $R_{CO} = R_{C_2F_6}$ and no CO_2 appeared. This is in agreement with Ayscough and Steacie[5] but is in total disagreement with the results of Gordon[7] who found no CO_2, obtained the addition product $(CF_3)_3COCF_3$ from 50–337°, and obtained $R_{C_2F_6}/R_{CO} \sim 2$. The fact that $R_{C_2F_6}$ was greater than R_{CO} cannot be accounted for by the formation of the perfluoroether. It could be explained by the formation of $(CF_3CO)_2$ which has been found in the photolysis of HFA at high intensities at

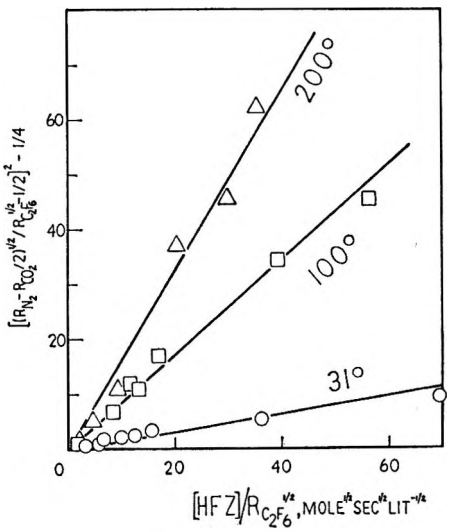

Figure 1. Photolysis of HF; Ztest of eq 6.

−80° by McIntosh and Porter.[6] Gordon[7] used high intensities and unfiltered light but it seems unlikely that perfluorobiacetyl could be a product at 300° and it is difficult to account for the deficiency of CO in his products.

The photolysis of HFZ may be represented by

$$(CF_3)_2N_2 + h\nu \longrightarrow 2CF_3 + N_2 \qquad (0')$$

$$CF_3 + (CF_3)_2N_2 \longrightarrow (CF_3)_2NNCF_3 \qquad (3)$$

$$CF_3 + (CF_3)_2NNCF_3 \longrightarrow (CF_3)_2NN(CF_3)_2 \qquad (4)$$

$$2(CF_3)_2NNCF_3 \longrightarrow (CF_3)_6N_4 \qquad (5)$$

together with reactions 1 and 2. We did not measure the heavier products in this investigation but their presence has been well substantiated.[8-11] Assuming steady states in CF_3 and $(CF_3)_2NNCF_3$ and assuming[17,18] that $k_4/k_1^{1/2}k_5^{1/2} = 2$, we have

$$\left[\left\{\frac{R_{N_2} - {}^1/_2R_{CO_2}}{R_{C_2F_6}}\right\}^{1/2} - {}^1/_2\right]^2 - {}^1/_4 = \frac{k_3[HFZ]}{2k_1^{1/2}R_{C_2F_6}^{1/2}} \qquad (6)$$

A plot of the left-hand side of eq 6 against [HFZ]/$R_{C_2F_6}^{1/2}$, using the data in Table III, is given in Figure 1. The effect of R_{CO_2} on the slope is appreciable only at 200°. Twice the slopes of the lines should equal $k_3/k_1^{1/2}$ and this is shown as an Arrhenius plot in Figure 2 together with the data of Pritchard and coworkers.[10] The estimated straight line corresponds to $k_3/k_1^{1/2} = 260 \pm 80e^{-(3900 \pm 200)/RT}$ l.$^{1/2}$ mol$^{-1/2}$ sec$^{-1/2}$. This coupled with Ayscough's value[19] for k_1 gives $k_3 = 3.9 \times 10^7 e^{-3900/RT}$ l. mol^{-1} sec^{-1} assuming $E_1 = 0$. The good agreement between the two sets of points shown in Figure 2 is a check on the validity of the rate law given by eq 6 since Pritchard and coworkers[10] obtained their values of $k_3/k_1^{1/2}$ by a quite different method, involving the measurement of pressure change after photolysis. By way of comparison the rate constant for the addition of methyl radicals to azomethane has been reported[20] as $10^{8.7}e^{-7100/RT}$.

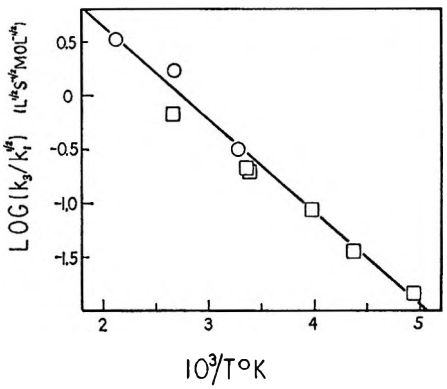

Figure 2. Arrhenius plot of $k_3/k_1^{1/2}$: □, data of Pritchard, *et al.*;[10] O, this work.

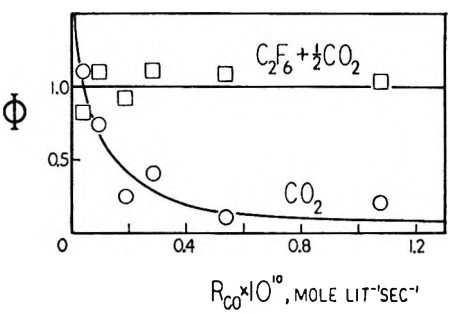

Figure 3. Photolysis of HFA; plot of $\Phi(CO_2)$ and $\Phi(C_2F_6) + {}^1/_2\Phi(CO_2)$ against intensity at 200°.

Formation of CO_2. This product is formed heterogeneously and its rate of formation was somewhat erratic. Nevertheless, some useful conclusions may be drawn from the data in our tables. CO_2 was an important product in the photolysis of HFA at 200° especially at low intensities as shown in Figure 3, which is taken from data in Table II. The mechanism given by reactions 0, 1, and 2 leads to the relationship

$$\Phi(C_2F_6) + {}^1/_2\Phi(CO_2) = 1 \qquad (7)$$

The validity of eq 7 is clearly shown in Figure 3 and shows that the only fate for a CF_3 radical, apart from C_2F_6 formation, is to form a molecule of CO_2. In the case of the photolysis of HFZ the ready addition of CF_3 to the parent molecule invalidates eq 7 but the rapid increase of $\Phi(CO_2)$ at low intensities to a limit of 2 still holds and is seen in Figure 4. Both HFA and HFZ mechanisms predict that $R_{CO_2}/R_{C_2F_6}^{1/2} = k_2/k_1^{1/2}$, where k_2 is a heterogeneous rate constant. Our results at 200° show that although $R_{CO_2}/R_{C_2F_6}^{1/2}$ appears independent of intensity over a 30-fold range, it increases

(17) J. A. Kerr and A. F. Trotman-Dickenson, *Progr. React. Kinet.*, 1, 105 (1961).

(18) J. M. Tedder and J. C. Walton, *ibid.*, 4, 39 (1967).

(19) P. B. Ayscough, *J. Chem. Phys.*, 24, 944 (1956).

(20) J. A. Kerr and J. G. Calvert, *J. Phys. Chem.*, 69, 1022 (1965).

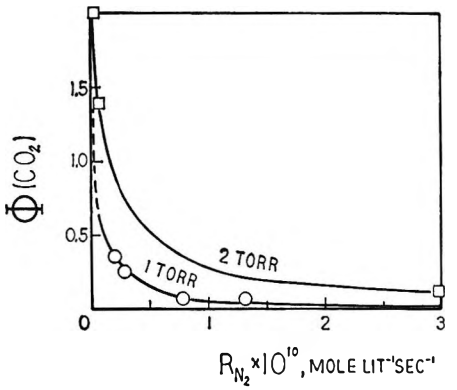

Figure 4. Photolysis of HFZ—plot of $\Phi(CO_2)$ against intensity at 200°.

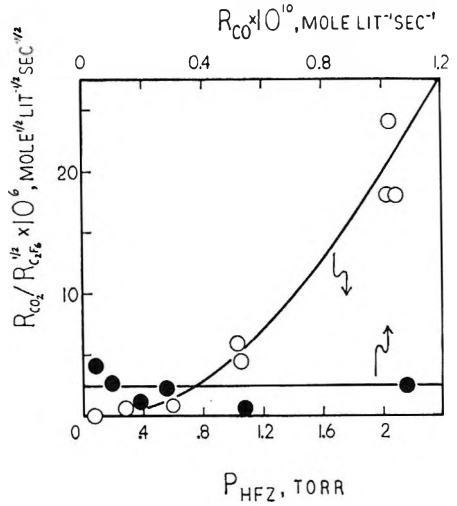

Figure 5. Plots of $R_{CO_2}/R_{C_2F_6}^{1/2}$ against HFZ pressure (open circles) and against intensity in HFA photolysis (filled circles) at 200°.

with pressure, as seen in Figure 5. Data at 100° were extremely scattered but a similar trend appeared to hold.

Effect of Added Gases. The effect of up to 250 Torr of helium is seen to have no effect on $R_{CO_2}/R_{C_2F_6}^{1/2}$ in the photolysis of 0.2 Torr of HFZ, as shown in Table IV. However, similar amounts of carbon monoxide caused a large increase in $R_{CO_2}/R_{C_2F_6}^{1/2}$, shown in Table V. Checks were made to ensure that this increase was not due to CO_2 as an impurity or to a dark reaction. It seems unlikely for collisional deactivation to increase the rate of formation of CO_2, and we have no satisfactory explanation for this effect.

Most of our experiments were carried out under conditions where collisional deactivation of the parent molecule was unimportant. For HFA at 2 Torr and 100°, and 7.5 Torr at 200° $\Phi(CO)$ would be expected to be very close to unity.[5] Similarly, $\Phi(N_2)$ should be unity for the HFZ runs in the absence of added gases, but consideration must be given to deactivation in their presence. Ayscough and Steacie[5] found that 95 Torr of H_2 had no effect on $\Phi(CO)$ in the photolysis of 10 Torr of HFA at 78°. We found (Table IV) that product formation was unaffected by added helium in the photolysis of HFZ at 200°. However, in the case of added CO, a clear decrease of C_2F_6 formation is seen (Table V). We cannot be certain whether this decrease was due to HFZ* deactivation or to possible scavenging by traces of O_2 in the CO (the manufacturer's specifications state less than 20 ppm of O_2). But it is clear that we have no evidence for third-body effects in the combination of CF_3 radicals at 200°. Kibby and Weston[21] have obtained evidence for pressure effects at 331° and about 1 Torr and although our experiments were unsuccessful in this regard it is clear that studies of deactivation of vibrationally excited C_2F_6 would be feasible and worthwhile.[22]

Acknowledgment. We are grateful to the National Science Foundation for the support of this work.

(21) C. L. Kibby and R. E. Weston, Jr., *J. Chem. Phys.*, 49, 4825 (1968).

(22) E. Tschuikow-Roux, *ibid.*, 49, 3115 (1968).

The γ Radiolysis of Cyclohexane–Perfluorocyclohexane Solutions[1]

by Michael B. Fallgatter and Robert J. Hanrahan

Chemistry Department, University of Florida, Gainesville, Florida *(Received January 13, 1970)*

An investigation has been made of the products from the ^{60}Co γ radiolysis of liquid-phase mixtures of cyclohexane and perfluorocyclohexane over the entire concentration range from pure fluorocarbon to pure hydrocarbon. All experiments were done at 64°, at which temperature the two compounds are completely miscible. In general, the products obtained over most of the concentration range are the main products characteristic of the radiolysis of pure cyclohexane, namely hydrogen, cyclohexene, and dicyclohexyl. The yields of hydrogen and cyclohexene are decreased in such a way as to suggest fairly efficient scavenging, but the dicyclohexyl yield is actually enhanced compared to pure cyclohexane. The only major organic product deriving from perfluorocyclohexane is c-$C_6F_{11}H$. A small yield of mixed dimer, possibly formed in a spur reaction, is also found. These results apparently require that cyclohexyl radicals do not react with perfluorocyclohexane, but that perfluorocyclohexyl radicals efficiently abstract hydrogen from cyclohexane. It is suggested that perfluorocyclohexane undergoes electron capture followed by dissociation, either directly or in a subsequent step.

Introduction

The fluorocarbons are interesting in that they are exactly analogous to the hydrocarbons structurally and have similar volatilities and other physical properties for a given chain length, yet differ markedly in other respects such as bond strength, electron affinity, ionization potential, and thermal stability. Accordingly, we decided several years ago, that it would be worthwhile to investigate the radiolysis of fluorocarbon–hydrocarbon mixtures. The cyclic C_6 system was chosen because of the relative simplicity of the radiation chemistry of cyclohexane and because the complete range of liquid mixtures can be achieved at only slightly elevated temperatures. Since the radiolysis of pure F-cyclohexane[2] had not been investigated, it was necessary first to investigate this subject.[3] Several recent studies[4-8] on other fluorocarbon systems provide additional insight into the behavior of these compounds under radiolysis.

During the course of the present work a study of hydrogen production in hydrocarbon–fluorocarbon mixtures was published, with experimental results closely paralleling that aspect of the present work, but with a different mechanistic interpretation.[9] More recent publications[10,11] dealing with dilute solutions of F-cyclohexane in cyclohexane in both the liquid and gas phase present conclusions similar to those reached in the present work.

The data reported here include measurements of the yields of hydrogen, cyclohexene, dicyclohexyl, a mixed dimer, and undecafluorocyclohexane as a function of mixture composition over the entire range from pure cyclohexane to pure F-cyclohexane, and also as a function of radiation dose for one selected composition. Results are discussed in terms of radical abstraction reactions and electron capture by the fluorocarbon.

Experimental Section

Purification of Materials. The cyclohexane used in these experiments was Phillips research grade, further purified by passage through silica gel. The F-cyclohexane used was obtained from Imperial Smelting Corp., Ltd. and was purified by preparative scale gas–liquid chromatography as previously described.[3]

Preparation and Irradiation of Samples. Samples of 1.0 and 0.15 ml were irradiated, the smaller volume being used for the mixtures containing over 90% fluorocarbon. Cells made from 8-mm Pyrex tubing were used for the 1.0-ml samples and cells made from 6-mm Pyrex tubing for 0.15-ml samples. Samples to be irradiated were prepared on a vacuum line. Cyclohexane was dried over BaO and F-cyclohexane by passage through a bed of P_2O_5. Both materials were degassed by several freeze–pump–thaw cycles before the amounts required were measured out and sealed off in the irradiation cells. F-cyclohexane was measured using PVT techniques as was cyclohexane when 0.15-ml samples

(1) Presented at the 154th National Meeting of the American Chemical Society, Chicago, Ill., Sept 1967.

(2) The prefix F- will be used as an abbreviation for perfluoro-.

(3) M. B. Fallgatter and R. J. Hanrahan, *J. Phys. Chem.*, **69**, 2059 (1965).

(4) L. Kevan and P. Hamlet, *J. Chem. Phys.*, **42**, 2255 (1965).

(5) L. Kevan, *J. Chem. Phys.*, **44**, 683 (1966).

(6) J. Fajer, D. R. MacKenzie, and F. W. Bloch, *J. Phys. Chem.*, **70**, 935 (1966).

(7) D. R. MacKenzie, F. W. Bloch, and R. H. Wiswall, Jr., *ibid.*, **69**, 2526 (1965).

(8) W. C. Askew, T. M. Reed, III, and J. C. Mailen, *Radiat. Res.*, **33**, 282 (1968).

(9) L. A. Rajbenbach, *J. Amer. Chem. Soc.*, **88**, 4275 (1966).

(10) N. H. Sagert, *Can. J. Chem.*, **46**, 95 (1968).

(11) N. H. Sagert and A. S. Blair, *ibid.*, **46**, 3284 (1968).

were used. For the 1.0-ml samples, cyclohexane was measured using a vacuum line buret.[12]

All samples were irradiated in a ^{60}Co γ irradiator at a flux of about 0.5 Mrad/hr. Irradiations were performed at 64 ± 1°, a temperature at which all the samples were liquid and at which c-C_6H_{12} and c-C_6F_{12} are miscible in all proportions.

Analysis of Radiolysis Products. Qualitative analyses of the radiolysis products was accomplished using comparative gas–liquid chromatographic retention volumes and mass spectra, the latter obtained using a Bendix Time-of-Flight mass spectrometer coupled directly to the output of a gas chromatograph.[3]

Hydrogen was quantitatively determined by irradiating 1.0-ml samples in cells fitted with break-seals. After irradiation, the cells were opened under vacuum and the contents distilled into a trap at liquid nitrogen temperature. The residual gas was then collected and measured using a Toepler pump.

The remaining major radiolysis products measured in this study, including c-$C_6F_{11}H$, c-C_6H_{10}, dicyclohexyl, and a product tentatively identified as perfluorocyclohexyl cyclohexane ("mixed dimer"), as well as two unidentified species formed with lower yields, were determined by quantitative gas–liquid chromatography using flame ionization or electron capture detection. The chromatographic conditions used were: for c-$C_6F_{11}H$, a 7-m column, packed with 10% silicone gum rubber on Chromosorb W and operated at 45°; for c-C_6H_{10}, a 6.4-m column, packed with 5% β,β′-oxydipropionitrile on Chromosorb W and operated at 50°; for mixed dimer and dicyclohexyl, a 0.8-m column packed with 10% silicone gum rubber on Chromosorb W and operated at 160° (used for dicyclohexyl only), or a 1.8-m column, packed with 10% silicone gum rubber on Chromosorb W and operated at 100° until elution of the solvent, 150° thereafter until elution of the mixed species and 180° thereafter until elution of dicyclohexyl. Flame ionization detection was used in all cases except for detection of F-dicyclohexyl, in which case electron capture detection and the same column as was used for cyclohexene were used.

The cyclohexene, F-dicyclohexyl, and dicyclohexyl used as chromatographic standards were obtained from Phillips Petroleum Co., Imperial Smelting Co., Ltd., and Columbia Organic Chemical Co., respectively, and were used, after a chromatographic check of purity, without further purification.

Results

Identification of Products. Several of the radiolysis products were readily identified since they are also the main products from pure cyclohexane; these are hydrogen, cyclohexene, and dicyclohexyl. The major product containing a fluorocarbon residue was found to be c-$C_6F_{11}H$; this compound elutes just after c-C_6F_{12} on a silicone gum rubber column. It was found to be identical with a known sample both in its gas chromatographic retention time and in its mass spectrometric fragmentation pattern. A minor product which we refer to as "mixed dimer" was found, having a chromatographicelution time midway between cyclohexane and dicyclohexyl. Mass spectrometric analysis showed that it consists of a C_6 hydrocarbon portion and a C_6 fluorocarbon portion. However, a detailed consideration of the spectrum left some doubt whether the compound was, in fact, the simple dimer c-C_6H_{11}–c-C_6F_{11} as might perhaps be expected. The fragmentation pattern suggested that one or both portions of the molecule might be open chain. No clear conclusion on this point could be reached, however, since the yield of this product is low and the resulting spectra were of poor quality. Two additional products were found eluting between the "mixed dimer" and dicyclohexyl, called products E and F for convenience. Their yields could be measured with a flame detector and are reported below. However, these compounds are produced in such small amounts that efforts to identify them were not successful.

As in the case of pure F-cyclohexane, no F-cyclohexene was produced. It was also shown by chromatographic comparison with a known sample that c-$C_6H_{11}F$ is not a radiolysis product.

A product which is important in pure F-cyclohexane but not in the mixtures is the fluorocarbon dimer, $(c$-$C_6F_{11})_2$. Although it has a yield of 0.95 mol/100 eV in pure F-cyclohexane,[13] it is decreased to *ca.* 5×10^{-3} by the addition of 0.1% cyclohexane. The yield decreases further to 1×10^{-3} at about 5% cyclohexane.

Concentration Dependence of Product Yields. Radiolysis yields of hydrogen gas, cyclohexene, and dicyclohexyl are shown as a function of composition in Figures 1a, 1b, and 1c. Due to analytical difficulties we were not able to obtain data on cyclohexene formation for solutions containing more than 50% cyclohexane. Figure 1d shows the concentration dependence of the yield of c-$C_6F_{11}H$. Figures 2a and 2b show the yields of the mixed dimer and of the two unidentified products E and F over part of the composition range. Figure 2b suggests that these species are partially or entirely fluorocarbon in nature, since their yields increase with fluorocarbon concentration.

Dose Dependence of Product Yields. Figures 3 and 4 show the effect of total dose on the yields, respectively, of the major products hydrogen, cyclohexene, dicyclo-

(12) R. J. Hanrahan, *J. Chem. Educ.*, **41**, 623 (1964).

(13) Yields of the major products from the radiolysis of pure F-cyclohexane have recently been redetermined in this laboratory by Mr. George A. Kennedy. The following G values were obtained: F-cyclohexylhexane, 0.11; F-cyclohexylhexene, 0.43; F-dicyclohexyl, 0.95. These yields are in fairly good agreement with some early, unpublished results of M. B. Fallgatter in this laboratory, and also are considerably closer to the yields obtained by MacKenzie and coworkers[7] than were the figures originally published by Fallgatter and Hanrahan.[3] It appears that the latter results were too high due to an error in a dosimetry calculation.

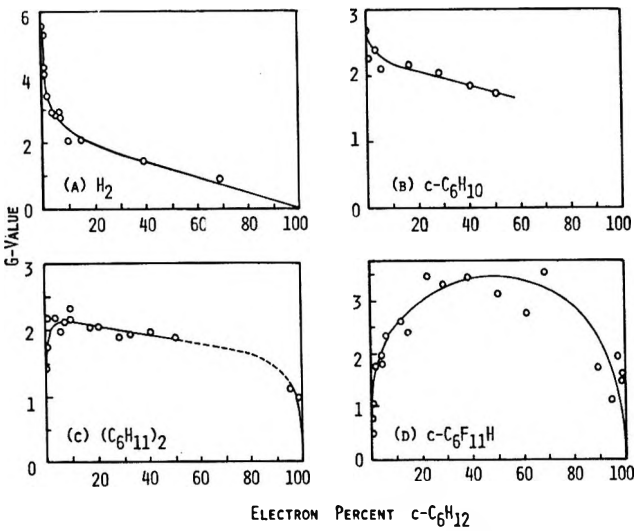

Figure 1. Dependence of major product yields on mixture composition in the radiolysis of c-C_6F_{12}–c-C_6H_{12} solutions: (a) hydrogen, (b) cyclohexene, (c) dicyclohexyl, (d) undecafluorocyclchexane.

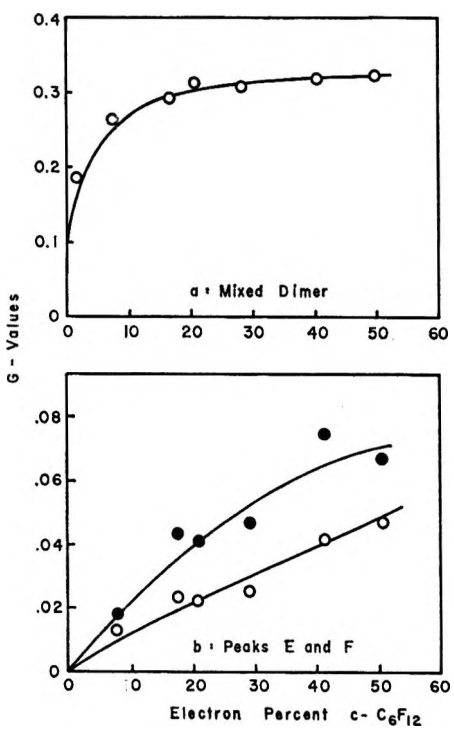

Figure 2. Dependence of minor product yields on mixture composition in the γ radiolysis of c-C_6F_{12}–c-C_6H_{12} solutions: (a) mixed dimer, (b) peaks E and F.

hexyl, and undecafluorocyclohexane, and the minor products, mixed dimer and products E and F. All of these measurements were made on solutions containing 10.2 electron % cyclohexane. Figure 4b shows one of the reasons we had difficulty in identifying compounds E and F: their yields do not increase regularly with dose, but instead essentially reach a plateau. As might be expected, the cyclohexene yield is also strongly dose dependent.

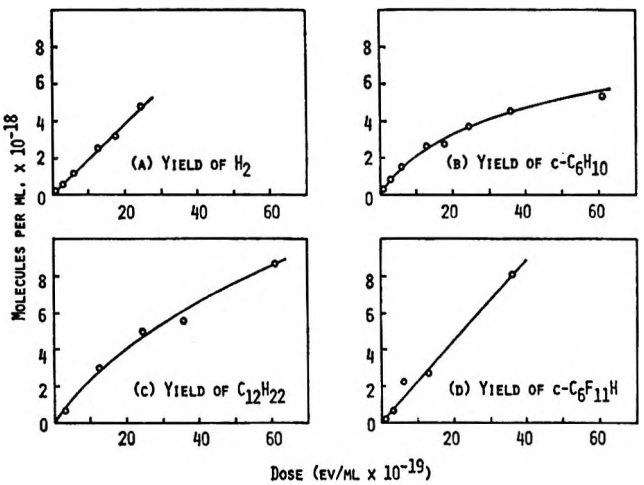

Figure 3. Major product yields as a function of dose for mixtures containing 10.2 electron % cyclohexane in F-cyclohexane: (a) hydrogen, (b) cyclohexene, (c) dicyclohexyl, (d) undecafluorocyclohexane.

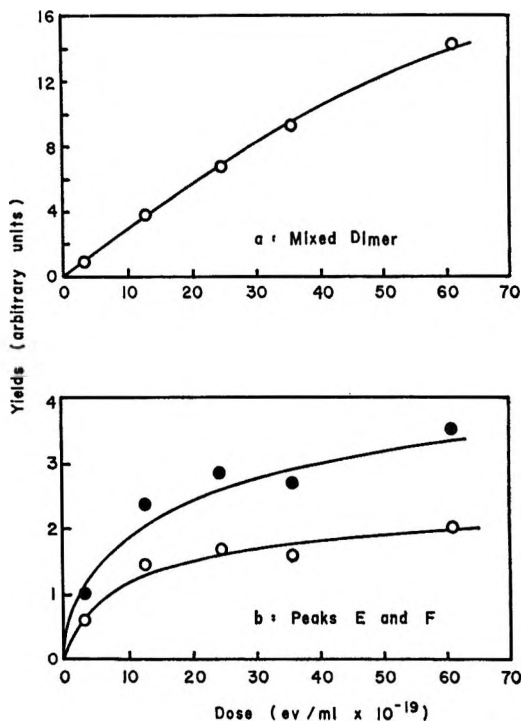

Figure 4. Minor product yields as a function of dose for mixtures containing 10.2 electron % cyclohexane in F-cyclohexane: (a) mixed dimer, (b) peaks E and F.

Discussion

From a mechanistic viewpoint, the most important observations on the effects of added F-cyclohexane in the radiolysis of cyclohexane are probably the decrease in the H_2 yield, originally noted by Rajbenbach,[9] and the efficient production of c-$C_6F_{11}H$, reported first by this laboratory[14] and subsequently by Sagert.[10] These

(14) M. B. Fallgatter and R. J. Hanrahan, Paper No. 127, Division of Physical Chemistry, 148th National Meeting of the American Chemical Society, Chicago, Ill., Sept 1964.

effects, as well as an increase in the dicyclohexyl yield, develop at low concentrations of added fluorocarbon.[10] The present study shows that these trends continue smoothly to 50 mol % fluorocarbon and beyond. We also find a slight decrease in the cyclohexene yield up to equimolar mixtures, while Sagert's data show a nearly constant yield between 0.03 and 0.3 *M* fluorocarbon.[10]

Effects in the region of dilute hydrocarbon (concentrated fluorocarbon) appear to raise no interpretational difficulties. It is reasonable to postulate that there is a substantial yield of $c\text{-}C_6F_{11}\cdot$ radicals, formed in a direct process, which abstract hydrogen from cyclohexane to give $c\text{-}C_6F_{11}H$. The residual cyclohexyl radicals then undergo combination–disproportionation reactions. Of course, the precursors of $c\text{-}C_6F_{11}\cdot$ may be ionic.

The radiation chemistry of cyclohexane–F-cyclohexane solutions resembles that of the pure hydrocarbon much more closely than that of the pure fluorocarbon at all concentrations studied in this work. None of the major products from the pure fluorocarbon are found in substantial yield, while considerable amounts of all of the major products from the pure hydrocarbon are found. Hence, an attempt to interpret this system most conveniently begins with a mechanism for cyclohexane radiolysis. Such a scheme was presented for this purpose by Sagert.[10]

Sagert[10,11] and Rajbenbach[15,16] and their respective coworkers have presented a number of possible mechanistic steps pertinent to the understanding of the behavior of solutions of F-cyclohexane in cyclohexane under radiolysis

$$c\text{-}C_6F_{11}\cdot + c\text{-}C_6H_{12} \longrightarrow c\text{-}C_6F_{11}H + c\text{-}C_6H_{11}\cdot \quad (1)$$

$$H\cdot + c\text{-}C_6F_{12} \longrightarrow HF + c\text{-}C_6F_{11}\cdot \quad (2)$$

$$e^- + c\text{-}C_6F_{12} \longrightarrow F^- + c\text{-}C_6F_{11}\cdot \quad (3)$$

$$e^- + c\text{-}C_6F_{12} \longrightarrow c\text{-}C_6F_{12}^- \quad (4)$$

$$c\text{-}C_6F_{12}^- + c\text{-}C_6H_{12}^+ \longrightarrow c\text{-}C_6F_{11}\cdot + c\text{-}C_6H_{11}\cdot + HF \quad (5)$$

Reaction 1 is proposed as the origin of the substantial yield of $c\text{-}C_6F_{11}H$. The analogous reaction in which cyclohexyl radical would attack F-cyclohexane is not postulated, since $c\text{-}C_6H_{11}F$ is not an observed product.

In his initial efforts to interpret the decrease in the H_2 yield in fluorocarbon–hydrocarbon systems, Rajbenbach emphasized the possibility of process 4, nondissociative electron capture, and argued against the plausability of reactions 2 and 3 on energetic grounds. However, the nondissociative attachment process fails to account for efficient production of $c\text{-}C_6F_{11}H$ in this system.[10,14] Sagert proposed reaction 5 to bring C–F bond rupture within the scope of Rajbenbach's postulate. Both Rajbenbach[16] and Sagert[10] have recognized that if fluorocarbon negative ions play an important role in these systems, the lifetime of the particular ion involved in various fluorocarbon systems would be significant in interpreting such systems. For example, the fact that the lifetime of $c\text{-}C_4F_8^-$ is 100 times shorter[17] than that of $c\text{-}C_6F_{12}^-$ may be related to observed differences in the behavior of F-cyclohexane systems[11] and F-cyclobutane systems[18,19] in the gas phase.

However, there exists no independent confirmation, either experimental or theoretical, of the occurrence of reaction 5. In fact, one might object to it on the basis of arguments given by Magee[20] against the likelihood of metathetical reactions of the type

$$A^+ + B^- \longrightarrow C + D \quad (6)$$

Although reaction 5 is of a somewhat different type, Magee's arguments appear to apply equally against it.

In our original consideration of the F-cyclohexane–cyclohexane system,[14] we suggested the participation of reaction 2, since arguments against it did not appear to be convincing (and such data as do exist refer to the gas phase). In an attempt to search experimentally for the possible occurrence of reaction 2 in the liquid phase, Mr. George Kennedy of this laboratory carried out photolysis of HI in liquid F-cyclohexane at 60° with an Hg-2537 resonance lamp. At this wavelength HI absorbs fairly efficiently, while the fluorocarbon is essentially transparent. Although extensive production of I_2 occurred in the experiment, no $c\text{-}C_6F_{11}H$ could be detected by gas chromatography. This indicates that F-cyclohexane did not effectively compete with HI as a trap for hydrogen atoms in spite of being present at a concentration 10^4 times greater. Although reaction 2 may occur to a small extent with hot hydrogen atoms, it cannot be the main route to production of $c\text{-}C_6F_{11}H$.

This result appears to rule out the only alternative to the conclusion reached by both Sagert and Rajbenbach that the special effects in fluorocarbon–hydrocarbon systems are due to primary processes involving charged species: electron capture by the fluorocarbon followed by rupture of a C–F bond, either directly or in a subsequent step. It is not at present possible to argue strongly for or against either alternative. All work published to date appears to be consistent with the view that most of the secondary reactions in the system are of the free radical type.

Several other aspects of the present results deserve brief comments. First, since the present study, done

(15) L. A. Rajbenbach and U. Kaldor, *J. Chem. Phys.*, **47**, 242 (1967).

(16) L. A. Rajbenbach, *J. Phys. Chem.*, **73**, 356 (1969).

(17) W. T. Naff and C. D. Cooper, *J. Chem. Phys.*, **49**, 2784 (1968).

(18) E. Heckel and R. J. Hanrahan, Advances in Chemistry Series, No. 82, American Chemical Society, Washington, D. C., 1968, p 120.

(19) E. Heckel and R. J. Hanrahan, Paper No. 140, Division of Physical Chemistry, 158th National Meeting of the American Chemical Society, New York, N. Y., Sept 1969.

(20) J. L. Magee, *Discuss. Faraday Soc.*, **12**, 33 (1952).

at 65°, gave results very similar to those of Sagert[10] at 25°, it appears that no reactions with a substantial temperature coefficient are involved. Next, the small yields of mixed fluorocarbon–hydrocarbon products are consistent with the assumption that reaction 1 occurs efficiently, dropping the steady-state concentration of F-cyclohexyl radicals to a low level. The small yields which are found may be formed in spurs. Finally, the observed dose effect on the cyclohexene yield and the lack of effect on hydrogen and $C_6F_{11}H$ are compatible with the nature of these compounds. The small dose effects on the hydrocarbon dimer and mixed dimer are not unreasonable. The dose–plateau behavior of products E and F is rather intriguing, but we have no evidence on the identities of these substances, except that they are likely to be partially fluorocarbon in composition.

Acknowledgment. This work was supported by the Atomic Energy Commission under Contract AT-(40-1)-3106 and by the University of Florida Nuclear Science Program. During a part of the work M. B. F. was a participant in the NSF-sponsored Summer Research Program for College Teachers. This is Document Number ORO-3106-24.

The Study of Second Coordination Sphere of Complex Ions by Nuclear Magnetic Resonance

by Amos J. Leffler

Department of Chemistry, Villanova University, Villanova, Pennsylvania 19085 *(Received October 27, 1969)*

Methylene chloride functions as an inert "probe" in aqueous solutions of paramagnetic ions to study the effect of second coordination sphere solvent ordering. A series of hexaaquo 3d transition metal ions was studied and it was found that the correlation time was controlled either by the electron spin relaxation or by the rotational tumbling of the methylene chloride depending on which is shorter. In the case of a series of Cr^{3+} complexes it was found that cations more effectively order the second coordination sphere than do anions. A brief study of the effect of temperature showed that there is no basic change of solution structure around the ions between 20 and 74°. The behavior of methylene chloride in comparison with the hydrogen molecule and its relative "inertness" as a probe are discussed.

Introduction

Progress in the understanding of aqueous solution structure using nmr techniques has been comprehensively described by Hinton and Amis.[1] It is evident from the review that most study has been directed toward the first or inner coordination sphere and much less progress has been made in understanding of the second or outer-sphere structure. The major drawback to understanding of outer-sphere structure has been the lack of a suitable probe to study the effect of outer-sphere structure without trying to separate the much larger inner-sphere effects. In the majority of complexes the ligands are rapidly exchanged between inner- and outer-coordination spheres and the major factors controlling the relaxation of the nuclei are the rates of exchange, the change in precessional frequency between coordinated and uncoordinated states, or the electron spin relaxation time. Outer-sphere effects must be determined by subtraction of the inner-sphere effect from the total relaxation process. Only in the cases of Cr(III) and Co(III) of the common ions is it possible to examine the outer-sphere effects directly because of their slow ligand exchange rates. Even in the case of the former it is necessary to use ^{17}O values because the water protons are rapidly exchanged by the reaction[2]

$$Cr(H_2O)_6^{3+} + H^*HO \longrightarrow Cr(H_2O)(OH)^{2+} + H^*H_2O^+$$

$$Cr(H_2O)_5(OH)^{2+} + H^*H_2O^+ \longrightarrow Cr(H_2O)_5(H^*HO)^{3+} + H_2O$$

(1) J. F. Hinton and E. S. Amis, *Chem. Rev.*, **67**, 367 (1967).

(2) R. G. Pearson, J. Palmer, and A. L. Allred, *Z. Elektrochem.*, **64**, 110 (1960).

A suitable probe to study the outer-coordination sphere must possess certain properties. It must be completely excluded from the inner-coordination sphere under all conditions. In addition, it must be mobile enough and small enough in size to diffuse rapidly through the bulk solution to the second coordination sphere at a rate which will give the same average distribution as that of the bulk solvent. Also, it must have sufficient solubility to give a detectable response. Finally, it should behave in a similar manner to the solvent molecules except for first-sphere exclusion. The most ideal probe would be the hydrogen atom itself but since this cannot exist as such in solution the hydrogen molecule would be the next best choice.

The para–orthohydrogen transition has been extensively studied in solution[3-5] but only in the integrated form of observing the kinetics of conversion. The solubility of H_2 in an aqueous solution is too low to permit the direct observation of transitions between the orthohydrogen triplet states. The integrated transition rate is a composite of the transfer of the gas into solution, diffusion in solution, rate of conversion, and finally transfer out of solution, and therefore cannot readily give information about the conversion process alone.

It has been found that both methylene chloride and chloroform fit the requirements outlined above for a suitable probe. Methylene chloride is superior at ambient temperatures because of its greater solubility and two protons. It was used exclusively in the present work. Since the proton resonance peaks for water and methylene chloride are relatively close together the water in a normal aqueous solution would swamp out the relatively small CH_2Cl_2 peak. Therefore all studies were run using D_2O as the solvent. In this work the effect of a number of aquo transition metal complexes and various chromium complexes on the proton peak width of methylene chloride was studied as a function of concentration and temperature.

Experimental Section

Materials. The deuterium oxide used was from Merck Sharp and Dohme of Canada and was nominally 99.5% D_2O. The methylene chloride was Matheson Coleman and Bell Spectroquality reagent. Saturated CH_2Cl_2 in D_2O was prepared by allowing the two materials to stand together with occasional shaking for a minimum of 24 hr. The upper D_2O layer was drawn off using a 1-ml syringe.

$Co(NO_3)_2 \cdot 6H_2O$, $CuCl_2 \cdot 2H_2O$, and $MnSO_4 \cdot H_2O$ were CP reagents and were obtained from Baker. They were used as received. $Ni(ClO_4)_2 \cdot 6H_2O$, $Cr(ClO_4)_3 \cdot 6H_2O$, and $Co(ClO_4)_2 \cdot 6H_2O$ were obtained from Alfa Inorganics while $Cu(ClO_4)_2 \cdot 6H_2O$ was received from Frederick Smith Co. All were used as received. $FeCl_2 \cdot 4H_2O$ and $NiCl_2 \cdot 6H_2O$ were obtained from Fisher Scientific Co. and were used as received.

$Cr(NH_3)_6(NO_3)_3$ was prepared as described by Brauer.[6] *Anal.* Calcd for $Cr(NH_3)_6(NO_3)_3$: Cr, 15.28. Found: Cr, 15.48. $K_3Cr(CN)_6$ was prepared from the procedure of Brauer.[6] *Anal.* Calcd for $K_3Cr(CN)_6$: Cr, 15.98. Found: Cr, 16.11. $K_3Cr(CNS)_6$ was prepared from the procedure of Brauer.[6] *Anal.* Calcd for $K_3Cr(CNS)_6$: Cr, 8.82. Found: Cr, 8.22. The difference appears to be water of hydration and the product is formulated as $K_3Cr(CNS)_6 \cdot 6.36 H_2O$. $Cr(CO(NH_2)_2)_6Cl_3$ was synthesized according to King's[7] description. *Anal.* Calcd for $Cr(CO(NH_2)_2)_6Cl_3$: Cr, 9.08; Cl, 18.5. Found: Cr, 10.02; Cl, 20.00. This material is formulated as the anhydrous material instead of the trihydrate described by King. $CoCl_2$ was dehydrated by reaction of the hydrate with $SOCl_2$ as described by Brauer.[6]

Solutions. Stock solutions were prepared by weighing the solids in 1-ml volumetric flasks and making up the required volume of solution at 25°. Since the amount of solids was small in all cases the concentrations of the solutions were calculated on the basis of pure deuterium oxide. The measured solubility of methylene chloride in deuterium oxide was found to be 9.0 g/1000.0 g of deuterium oxide at 25° while the density of the saturated solution was measured to be 1.1090 g/ml *vs.* 1.1059 g/ml for pure deuterium oxide. The increase in density of the solutions means that there is almost the same amount of deuterium oxide as in the pure material. The uncertainties introduced by these approximations are much smaller than those due to line width measurements. When very dilute salt solutions were required the stock solutions were diluted by taking known amounts of stock solution with either a 10- or 25-ml syringe and diluting to 1 ml in the volumetric flask. In the case of cobaltous chloride it was found that the amount of salt required introduced enough H_2O to mask the methylene chloride resonance peak. Therefore the anhydrous salt was prepared as described above.

Nmr Spectra. All nmr spectra were obtained with a Varian A-60 instrument equipped with a variable temperature control accessory. Spectra were run in standard 5-mm diameter tubes. When variable temperatures runs were made the solutions were sealed in the tube under vacuum after degassing. In all spectra HDO resonance was observed. Its source was mainly the water of hydration of the added salt.

Solubility of Methylene Chloride in Deuterium Oxide. Although a solubility value of methylene chloride in

(3) H. Sachsse, *Z. Phys. Chem., Abt. B*, **24**, 429 (1934).

(4) G. M. Schwab, J. Voilaender, and V. Penka, *Z. Phys. Chem.* (Frankfurt am Main), **36**, 378 (1963).

(5) W. K. Wilmarth and F. Baes, *J. Chem. Phys.*, **20**, 116 (1952).

(6) G. Brauer, "Handbook of Preparative Inorganic Chemistry," Vol. II, Academic Press, New York, N. Y., 1963.

(7) A. King, "Inorganic Preparations," Van Nostrand, Princeton, N. J., 1936, pp 48, 106.

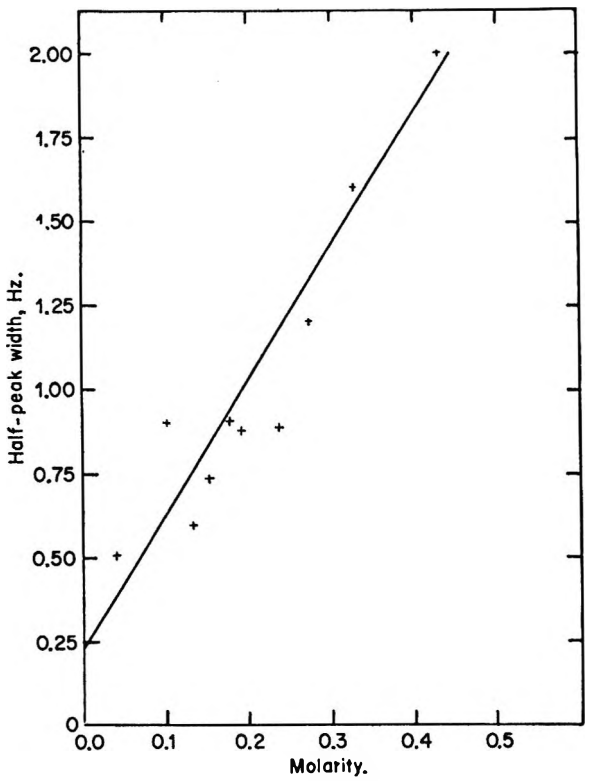

Figure 1. Peak broadening of CH_2Cl_2 by $Co(H_2O)_6(NO_3)_2$.

normal water of 2 g, 100 g of solvent at 20° is given in the literature,[8] the solubility was determined in deuterium oxide at 20, 25, and 30°.[9] Saturated solutions were prepared by allowing the materials to stand for 24 hr in a thermostated bath with occasional shaking. Weighed samples were taken in 1-ml volumetric flasks held at the respective temperature and weighed amounts of *p*-dioxane were added to calibrate the proton response of the nuclear magnetic resonance peaks. Each sample was run at the thermostated temperature in the nmr, and the peaks on the chart paper for the *p*-dioxane and methylene chloride were cut out and weighed. The solubility results in grams of methylene chloride per 1000 g of deuterium oxide are 20, 9.2, 25, 9.0, 30, and 7.3°. The estimated accuracy is 10% but it is clear that the results are much lower than the value in the literature.

Peak-Width Measurements. A series of peak-width measurements were carried out at 30° for Cu^{2+}, Cr^{3+}, Co^{2+}, Fe^{2+}, Mn^{2+}, and Ni^{2+} hexaaquo ions. Various diamagnetic anions were used but did not affect the methylene chloride peak-width values. The best fit of the peak widths as a function of metal ion concentrations was determined by a least-squares program. Peak broadening of methylene chloride in pure deuterium oxide was evaluated by extrapolation to zero metal ion concentration and this value subtracted from the observed value at each concentration to determine the peak broadening due to the metal ion. A typical plot for Co^{2+} is shown in Figure 1. The scatter is primarily due to instrument limitation.

A similar set of measurements was carried out for the $Cr(NH_3)_6^{3+}$, $Cr(CN)_6^{3-}$, $Cr(CNS)_6^{3-}$, and $Cr(CO(NH_2)_2)_6^{3+}$ complexes. In no case were the solutions allowed to stand over an hour after being prepared to minimize decomposition.

Results and Discussion

Aquated Metal Ion Measurements. The peak broadening due to unpaired electron–nuclear coupling is described by the Bloembergen–Solomon formula[10] given in eq 1.

$$\frac{1}{T_{2M}} = {}^4/_3 S(S+1)\frac{g^2\beta^2 g_N{}^2\beta_N{}^2\tau_c}{\hbar^2 r^6} + {}^1/_3 S(S+1)\frac{a^2}{\hbar^2}\tau_e \quad (1)$$

In (1) T_{2M} is the relaxation time of methylene chloride protons in the second coordination sphere, S the unpaired electron spin value, g and g_N have the values 2.002 and 5.585, respectively, β and β_N are the Bohr and nuclear magnetons, respectively, τ_c is the effective dipolar correlation time, a is the isotropic hyperfine interaction constant, τ_e is the effective contact correlation time, and r the distance of closest approach of the methylene chloride to the metal ion. The observed peak broadening is a function of the metal ion concentration and mole fraction of methylene chloride as well the coordination geometry of the complex and is given by

$$\frac{1}{T_2} = \frac{N_{CH_2Cl_2}n}{N_{D_2O} + N_{CH_2Cl_2}}\frac{1}{T_{2M}} \quad (2)$$

where T_2 is the observed peak broadening, $N_{CH_2Cl_2}$ and N_{D_2O} are the moles of methylene chloride and deuterium oxide, respectively, and n is the allowable number of protons coordinated in the second sphere. In eq 1 peak broadening can occur by both dipolar and contact mechanisms and it was necessary to determine whether both were operative. This was tested by plotting the absolute peak shifts in Hz as a function of the metal ion concentrations. If we assume that methylene chloride only undergoes bulk susceptibility shifts then the shift in Hz between HDO and methylene chloride gives the contact shifts of the HDO due to spending part of its time in the first coordination sphere. The apparent contact shifts of HDO due to Fe^{2+} and Co^{2+} were found to be directly proportional to the metal ion concentration as shown in Figure 2. The values for the other ions at the concentrations used were too small to be measured. The ratio of Δ contact for Fe^{2+}/Co^{2+} was very

(8) N. A. Lange, "Handbook of Chemistry," 10th ed, McGraw-Hill, New York, N. Y., 1961.

(9) One of the referees requested these data and thanks are due to him since the calculated distance of closest approach of the methylene chloride is considerably changed as a result of this measurement.

(10) A. Abragam, "Nuclear Magnetism," Oxford University Press, New York, N. Y., 1961.

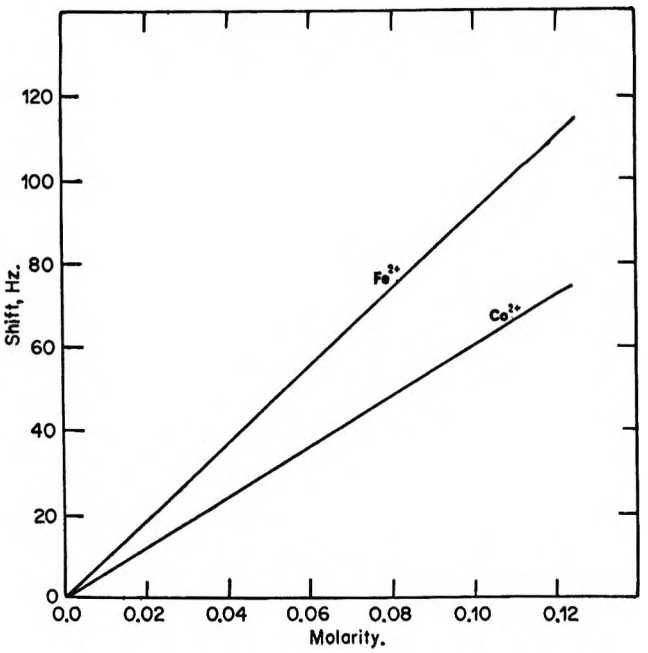

Figure 2. Apparent contact shift of H_2O against CH_2Cl_2 due to $Fe(H_2O)_6^{2+}$ and $Co(H_2O)_6^{2+}$ ions.

close to that observed by Wayland and Rice.[11] Therefore it was concluded that only the dipolar broadening mechanism is effective.

Although all peak broadenings were proportional to metal ion concentrations, large differences were found between various metals. The ions Co^{2+}, Fe^{2+}, and Ni^{2+} were very inefficient in broadening the methylene chloride peak and concentrations up to about 0.1 M were required for appreciable broadening. In the case of Mn^{2+} the resonance peak disappeared at metal concentrations greater than 0.1 M while Cu^{2+} and Cr^{3+} were intermediate between the two extremes. In comparison to these results the reaction rate constants for the para–orthohydrogen reaction in aqueous solution showed a factor of 2 over the same metals when corrected for the number of unpaired electrons. The values are shown in Table I. Since both methylene chloride peak broadening and para–orthohydrogen conversion are electron–nuclear interactions the difference in metal ion efficiencies can be due either to the electron or rotational correlation time for the former but only the rotational correlation time for the latter. The rotational correlation time for H_2 can be approximated from the Debye relation[10]

$$\tau_r = \frac{4\pi\eta a^3}{3kT} \tag{3}$$

where η is the viscosity of the solvent and a the radius of the hydrogen molecule. Using a value of 0.075 nm for the latter, a value of 4.3×10^{-13} sec at 298°K is obtained. The value is shorter than all electron spin relaxation times of the ions as listed in Table II. The value of τ_r for methylene chloride using a molecular radius of 0.20 nm is 8.4×10^{-12} sec which is longer than τ_s for Ni^{2+}, Co^{2+}, and Fe^{2+}. In these cases the τ_s of the electrons control peak broadening. The remaining ions have long τ_s values so that the rotational correlation time of the methylene chloride is controlling.

Table I: Para to Orthohydrogen Conversion Rate Constants for Hexaaquometal Ions[a]

Metal	Rate constant, min^{-1}	Magnetic moments in BM	k/μ^2
Cr^{3+}	2.22	3.83	0.150
Ni^{2+}	1.84	3.22	0.177
Co^{2+}	5.34	5.04	0.210
Mn^{2+}	7.65	5.91	0.219
Fe^{2+}	5.81	4.91	0.240
Cu^{2+}	1.06	1.94	0.284

[a] Normalized to 1 M metal concentration at ambient temperature.

Table II: Correlation Times for Heaxaquometal Ions Assuming Distance of Closest Approach of 0.354 nm

Metal	τ_c, sec	τ_s, sec (lit.)
Co^{2+}	5.0×10^{-13}	5.0×10^{-13}
Cr^{3+}	1.2×10^{-11}	5.0×10^{-10}
Ni^{2+}	2.0×10^{-12}	3.0×10^{-12}
Fe^{2+}	1.0×10^{-12}	1.4×10^{-12}
Cu^{2+}	1.6×10^{-11}	2.0×10^{-8}
Mn^{2+}	2.3×10^{-11}	3.5×10^{-9}

The most carefully measured short electron spin relaxation time is that for Co^{2+} which was found by Fiat and Chmelnick[12] to have the value of 5.0×10^{-13} sec. Using this value in (1) and assuming eight coordination sites in the second sphere[13] the distance of closest approach of methylene chloride to Co^{2+} is found to be 0.354 nm, which is reasonable based on molecular geometry. The calculation assumes that methylene chloride behaves just as does deuterium oxide except that it does not enter the first coordination sphere. Although this cannot be shown conclusively to be the case it must be approximately so. The extreme alternatives can easily be rejected. If methylene chloride "clustered" around the complex ion the proton resonance would be broadened and shifted beyond the instrument range even at very low metal ion concentrations. On the other hand, if methylene chloride did not enter the second coordination sphere then it would not be appreciably broadened by any metal ion con-

(11) B. B. Wayland and W. L. Rice, *Inorg. Chem.*, **5**, 54 (1966).
(12) A. M. Chmelnick and D. Fiat, *J. Chem. Phys.*, **47**, 3986 (1967).
(13) K. Wüthrich and R. E. Connick, *Inorg. Chem.*, **7**, 1377 (1968).

centration. If we assume that the third coordi sphere is about 0.50 nm from the ion then th broadening would be decreased by an order o tude from that observed assuming an equal r for the methylene chloride and deuterium present. The larger distance of closest app d only be compensated for by assuming a corres gly greater likelihood of finding the methylene chloride at this particular distance.

Using the calculated distance of closest approach between Co^{2+} and methylene chloride, values of τ_c were calculated for the remaining ions. The values for Ni^{2+} and Fe^{2+} are very short due to their short τ_s values. In the latter species some concern was felt about the possible oxidation to Fe^{3+} which would affect the value of S and therefore a small amount of $SnCl_2$ and DCl were added in some runs. No effect was found. The remaining correlation times reflect the rotational correlation time of methylene chloride and are shown in Table II. These calculated correlation times are further evidence for methylene chloride having an approximately equal probability as deuterium oxide of being in the second coordination sphere. A factor of 2 difference in probability would change the correlation time by a corresponding amount. Based on the fairly large negative enthalpy and entropy of solution of hydrocarbons[14] in water it was concluded that such species exist as isolated molecules with an ordered arrangement of water molecules around them. Assuming that this is also true for methylene chloride it will be present as isolated molecules weakly hydrogen bonded to the surrounding deuterium oxide molecules. This latter interaction is likely small and allows the rapid rotational correlation time calculated from eq 2. Its close agreement with the value found for a free sphere in the Debye eq 3 is in agreement with this model.

The good agreement of the calculated τ_c values in Table II with that of the free molecule is also evidence that the approximation of a constant radius for the complex ions is valid. Estimates using Morgan's[15] method show only a slight variation in radius from ion to ion. Only in the case of Cu^{2+} would there be any serious doubt of this approximation but even in these cases the calculated τ_c values are close enough to those expected.

Further evidence that the values measured reflect only the second coordination sphere of the metal ion and are independent of the bulk solution is the lack of effect of potassium chloride on the peak width. Concentrations up to 3 M were added to the hexaaquochromium(III) solutions and no appreciable broadening was noted. Similar results were reported by Calvin[16] many years ago for the para–orthohydrogen conversion.

Chromium Complex Ion Measurements. In addition to the hexaaquometal ion complexes a set of peak broadening studies was carried out with a series of chromium complexes. As with the hexaaquo ions the peak broadenings were proportional to metal complex concentrations. Since all of the complexes contained the same metal with essentially the same τ_s value any variation in the peak broadening can be attributed to the complexing ligands. The observed half-height peak widths at 0.01 M metal concentration were plotted as a function of the k/u^2 values for the para–orthohydrogen conversion for each complex ion using the data of Wilmarth and Baes.[5] The result is shown in Figure 3. No attempt was made to estimate the accuracy of the data but the proportionality is evident. It is clear from the results that the complex ion radius is not the controlling factor since the urea complex is larger than the aquo complex but is more efficient as a catalyst. This was even more clearly shown by other ions in the series of Wilmarth and Baes, notably the very large antipyrine complex which falls between the hexaaquo and hexaamino in efficiency. A second observation is that the anion complexes tend to be more efficient than the cationic complexes for catalysis and peak broadening of methylene chloride. Based on these two observations a reasonable explanation of the relative ability of complex

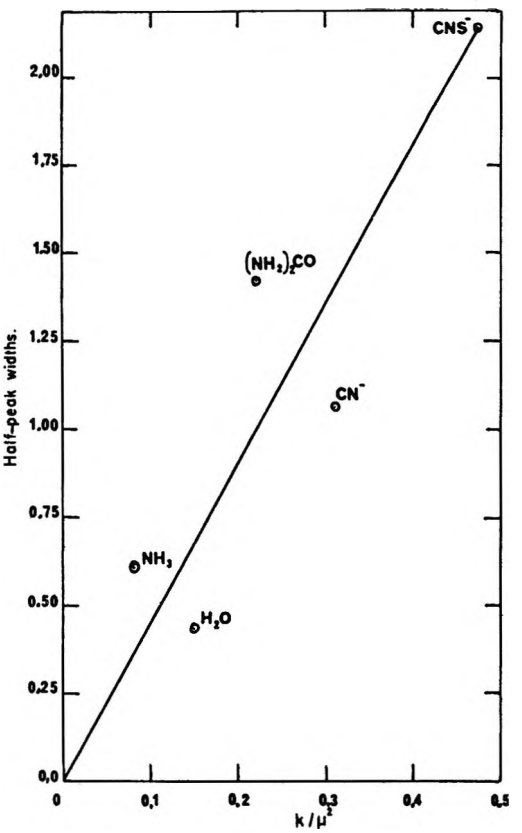

Figure 3. Peak broadening of CH_2Cl_2 by 0.01 M Cr complexes *vs.* k/μ^2 for p → o-H_2 rate constant.

(14) G. Nemethy and H. A. Scheraga, *J. Chem. Phys.*, **36**, 3401 (1962).

(15) L. O. Morgan, *ibid.*, **38**, 2788 (1963).

(16) M. Calvin, *J. Amer. Chem. Soc.*, **60**, 2003 (1938).

ions as catalysts is their power to structure the solvent beyond the first-coordination sphere. A large cation such as antipyrine has a greater ability to affect the water structure than a relatively small anion such as hexacyanide. Cations break down the icelike structure of water more effectively than do anions and thereby decrease the aqueous microviscosity around the ions. The decrease in viscosity reduces the value of τ_c in (1), reducing both the peak broadening of methylene chloride and the correlation time for the para–ortho-hydrogen reduction. This conclusion is in agreement with the work of Horne,[17] who showed that a decrease in the viscosity of water at high pressures is due to the collapse of the icelike structure.

With the present data it is not possible to calculate the distance of closest approach of either methylene chloride or hydrogen molecules to the various chromium complex ions. In neither case is the distance of closest approach to the complex of the correlation times known. However, since both equations have the same inverse r^6 relation and proportional correlation times, the relative efficiency of a series of complexes can be compared. The proportionality between the methylene chloride and hydrogen results for the series of complex ions is evidence that similar mechanisms are operative.

The interaction of both methylene chloride and hydrogen with charged metal complexes appears to be independent of the charge on the ions. A comparison with the effect of a charged species can be made by using Stengle and Langford's[18] data on the peak broadening of ^{19}F in PF_6^- in the presence of a series of chromium complexes. In order to obtain a relation between their results and the para–orthohydrogen results it is necessary to plot the reciprocal of the ^{19}F peak broadenings as shown in Figure 4. Thus the cations are more effective than the anions in contrast to the present work. The authors suggest that ion pairs are formed between the complexes and PF_6^- ions. In their calculation of complexation constants they assumed a similar aqueous structure around each complex ion but pointed out that this is an approximation. The present work shows that the structure does vary with the complex and their complex constants are larger than originally estimated.

A small number of measurements were carried out over a temperature range from 21 to 74° for aquo Cr^{3+}, Ni^{2+}, and Cu^{2+} ions. The broadening due to the ions was obtained by subtracting the peak width of a pure methylene chloride–deuterium oxide solution. Metal ion concentrations were chosen to give convenient peak widths and the results are shown in Table III. Although the results are of low precision there is almost no change in the effectiveness of the metal with temperature. Since metal free broadening has been subtracted we can conclude that there is no appreciable structure change of the solution around the ion. This is rather interesting especially in the case of copper

Table III: Peak Broadening in Hz as a Function of Temperature

Temp, °C	Cr^{3+}, 0.0394 *M*	Ni^{2+}, 0.1182 *M*	Cu^{2+}, 0.0900 *M*
21	2.6	1.2	
27	2.6	1.0	1.8
55	3.2	1.0	1.8 (53°)
67			2.0
74	2.8		

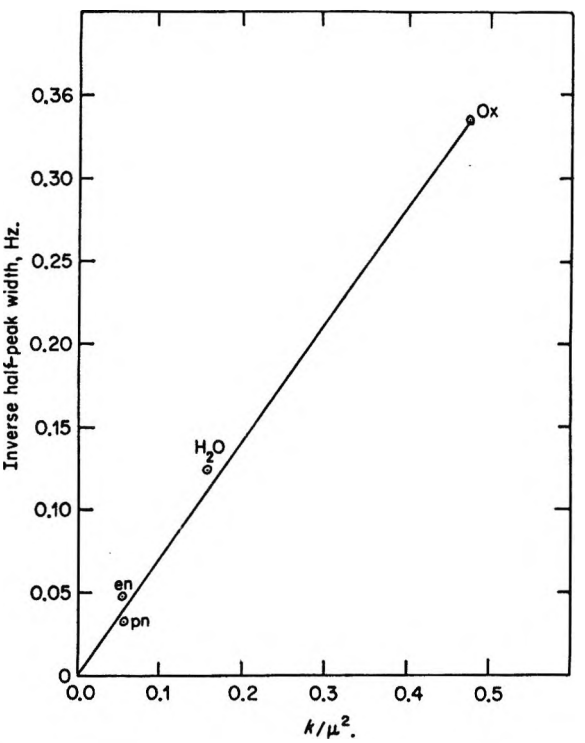

Figure 4. Inverse peak broadening of ^{19}F in 0.05 *M* PF_6 *vs.* k/μ^2 for p → o-H_2 rate constant.

where the loose coordination of the fifth and sixth ligands might have permitted the methylene chloride to enter the primary coordination sphere. Such a process may be possible at higher temperatures but further work will be necessary to demonstrate this.

A comparison of the present work with recent results of Wüthrich and Connick and with Olson, Kanazawa, and Taube[19] indicates the difference in the behavior of the methylene chloride and water in the second coordination sphere. The latter authors find that a correlation time of 2.5×10^{-10} sec for H_2O around the hexaaquochromium(III) ion which is more than an order of magnitude greater than that in the present work. Since this value is so much longer than the rotational correlation time of the water molecule itself it is con-

(17) R. M. Horne and D. S. Johnson, *J. Phys. Chem.*, **70**, 2182 (1966).

(18) J. R. Stengle and C. H. Langford, *ibid.*, **69**, 3299 (1965).

(19) M. V. Olson, Y. Kanazawa, and H. Taube, *J. Chem. Phys.*, **51**, 289 (1969).

cluded that the entire second coordination sphere remains intact during rotation. The present results give a rotational correlation time which is only a factor of 2 greater than that for the methylene chloride in pure deuterium oxide, indicating that the molecule is not held to the complex and has been cited above as evidence that methylene chloride is an "inert" probe. In both papers there is considerable uncertainty of whether both dipolar and scalar coupling mechanisms are operative in the second coordination sphere. Our evidence of solely dipolar coupling is clear. Wüthrich and Connick estimate distances of 0.314 nm and 0.383 nm for the V–O and V–H distances, respectively, for water in the second coordination sphere of the VO^{2+} complex. The value of 0.354 nm for the metal proton distance in the present work is a reasonable one assuming that the methylene chloride molecule is rotating so that only the average distance is found.

Acknowledgments. The author wishes to thank Mr. R. Windolph for the analytical data and Mr. Nyal Walker for the Synthesis of the chromium urea complex, and Messrs. V. Spaziano and B. Burns for many of the nmr spectra.

Nuclear Magnetic Resonance Spectral Parameters and Ring Interconversion of a Series of Piperazines

by R. G. Lett, L. Petrakis,[1] A. F. Ellis, and R. K. Jensen

Gulf Research and Development Company, Pittsburgh, Pennsylvania 15230 *(Received January 6, 1970)*

Several N,N′-, 2,5-, and 2,6-disubstituted piperazines have been examined by high-resolution proton nmr in a variety of solvents and as a function of temperature. Spectral parameters have been extracted by utilizing proton decoupling and iterative computer fitting techniques. Substituents in the compounds which are locked in a chair conformation at room temperature are shown to occupy equatorial sites. Thermodynamic functions for the chair–chair ring interconversion of piperazine and N,N′-dimethylpiperazine have been redetermined by line shape methods. N,N′-Dinitroso- and N,N′-diphenylpiperazine interconvert too rapidly at conveniently accessible temperatures for study using 60-MHz apparatus. The trends of the spectral parameters and the free energies for ring interconversion in various solvents are discussed in terms of their structural implications and significance.

Introduction

The tremendous utility of nuclear magnetic resonance as a structure determining tool is well established. In addition, nmr spectroscopy has found very wide application as a powerful probe in conformational analysis, in general, and ring inversion of six-membered compounds, in particular.[2] The numerous recent publications on this latter subject reflect both the high hopes held for the potential of the technique as well as the care that must be exercised in arriving at conclusions from the nmr data.[2,3]

At low temperatures, distinct, chemically shifted signals are obtained from axially and equatorially placed groups, but when interconverting rapidly at higher temperatures, only one signal is obtained which is the average of the two distinct signals. From the careful determination of the temperature dependence of the rate of interconversion, one can obtain not only the Gibbs free energy for inversion but also the energy of activation and the enthalpy and entropy of activation. Among the various approaches that can be taken in the solution of the problem is the double resonance method, the determination of the coalescence temperature, complete line shape analysis, and spin-echo techniques.[2–5]

We report in this work the detailed investigation of a series of piperazines hereto unreported, as well as the reinvestigation of some that have already been

(1) To whom all correspondence should be addressed.

(2) W. A. Thomas, *Ann. Rev. NMR Spectrosc.*, **1**, 43 (1968), and references therein.

(3) (a) A. Allerhand, H. S. Gutowsky, J. Jonas, and R. A. Meinzer, *J. Amer. Chem. Soc.*, **88**, 3185 (1966); (b) F. A. L. Anet and A. J. R. Bourn, *ibid.*, **89**, 760 (1967).

(4) F. R. Jensen, D. S. Noyce, C. H. Sederholm, and A. J. Berlin, *J. Amer. Chem. Soc.*, **82**, 1256 (1960); **84**, 386 (1962).

(5) L. W. Reeves, *Advan. Phys. Org. Chem.*, **3**, 187 (1965)

reported in certain solvents.[6-9] The determination of the thermodynamic parameters has been made by employing the various techniques indicated above. Also, some determinations have been made in a variety of solvents. When feasible, we have extracted as precise spectral parameters as possible by spectral fitting and decoupling techniques, and have examined the role of substituents and solvents in determining both the spectral parameters, as well as the thermodynamic functions of the interconversion of these systems.

Experimental Section

The dimethylpiperazines were Aldrich Chemical Co. products used without further purification. The purity of *cis*-2,5-dimethylpiperazine was checked by ir and gc. Since the nmr spectra of the other commercial products were consistent with their expected structure, only routine ir spectra were obtained for verification of their structure. The remaining 2,5-disubstituted piperazines were synthesized by a method developed by Ellis.[10] The solid compounds were dried before use by evacuation in a vacuum oven or on a vacuum line. Fresh solutions were run immediately after preparation since samples tend to decompose slowly upon standing. The N,N′-disubstituted piperazines were commercial products also from the Aldrich Chemical Co. and were used without further purification, except for N,N′-dimethylpiperazine which was redistilled before use. Since the quality of the spectra depends on degassing, we bubbled N_2 through the sample and used repeated freeze–pump–thaw techniques before running. The solid compounds are poorly soluble in most solvents at room temperature and rapidly precipitate from cold solutions. Freshly prepared samples were used since solutions tend to decompose upon standing also.

Spectra were obtained on a Varian HA-60-IL. Frequency sweep decoupling experiments utilized a Hewlett–Packard 200 AB or Wavetek III VCG as the external oscillator. Chloroform was used as a lock in the decoupling experiments. Frequencies were counted to ±0.1 Hz using an Hewlett–Packard 521C frequency counter and 10-sec counting periods. Frequency measurements were made on 50- or 100-Hz sweeps run at 250- or 500-sec sweep rates. The final frequency measurements were made relative to tetramethylsilane (TMS) using a TMS lock.

Spectra were fit using LAOCN3 as written by Castellano and Bothner-By.[11] The ABC ring proton spectra were analyzed after they were decoupled from the alkyl side chain protons, and then they were checked by comparison of calculated cathrode ray tube plots of five- and six-spin systems (decoupled) *vs.* observed normal spectra. Iterations were generally convergent to approximately ±0.1 Hz on each measured line. Five per cent solutions were used for temperature measurements. The V-4332 probe was calibrated using a standard ethanol sample, and temperature was maintained to better than ±1° by means of a V4341 temperature controller. The TMS line width was monitored as an indication of T_2.

Results

A. Dialkyl Piperazines. The molecules examined are generally locked in the most stable chair configuration at room temperature. *cis*-2,5-Dimethylpiperazine having one axial substituent is an exception and interconverts rapidly at room temperature. Coalescence temperature was reported[9] to be −74°, $\Delta G^{\ddagger}$ = 9.6 kcal/mol, and at 100 MHz in CH_2Cl_2, $\nu_0\delta_{ae}^{CH_3}$ = 26 Hz. The interconversion can be slowed below −90° at 60 MHz, but the ring proton multiplet shows insufficient resolution for a detailed analysis. The only significant change noted in the spectra of *trans*-2,5-dimethylpiperazine and *cis*-2,6-dimethylpiperazine upon heating to 180° in nitrobenzene was a slight loss of intensity due to decomposition. The interconversion barrier in these molecules may be as high as 20 kcal/mol, or alternatively, the lack of changes in the spectra may be entirely due to the equilibria involved, since both of these molecules exist primarily in the diequatorial form.

The ring proton multiplets are deceptively simple due to the broad lines observed and extensive overlapping. The ring proton patterns of the *trans*-2,5-dibutyl and dioctyl derivatives were identical to within the experimental error. The coupling constants $J_{ae'}$ and $J_{aa'}$ were not independently variable in the diethyl, dibutyl, and dioctyl derivatives and iterations were carried out using an assumed value of $J_{ae'}$. Attempts were made to refine the constants characterizing the spectra of the dimethyl and diethyl derivatives by five- and six-spin calculations with only limited success. Due to the poor resolution, it was not possible to accurately determine the coupling constants between the axial ring proton and methylene protons of the dibutyl and dioctyl derivatives. Computer plots indicate the coupling is similar to that of the diethyl. It was necessary to utilize Lorentzian lines of ∼1.0 Hz half-width to satisfactorily reproduce the observed spectra although spiking with impurities indicated spectrometer resolution was within 0.4 Hz during the experiments. This may be due to the effect of the ^{14}N quadrupole or small cross-ring coupling constants. Similar line widths are observed in N,N′-dimethylpiperazine and other six-membered N containing ring compounds. Unless dealing with ^{14}N decoupled spec-

(6) R. K. Harris and R. A. Spragg, *Chem. Commun.*, 134 (1966).
(7) R. J. Abraham and D. B. MacDonald, *ibid.*, 188 (1960).
(8) J. L. Sudmeier, *J. Phys. Chem.*, **72**, 2344 (1968).
(9) R. K. Harris and R. A. Spragg, *J. Chem. Soc., B*, 684 (1968).
(10) A. F. Ellis, U. S. Patent 3,453,278 (1969).
(11) S. Castellano and A. A. Bothner-By, *J. Chem. Phys.*, **41**, 3832 (1964).

Table I: Spectral Parameters of Diallylpiperazines in Deuteriochloroform, and D_2O Dilute Solutions (All Parameters in Hz; Chemical Shifts Relative to TMS. Dimethylpiperazine Parameters ±0.1 Hz; Others ±0.2 Hz Unless Otherwise Noted)

	trans-2,5-Dimethylpiperazine		*cis*-2,5-Dimethylpiperazine	*cis*-2,6-Dimethylpiperazine	*trans*-2,5-Diethylpiperazine		*trans*-2,5-Dibutylpiperazine		*trans*-2,5-Dioctylpiperazine
	$CDCl_3$	D_2O[a]	$CDCl_3$	$CDCl_3$	$CDCl_3$	C_6H_6	$CDCl_3$	C_6H_6	$CDCl_3$
$\nu_0\delta_e$	176.45	171.54	Multiplet centered	172.00	184.36	163.5	178.08	167.3	178.28
$\nu_0\delta_{a'}$	163.00	158.64	About 164.50	166.86	154.41	141.1	153.61	146.0	153.93
$\nu_0\delta_a$	145.60	137.58	...	135.93	147.10	134.3	144.68	137.7	144.92
$\nu_0\delta_{a'e}$	30.85	33.06	...	37.07	37.26	29.3	33.4	29.6	33.4
$J_{ea'}$	2.71	2.9	...	2.46	2.71 ± 0.5	...	2.80 ± 0.5[c]	...	2.70 ± 0.5
$J_{ae'}$	−11.78	−12.5	...	−12.14	−11.27 ± 0.5	...	−11.73 ± 0.5	...	−11.78 ± 0.5
$J_{aa'}$	10.52	10.8	...	10.51	9.58	...	10.41	...	10.67
$\nu_0\delta_{CH_3}$	60.18	57.60	$\langle 66.60\rangle_{av}\begin{Bmatrix}58.8(eq)\\74.4(ax)\end{Bmatrix}$[b]	60.75	54.93	49.2	53.60	52.5	52.36
$J_{Ha'-CH_3}$	5.85	6.4	$\langle 6.20\rangle_{av}$	5.95	6.20	...	...	...	...
$\nu_0\delta_{CH_2}$	...	...	...	...	80.3	71.5	77.3	73.0	77.4
$J_{CH_2-CH_3}$	...	...	...	...	6.85	...	4.95	...	4.95
$\nu_0\delta_{N-H}$	98.18	...	91.80	91.15	97.10	...	95.71	...	95.15

[a] Reference 8. [b] Reference 9. [c] $(J_{ae} + J_{ea'}) = 8.90 \pm 0.1$ Hz.

tra, the introduction of cross-ring coupling constants to improve the calculated fit of the spectrum is unjustified.[12]

The parameters extracted from spectra in dilute $CDCl_3$ solutions are summarized in Table I. The spin–spin coupling constants indicate unambiguously that both substituents occupy the preferred equatorial positions with the exception of *cis*-2,5-dimethylpiperazine. The relative chemical shifts and coupling constants are reliable to about ±0.1 Hz unless otherwise noted. Absolute chemical shifts relative to TMS are reliable to about ±0.3 Hz with the exception of the N–H band. A comparison of computer synthesized *vs.* observed spectra for *trans*-2,5-diethylpiperazine (ring protons) is shown in Figure 1. The ring proton multiplets of the dibutyl- and dioctylpiperazine spectra are characterized by identical parameters. The alkyl methylene chemical shift given for the latter compounds is only the center of the unresolved alkyl methylene band. Table I also summarizes the ring proton chemical shifts of the diethyl and dibutyl derivatives in benzene relative to TMS. These spectra were repeated in benzene as a check upon the analysis of the $CDCl_3$ spectra.

An analysis of the *trans*-2,5-dimethylpiperazine spectrum in D_2O has been reported by Sudmeier.[8] The constants characterizing the spectrum in $CDCl_3$ are significantly different from those found in a D_2O solution. Of course, D_2O is in no sense a noninteracting solvent for amines. The relative axial–equatorial chemical shifts are ~4 Hz larger in $CDCl_3$. The geminal coupling constant, J_{ae} is less negative and the vicinal couplings smaller. These effects may be largely due to hydration of the piperazine derivative in D_2O. The analysis in $CDCl_3$ given here for a 60-MHz spectrum is also in satisfactory agreement with the decoupled 100-MHz spectrum (kindly provided by Dr. L. A. Wilson, Varian Associates, Springfield, N. J.).

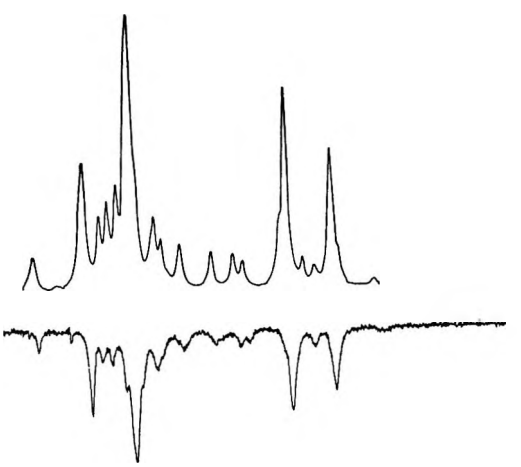

Figure 1. Comparison of computer-synthesized and observed spectra for *trans*-2,5-diethylpiperazine (ring protons).

B. Piperazine and N,N'-Disubstituted Piperazines. Piperazine. The spectrum consists of a single N–H peak at 98.8 Hz and a single ring proton peak at 169.8 Hz from TMS at room temperature in $CHCl_3$ solution. In CH_2Cl_2 solution, the NH peak does not shift, but the ring proton shifts to 164.9 Hz. Broadening of ring proton line is observed as the temperature is lowered. A well-defined AA'BB' pattern is not observed even at −100°. A broad doublet separated by about 2.5 Hz was observed in an ethanol–methylene chloride mixed solvent near −100°. The result is readily understood if the 60-MHz spectrum is pre-

(12) Similar effects were observed in the spectra of N,N,-dinitropiperazine, but H{^{14}N} decoupling did not sharpen the spectra in that case. R. K. Harris, *J. Mol. Spectrosc.*, 15, 100 (1964).

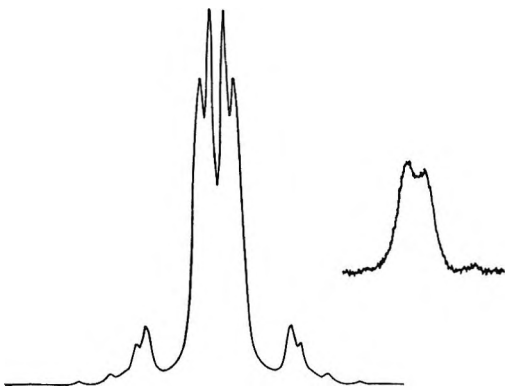

Figure 2. Comparison of observed and synthesized spectrum of piperazine at −100° in ethanol–methylene chloride mixed solvent.

dicted using $\nu_0\delta_{ae}$ = 9.6 Hz derived from 100 MHz results. A plot of the expected low-temperature spectrum is shown in Figure 2. A poorly resolved doublet is also observed in methylene chloride just above the freezing point.

The ring proton interconversion has been frozen out by Harris and Spragg[9] in a methylene chloride solution at 100 MHz. A value of $\Delta G^{\ddagger}$ = 10.3 kcal/mol was determined from the coalescence temperature (−65° at 100 MHz), and the axial–equatorial chemical shift difference was estimated to be 16 Hz. No further parameters have been published indicating a problem extracting coupling constants from the 100-MHz spectrum also. The following parameters are known from an analysis of the ^{13}C spectrum[13] of the rapidly interconverting form

$$^1/_2\langle J_{aa'} + J_{ee'}\rangle = 6.54$$

$$^1/_2\langle J_{ae'} + J_{a'e}\rangle = 3.04$$

Measurements of the ring proton line width with temperature were made using a dilute (~5%) solution in methylene chloride with TMS added as a reference. Reliable measurements were only obtained in a narrow region from −30 to −65°. The results were analyzed using the value[9] $\nu_0\delta_{ae}$ = 9.6 Hz and the line shape function of Gutowsky and Holm[14] for intermediate exchange rates. The free energy of activation was calculated at each temperature, and the values varied from 10.3 to 11.7 kcal/mol. The average value of $\Delta G^{\ddagger}$ ~10.4 kcal/mol in the −30 to −60° temperature range is in good agreement with the 100-MHz value from the coalescence temperature.[9] The Eyring plot indicated that a reliable estimate of $\Delta H^{\ddagger}$ or $\Delta S^{\ddagger}$ is unobtainable from data over the restricted temperature range. A straight line drawn to give a free energy of activation of 10.5 kcal/mol at 298°K yields reasonable values of $\Delta H^{\ddagger}$ (10.1 kcal/mol) and $\Delta S^{\ddagger}$ (−1.6 eu).

N,N-Dimethylpiperazine. This molecule has been extensively studied in conjunction with other six-membered rings.[6,9,15,16] The ring proton line is slightly broadened at room temperature due to axial–equatorial proton exchange. This line broadens and completely collapses near −10°. Below −30°, the ring proton absorption reverts to the AA′BB′ pattern of the non-interconverting molecule.

The AA′BB′ ring proton pattern observed at low temperature is deceptively simple but dependent upon five parameters. A unique set of parameters was unobtainable from a 60-MHz spectrum; therefore, a 100-MHz spectrum was also obtained. A number of lines overlap to form broad bands. There is additional broadening due to the ^{14}N quadrupole nucleus as indicated by a methyl line width at half peak height ~1.8 Hz at −60°. Spectral parameters for a dilute solution spectrum in methylene chloride are summarized in Table II. The errors are estimated from the standard deviations and are a reflection of the internal consistency of the analysis rather than absolute confidence limits. The relative axial–equatorial chemical shift is well determined, but the small vicinal coupling constants can only be estimated. Similar results have been reported by Harris and Spragg.[6] The parameters originally reported by Reeves and Stromme[15] from a 40-MHz spectrum are known to be wrong due to a faulty assumption in their analysis. The ^{13}C satellite spectrum has been investigated by Harris and Sheppard.[16] The chemical shifts of the methyl and ring proton groups relative to TMS at room temperature are summarized in Table III.

Table II: Spectral Parameters Obtained from an Analysis of the Low-Temperature Spectrum of N,N-Dimethylpiperazine in Methylene Chloride

	60 MHz	100 MHz	Lit.[a] (100 MHz)
$\nu_0(\delta_a - \delta_e)$	38.0 ± 0.1	64.3 ± 0.2	63
J_{ae}	−11.3 ± 0.2	−11.4 ± 0.3	...
$J_{ee'}$	2.4 ± 0.2	3.3 + 0.3	$(J_{aa'} + J_{ee'})$ = 13.6
$J_{aa'}$	11.5 ± 0.2	12.0 ± 0.3	...
$J_{ea'}$	3.2[b]	3.2[b]	3.2

[a] References 6 and 7. [b] Fixed.

Temperature runs were made in several solvents using 5% solutions bubbled with N_2 before capping. The methyl absorption was monitored during each sweep as an indication of T_2. The data were first treated using the Piette–Anderson equation.[17] Experimental problems and approximations in the treat-

(13) J. B. Lambert, *J. Amer. Chem. Soc.*, **89**, 1836 (1967).

(14) H. S. Gutowsky and C. H. Holm, *J. Chem. Phys.*, **25**, 1228 (1956).

(15) L. W. Reeves and K. O. Stromme, *ibid.*, **34**, 1711 (1961).

(16) R. K. Harris and N. Sheppard, *J. Chem. Soc., B*, 200 (1966).

(17) L. H. Piette and W. A. Anderson, *J. Chem. Phys.*, **30**, 899 (1959).

Table III: Observed Chemical Shifts of N,N'-Dimethylpiperazine at Room Temperature and Activation Parameters Determined by Various Methods

	Chemical shifts, Hz, relative to TMS			Activation parameters, kcal/mol		
Solvent	CH_2	CH_3	$\nu_0\delta_{ac}$	E_a[a]	$\Delta G^{\pm}_{298}$[b]	$\Delta G^{\pm}_{298}$[c]
CCl_4	137.6	129.5	34.0	12.2	13.6	13.1
$CDCl_3$	146.8	137.0	39.5	16.2	13.5	13.4
CH_2Cl_2	141.4	132.2	38.5	13.8	13.3	13.2
CS_2	138.4	129.6	32.6	12.7	12.4	12.7
Acetone	136.4	128.5	...	...	...	...
Benzene	138.6	127.3	...	...	...	...
Methanol	148.3	135.9	40.6	14.4	14.1	13.5

[a] Piette–Anderson equation, ref 17. [b] Gutowsky–Holm equation, ref 18. [c] Density matrix treatment for AB system, ref 19.

ment lead to considerable distortion of the plots at both high and low temperature. The uncertainty in the slope of these plots is sufficient to render changes in E_a for different solvents of little quantitative significance. Free energies of activation were determined by two methods (Table III). The line shape function derived by assuming two site exchanges in the absence of spin–spin coupling was initially used.[18] Eyring plots constructed using rate constants determined from this approach indicate that reliable values of $\Delta H^{\pm}$ and $\Delta S^{\pm}$ cannot be determined without data over a wider temperature range. A reanalysis was made using a program written by Newmark[19] based on density matrix methods. The molecule was assumed to be a strongly coupled AB system. Free energies determined by this approach show little variation over the range of accessible temperatures indicating a relatively small value of $\Delta S^{\pm}$ ($|\Delta S^{\pm}|<5$ cal/deg mol). The results are summarized in Table IV also.

Table IV: Observed Spectrum of N,N'-Diphenylpiperazine Chemical Shifts in Hz Relative to TMS

	N,N'-Diphenylpiperazine	
Solvent	Aliphatic	Aromatic
CCl_4	196.2 ± 0.1	~420
$CDCl_3$	197.0 ± 0.1	~420
CH_2Cl_2	195.2 ± 0.1	~420
Acetone	199.1 ± 0.1	~420
Benzene	177.0 ± 0.1	~420

N,N-Diphenylpiperazine. This compound is poorly soluble in most of the suitable nmr solvents. At room temperature, the spectrum consists of only a sharp ring proton line due to rapid axial ↔ equatorial conversion and a five-spin multiplet in the aromatic region. The results are summarized in Table IV. The aromatic region is not completely analyzed but estimates of the chemical shifts in chloroform are: $\nu_0\delta_{ortho} \approx 415$ Hz (rel TMS), $\nu_0\delta_{meta} \approx 435$ Hz, and $\nu_0\delta_{para} \approx 414$ Hz. The ring interconversion process is too rapid to give any significant temperature effects in the range 25 to −100° in methylene chloride.

N,N'-Dinitrosopiperazine. The observed spectrum consists of two sets of lines corresponding to the *cis* and *trans* forms of the compound. In acetone at room temperature,[12] approximately 39.7% is in the *cis* form and 61.3% *trans*. Thus, the energy difference between the isomers is only ~250 cal/mol but a relatively high barrier, typically 20–25 kcal/mol, must be exceeded before interconverting them. Rotation about the N–N bond is restricted by overlap between the nitrogens. The spectrum indicates that rapid axial–equatorial conversion does occur at room temperature. A pair of sharp lines results for the *cis* form due to the anisotropy of the nitroso group. In the *trans* form, the coupled protons do not have the same average chemical shift leading to a multiplet pattern depending on only three parameters. The results obtained on our external lock system in acetone are compared with the results published by Harris[12] in Table V. The spectrum was rerun on our internal lock system in $CDCl_3$ with resolution ~0.3 Hz. The average RMS error between calculated and observed spectra is less than 0.1 Hz for the parameters in Table V. The assignment of protons A and B previously indicated can be made on the basis that protons *cis* to the nitroso group are shifted upfield from those *trans*.[20] The value of $J_{gem} = -10.8$ Hz has been assumed for comparison with previous work.[12] A value of ~−13.0 Hz is expected on the basis of similar compounds,[21] but the value assumed has little effect on the other parameters determined. Attempts were made to observe the spectrum at reduced temperatures although the compound precipitates out of most cold solutions. A sample was taken to its freezing point in methylene chloride (<−97°) with no significant changes in the ring proton pattern other than those due to poor field homogeneity and viscosity.

Discussion

A. Chemical Shifts of Dialkylpiperazines. Chemical shifts of the amine protons are solvent and concentration dependent, being displaced to higher fields upon increasing dilution or by use of nonhydrogen bonding solvents. Dilute chloroform solutions show a definite upfield shift of the amine proton resonance as expected in proceeding from piperazine to 2,5-dibutylpiperazine. The N–H band of *cis*-2,5-dimethylpiperazine appears to be at lower field than that of the *trans*-2,5-dimethyl.

(18) J. A. Pople, W. G. Schneider, and H. G. Bernstein, "High Resolution Nuclear Magnetic Resonance," McGraw-Hill, New York, N. Y., 1959, p 223.

(19) R. A. Newmark, Thesis, University of California, Berkeley, Calif., Nov 1964.

(20) H. W. Brown and D. P. Hollis, *J. Mol. Spectrosc.*, **13**, 305 (1964).

(21) R. K. Harris and R. A. Spragg, *ibid.*, **23**, 158 (1967).

Table V: Parameters Characterizing the Spectrum of N,N′-Dinitrosopiperazine in Acetone and $CDCl_3$

	cis isomer			*trans* isomer		
	$CDCl_3$	In acetone	Lit.[a]	$CDCl_3$	In acetone	Lit.[a]
$^1/_2\nu_0(A + B)$	250.9 ± 0.2	256 ± 2Hz	253	252.9	253.0	255.7
$\nu_0\delta_{AB}$	44.8	47.1 ± 0.1Hz	46.9	21.5	30.1	29.4
J_{trans}		...	...	6.86 ± 0.05	6.94	7.17
J_{cis}		...	...	4.54 ± 0.05	4.73	4.88
J_{ae}		...	...	−10.8 (assumed)	−10.8 (assumed)	

$J_{trans} = {}^1/_2\langle J_{aa'} + J_{ee'}\rangle$
$J_{cis} = {}^1/_2\langle J_{ee'} + J_{e'a}\rangle$

[a] Reference 12.

Since the former is an average between N–H with an equatorial and axial methyl substituent, this implies that the axial methyl substituent is less effective than the equatorial in shielding the amine group. The alkyl methyl absorption also shows the anticipated upfield shift with increasing chain length. The downfield shift of the average methyl absorption in *cis*-2,5-dimethylpiperazine indicates that the axial methyl resonance is at lower field than the equatorial.

The relative axial–equatorial chemical shift of protons on the same carbon in a six-membered ring is generally 25–30 Hz in the absence of substituent or heteroatom effects. Jackman[22] has shown that this shift difference can be explained in terms of the diamagnetic anisotropy of the neighboring C–C bonds in the chair conformation. This effect is such that the equatorial protons are deshielded relative to the axial protons. In the case of piperazine,[9] the nitrogen atoms with lone pairs probably occupying equatorial positions cause a pronounced decrease in the relative shift, $\nu_0\delta_{ae}$, to ~9 Hz. Alkyl substitution elsewhere in the ring is not expected to alter the lone pair conformation. However, substituents on the amine group could force the lone pair into an axial position increasing $\nu_0\delta_{ae}$ of ~20 Hz to 30.7 Hz in *trans*-2,5-dimethylpiperazine. The principal change in $CDCl_3$ is a 19.4-Hz upfield shift of the axial protons relative to their position in piperazine. The only difference in the immediate environment of the ring methylene protons in *trans*-2,5- and *cis*-2,6-dimethylpiperazine is the presence of a β methyl substituent in the *cis*-2,6 derivative. The β methyl substituent appears to enhance $\nu_0\delta_{ae}$ ~6 Hz to 37.1 Hz in *cis*-2,6-dimethylpiperazine. The shielding effect of the β methyl is about twice as great on the axial protons (10.3 Hz) as the equatorial (3.9 Hz).

The effect of substituting ethyl for methyl in the 2,5-derivatives is a deshielding of the equatorial, and to a lesser extent axial, protons resulting in a rather large value of $\nu_0\delta_{ae}$ = 37.3 Hz. However, the deshielding effect is decreased in the longer alkyl chains giving an intermediate value of $\nu_0\delta_{ae}$ ~33.4 Hz. Chemical shifts of axial protons on the same carbon as the substituent follow the shielding trend expected on the basis of inductive effects.

The relative axial–equatorial chemical shift differences are not particularly solvent dependent. Dilute benzene solutions of 2,5-diethyl and 2,5-dibutylpiperazine give the expected upfield shift of the spectrum as indicated in Table I. The value of $\nu_0\delta_{ae}$ is somewhat reduced, particularly in 2,5-diethylpiperazine. The reduction is due to a greater upfield shift of the equatorial than axial protons. The two axial ring protons in each molecule undergo nearly identical solvent shifts. The enhanced solvent shifts in *trans*-2,5-diethylpiperazine may indicate a tendency to orient relative to neighboring solvent molecules which is partially destroyed by the introduction of longer alkyl chains.

B. Coupling Constants of Dialkylpiperazines. A self-consistent analysis is obtained by assuming that the geminal coupling constants are of opposite sign to the vicinal constants. The geminal constants are almost certainly negative on the basis of similar compounds and have the magnitude expected for essentially sp^3 hybridization of the carbon.[23] Geminal coupling constants are sensitive to both the nature and orientation of substituents. For the molecules examined here, the MO approach[24] predicts that electronegative substituents in the α position cause negative shifts and electronegative β substituents cause positive shifts in these constants. It is interesting to compare values of J_{gem} in *trans*-2,5-dimethyl and *cis*-2,6-dimethylpiperazine. The α substituents are identical in each case. However, the β substituents in *trans*-2,5-dimethylpiperazine are amine and methylene groups; in *cis*-2,6-dimethylpiperazine, amine and $-CH-CH_3$ groups. The coupling constant is slightly more positive in the *trans*-2,5 derivative as predicted.

The replacement of the methyl by larger alkyl groups would be expected to lead to a small positive shift in J_{gem} if α-substituent effects dominate. It does appear that the value of J_{gem} becomes less negative upon proceeding from 2,5-dimethyl to 2,5-diethylpiperazine.

(22) L. M. Jackman, "Nuclear Magnetic Resonance Spectroscopy," Pergamon Press, Oxford, 1959, p 117.

(23) Approximate values in cyclohexane are J_{gem} = 12.6 Hz, $J_{aa'}$ = 11.8 Hz, $J_{ae'}$ = 3.9 Hz, $J_{ee'}$ = 3.9 Hz. N. Muller and P. J. Schultz, *J. Phys. Chem.*, **68**, 2026 (1964).

(24) J. A. Pople and A. A. Bothner-By, *J. Chem. Phys.*, **42**, 1339 (1965).

Results for the *trans*-2,5-dibutyl and dioctyl derivatives are inconclusive due to the large uncertainties in the values extracted from the spectra.

As predicted by VB theory,[25,26] vicinal coupling constants are sensitive to the dihedral angle and electronegativity of substituents among other factors. For a regular chair conformation, $J_{aa'}$ should be near a maximum value ($\phi \sim 180°$) and $J_{ae'}$ should be only slightly larger than the minimum value. The value of $J_{aa'}$ 10.5 Hz is only slightly lower than the value of approximately 11.8 Hz in cyclohexane.[23] Barring no ring distortion, most of the decrease can be attributed to the substitution of nitrogen in the ring for the less electronegative carbon. One is tempted to attribute the decrease of $J_{aa'}$ in 2,5-diethylpiperazine to a small degree of ring distortion tending to decrease the dihedral angle between C–H bonds. However, the situation is more complex since $J_{aa'}$ apparently increases in the 2,5-dibutyl and dioctyl derivatives. A value of $J_{a'e}$ of 2–4 Hz is expected.[27] This constant was reliably determined only in the dimethylpiperazines analyzed.

C. N,N′-Disubstituted Compounds. Where determined, the coupling constants have the values expected on the basis of similar molecules. The geminal coupling in N,N′-dimethylpiperazine must be opposite in sign to the vicinal coupling constants for any reasonable analysis. The axial–equatorial vicinal coupling constants in molecules of this type are small, generally in the range 2.0–4.0 Hz. The value of J_{cis}/J_{trans} is usually near 2.0 for molecules such as piperazine, which are thought to exist in a chair form.[12] Lower values such as obtained for N,N′-dinitrosopiperazine may indicate the stable configuration is a distorted chair form.[14,16] The placement of the electronegative N–O groups on the nitrogen leads to some double bond character in the N–N bond and subsequent flattening of the ring. On the basis of the trends in vicinal coupling constants with dihedral angle, $J_{aa'}$ and $J_{ee'}$ are decreased but $J_{ae'}$ increased from their values in the normal chair form. Hence, a smaller J_{cis}/J_{trans} ratio is predicted.

The relative axial–equatorial chemical shift is approximately 30 Hz except in piperazine. It is relatively independent of the particular substituent on the nitrogen. The small value of 9.6 Hz in piperazine can be attributed to a conformational preference of the lone pair for the equatorial position in this molecule. Larger substituents than hydrogen occupy the equatorial position forcing the lone pair into an axial position. Comparison of the CH_2 shifts of piperazine and N,N′-dimethylpiperazine indicates that the change in $\nu_0\delta_{ae}$ is largely due to an upfield shift of the axial ring protons. Similar results are known in piperidine and N-methyl piperidine.[28] The axial ring protons are anticoplanar to the nitrogen lone pair if it is axial. The enhanced axial chemical shift has been attributed[29] to the bonding of the axial lone pair with the anti-coplanar $\sigma^*(C\text{–}H_{ax})$ orbital.

The interpretation of the free energies of activation requires a model for the ground state and also transition state. It has been proposed[30] that for chair $\leftrightarrow$ chair interconversion the most stable transition state would be one of the possible half chair forms as shown

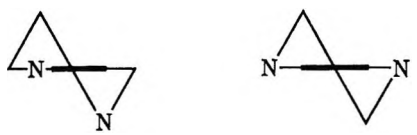

below. Hendrickson[30] has estimated the energies involved for the case of cyclohexane. On the basis of this work, Harris[9] has correlated the $\Delta G^{\ddagger}$ values for a number of cyclohexane-like molecules assuming that changes in torsional energies dominate changes in the observed enthalpies of activation. Assuming the relative axial–equatorial chemical shifts are similar, the inversion barriers in N,N-diphenyl and N,N-dinitrosopiperazine must be much lower than in N,N-dimethylpiperazine. Similar results[9] have been reported at 100 MHz for N-methylpiperazine ($T_c = -26°$, $\Delta G^{\ddagger} = 11.5$ kcal/mol), 1-methyl-4-nitrosopiperazine ($T_c < -95°$), N-methylmorpholine ($T_c = -31°$, $\Delta G^{\ddagger} = 11.5$ kcal/mol), and N-phenyl-morpholine ($T_c < -95°$). In each of these cases, partial delocalization of the nitrogen lone pair onto the substituent gives some double bond character to the C–N or N–N bond. The resulting flattening of the ring in the chair form is expected to reduce the torsional and bond angle strain in going from a chair to a half chair form.

The free energy of activation in N,N′-dimethylpiperazine is relatively independent of solvent if detailed line shape methods are used in the rate analysis. The slightly higher free energy values observed in "interacting" solvents such as methanol are probably real. For example, the free energy of activation for N-methylmorpholine is approximately 0.3 kcal/mol lower in methylcyclohexane than in methylene chloride.[9]

(25) M. Karplus, *J. Chem. Phys.*, **30**, 11 (1959).
(26) M. Karplus, *J. Amer. Chem. Soc.*, **85**, 2870 (1963).
(27) A. A. Bothner-By, *Advan. Mag. Res.*, **1**, 195 (1965).
(28) J. B. Lambert and R. G. Keske, *J. Amer. Chem. Soc.*, **88**, 620 (1966).
(29) H. P. Hamlow, S. Okuda, and N. Nakagawa, *Tetrahedron Lett.*, **37**, 2553 (1964).
(30) J. B. Hendrickson, *J. Amer. Chem. Soc.*, **83**, 4537 (1961).

Adsorbed Residues from Formic Acid and Formate Ion Generated under Steady-State Potentiostatic Conditions

by Sigmund Schuldiner and Bernard J. Piersma

Naval Research Laboratory, Electrochemistry Branch, Washington, D. C. 20390 *(Received December 15, 1969)*

The free radicals generated when formic acid and sodium formate dehydrogenate on a clean platinum surface interact with each other and with the surface to form organic residues that hinder further dehydrogenation. Steady-state potentiostatic current density *vs.* potential relations were determined. By rapid switching from potentiostatic to galvanostatic control, the number of coulombs required to oxidize the organic residue adsorbed at a given potential was determined. It was shown that the amount of residue was time dependent for hours. Both hydrogen and increased pH lowered the number of coulombs of charge required to oxidize the organic residue and allowed higher current densities at low polarization potentials. Activation of a Pt electrode by an anodic charging pulse appeared to have long-time effects on increasing the rate of formate oxidation. The effect was most pronounced in hydrogen-saturated 1 *M* HCOONa.

Introduction

A limitation to the use of organic fuels for low-temperature fuel cell applications is the formation of organic residues primarily from the free radicals which are generated at the surface. To better understand these residues it is necessary to study their formation, to characterize their electrochemical behavior, and to determine their chemical composition. Electrochemical studies of bulk species can only avoid the effects of these residues if the measurements are made on a surface before residues are significantly formed; however, such control is very limited. Since the character of the surface is constantly changing, the steady-state behavior is of real importance from both a fundamental and a practical viewpoint.

When a clean platinum electrode is exposed under open circuit conditions to formic acid or sodium formate solutions there is a rapid dehydrogenation reaction followed by a much slower interaction of adsorbed H atoms with formic acid or formate ions to give molecular hydrogen and free radicals.[1,2] The free radicals formed by this reaction and by the initial dehydrogenation reactions interact with the surface and each other to form residues which then hinder further dehydrogenation. Upon anodic potentiostating of the Pt electrode, one would expect that any atomic hydrogen formed by dehydrogenation would be readily oxidized. A previous steady-state potentiostatic study[3] on the anodic oxidation of formic acid and hydrogen in formic acid and formic acid–sulfuric acid mixtures showed that even though the initial rates of oxidation are quite high, there is a gradual decrease in rates until at steady-state, the reaction rates are considerably reduced. Apparently, the formation of free radicals also occurs under anodic potentiostatic conditions, and the resulting residue can affect the rates of oxidation of both formate species and hydrogen.

The present investigation was for the purpose of determining the relation between potential and the steady-state amount of charge required to oxidize the organic residue formed on Pt in formic acid and formate ion solutions, both under helium and hydrogen saturated conditions. High current density anodic galvanostatic pulses give charging curves that show an increase in the number of $\mu C/cm^2$ required to form a monolayer of adsorbed oxygen atoms on the surface of the Pt electrode ($Pt–O_{ad}$). This increase beyond the 420 $\mu C/cm^2$ required to form a monolayer of $Pt–O_{ad}$ on a clean Pt electrode plus 36 $\mu C/cm^2$ for double layer charging is attributed[4] to oxidation of the organic residue on the electrode. Such measurements only show the number of coulombs of charge required to oxidize adsorbed organic material plus water. Unreactable species on the surface may not be oxidized by the anodic galvanostatic pulse, but may cause an increase in overvoltage for the formation of oxygen atoms. Because of the complexity of interpretation of the anodic charging curves and because qualitative identification of the organic residues or of the oxidized or desorbed products is extremely difficult, it is not possible to associate the amount of charge actually determined by this technique to specific reactants, reactions, or products. Therefore, the use of such terms as degree of surface coverage has little real meaning. Hence, in this study the number of electrons generated in the atomic oxygen adsorption region (from ~0.9 to 1.8 V), after subtracting the monolayer contribution due to $Pt–O_{ad}$ plus the double layer, is expressed as

(1) J. Fahrenfort, L. L. Van Reyen, and W. M. H. Sachtler in "The Mechanisms of Heterogeneous Catalysis," J. H. de Boer, Ed., Elsevier, Amsterdam, 1960, pp 23–48.

(2) S. Schuldiner and B. J. Piersma, *J. Catal.*, **13**, 413 (1969).

(3) S. Schuldiner, *J. Electrochem. Soc.*, **116**, 767 (1969).

(4) S. Schuldiner and R. M. Roe, *ibid.*, **110**, 332 (1963).

q_{org} and solely represents the amount of charge used to remove the reactable organic species adsorbed on the Pt surface at specific, steady-state anodic potentials.

Experimental Section

The solutions investigated were: (a) 1 *M* HCOOH + 1 *M* H_2SO_4 (pH ≈0), (b) 1 *M* HCOOH + 1 *M* HCOONa (pH 3.5), and (c) 1 *M* HCOONa (pH 7.9). The formic acid was reagent grade, the H_2SO_4 was ultrapure (E. Merck, Darmstadt). Measurements were made in both helium- and hydrogen-saturated solutions (see ref 2 for details of experimental techniques). The Pt working electrode potentials were controlled with a Wenking 61RS potentiostat, galvanostatic pulses (1–2 A/cm²) were applied with either an Electro-Pulse 3450C or 3450D pulse generator, and traces were photographed from a Tektronix 547 oscilloscope with a 1A1 plug-in. The circuitry used and the fast switching between potentiostatic and galvanostatic control were as previously described.[5]

Generally, the time required to reach steady-state conditions was at least 14 hr. Figure 1 gives two examples of the q_{org} relation with time. Even though, in many cases, there was little change in q_{org} within the first 5 min, steady-state values were reached only after several hours and were considerably larger than initial values.

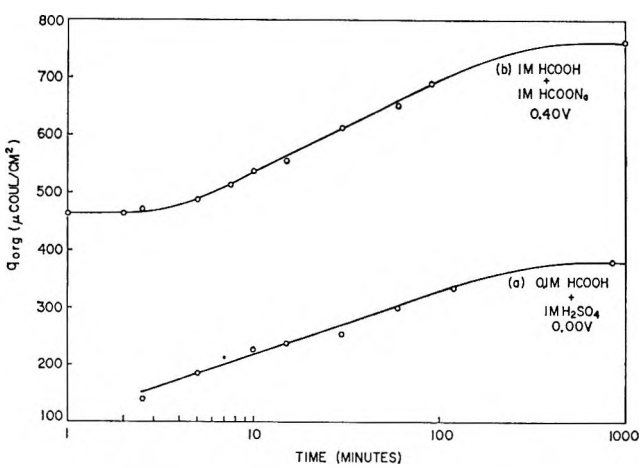

Figure 1. Typical buildup of organic residue with time.

All potentials, except those otherwise noted, are referred to the reversible hydrogen electrode (RHE) in the same solution. The temperature was 25 ± 1°.

Results

Steady-state potentiostatic polarization curves for formic acid and formic acid–sulfuric acid mixtures were published previously.[3] Figures 2 and 3 show the polarization behavior for 1 *M* HCOOH + 1 *M* HCOONa and 1 *M* HCOONa solutions. These figures show that the net oxidation rates in H_2-saturated solutions are generally higher than in He-saturated solutions. Thus the steady-state rate of H_2 oxidation, even though considerably reduced by the presence of the organic species, is generally faster than the rate of oxidation of the formate species. Both curves show hysteresis similar to those found in other formic acid solutions.[3] There are some important differences, however. In the 1 *M* HCOOH + 1 *M* HCOONa (He-saturated) solution (Figure 2), the current densities on the decreasing po-

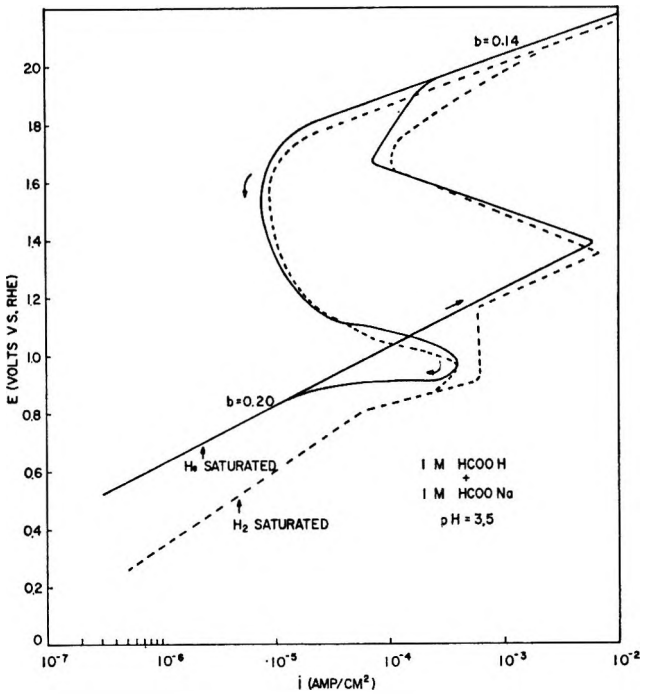

Figure 2. Steady-state potentiostatic current density *vs.* potential relation in 1 *M* HCOOH + 1 *M* HCOONa.

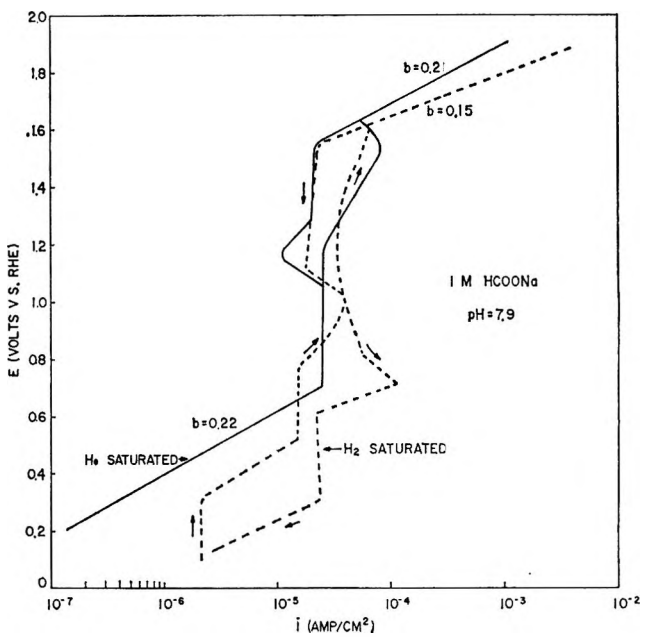

Figure 3. Steady-state potentiostatic current density *vs.* potential relation in 1 *M* HCOONa.

(5) T. B. Warner and S. Schuldiner, *J. Electrochem. Soc.*, 114, 359 (1967).

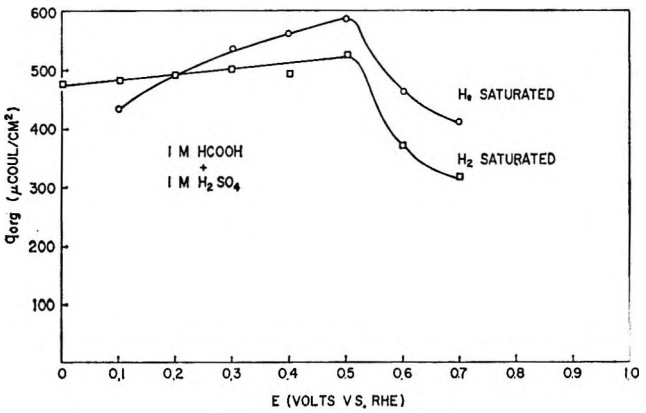

Figure 4. Steady-state dependence of amount of charge, q_{org}, required to oxidize organic residue at set potentials; 1 *M* HCOOH + 1 *M* H_2SO_4.

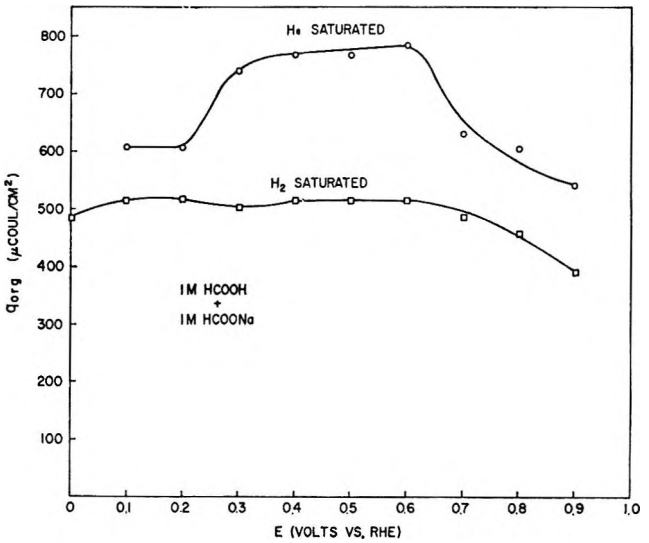

Figure 5. Steady-state dependence of amount of charge, q_{org}, required to oxidize organic residue at set potentials; 1 *M* HCOOH + 1 *M* HCOONa.

tential branch are greater than the values found for the increasing potential branch at potential between 1.0 and 0.8 V. Similarly, in the 1 *M* HCOONa solution (Figure 3), the current density is larger for decreasing potentials from 1.0 to 0.1 V in H_2-saturated solution.

Previous work[6,7] has shown that in the presence of an inert anion (sulfate ion) a reduction in the rate of hydrogen oxidation (passivation) occurred at 0.7 V (*vs.* NHE). This reduction in hydrogen oxidation rate was explained as being due to sulfate ion adsorption rather than to formation of an oxygen species since it was found that the rate of reaction of molecular hydrogen with oxygen species was much faster than the rate of oxidation of water in the absence of hydrogen. Further work[3] in formic acid containing solutions verified the conclusion that an oxygen species would not cause passivation of the hydrogen oxidation reaction at 0.7 V (NHE). Figure 2 confirms the conclusion that in the presence of an oxidizable ion a passivating oxygen species is not formed at potentials below 1.4 V.

A slight passivation effect in He saturated 1 *M* HCOONa (Figure 3) occurs at about 1.5 V but this also is well above the potential at which water can be oxidized to form Pt–O_{ad}. In H_2-saturated 1 *M* HCOONa there is a slight decrease in oxidation rate at potentials positive to 1.0 V and a marked activation on the decreasing potential arm starting at about the same potential. However, these effects show that oxidation of formic acid and formate ion are easier than water and indicates that the formation of oxygen species on Pt do not retard the oxidation of formic acid or formate ion below 1.4 V. This behavior supports previous conclusions[3,6,7] that passivation which occurs below 1 V (NHE) in the presence of easily oxidized hydrogen or organic species is due to inert anion adsorption rather than to the formation of oxygen species from water.

Figures 4, 5, and 6 show the relationships between potential and the steady-state amount of charge required to oxidize the adsorbed residue in formic acid and formate ion solutions. Both the q_{org} values in Figure 4 start at about 450 μC/cm^2 at open circuit (0 V for H_2 saturated solution and 0.1 V for He-saturated solution) and go to maximums of about 525 to 575 at 0.5 V. If one assumes monolayer coverage by the residue, then a little over two electrons per Pt site (210 μC/cm^2 = 1 electron/Pt site) would be required to oxidize the residue. Contrasting these results with those of Breiter,[8] Brummer and Makrides,[9] Brummer,[10] Minakshisandaram, *et al.*,[11] and Urbach and Smith,[12] we see that the amount of charge required to strip the adsorbed residue is more than twice the amount found by these investigators. Is should be remembered, however, that we have measured the steady-state values, and as can be seen in Figure 1, these are about twice the values found for the coverages at the short adsorption times used in ref 8–12. In addition, although the general shape of the curves in Figure 4 is similar to those in ref 8–11, the details are quite different. For example, instead of the plateau found in ref 8–11 a linear increase in q_{org} with a potential up to a maximum at about 0.5 V was found here. The drop in q_{org} was also less abrupt. It is obvious that the residue formed under steady-state conditions is quite different from the one adsorbed on the surface after only short times. The adsorption results of Urbach and Smith[12] were

(6) S. Schuldiner, *J. Electrochem. Soc.*, 115, 362 (1968).

(7) S. Schuldiner, *ibid.*, 115, 897 (1968).

(8) M. W. Breiter, *Electrochim. Acta*, 8, 457 (1963).

(9) S. B. Brummer and A. C. Makrides, *J. Phys. Chem.*, 68, 1448 (1964).

(10) S. B. Brummer, *ibid.*, 69, 562 (1965).

(11) N. Minakshisandaram, Yu. B. Vasil'ev, and V. S. Bagotskii, *Elektrokhimiya*, 3, 193 (1967).

(12) H. B. Urbach and R. E. Smith, submitted to *J. Phys. Chem.*

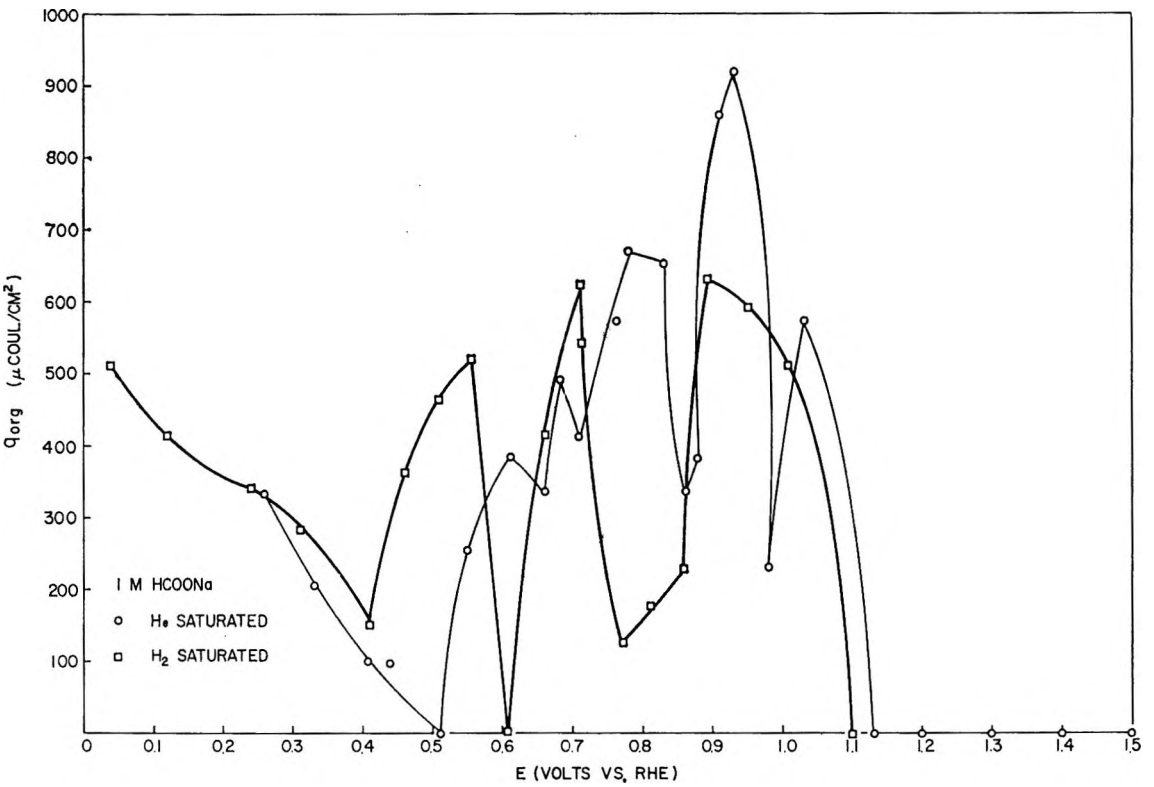

Figure 6. Steady-state dependence of amount of charge, q_{org}, required to oxidize organic residue at set potentials; 1 *M* HCOONa.

different from the results of other workers[8-11] and those shown here. However, Urbach and Smith determined coverage from radiometric measurements of tagged formic acid and were, in fact, determining the concentration of adsorbed tagged carbon rather than the concentration of adsorbed oxidizable species. It is possible that the differences found by the various workers are due to the differences in the constantly changing composition of the surface species. Results which are comparative to the literature values[8-11] can be seen in Figure 1, curve a where the initial 2.5 to 5 min results gave q_{org} of 140 to 180 μC/cm^2. On the basis 210 μC/cm^2 for fraction of surface coverage, $\theta = 1$, a θ of about 0.7 to 0.9 is obtained.

In H_2-saturated solution of 1 *M* HCOOH and 1 *M* HCOONa (Figure 5) the relationship between q_{org} and potential is similar to the sulfuric acid case (Figure 4) except that the drop in q_{org} is less at potentials above 0.5 V. In He-saturated solution, however, the character of the residue must be quite different since the q_{org} runs considerably higher than in sulfuric acid solutions. In this case q_{org} runs as high as 775 μC/cm^2 or about 3.7 electrons/Pt site. These high values of q_{org} as compared to the 210 μC/cm^2 which would be found for a monolayer coverage of the free radicals formed after dehydrogenation indicates that the organic residue which is oxidized consists of complex molecules with oxidizable sites which extend several atomic distances away from the surface.

One cannot attribute an increase in q_{org} with time to the adsorption of trace amounts of nonoxidizable impurities since such species would lower the amounts of oxidizable residue. In addition, experience at this laboratory has shown that the adsorption of trace amounts of oxidizable impurities would not require such a high number of coulombs for oxidation. The abnormally high number of coulombs can be most easily explained by the interaction of the free radicals (formed by dehydrogenation) to form a complex multilayer polymeric structure on the surface. It appears that the organic residues formed at the various potentials are of such high concentration that possible effects of trace amounts of impurities only could interfere in an indirect complex way, such as by catalytic influence of the composition of the residue.

The complexity of the potential *vs.* q_{org} relation shown in Figure 6, which was repeatedly checked, makes analysis virtually impossible. There are some similarities between the peaks and valleys for the He- and H_2-saturated solutions, but the most obvious difference is the fact that in He-saturated solution, the adsorption behavior is both more complex, and q_{org} can rise to substantially higher peak values. The 0.95 V value of 925 μC/cm^2 is equivalent to 4.4 electrons/Pt atom.

Discussion

The most obvious effect of hydrogen in the solutions investigated is that the measured q_{org} is substantially

lower at essentially all potentials. In H_2-saturated solutions, the open-circuit potentials were the equilibrium hydrogen potentials, even though the charging curves taken under steady-state conditions showed no visible hydrogen oxidation region. It appears that the trace amounts of hydrogen present on the electrode were sufficient to maintain the equilibrium hydrogen reaction at open circuit.[2] Some of the hydrogen from the H_2 can associate with the surface and/or organic residue on the surface affecting the structure and composition of this residue. Previously reported work[13] has indicated that atomic hydrogen at potentials negative to 0.3 V can interact with CO_2 which then prevents oxidation of this hydrogen at potentials below 0.9 V with a high-amplitude galvanostatic pulse. The interaction of hydrogen with formic acid and formate ion is much more complex, but it is apparent that the presence of hydrogen does affect the character of the steady-state organic residue.

Another factor which may also affect the character of the organic residue is the pH, but there is no apparent simple relationship. This can be especially seen for the He-saturated solutions shown in Figures 4, 5, and 6 where the interfering effect of hydrogen is minimized. The fact that the 7.9, 1 *M* HCOONa solution (Figure 6) is more sensitive to potential indicates that in the more alkaline solution the adsorbed species may have a stronger anionic character. At lower pH, adsorption is less dependent on potential and significant desorption does not occur below 0.5 V.

Further evidence for the pH effect on the adsorbed species and its effects on retardation of the net oxidation rate can be seen from the He-saturated potentiostatic polarization curves shown in Figures 2 and 3. The higher pH results (Figure 3) show a limiting current density at 2.5×10^{-5} A/cm^2 from 0.7 to about 1.2 V followed by a range of increasing oxidation rates with increasing potential. The hysteresis effect in the decreasing potential branch is relatively small. This effect and the data in Figure 6 (which shows a strong coverage dependence on potential) indicate that the oxidation of formate ion itself is rate determining and is not limited by the amount or character of the organic residue on the surface. At potentials above 1.2 V, the surface is essentially free of the organic residue, and the rate of oxidation gradually increases as the potential is increased to about 1.5 V.

In Figure 3 there is no pronounced passivation on the increasing potential branch for the He-saturated solution. It also is significant that in H_2-saturated solution, the organic residue only slightly passivates the H_2 oxidation component to the oxidation rate of the formate itself on the increasing potential branch above 1.0 V. In fact, there only is a little difference between the H_2- and He-saturated solutions from 0.7 to 1.6 V on the increasing potential branch. On the other hand, for the decreasing potential branch there is a significant activation effect which reaches a maximum at 0.7 V. The hysteresis at potentials below 1.0 V in H_2-saturated solution show increased activity for hydrogen oxidation. This increased activity and the increased activity shown in Figure 2 for decreasing potentials are the first times such increases have been noted in the various formic acid, formate, sulfuric acid, and alkali solutions investigated here. Although these points were repeatedly checked and critical points kept potentiostated at a given value for three to four days, it is likely that very slow changes in reaction rate may still be occurring and that eventually a return to the values on the potential increasing curve would be obtained. Another possibility is that the residue formed at high positive potentials is different from the one formed at low potentials and that the high-voltage residue does not retard hydrogen oxidation as much as does the low-voltage residue.

Contrasting the behavior in 1 *M* HCOONa (Figure 3) with that in 1 *M* HCOOH and 1 *M* HCOONa (Figure 2), one notes important differences. In the first place, Figure 2 shows little difference in the behavior in He- and H_2-saturated solutions except in the potential range from open circuit to about 0.9 V. At lower potentials the current densities are higher in the presence of H_2. The increased reaction rates for both the data shown in Figure 2 and 3 are due to the contribution of H_2 oxidation which is faster in this potential range than is the oxidation of formate species. The fact that the net oxidation rate in Figure 2 reaches a peak of about 7×10^{-3} A/cm^2 at about 1.4 V is of interest because this rate of oxidation is 3.5 times faster than the maximum rate of oxidation of hydrogen in sulfuric acid solution.[6] The pronounced passivation which occurs at higher potentials can be explained by adsorbed oxygen atoms generated by the oxidation of water. The marked hysteresis for the decreasing potential arm indicates the strong effect of dermasorbed oxygen atoms on the reaction rates.

Conclusions

The determination of adsorption isotherms[8-12] implies an equilibrium between an adsorbed or dissociated species and the original compound in solution. This investigation has shown that such equilibria do not exist for formic acid or formates. There is an irreversible dehydrogenation followed by free radical interaction to form a complex residue at the surface that appears to be dependent on the potential sequence and the presence of H_2. It appears that the "adsorption isotherms" for such systems are, in fact, of kinetic rather than thermodynamic significance.

The work reported here shows that at low polarization potentials the rates of hydrogen, formic acid, and

(13) B. J. Piersma, T. B. Warner, and S. Schuldiner, *J. Electrochem. Soc.*, **113**, 841 (1966).

formate ion oxidation are strongly retarded by the organic residues formed on the surface. This most likely occurs by covering sites at which dehydrogenation of the organic material can take place.[2] Dehydrogenation can produce easily oxidizable H atoms which make an organic species an effective fuel for fuel cell applications at low polarization. It appears that oxidation of carbon itself can readily occur at higher potentials, but this reaction would be of no obvious value for fuel cell operation. Dissociation of organic fuels to atomic hydrogen also implies that full low-temperature oxidation of the fuel to CO_2 and H_2O would not be practicable in many cases, and that a large part of the chemical energy of the fuel could not be utilized in the generation of electricity.

Some degree of control of the organic residue results from the presence of molecular hydrogen and by changing the pH. Hydrogen lowers the number of coulombs of charge required to oxidize the organic residue and allows higher anodic current densities at low polarization potentials.

Activation of a Pt electrode by polarizing to high anodic potentials appears to have long-time effects on increasing the rate of fuel oxidation. This effect is most pronounced in H_2-saturated 1 M HCOONa.

Acknowledgments. The authors are indebted to a reviewer and to Drs. Murray Rosen and David R. Tilman for their careful reading and criticisms of this paper.

Statistical Thermodynamics of Adsorption from Liquid Mixtures on Solids. I. Ideal Adsorbed Phase

by S. Sircar and A. L. Myers

School of Chemical Engineering, University of Pennsylvania, Philadelphia, Pennsylvania 19104 *(Received June 4, 1969)*

The cell model is applied to the adsorption of binary liquid mixtures on solids. The theory is based upon the assumption of an ideal adsorbed phase. Experimental data are reported for the adsorption of seven binary liquid mixtures on silica gel and on activated carbon at 30°. Comparison of the theory with experiment shows that the model is adequate for liquids which form ideal or nearly ideal liquid mixtures.

Theory

The surface thermodynamics of adsorbed solutions has been studied for the gas–solid interface.[1] The concept of an ideal adsorbed solution has been useful not only for classifying observed data but for predictive purposes as well.[2] Unfortunately, the results obtained for mixed gas adsorption do not apply to adsorbed liquid solutions. The reason is that the amount adsorbed at the liquid–solid interface is not a meaningful experimental variable.[3] The pertinent experimental variable for the liquid–solid interface is the surface excess. The purpose of this work is the derivation of an expression for the surface excess for the case of an ideal adsorbed phase.

The Thermodynamic System. The system is a liquid phase (the adsorbate) in contact with a solid phase (the adsorbent). The portion of the liquid phase in close proximity to the adsorbent is called the adsorbed phase. Variables which refer to the adsorbed phase will be identified by the prime symbol ($'$). The adsorbate and adsorbent are assumed to be mutually insoluble.

Assumptions. The following assumptions are made for the derivation of an expression for the surface excess. (a) The adsorbate may be divided into two parts: an adsorbed phase of N' molecules and a bulk phase of N molecules. (b) The total number of molecules in the adsorbed phase is a constant ($N' = M$). (c) The cell model, with one molecule in each cell, is used for the adsorbed phase and for the bulk phase. (d) The potential energy for the adsorbate–surface interaction, U_{is}', is approximated by the square-well potential. For the ith component, U_{is}' has a constant value if the molecule is in the adsorbed phase and U_{is} has a value of zero if the molecule is in the bulk phase. (e) Adsorbate–adsorbate molecular

(1) A. L. Myers and J. M. Prausnitz, *AIChE J.*, **11**, 121 (1965).
(2) A. L. Myers, *Ind. Eng. Chem.*, **60**, 45 (1968).
(3) S. Sircar and A. L. Myers, *AIChE J.*, in press.

interactions in the adsorbed phase can be neglected in comparison with the adsorbate–surface interactions. (f) The PV product is negligibly small in comparison with energy terms. It follows that the Helmholtz and Gibbs free energies are equivalent.

Derivation. The surface tension of the liquid–solid interface for pure i adsorbate, σ_i^0, is calculated using the canonical ensemble. Then the surface tension of the liquid–solid interface for a binary liquid mixture, σ, is calculated using the grand canonical ensemble. Finally, after expressing σ in terms of σ_1^0 and σ_2^0, the surface excess is calculated by means of the Gibbs adsorption isotherm.

Assumptions a, d, and e ensure that the adsorbed phase–bulk phase molecular interactions can be neglected. The surface tension of pure i adsorbate can be written as the actual free energy of the adsorbate less the free energy of the adsorbate in the absence of an interface[4]

$$\sigma_i^0 A = (F_i + F_i') - (N_i + N_i')\mu_i^0 \quad (1)$$

According to assumption b

$$N_i' = M \quad (2)$$

The free energies of the bulk phase and the adsorbed phase are given by the ordinary partition functions for these phases

$$F_i = -kT \ln Q_i \quad (3)$$

$$F_i' = -kT \ln Q_i' \quad (4)$$

Based upon assumptions c, d, and e, the partition functions for the bulk and adsorbed phases may be written in terms of the molecular partition functions[5]

$$Q_i = (q_i)^{N_i}(e^{-N_i U_{ii}/kT}) \quad (5)$$

$$Q_i' = (q_i')^{N_i'}(e^{-N_i' U_{is}'/kT}) \quad (6)$$

Combination of eq 1–6 gives an expression for the surface tension of pure i adsorbate

$$\sigma_i^0 A = -Mkt \ln q_i' + MU_{is}' - N_i kT \ln q_i + N_i U_{ii} - (N_i + M)\mu_i^0 \quad (7)$$

The chemical potential of pure i adsorbate is obtained from the thermodynamic expression

$$\mu_i^0 = \left[\frac{\partial F}{\partial N_i}\right]_{T,V} \quad (8)$$

Using eq 3 and 5, eq 8 may be written

$$\mu_i^0 = -kT \ln q_i + U_{ii} \quad (9)$$

Substitution of μ_i^0 from (9) into (7) gives an expression for the surface tension of pure i adsorbate in terms of molecular parameters

$$\sigma_i^0 A = MkT \ln\left[\frac{q_i}{q_i'}\right] + M(U_{is}' - U_{ii}) \quad (10)$$

For the mixture the surface tension is most easily evaluated by means of the grand partition function[6]

$$-\sigma A = kT \ln \Xi' \quad (11)$$

$$\Xi' = \sum_{N_1'} \sum_{N_2'} Q'(N_1', N_2', T)(e^{N_1'\mu_1'/kT})(e^{N_2'\mu_2'/kT}) \quad (12)$$

In accordance with assumptions c, d, and e, the molecules in the adsorbed phase are distributed randomly in the M cells. Therefore the ordinary partition function for the adsorbed phase, Q', is related to the molecular partition functions by the expression[5]

$$Q' = (q_1')^{N_1'}(q_2')^{N_2'}\left[\frac{(N_1' + N_2')!}{(N_1')!(N_2')!}\right] \times (e^{-N_1' U_{1s}'/kT})(e^{-N_2' U_{2s}'/kT}) \quad (13)$$

The chemical potential may be expressed in terms of the activity in the bulk solution

$$\mu_i = \mu_i^0 + kT \ln a_i \quad (14)$$

At equilibrium the chemical potential in the adsorbed phase is equal to the chemical potential in the bulk phase

$$\mu_i' = \mu_i \quad (15)$$

Assumption e is tantamount to the equality of the molecular partition function for the mixture and the molecular partition function for the pure liquid. Therefore q_i' in eq 10 and 13 has the same value. Combination of eq 9, 10, and 12–15 yields

$$\Xi' = \sum_{N_1'} \sum_{N_2'} \left[\frac{(N_1' + N_2')!}{(N_1')!(N_2')!}\right] \times (e^{-\sigma_1^0 A N_1'/MkT})(e^{-\sigma_2^0 A N_2'/MkT})(a_1)^{N_1'}(a_2)^{N_2'} \quad (16)$$

According to assumption b, eq 16 is subject to the constraint that

$$N_1' + N_2' = M \quad (17)$$

Using eq 17, the expression for Ξ' may be written as

$$\Xi' = \sum_{N_1'=0}^{M} \frac{M!}{(N_1')!(M - N_1')!} [a_1 e^{-\sigma_1^0 A/MkT}]^{N_1'} \times [a_2 e^{-\sigma_2^0 A/MkT}]^{(M - N_1')} = [a_1 e^{-\sigma_1^0 A/MkT} + a_2 e^{-\sigma_2^0 A/MkT}]^M \quad (18)$$

Alternatively, eq 18 may be derived from eq 16 by the conventional method of replacing the sum by the maximum term.[5] Equations 11 and 18 are combined to obtain

$$e^{-\sigma A/MkT} = a_1 e^{-\sigma_1^0 A/MkT} + a_2 e^{-\sigma_2^0 A/MkT} \quad (19)$$

(4) E. A. Guggenheim, *Trans. Faraday Soc.*, 41, 150 (1945).

(5) T. L. Hill, "An Introduction to Statistical Mechanics," Addison-Wesley, Reading, Mass., 1960, p 382.

(6) E. A. Guggenheim, "Mixtures," Oxford University Press, London, 1952, p 173.

Equation 19 describes the variation of the surface tension at the liquid–solid interface with the activities and therefore composition in the bulk liquid phase.

An equation similar to eq 19 has been derived by Guggenheim[4] for calculating the liquid–vapor interfacial tension of ideal liquid mixtures. His expression contains mole fractions in place of activities. It will be shown later that the liquid–liquid interactions in the bulk phase play a significant role in the adsorption of liquid mixtures on solids. Equation 19, therefore, represents a first correction for the nonideality of the system.

The Surface Excess. The pertinent experimental variable for the adsorption of liquid mixtures on solids is the surface excess.[3] The surface excess is defined by[7]

$$n_i^e = n^*(x_i^* - x_i) \tag{20}$$

where n^* is the total number of moles of binary liquid mixture brought into contact with unit mass of adsorbent. x_i^* and x_i are, respectively, the mole fraction of component i in the bulk liquid before and after contact with the solid adsorbent. All quantities in eq 20 are experimentally measurable.

The Gibbs adsorption isotherm relates the surface tension to the surface excess[3]

$$\frac{A}{kT}\frac{d\sigma}{da_1} = -\frac{N_i^e}{a_1 x_2} \tag{21}$$

N_1^e is the molecular surface excess of species number 1.

The bulk liquid activities are related by the isothermal Gibbs–Duhem equation[8]

$$x_1 \, d \ln a_1 + x_2 \, d \ln a_2 = 0 \tag{22}$$

Combination of eq 19, 21, and 22 yields, after some simplification

$$\frac{N_1^e}{M} = \frac{a_1 - x_1(a_1 + Ka_2)}{a_1 + Ka_2} \tag{23}$$

where

$$K = e^{A(\sigma_1^0 - \sigma_2^0)/MkT} \tag{24}$$

Equation 23 provides the desired relationship between the surface excess and the composition of the bulk liquid; (23) may be written in terms of molar quantities

$$\frac{n_1^e}{m} = \frac{a_1 - x_1(a_1 + Ka_2)}{a_1 + Ka_2} \tag{25}$$

where

$$K = e^{A(\sigma_1^0 - \sigma_2^0)/mRT} \tag{26}$$

m, a constant, is the number of moles in the adsorbed phase; (25) obeys the boundary conditions that

$$\lim_{x_1 \to 0} n_1^e = \lim_{x_1 \to 1} n_1^e = 0 \tag{27}$$

An exchange of subscripts in 25 and 26 provides an expression for the surface excess of component 2

$$\frac{n_2^e}{m} = \frac{a_2 - x_2(a_2 + a_1/K)}{a_2 + a_1/K} \tag{28}$$

Comparison of 25 and 28 shows that

$$n_1^e = -n_2^e \tag{29}$$

as required.

Integration of eq 21 yields

$$\frac{A(\sigma_1^0 - \sigma_2^0)}{RT} = -\int_{x_1=0}^{1} \frac{n_1^e}{x_1(1 - x_1)\gamma_1} \, d(\gamma_1 x_1) \tag{30}$$

In (30) the activity is written in terms of the activity coefficient for component number 1 in the bulk liquid

$$a_1 = \gamma_1 x_1 \tag{31}$$

The integral in (30) may be evaluated using the experimental isotherm for the surface excess. The remaining parameter, m, may then be determined by a best fit of (25) to the experimental isotherm.

Prediction of Surface Excess. For mixtures which obey this model, the requirement of thermodynamic consistency leads to a constraint on the parameter K. Consider, for example, the liquid mixture pairs 1–2, 1–3, and 2–3 adsorbed on the same adsorbent. Using (26), the constant K_{ij} for the i–j binary may be written

$$K_{ij} = e^{A(\sigma_i^0 - \sigma_j^0)/mRT} \tag{32}$$

According to (32)

$$K_{ij} = 1/K_{ji} \tag{33}$$

For the three liquids under consideration, it follows from (32) that

$$K_{13} = K_{12}K_{23} \tag{34}$$

Therefore the surface excess for liquid binary 1–3 can be predicted from data for the pairs 1–2 and 2–3.

Special Case of Ideal Liquid Mixture. If the bulk liquid, as well as the adsorbed phase, forms an ideal liquid mixture, (31) reduces to

$$a_1 = x_1 \tag{35}$$

Using (35), eq 25 reduces to

$$\frac{n_1^e}{m} = \frac{x_1 x_2(1 - K)}{x_1 + Kx_2} \tag{36}$$

K in (36) is given by (26). An expression (using volume fractions instead of mole fractions) of this form has been suggested by Schiessler and Rowe[9] as a method of plotting experimental data. More recently, Everett[10]

(7) J. J. Kipling, "Adsorption from Solutions of Non-Electrolytes," Academic Press, New York, N. Y., 1965, p 27.

(8) K. Denbigh, "The Principles of Chemical Equilibrium," Cambridge University Press, London, 1966, p 127.

(9) R. W. Schiessler and C. N. Rowe, *J. Amer. Chem. Soc.*, **75**, 4611 (1953); **76**, 1202 (1954).

(10) D. H. Everett, *Trans. Faraday Soc.*, **60**, 1803 (1964).

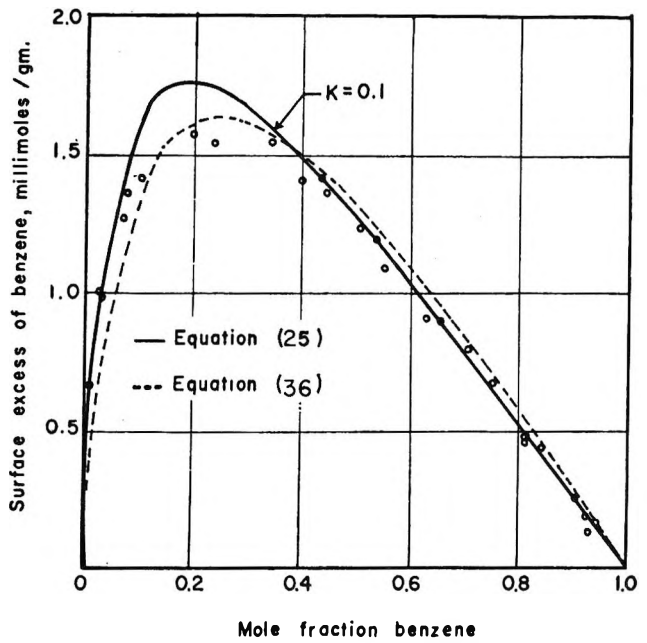

Figure 1. Adsorption of benzene–cyclohexane mixtures on silica gel at 30°.

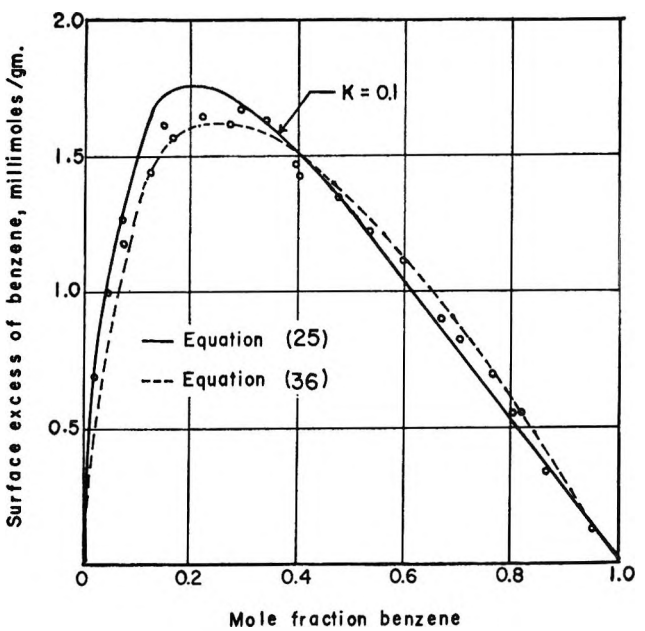

Figure 2. Adsorption of benzene–*n*-heptane mixtures on silica gel at 30°.

developed an expression similar to eq 36 using a "phase exchange reaction" model of adsorption originally proposed by Klinkenberg.[11]

Equation 36 can be written in the form

$$\frac{x_1 x_2}{n_1^e} = \left(\frac{1}{m}\right) x_1 + \frac{K}{(1 - K)m} \tag{37}$$

According to this equation, a plot of (x_1x_2/n_1^e) against x_1 would be a straight line with slope $(1/m)$ and intercept $K/(1 - K)m$.

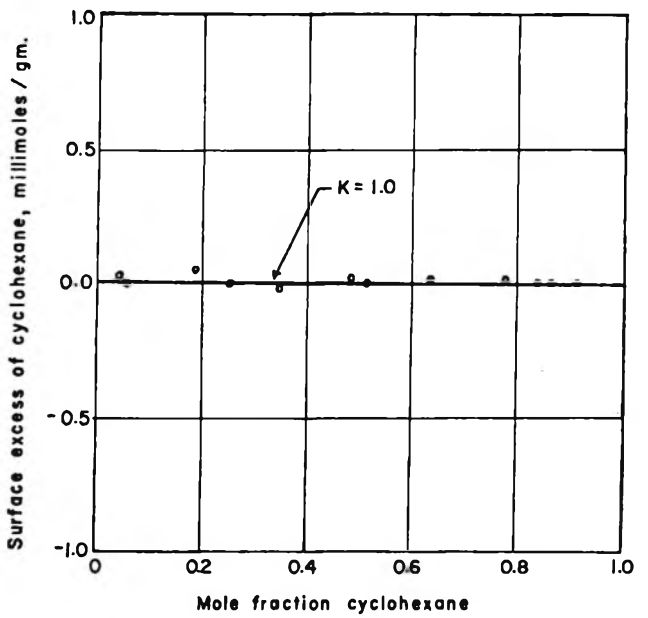

Figure 3. Adsorption of cyclohexane–*n*-heptane mixtures on silica gel at 30°.

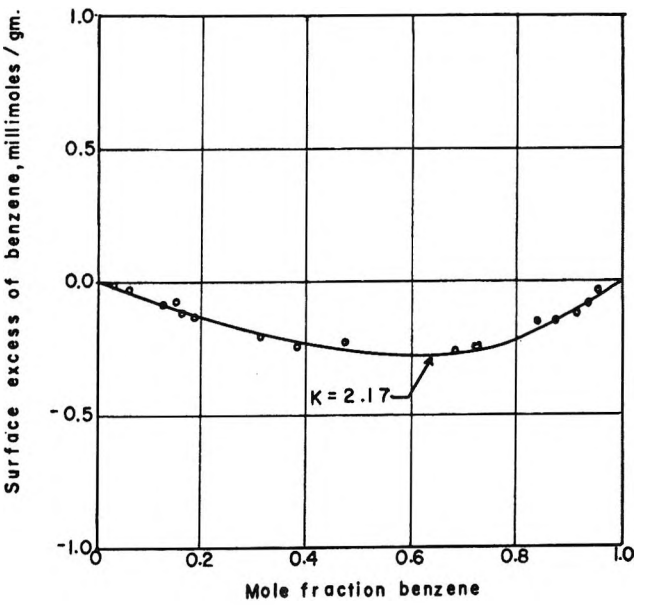

Figure 4. Adsorption of benzene–1,2-dichloroethane mixtures on silica gel at 30°.

Equation 36 shows that component number 1 will be preferentially adsorbed if

$$K < 1 \tag{38}$$

According to eq 26, the inequality 38 will hold provided that

$$\sigma_1^0 - \sigma_2^0 < 0 \tag{39}$$

Thus the model predicts that the component exhibiting the more negative value of the surface tension is selectively adsorbed from solution.

(11) A. Klinkenberg, *Recl. Trav. Chim. Pays-Bas*, 77, 83 (1959).

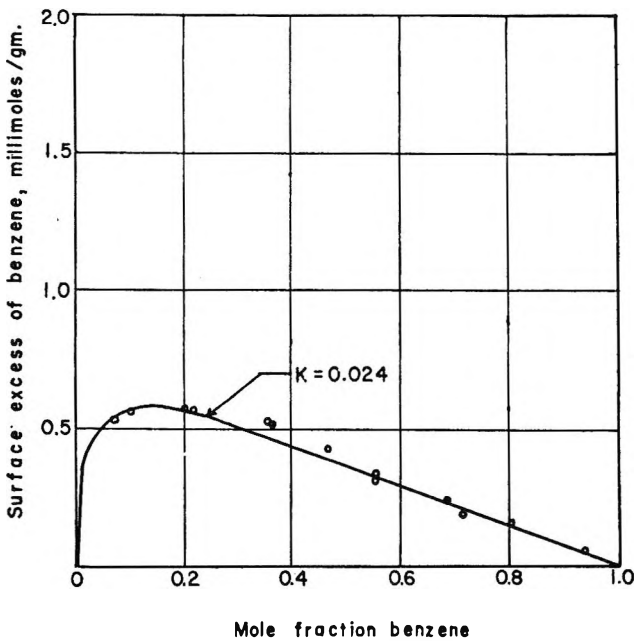

Figure 5. Adsorption of benzene–1,2 dichloroethane mixtures on activated carbon at 30°.

Experimental Section

Experiments were conducted to test the range of application of the model. Of particular interest was the possible application of eq 25 to mixtures which form nonideal liquid solutions.

Chemicals. The chemicals were Spectroquality reagents obtained from Matheson Coleman and Bell Co. The silica gel was supplied by the Davison Chemical Co. (Davison Grade PA 400) and was reactivated by heating it to 430° for 6–8 hr under vacuum. The carbon was obtained from Pittsburgh Activated Carbon Co. (BPL 4 × 10 number 23) and was reactivated at 150°.

Procedure. A binary mixture was prepared for each experimental point; its mass was determined gravimetrically and its concentration was analyzed refractometrically. A weighed amount of adsorbent was then added to the binary mixture. The system consisting of the binary mixture and the adsorbent was shaken for 10–12 hr in a screw-capped erlenmeyer flask, using a reciprocating shaker. The temperature was thermostatically controlled to 30 ± 0.1°. The equilibrium composition of the bulk liquid, x_1, was then analyzed refractometrically; the calibration curves needed for the refractometric analyses were prepared by us. Finally, the surface excess was calculated by eq 20.

Results

The following systems were studied at 30°: (a) benzene (1) + cyclohexane (2) on silica gel; (b) benzene (1) + *n*-heptane (2) on silica gel; (c) cyclohexane (1) + *n*-heptane (2) on silica gel; (d) benzene (1) + 1,2-dichloroethane (2) on silica gel; (e) benzene (1) + 1,2-dichloroethane (2) on activated carbon; (f) benzene (1) + ethyl alcohol (2) on activated carbon; (g) cyclohexane (1) + ethyl alcohol (2) on activated carbon. The surface excess of component number 1 as a function of the equilibrium composition of the bulk liquid is reported in Tables I–VII and Figures 1–7.

Table I: Adsorption of Benzene (1)–Cyclohexane (2) Mixtures on Silica Gel at 30°

x_1	n_1^e, mmol/g	x_1	n_1^e, mmol/g	x_1	n_1^e, mmol/g
0.011	0.674	0.398	1.410	0.740	0.683
0.030	1.008	0.434	1.415	0.755	0.680
0.033	0.986	0.443	1.362	0.810	0.488
0.074	1.274	0.508	1.240	0.811	0.460
0.078	1.361	0.536	1.192	0.844	0.451
0.107	1.425	0.549	1.096	0.906	0.261
0.145	1.454	0.630	0.908	0.927	0.191
0.202	1.579	0.652	0.900	0.930	0.130
0.240	1.552	0.703	0.785	0.945	0.173
0.344	1.555	0.708	0.802		

Table II: Adsorption of Benzene (1)–*n*-Heptane (2) Mixtures on Silica Gel at 30°

x_1	n_1^e, mmol/g	x_1	n_1^e, mmol/g	x_1	n_1^e, mmol/g
0.006	0.466	0.224	1.641	0.675	0.915
0.022	0.695	0.278	1.615	0.693	0.963
0.044	1.005	0.295	1.672	0.709	0.836
0.071	1.273	0.340	1.624	0.769	0.703
0.076	1.180	0.396	1.464	0.806	0.560
0.126	1.440	0.405	1.429	0.819	0.563
0.153	1.608	0.480	1.352	0.866	0.333
0.169	1.572	0.542	1.230	0.955	0.124
0.174	1.546	0.596	1.122		

Table III: Adsorption of Cyclohexane (1)–*n*-Heptane (2) Mixtures on Silica Gel at 30°

x_1	n_1^e, mmol/g	x_1	n_1^e, mmol/g	x_1	n_1^e, mmol/g
0.041	0.036	0.349	−0.021	0.831	0.000
0.055	0.000	0.484	0.021	0.862	0.000
0.157	0.014	0.513	0.000	0.911	0.000
0.190	0.054	0.633	0.020		
0.250	0.000	0.780	0.020		

Table IV: Adsorption of Benzene (1)–1,2-Dichloroethane (2) Mixtures on Silica Gel at 30°

x_1	n_1^e, mmol/g	x_1	n_1^e, mmol/g	x_1	n_1^e, mmol/g
0.037	−0.011	0.311	−0.214	0.872	−0.167
0.066	−0.025	0.386	−0.246	0.918	−0.128
0.129	−0.080	0.476	−0.233	0.931	−0.095
0.153	−0.071	0.683	−0.268	0.954	−0.039
0.164	−0.120	0.727	−0.241		
0.190	−0.136	0.838	−0.156		

Table V: Adsorption of Benzene (1)–1,2-Dichloroethane (2) Mixtures on Activated Carbon at 30°

x_1	n_1^e, mmol/g	x_1	n_1^e, mmol/g	x_1	n_1^e, mmol/g
0.074	0.529	0.364	0.519	0.713	0.186
0.102	0.575	0.471	0.429	0.803	0.151
0.209	0.568	0.551	0.298	0.939	0.047
0.221	0.572	0.556	0.342		
0.359	0.538	0.687	0.234		

Table VI: Adsorption of Benzene (1)–Ethyl Alcohol (2) Mixtures on Activated Carbon at 30°

x_1	n_1^e, mmol/g	x_1	n_1^e, mmol/g	x_1	n_1^e, mmol/g
0.014	0.74	0.205	2.13	0.758	0.78
0.036	1.29	0.273	2.18	0.850	0.35
0.061	1.66	0.429	1.99	0.914	0.13
0.118	2.00	0.581	1.43	0.940	0.02
0.177	2.11	0.671	1.05	0.958	0.03

Table VII: Adsorption of Cyclohexane (1)–Ethyl Alcohol (2) Mixtures on Activated Carbon at 30°

x_1	n_1^e, mmol/g	x_1	n_1^e, mmol/g	x_1	n_1^e, mmol/g
0.042	0.295	0.286	0.532	0.756	−1.230
0.051	0.485	0.341	0.383	0.848	−1.310
0.072	0.517	0.391	0.192	0.893	−1.180
0.148	0.586	0.440	0.065	0.920	−1.230
0.160	0.669	0.470	0.000	0.953	−0.996
0.213	0.661	0.521	−0.129	0.974	−0.470
0.216	0.583	0.537	−0.362		
0.249	0.595	0.610	−0.643		

Analysis of Results. The liquid mixtures may be classified according to the degree of nonideality of the bulk liquid.

System	Classification
a,b	Small deviations from Raoult's law
c,d,e	Ideal
f,g	Large deviations from Raoult's law

For systems a and b the mixtures are nearly ideal; the activity coefficients at infinite dilution are 1.5. Experimental values for the activity coefficients were obtained from ref 12 for the benzene–cyclohexane mixture and from ref 13 for the benzene–*n*-heptane mixture. The value of $A\Delta\sigma/RT$ was obtained by evaluating the integral of equation 30. Then the parameter m was obtained by a best fit of eq 25 to the experimental data. Values of $A\Delta\sigma/RT$, m, and K are tabulated in Table VIII. Comparison of eq 25 on Figures 1 and 2 (solid lines) with the observed data (circles) shows that there is good agreement between the theory and the experimental results.

Table VIII: Parameters of Eq 25 and 36 for Systems Studied Experimentally

System	$A(\sigma_1^0 - \sigma_2^0)/RT$, mmol/g	Eq 25		Eq 36	
		K	m	K	m
a	−7.2	0.1	3.1	0.107	3.24
b	−7.2	0.1	3.1	0.119	3.36
c	0	...	...	1.0	3.1
d	1.11	...	...	2.17	1.44
e	−2.95	...	...	0.024	0.79
f	−6.26	0.25	4.5	0.25	4.5
g	0.90	1.33	3.18	1.33	3.18

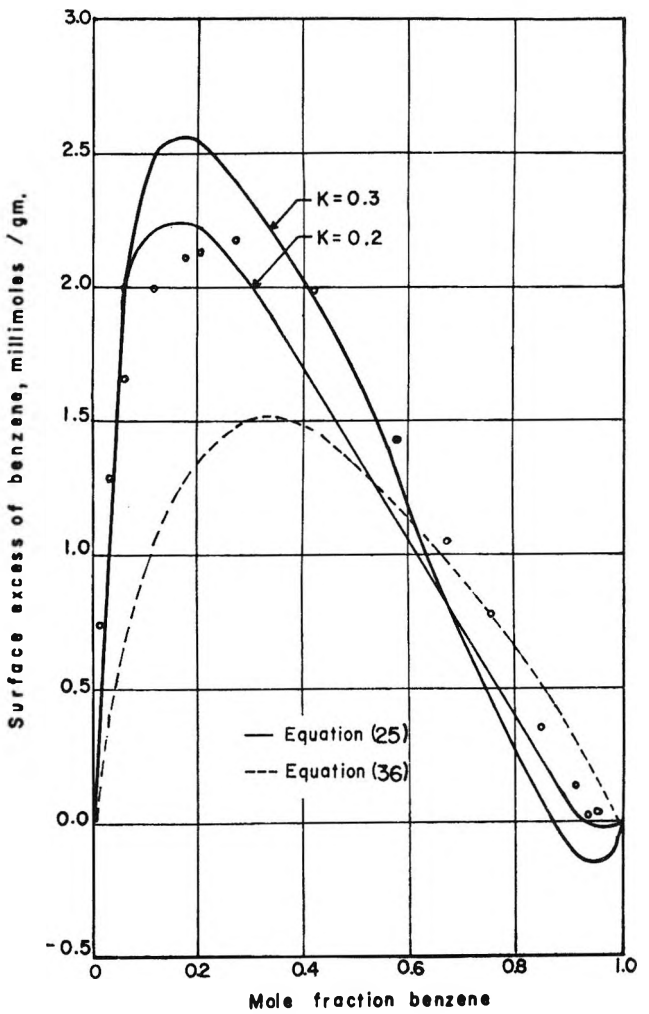

Figure 6. Adsorption of benzene–ethyl alcohol mixtures on activated carbon at 30°.

Systems a and b are nearly ideal and it is posssible to fit the data with eq 36, too. As before, the parameter m was obtained by a best fit of the experimental data using the known value of $A\Delta\sigma/RT$; values of the parameters are given in Table VIII. Equation 36 for

(12) G. Scatchard, S. E. Wood, and J. M. Mochel, *J. Phys. Chem.*, **43**, 119 (1939).

(13) I. Brown and A. H. Ewald, *Australian J. Sci. Res., Ser. A*, **44**, 198 (1951).

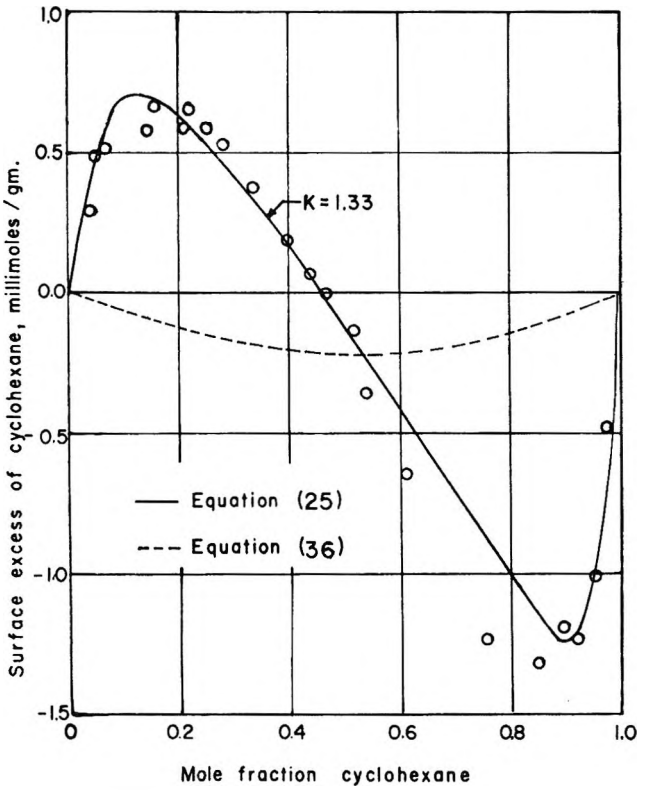

Figure 7. Adsorption of cyclohexane–ethyl alcohol mixtures on activated carbon at 30°.

an ideal bulk solution is plotted in Figures 1 and 2 as a dashed line and should be compared with eq 25 for the nonideal solution. Since the mixture is nearly ideal there is little difference between the two equations. For the same reason, the parameters for eq 25 and for eq 36 are nearly equal as shown in Table VIII.

The liquid mixture benzene–1,2-dichloroethane is ideal.[14] Therefore eq 36 may be applied to systems d and e. For these systems the experimental data, plotted in the form of eq 37, form a straight line. The parameters were derived from this plot using the method described previously and are reported in Table VIII. Equation 36, shown in Figures 4 and 5 as a solid line, provides a quantitative fit of the experimental data. In the case of silica gel the preferential adsorption is for the dichloroethane but the activated carbon preferentially adsorbs the benzene.

Systems a, b, and c form a set of three binary mixtures adsorbed on the same adsorbent. Therefore the thermodynamic consistency relationship, eq 34, can be used with the parameters found for systems a and b to predict the surface excess for system c: $m = 3.1$ mmol/g, $K = 1$. Since system c is ideal, eq 36 applies. The prediction of eq 36 for $K = 1$ is that silica gel has no preference for either component. Figure 3 shows that this prediction is in agreement with the experimental observation of zero surface excess.

Systems f and g provide a stringent test of eq 24 because the mixtures are highly nonideal. In the manner described previously, the value of $A\Delta\sigma/RT$ was evaluated by eq 30 and then the parameter m was obtained by a best fit of the experimental data. Activity coefficients for the bulk liquids were obtained from ref 15. The parameters of eq 25 and 36 are reported in Table VIII. Equation 25 for the nonideal bulk solution (solid line) and eq 36 for the ideal bulk solution (dashed line) are plotted in Figures 6 and 7. The two solid lines plotted in Figure 6 are for different values of the parameter K and show that eq 25 does not provide a quantitative fit of the experimental data for system f. But the superiority of eq 25 over eq 36 is evident on Figures 6 and 7.

The dashed line in Figure 7 is a plot of eq 36 using the same values of m and K used for eq 25. The difference between the solid line and the dashed line is due entirely to nonideality in the bulk phase. Equation 36, derived for an ideal bulk solution, fails to interpret the sigmoidal type of isotherm.

Conclusions

Ideal and slightly nonideal liquid mixtures may be interpreted in terms of an ideal adsorbed solution. The surface excess for mixtures of this type is given by eq 36.

If the liquid mixture exhibits strong deviations from Raoult's law, it is found that eq 36 is unsatisfactory. Equation 25, which takes into account the nonideality in the bulk phase, provides much better (but not quantitative) agreement with the observed data.

The thermodynamic consistency relationship for adsorption of binary mixtures, eq 34, predicts the surface excess for liquid mixtures which are ideal or nearly ideal.

Acknowledgment. Financial support by the National Science Foundation is gratefully acknowledged.

Appendix. Notation

a	Activity
A	Specific surface area of adsorbent
F	Helmholtz free energy
k	Boltzmann constant
K	A constant, eq 26
M	Number of molecules in adsorbed phase, a constant
m	Number of moles in adsorbed phase, a constant
N	Number of molecules
n	Number of moles
P	Pressure
q	Cell partition function
Q	Canonical partition function
R	Gas constant
T	Absolute temperature
U_{ii}	Cell potential energy for like molecular interactions
U_{is}	Cell potential energy for interaction of molecule i and surface
V	Volume
x	Mole fraction

(14) J. J. Kipling and D. A. Tester, *J. Chem. Soc.*, 4123 (1952).
(15) I. Brown and F. Smith, *Aust. J. Chem.*, 7, 264 (1954).

Greek letters
γ Activity coefficient
μ Chemical potential
Ξ Grand partition function
σ Surface tension
Subscripts
1 Component 1
2 Component 2
i Component i
Superscripts
$'$ Adsorbed phase
^{0} Pure liquid adsorbate
e Surface excess
* Initial value before contacting adsorbent

Association Theory. The Discontinuous Case and the Structure of Liquids and Solids

by Robert Ginell and Albert S. Kirsch

Chemistry Department, Brooklyn College of the City University of New York, Brooklyn, New York 11210
(Received December 12, 1969)

The assumption of the continuous case of association which is that all species of particles are always present is discussed. It is shown that a more appropriate model of the liquid or solid is given by the discontinuous case which postulates that certain smaller species are completely absent. A discussion of the nature and cause of the gas–liquid transition is given. This transition coincides with the change from a treatment by the continuous case to the discontinuous case. Various modifications of the mathematical treatment are derived and discussed.

In previous work[1,2] a theory of association of matter was presented which led to an equation of state[3] and finally to a derivation of Tait's equation.[4] This theory was applied both to liquids[5] and solids[6] and showed success in enabling us to calculate the atomic radii[7] of the five alkali metals from a knowledge of their compressibility data and their crystal form. However, a further detailed examination of the equations in this theory showed that there were some difficulties both conceptually and mathematically. Among other things, the number of 1-mers in liquids and solids under high pressure calculated by this theory were found to be too great. Careful analysis of the equations traced the difficulties to one assumption in the original derivation; this is the assumption that all species from 1-mer to m-mers were always present. If in these derived equations the concentration of any species became zero, then the mathematical equations broke down giving a singular case. This paper then is devoted to an examination of this assumption and to the consequences of removing its restrictions.

The Assumption of Continuous Distribution. The origin of this assumption probably lies in the kinetic derivation of the distribution equations, which assumes that we start with a hypothetical matrix of single atoms and from this build an associated substance. This is equivalent to assuming that we start a mass of matter at infinite volume where there are no collisions and suddenly compress it to some arbitrary volume where the molecules start colliding and associating. This is an unnecessary concept, although a convenient one, since the same equations can be obtained by considering the equilibrium situation.[8] The concept of this assumption was reinforced by the thought experiment[1] in which the individual frames of a hypothetical motion picture of a gas were examined one by one. In such examination, 1-mers, 2-mers, 3-mers, etc., were seen. From a dynamic point of view the 2-mers were static representations of binary collisions, the 3-mers, ternary collisions, etc. This picture is the one presented by the kinetic–molecular theory and is undoubtedly true of a gas. The extrapolation to liquids and solids came with

(1) For a review article see: R. Ginell, p 41–48, "Advances in Thermophysical Properties at Extreme Temperatures and Pressures," S. Gratch, Ed., American Society of Mechanical Engineers, New York, N. Y., 1965.

(2) R. Ginell, *Ann. N. Y. Acad. Sci.*, **60**, 521 (1955).

(3) R. Ginell, *J. Chem. Phys.*, **23**, 2395 (1955).

(4) R. Ginell, *ibid.*, **34**, 1249 (1961); **34**, 2174 (1961); **35**, 1135 (1961).

(5) R. Ginell, *ibid.*, **35**, 473 (1961).

(6) R. Ginell and T. J. Quigley, *J. Phys. Chem. Solids*, **26**, 1157 (1965).

(7) R. Ginell and T. J. Quigley, *ibid.*, **27**, 1173 (1966).

(8) R. Ginell and J. Shurgan, *J. Chem. Phys.*, **23**, 964 (1955).

the derivation of Tait's law, and the successes and troubles started at this point.

The Liquid and Solid State. The correct approach is to extrapolate our thought experiment from the gas case described above to the liquid and solid cases. One must therefore look for an acceptable picture of a liquid and a solid. The subject of the nature of the liquid and solid state has been the subject of many papers and reviews, and an introduction to the current views can be found in a general text like Moelwyn-Hughes or Hirschfelder, *et al.*,[9] and need not be detailed here. However, the association approach to liquids and solids is not widely known. Part of this problem has been considered[10,11a] in connection with a discussion of close-packing in j-mers of large size, and the suggestion has been made that the essential difference between liquids and solids is one of symmetry. From this work it appears that higher j-mers that are packed in 4- or 6-symmetry give rise to particles of regular form which are recognizable as prototypes of crystals, while on the other hand higher j-mers that are packed in approximate 5-symmetry form particles of irregular shape, full of voids that seem to correspond to our current views of the structure of liquids. This work showed, moreover, that particles in 5-symmetry had more bonds and hence are more stable, at least in the smaller sizes, than particles in 6-symmetry. This symmetry difference leads to an explanation of the mechanism of nucleation. From our present work it seems that we must consider a liquid to consist of an array of such 5-symmetry particles separated by defects, all in equilibrium. The equilibrium is due to 1-mers breaking off one particle (j-mer), crossing the defect volume and joining another j-mer. The equation would be

$$n_1 + n_j \rightleftarrows n_{j+1}$$

The number of such 1-mers in the liquid is very small, the main bulk consisting of 5-symmetry j-mers. The equilibrium mechanism postulated here is very similar to the mechanism for the growth of crystals after heterogeneous nucleation.[11b]

If one lowers the pressure on the liquid, one ultimately reaches the vapor pressure of the liquid. This is the pressure which these 1-mers exert in the liquid at this temperature. In solids, the process is the same except that the particles are now in 4- or 6-symmetry. Thus the liquid and solid both consist of large particles in 5- or 6- (or 4-) symmetry, respectively, in equilibrium with 1-mers. The question of whether 2-mers exist in the liquid depends in part on the abundance of 1-mers. The quantity of 3-mers is still smaller and there undoubtedly is a gap between these small particles and the large j-mers which form the bulk of the liquid or solid. In many ways this concept resembles Eyring's significant structures theory.[12] This theory postulates that liquids are composed of a mixture of gas-like particles and solid-like particles. This is equivalent to our 1-mers and j-mers. The difference in the theories is that we specify that the j-mers are 5-symmetric in liquids and 6- (or 4-) symmetric in solids, while Eyring's theory considers the solid-like particles to have the properties of solids and contains some arbitrary parameters. Our theory enables one to explain nucleation and the conversion of liquids to solids. This is impossible in Eyring's theory.

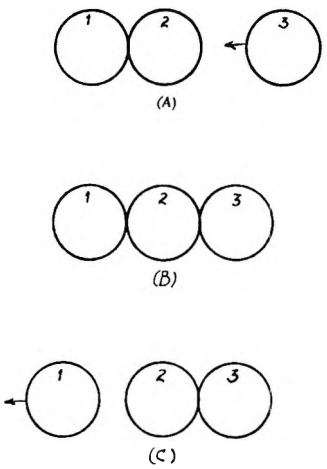

Figure 1. Straight line collision. The transfer of kinetic momentum is complete: (A) approach (origin of coordinates is on the 2-mer); (B) collision (the shapes of the molecules are distorted from spherical symmetry during the collision although this is not shown. During the lifetime of the 3-mer, the energy of the collision is stored as potential energy of distortion); (C) departure (molecule at opposite end departs taking all the kinetic energy. This is only true for a strictly straight line molecule).

Liquid–Gas Transition. The concept of a discontinuous distribution raises several questions. The first: how and why does this distribution arise, and why is it more applicable to liquids and solids. Qualitatively this can be approached by a picture of this sort which turns out to give us a clearer understanding of the nature of the gas–liquid transition.[13] Let us imagine that we have a gas at some elevated temperature. The particles present will probably be linear forms of the 1-mer, 2-mer, 3-mer, 4-mer, and perhaps 5-mer. (Occasionally a linear form of a higher j-mer may form.) The lifetime of such particles is very short. Let us reduce the temperature of the gas. The effect would be to decrease the energy and hence the velocity and momen-

(9) E. A. Moelwyn-Hughes, "Physical Chemistry," Pergamon Press, New York, N. Y., 1957; J. O. Hirschfelder, C. P. Curtiss, and R. B. Bird, "Molecular Theory of Gases and Liquids," Wiley, New York, N. Y., 1954.

(10) R. Ginell, *J. Chem. Phys.*, **34**, 992 (1961).

(11) (a) J. D. Bernal, *Nature*, **185**, 68 (1960); *Sci. Amer.*, **203**, 124 (1960); (b) S. E. Brown and R. Ginell, pp 109–118, "Symp. Nucleation and Crystallization in Glasses and Melts," M. K. Reser, C. Smith, and C. H. Insley, Ed., American Ceramic Society 1962.

(12) H. Eyring, T. Ree, and N. Hirai, *Proc. Natl. Acad. Sci. U. S.*, **44**, 683 (1958), and subsequent papers.

(13) R. Ginell, Proceeding of the 1st International Conference on Thermodynamics and Calorimetry, Sept 1–5, 1969, Warsaw, Poland, in press.

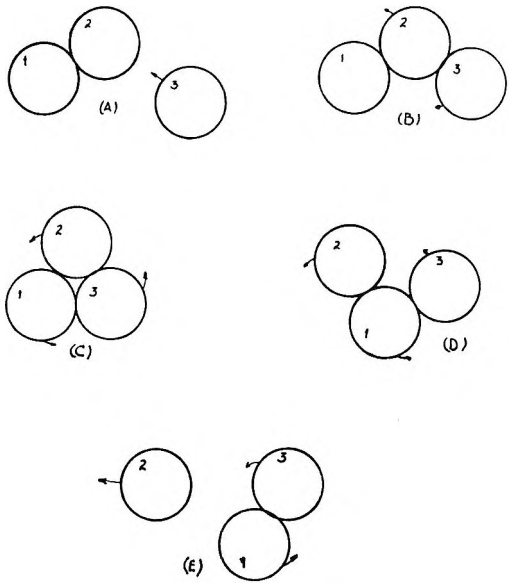

Figure 2. Collision of a 2-mer and a 1-mer. Partial transfer of kinetic momentum to rotational momentum. If the energy of impact is slight, collision may stop at step C. For a collision a little higher in energy, termination step may be step D. Step D is in equilibrium with step C and molecule will alternately have structure D and C. (A) approach; (B) collision: formation of first bond; (C) formation of second bond due to rotation (may stop at this stage); (D) degradation: breaking first bond. (Energy of collision too great to stop at C but may stop at this stage and oscillate between C and D); (E) complete degradation: breaking of second bond: (likelihood good that some rotational momentum remains, in part, in the molecule).

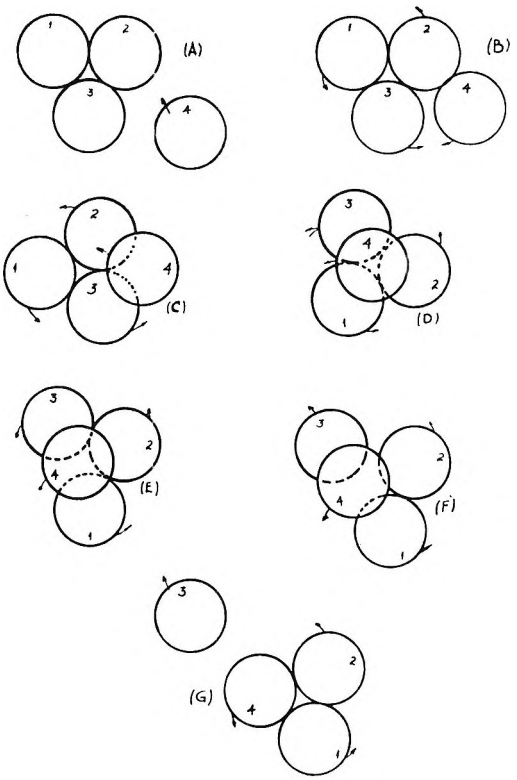

Figure 3. Bond formation in a 3-hole molecule: (A) approach; (B) first bond forms; (C) second bond forms; (D) third bond forms; (E) first bond breaks; (F) second bond breaks; (G) third bond breaks (departure). Process may stop at any of several stages. Transfer of kinetic momentum to rotational momentum most likely. Most stable structure (least energy) is D. The stages that are gone through and the amount of energy transferred depends largely on the quantity of energy in the collision and the exact geometry of the collision.

tum of the particles. Since every collision, except a direct line collision (Figure 1) results in the transfer of some of the kinetic momentum into rotational momentum, there is time for additional bonds to form. From geometric concepts, direct line collisions are rare, hence extra bonds are usually formed (see Figure 2). This means that as higher j-mers form, they tend to be more complex in terms of the number of bonds that an individual atom shares. The situation in the case of the formation of the 4-mer from the 3-mer and the 1-mer is shown in Figure 3. Here the 3-mer is triangular, and the rotation momentum of the 4-mer forces the formation of first, 1 additional bond and then 2 additional bonds. We would refer to such a bonding type as three-hole bonding (3-hole) since the triangular array of the 3-mer forms a hole bounded by 3 atoms. The breakup of such a bonded arrangement is simple. The bond was formed one bond at a time and breaks up one bond at a time. If we consider the energy of formation of a single bond to be the same, no matter where it occurs, and this is a plausible assumption at least as a first approximation, then the formation of a 3-hole bond consists of a series of three equally energetic steps while the reverse reaction of breakup of a 3-hole bond consists of the same three steps.

As the temperature is lowered and still higher compact forms have time to form, j-mers with 4 and 5 holes appear. The behavior of such bonds is in one way similar and in another way quite different from the formation of 3-hole bonds. In the formation of 4-hole bonds, the energy of the first step and the second step (Figure 4) is the same as in the 3-hole bond. However, the third step is different. In the 4-hole bond two bonds are formed simultaneously in the third step, while in the 3-hole bond only one bond is formed. The important difference is when we consider the process of breakup. In the 4-hole bond the first step demands that 2 bonds be broken simultaneously. This is energetically more difficult than breaking one bond. Hence energetics favor the 4-hole bond. It is more stable than the three-hole bond. In the 5-hole bond the stability of the bond increases still more, since 3 bonds are formed in the last step. Similar reasoning holds for the 6- and higher hole bonds. We call such highly stable particles multiply bonded structures. As the temperature of the gas is lowered, the point is reached where such multiply bonded structures start forming. Since they are more stable, they rapidly drain the gas of simply bonded

structures. Shortly this process results in the depletion of the simply bonded j-mers in the gas, and first the 2-mer and then the 3-mer and 4-mer disappear from the gas. The concentration of 1-mers is also decreased at this time. At this point where multiply bonded structures form there is an extra release of energy due to their formation. This compensates for the uniform dropping of the temperature, and a halt in the temperature drop ensues while the multiply bonded j-mers for either the liquid or the solid are forming. The fact that the species, 2-mer, 3-mer, etc. go to zero concentration results in a breakdown of the mathematics of the continuous case and results in a gap, giving rise to the discontinuous case.

Mathematical Derivation

The problem is now to put these ideas into mathematical form. For simplicity we shall consider the case where a gap exists between the 1-mers and the α-mer where α is some larger number. The general reactions existing are

	Equilibrium constants
$N_1 + N_\alpha \rightleftarrows N_{\alpha+1}$	$K_{1,\alpha}$
$N_1 + N_{\alpha+1} \rightleftarrows N_{\alpha+2}$	$K_{1,\alpha+1}$
.	
.	
.	
$N_1 + N_{m-1} \rightleftarrows N_m$	$K_{1,m-1}$

$$N_1 = N_1$$

$$N_j = 0 \quad 2 \leq j < \alpha$$

$$= N_j \quad \alpha \leq j \leq m$$

$$= 0 \quad m < j$$

where N_j = number of moles of particles of size j in a mass of substance of w grams.

The kinetic equations[2] or equilibrium equations[8] are the same as for the continuous case (where all species are present) as is the solution, if certain definitions are modified. In Table I are to be found the equations and definitions for both the continuous case and the discontinuous case (gap exists). As can be seen from the table, the discontinuous case can be considered a singular case of the continuous case; a case where K_x becomes zero as soon as any one of the species disappears, or better, the continuous case can be considered a special case of the discontinuous case where $\alpha = 1$. As can be seen, the discontinuous case reduces to the continuous case when $\alpha = 1$.

Equation of State. The derivation for the equation of state does not change, and the equation of state for both cases is

$$P(1 - \text{Б}/v) = \text{C}RT \qquad (1)$$

where C is $\sum_1^m C_x$ and $\text{Б}/v = \sum_1^m \text{Б}_x C_x$ where Б_x is the covolume of a mole of x-mers. Hence this equation of state is valid for gases, liquids, and solids.

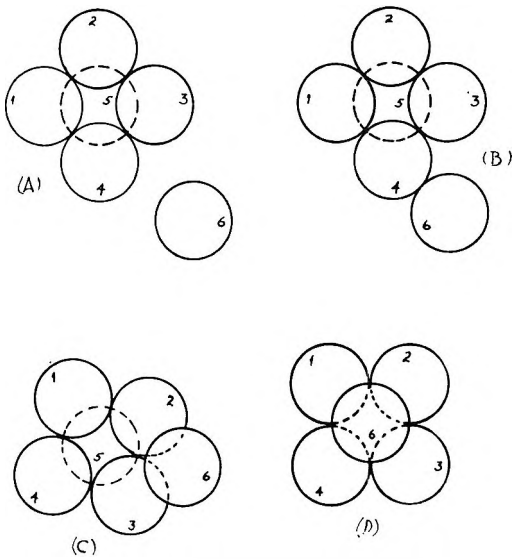

Figure 4. Bond formation in a 4-hole molecules: (A) approach; (B) first bond forms; (C) second bond forms; (D) third and fourth bonds form simultaneously. Degradation in reverse order. 2 bonds breaking simultaneously is the first step. Atom 5 as shown is necessary since without atom 5 the square planar structure of 1, 2, 3, 4 is not stable to kinetic forces and will rearrange to a tetrahedral structure.
In a collision of this sort kinetic momentum is transferred to rotational momentum. Loss of this energy may be by the same mechanism or by colliding with a more complex j-mer.

The Compressibility Equation. The point where the serious changes occur is in the equations derived from the compressibility equation. If one takes the derivative of the equation of state (eq 1) at constant temperature and rearranges it, one has

$$-\frac{dv}{dP} = \frac{u \Big/ \frac{du}{dv}}{\left(-RT \frac{dC}{dv} \Big/ \frac{du}{dv}\right) + P} \qquad T = \text{constant} \qquad (2)$$

where $u = (1 - \text{Б}/v)$, letting

$$u \Big/ \frac{du}{dv} = J \qquad (3)$$

and

$$\frac{-RTdC}{dv} \Big/ \frac{du}{dv} = L \qquad (4)$$

one has

$$-\frac{dv}{dP} = \frac{J}{L + P} \qquad T = \text{constant} \qquad (5)$$

If J and L are constant with pressure changes then the equation is identical with the so-called Tait equation. We say so-called Tait equation because as explained by

Table I: Association Equations for Continuous and Discontinuous Cases

Continuous case Condition—all species present	Discontinuous case Gap exists—some species absent
$C_1 = C_1$ $C_x = C_x;\ 2 \leq x \leq m$ $= 0;\ m < x$ m is the size of the largest species $C_x = N_x/v$ N_x = no. of moles of particles of size x in mass w v = volume	$C_1 = C_1$ $C_x = 0;\ 2 \leq x < \alpha$ $= C_x;\ \alpha \leq x \leq m$ $= 0;\ m < x$ m is the size of the largest species Note: The gap need not start at 2 but could start at 3 or 4. This entails only slight modification.
Equilibrium constants (double index)	Equilibrium constants (double index)
$C_1 + C_x \rightleftarrows C_{x+1}$ $K_{1,x} = \dfrac{C_{x+1}}{C_1 C_x} \quad 1 \leq x$	$C_1 + C_x \rightleftarrows C_{x+1}$ $K_{x,1} = \dfrac{C_{x+1}}{C_1 C_x} \quad \alpha \leq x$
Equilibrium constants (single index)	Equilibrium constants (single index)
$K_1 = 1$ $K_x = {}^1/_2 \prod_{y=1}^{x-1} K_{1,y} = \dfrac{C_x}{C_1^x} \quad 2 \leq x \leq m$ $K_x = 0;\ m < x$	$K_1 = 1$ $K_x = 0 \quad 2 \leq x < \alpha$ $K_\alpha = \dfrac{C_\alpha}{C_1^\alpha} \quad \alpha > 2$ $K_2 = \dfrac{C_2}{2C_1^2} = {}^1/_2 K_{1,1} \quad \alpha = 1$ $K_x = K_\alpha \prod_{y=\alpha}^{x-1} K_{1,y} \quad \alpha < x \leq m$ $K_x = 0;\ m < x$
$\sum_{x=1}^{m} C_x = \sum_{1}^{m} K_x C_1^x$	$\sum_{x=1}^{m} C_x = C_1 + \sum_{y=\alpha}^{m} K_y C_1^y$ Actually this definition is redundant, since considering the conditions on K_x and C_x the continuous definition can be used.

Hayward[14a] this is not the equation originally proposed by Tait but rather that called the Tait equation by Tamann. An interesting discussion of the various empirical two-constant compressibility equations is to be found in Hayward while a comparison of these equations is given by MacDonald.[14b] As discussed by Hayward, the fit of the various equations depends on the quality of the data. Up to rather high pressures most of the proposed equations fit about equally as well; therefore one has to employ other criteria in choosing which equation to use. For practicality in interpolation one would as a matter of course use the simplest equation compatible with the precision desired. For use in drawing theoretical deductions the equation to be used is the one with the soundest theoretical basis. On this ground we have chosen to use eq 5 which we shall name the general compressibility equation (GCE) or the Tamann–Tait equation. In this equation which from its derivation is applicable to gases, liquids, and solids, it is not predetermined whether J and L are constant with pressure, temperature or not. This depends entirely on the state and conditions. For gases, J and L are apparently variables. For liquids there are various cases; for liquid Helium I and II both J and L are constant with pressure;[5] for Helium I, stable above the λ point, J is constant with temperature, L varies; for Helium II, stable below the λ point, L/J is constant with temperature with both J and L varying; according to other authors for a single class of substances J/v_0 is constant (v_0 is specific volume at a reference temperature) with temperature, both J and L being constant with pressure.[15,16] In the case of the solid alkali metals[6] both J and L are constant with pressure (Tamann–Tait law holds). Evidently a discussion of the compressibility equation of state will revolve around the constancy of J and L.

(14) (a) A. T. J. Hayward, N. E. L. Report 295, Natl. Eng. Lab., E. Kilbride, Glasgow, Scotland, 1967; *Brit. J. Appl. Phys.*, **18**, 965 (1967). (b) J. R. MacDonald, *Rev. Mod. Phys.*, **41**, 316 (1969).

(15) See for instance: A. Wohl, *Z. Phys. Chem.*, **99**, 234 (1921); A. Carl *ibid.*, **101**, 238 (1922); R. E. Gibson and O. H. Loeffler, *J. Phys. Chem.*, **43**, 207–217 (1939).

(16) R. Ginell and A. M. Ginell, "Humidity and Moisture," Vol. III, A. Wexler and W. A. Wildhack, Ed., Reinhold Publishing Co., New York, N. Y., 1965, pp 363–386.

Some general relationships can be derived. One can rewrite eq 3 as

$$\frac{\mathrm{d} \ln u}{\mathrm{d}v} = \frac{1}{J} \tag{6}$$

from whence on integrating

$$u = Ee^{\int \mathrm{d}v/J} \tag{7}$$

E = constant of integration. From eq 7 and eq 1 we get that

$$\mathbf{C} = \frac{PEe^{\int \mathrm{d}v/J}}{RT} \tag{8}$$

J and L Constant with Pressure. An important case of the compressibility equation is that when J and L are constant with pressure. Here eq 7 becomes

$$\left(1 - \frac{Б}{v}\right) = Ee^{v/J} \tag{9}$$

$$\mathbf{C} = \frac{PE}{RT} e^{v/J} \tag{10}$$

and

$$Zn = \frac{\sum iC_i}{\sum C_i} = \frac{wRT}{M^0 vPEe^{v/J}} \tag{11}$$

where Zn is the number average degree of association. Zn exhibits a minimum with an increase in pressure. Differentiating eq 11 with respect to volume, and using eq 5 with J and L constant, we have

$$\frac{\mathrm{d}Zn}{\mathrm{d}v} = Zn\left[\frac{1}{v} - \frac{L}{PJ}\right]$$

Since at the minimum $\mathrm{d}Zn/\mathrm{d}v = 0$, hence at this point

$$\frac{v}{P} = \frac{J}{L} \tag{12}$$

All these equations are the same for both the continuous and the discontinuous cases, and the quantities $(1 - Б/v)$, $\mathbf{C}$ and Zn are all calculatable in terms of constant of integration, E. In previous publications[7] on the continuous case, the equations are slightly different from those given above, being given in terms of another integration constant, A. They can be reconciled by setting

$$E = ARTw/M^0 \tag{13}$$

where A is the constant of integration evaluated in ref 7. In that work A was evaluated by making the assumption that $Zn = Zw = 1$ when $P/v = L/J$. This is true at the point where Zn is a minimum.[1,7] Since Zw and Zn, the weight and number average degrees of association, are comparable quantities their behavior is similar and Zw should show a minimum around the same point where Zn does. However, since from ref 4b

$$\varphi = -\mathrm{d} \ln C_1/\mathrm{d}v = A(L/J)ve^{v/J} \tag{14}$$

and from ref 1, $Zw = 1/v\varphi$, then

$$Zw = \frac{1}{A(L/J)v^2e^{v/J}} \tag{15}$$

But the right-hand side of eq 15 exhibits no minimum, hence at pressures less than the pressure at the minimum, Zw becomes less than Zn. This is manifestly impossible, since from the definitions of Zw and Zn, their behavior must be parallel. Zw must always be greater than, or equal to Zn.

Examining the derivation of Zw in ref 1, we see that eq 16 is derived under the assumption that $\mathrm{d}K_x/\mathrm{d}v = 0$. If all the j-mers are present, as they are in the continuous case, this is probably justified, but if the j-mers between $j = 2$ and $j = \alpha$ are absent, α being a new variable, the size of the smallest of the multiply packed j-mers, then it is not justified. Since $K_x = 0$ for $x < \alpha$ and $K_x \neq 0$ for $x \geq \alpha$, then as the pressure changes and species appear and disappear, α changes in value. Under these conditions the assumption that $\mathrm{d}K_x/\mathrm{d}v = 0$ is invalid.

If we redefine φ to be

$$\varphi = -(\partial \ln C_1/\partial v)_\alpha \tag{16}$$

then $(\partial K_x/\partial v)_\alpha = 0$ and $Zw = 1/v\varphi$ in terms of the new definition of φ. This can readily be seen by rederiving the relationship of φ and Zw in the same way as in ref 4b.

Now from eq 1 we have

$$-\left(\frac{\partial v}{\partial P}\right)_\alpha = \frac{u/(\partial u/\partial v)_\alpha}{\dfrac{-RT(\partial \mathbf{C}/\partial v)_\alpha}{(\partial u/\partial v)_\alpha} + P} \tag{17}$$

$$= \frac{J_v}{L_v + P}$$

where

$$J_v = u/(\partial u/\partial v)_\alpha \tag{18}$$

and

$$L_v = \frac{-RT(\partial \mathbf{C}/\partial v)_\alpha}{(\partial u/\partial v)_\alpha} \tag{19}$$

These definitions of J_v and L_v are analogous to the definitions of J and L which one defined in terms of the total derivatives; but while J and L are constant with pressure changes, J_v and L_v are not constants.

Now since $\mathbf{C} = \sum K_x C_1^x$

$$(\partial \mathbf{C}/\partial v)_\alpha = \sum x K_x C_1^x (\partial \ln C_1/\partial v)_\alpha$$

$$= -\varphi \sum x C_x \tag{20}$$

Whence using eq 19

$$\lambda = \frac{L_v}{J_v} = RT\varphi \sum x C_x/u \tag{21}$$

From eq 1, $Pu = CRT$; hence

$$\lambda = \frac{P\varphi\sum xC_x}{C} = P\varphi Zn \tag{22a}$$

or

$$Zn = \frac{\lambda}{P\varphi} \tag{22b}$$

for the discontinuous case. This result is analogous to that in the continuous case where

$$Zn = L/JP\varphi \tag{22c}$$

From eq 15 and 22b one can see that when (and if) $Zn = Zw$, then $\lambda = P/v$; but there is no necessity for this to occur at the pressure corresponding to the minimum in Zn. In Table II we have summarized the relevant equations for the continuous and discontinuous cases.

It can be seen by examining Table II that the definition of Zn has not changed in going from the continuous case to the discontinuous case, but that the definition of Zw has changed due to the appearance of the new variable λ. The problem now has become the evaluation of the constants of integration. As yet this is not possible in all cases.

Table II: Summary of Equations for the Degree of Aggregation, Zn and Zw for the Continuous and Discontinuous Cases[a]

Continuous case	Discontinuous case
$Zn = \frac{L}{Jp\varphi}$	$Zn = \frac{\lambda}{P\varphi} = \frac{L_v}{J_vP\varphi}$
$= \frac{1}{APve^{v/J}}$	$= \frac{1}{A'Pve^{v/J}}$
$= \frac{RTw/M^0}{EPve^{v/J}}$	$= \frac{RTw/M^0}{E'Pve^{v/J}}$
$Zw = 1/v\varphi$	$Zw = 1/v\varphi$
$= \frac{J}{ALv^2e^{v/J}}$	$= \frac{1}{A'\lambda Pv^2e^{v/J}}$
$= \frac{JRTw/M^0}{ELv^2e^{v/J}}$	$= \frac{RTw/M^0}{E'\lambda v^2e^{v/J}}$
$\varphi = -\left(\frac{\mathrm{d}\ln C_1}{\mathrm{d}v}\right)$	$\varphi = -\left(\frac{\partial \ln C_1}{\partial v}\right)_\alpha$
$= (AvLe^{v/J})/J$	$= A'\lambda ve^{v/J}$

[a] The constant A is different for the continuous and discontinuous cases. J and L are experimental and independent of which case is chosen for analysis. [c] $\lambda = L_v/J_v$ and it is a variable with pressure.

Further work is in progress on the mathematical and conceptual development of this theory.

Hydrophobic Bonding in Alternating Copolymers of Maleic Acid and Alkyl Vinyl Ethers[1]

by Paul L. Dubin and Ulrich P. Strauss[2]

School of Chemistry, Rutgers University, The State University of New Jersey, New Brunswick, New Jersey 08903
(Received February 16, 1970)

The effects of hydrophobic bonding on macromolecular structure were investigated by potentiometric titration and viscosity studies on a series of hydrolyzed copolymers of maleic anhydride and alkyl vinyl ethers of varying side-chain length. While the copolymer with ethyl vinyl ether behaves as a normal weak polyacid, the butyl and hexyl copolymers exist in hypercoiled states at low pH and undergo conformational transitions to extended states as the degree of neutralization, α, is increased. The range over which the transition occurs is shifted to higher values of α with increasing side-chain length. The free energy of the transition from hypercoil to extended conformation at zero charge, $\Delta G_t°$, may be obtained from the potentiometric titration data. Values of $\Delta G_t°$ at 25° are 310 and 1110 cal/mol residue for the butyl and hexyl copolymers, respectively. The temperature dependence of $\Delta G_t°$ indicates that both $\Delta H_t°$ and $\Delta S_t°$ increase from negative to positive values with increasing temperature, a behavior previously observed for other systems involving hydrophobic bonding. From the difference in $\Delta G_t°$ for the hexyl and butyl copolymers we estimate the contribution of one methylene group to the hydrophobic stabilization of the hypercoiled form to be 400 cal/mol.

In view of the intense current interest in hydrophobic bonding and its influence on the conformation of macromolecules, it seems desirable to improve our understanding of this phenomenon by appropriate experimental studies. To this end we report here an investigation of the behavior of alternating copolymers of maleic acid and *n*-alkyl vinyl ethers in aqueous solution. Preliminary evidence suggests that with increasing ionization the butyl copolymer undergoes a transition from a compact, polysoap-like conformation to an expanded, polyelectrolyte-like form, whereas the ethyl copolymer behaves as a typical polyelectrolyte over its whole ionization range.[3] These findings which were based on potentiometric acid–base titrations have now been supplemented by the use of viscosimetry as well as by the inclusion of the hexyl copolymer in the investigation.

This series of copolymers provides a useful model system for elucidating the nature of hydrophobic bonding in biopolymers. By focusing on the differences in the experimental behavior of the members of this series, one may hope to isolate the contributions of alkyl side chains to the intra and intermolecular interactions; effects due to the common polymer backbone and the attached polar groups may be expected to cancel. In contrast, the determination of hydrophobic forces in a single biopolymer system would require the quantitative estimation of the effects of all other forces, a formidable task.[4]

Experimental Section

Materials. Copolymers. Samples of alternating 1–1 copolymers of maleic anhydride with ethyl vinyl ether (our sample A), with *n*-butyl vinyl ether (our sample B-II), and with *n*-hexyl vinyl ether (our sample C were prepared as follows: 1.10 mol of maleic anhydride and 1.10 mol of alkyl vinyl ether were dissolved in 880 g of benzene. After purging with oxygen-free nitrogen and adding 0.1 g of azobisisobutyronitrile (ABIN), the polymerization was allowed to proceed at 60° for 3 hr. The ethyl and butyl copolymer samples which had precipitated out of the benzene solution were washed with benzene, purified by successive precipitations from tetrahydrofuran (THF) into ethyl ether, and vacuum dried at 50° for 10 hr. The hexyl copolymer which was soluble in benzene was precipitated into ethyl ether and purified as described above.

A low molecular weight copolymer sample of maleic anhydride and *n*-butyl vinyl ether (our sample B-I) was prepared by dissolving 1.5 mol of each of the monomers in 865 g of THF. The polymerization was initiated with 0.25 g of ABIN and allowed to proceed at 60° for 3 hr. The soluble copolymer was precipitated into ethyl ether and purified as described above.

A high molecular weight copolymer sample of the same monomers (B-III) was prepared by mixing 1.5 mol of maleic anhydride, 4.5 mol of *n*-butyl vinyl

(1) The support of this research by grants from the United States Public Health Service (Grant GM12307) and from S. C. Johnson and Son, Inc., is gratefully acknowledged. This work constitutes a portion of a thesis to be presented by Paul L. Dubin to Rutgers University in partial fulfillment of the requirements for the Ph. D. degree.

(2) To whom all correspondence should be addressed.

(3) P. Dubin and U. P. Strauss, *J. Phys. Chem.*, **71**, 2757 (1967).

(4) A. Holtzer and D. Olander, *J. Amer. Chem. Soc.*, **90**, 4549 (1968).

Table I: Characterization of Copolymers

Code	Alkyl vinyl ether	Degree of conversion, %	% calcd C	% calcd H	% expt C	% expt H	$[\eta]_{THF}$, l./half-monomole of maleic anhydride	DP
A	Ethyl	25	56.4	5.9	55.8	5.8	11.8	650
B-I	Butyl	40	60.6	7.1	60.2	6.8	1.47	20
B-II	Butyl	60	60.6	7.1	59.6	6.9	9.85	500
B-III	Butyl	55	...	...	...	...	37.0	5000
C	Hexyl	66	62.1	7.6	62.7	8.0	20.4	1700

ether and 0.03 g of ABIN and letting the reaction proceed at 50°. After 6 hr, the solid polymeric mass was dissolved in THF and purified as described above. A portion of the polymer which was insoluble in THF, probably due to cross-linking, was discarded.

Various characteristics of these copolymers are summarized in Table I. The analyses were performed by Micro-tech Labs, Skokie, Ill. Intrinsic viscosities in THF at 30° are given in units of liters per half-monomole of maleic anhydride in order to maintain consistency with the units of liters per equivalent of acid groups used for the hydrolyzed form. Degrees of polymerization (DP) were estimated from the relation of Ito, Ono, and Yamashita.[5] Since their relation refers to copolymers of maleic anhydride and dodecyl vinyl ether, our DP values should be considered rough approximations only.

Polymerization Reagents. Maleic anhydride (Matheson Coleman and Bell) was vacuum distilled over calcium hydride. Ethyl vinyl ether (Eastman Organic Chemicals) was washed five times with water, dried over KOH, and distilled over sodium (bp 35–36°). Butyl vinyl ether (City Chemical Corp.) was water washed, dried, and distilled over sodium (bp 81–82°). Hexyl vinyl ether was prepared by refluxing 250 g of *n*-hexanol (City Chemical Corp., bp 68–71° at 18.2 mm) for 2 days with 1500 g of isobutyl vinyl ether (Eastman Organic Chemicals, bp 81–82°) and 1 g of mercuric acetate. After addition of 1 g of sodium carbonate, hexyl vinyl ether was separated by fractional distillation to yield 118 g (bp 42–44° at 17 mm).[6]

The initiator, azobisisobutyronitrile (Borden), was recrystallized from chloroform. The solvents THF and ethyl ether were distilled over lithium aluminum hydride. Pentane and benzene were distilled, the latter after drying with magnesium sulfate.

Other Materials. Sodium hydroxide and hydrochloric acid titrants were Fisher certified 0.2 *N* solutions. All water was deionized, distilled over potassium permanganate, and redistilled.

Preparation of Aqueous Polymer Solutions. Stock solutions for the titration experiments were prepared by first dissolving the samples in water at room temperature with shaking and then adjusting to the desired composition with additional water or aqueous-NaCl solution. Stock solutions for the viscosity experiments were prepared by shaking the sample in the dark at 4° with an equivalent amount of dilute sodium hydroxide. After the polymer was dissolved, the sodium hydroxide was neutralized with an equivalent amount of hydrochloric acid. The total carboxylate and NaCl concentrations of the stock solutions were then brought to 0.01 *N* and 0.04 *N*, respectively. While dissolution at such low temperatures proceeded very slowly for all but the ethyl copolymer, heating was considered undesirable because of possible degradation of the samples. Test experiments showed that dissolution at room temperature produced less than 10% degradation which was considered permissible for all but the viscosity measurements. It was also ascertained that the dissolution method used for the latter avoided degradation completely.

Methods. Viscosities were measured at 30.0° in a bath thermostated to within 0.01°. Four dilutions of the appropriate stock solutions were made in the appropriate Cannon–Ubbelholde viscometer over the polymer concentration range 0.05–0.0125 *N* for the THF solutions and 0.01–0.0025 *N* for the aqueous systems. The solvents for the latter were 0.04 *N* NaCl solutions adjusted to the pH of the polymer solution to be diluted. The degree of dissociation, α, corresponding to the experimental pH was obtained from titration curves in 0.04 *N* NaCl.

Potentiometric titrations were carried out under nitrogen with a Radiometer Model pHM26 pH meter equipped with Radiometer G202c glass and K4016 calomel electrodes. The temperature was controlled to within ±0.1°. Titrant was added from a 2-ml micrometer buret into the titration vessel containing 20–50 ml of polymer solution. Unless specified otherwise, the temperature was 30° and the initial polymer concentration 0.01 *N*. Since the titration curve of the ethyl copolymer was used as the reference for the titration curves of the other copolymers, the ethyl

(5) K. Ito, H. Ono, and Y. Yamashita, *J. Colloid Sci.*, **19**, 28 (1964).
(6) O. L. Brekke, *J. Amer. Oil Chem. Soc.*, **37**, 568 (1960).

copolymer was titrated in close succession with each copolymer and its blank. This procedure minimized the effects of possible meter and electrode changes.

Treatment of Titration Data. The degree of neutralization, α, of the carboxyl groups is defined by the equation

$$\alpha = [(\mathrm{NaOH}) + (\mathrm{H^+}) - (\mathrm{OH^-})]/C_p \qquad (1)$$

where (NaOH), (H^+), and (OH^-) are the molarities of added titrant, free hydrogen ion, and free hydroxyl ion, respectively, and C_p is the concentration of the polyacid, expressed in monomoles per liter. (One monomole contains one maleic acid and one alkyl vinyl ether residue.) The values of (H^+) and (OH^-) were obtained from titration of solvent neglecting any effects that the polymer might have on the activity coefficients of these ions. With this definition $\alpha = 2$ at complete neutralization of the dibasic acid units.

The pH of a solution of a poly(diprotic acid) may be given by the equation

$$\mathrm{pH} = \mathrm{p}K_1^0 - \log\left\{\frac{1}{2}\left(\frac{1-\alpha}{\alpha}\right) + \frac{1}{2}\left[\left(\frac{1-\alpha}{\alpha}\right)^2 + \frac{4K_2^0}{K_1^0}\left(\frac{2-\alpha}{\alpha}\right)\right]^{1/2}\right\} + \frac{1}{RT\ln 10}\left(\frac{\partial G_{ion}}{\partial \alpha}\right) \qquad (2)$$

where K_1^0 and K_2^0 are the first and second intrinsic ionization constants of a diprotic acid residue and dG_{ion} is the differential change in the electrostatic and conformational free energy which accompanies a differential change in α. The derivation of this equation is similar to that of the well-known corresponding equation for poly(monoprotic acids)[7,8]

$$\mathrm{p}K_1^a = \mathrm{pH} + \log\left(\frac{1-\alpha}{\alpha}\right) \qquad (3)$$

to which eq 2 reduces for values of α less than unity under conditions where the second term under the square root becomes negligible compared to the first. As has been shown, ΔG_t°, the free energy per residue for the process: (uncharged compact form) → (uncharged random coil form) is given by the integral $\oint dG_{ion}$ taken over the charge cycle: (compact form at $\alpha = 0$) to (coil form at an appropriate value of α) to (hypothetical coil form at $\alpha = 0$).[9,10] As has been described previously, we avoid the usual long extrapolation inherent in the last step by assuming that the extrapolated titration curves for coil forms of the butyl and hexyl copolymers coincide with the actual curve obtained for the ethyl copolymer.[3] The quantity, ΔG_t°, may then be obtained from the area between the two curves representing $\partial G_{ion}/\partial\alpha$ as a function of α for the copolymer undergoing the transition and for the ethyl copolymer.

The value of $\mathrm{p}K_1^0$ is obtained in the usual way by the extrapolation of $\mathrm{p}K_1^a$ to $\alpha = 0$. For the ethyl and butyl copolymers, the quantity of $\mathrm{p}K_2^0$ may be obtained from the relation

$$\frac{\mathrm{p}K_1^0 + \mathrm{p}K_2^0}{2} = \mathrm{pH}_{\alpha=1} - \frac{1}{RT\ln 10}\left(\frac{\partial G_{ion}}{\partial \alpha}\right)_{\alpha=1} \qquad (4)$$

This equation is equivalent to eq 2 at $\alpha = 1$, where $(RT\ln 10)^{-1}(\partial G_{ion}/\partial\alpha)_{\alpha=1}$ is the value of the smooth function ($\mathrm{p}K_1^a - \mathrm{p}K_1^0$) extrapolated to $\alpha = 1$ from the range of α over which the poly(monoprotic acid) form of eq 2 is valid ($0 < \alpha < 0.9$). This method of determining $\mathrm{p}K_2^0$ could not be applied to the hexyl copolymer because the conformational transition of this polymer extended beyond $\alpha = 1$. Since the ethyl and butyl copolymers were found to have identical values of $\mathrm{p}K_2^0$ (6.6 ± 0.1), the hexyl copolymer was assumed to have this value of $\mathrm{p}K_2^0$ also. This assumption is further justified by the finding that all three copolymers have identical values of $\mathrm{p}K_1^0$ (3.5 ± 0.1) even though the conformation of the ethyl copolymer differs from that of the other two at $\alpha = 0$. Finally, the observed convergence of the titration curves of the butyl and hexyl copolymers at values of α slightly greater than unity gives additional support to our assumption of uniform $\mathrm{p}K_2^0$.

We note from eq 2 that the difference in $(RT\ln 10)^{-1}(\partial G_{ion}/\partial\alpha)$ for two polyacids at any given value of α with identical values of K_1^0 and K_2^0 becomes $\Delta\mathrm{p}H$. Hence we may expect to obtain identical areas from titration curves plotted as $(RT\ln 10)^{-1}(\partial G_{ion}/\partial\alpha)$ *vs.* α, as pH *vs.* α or as $\mathrm{p}K_1^a$ *vs.* α. In the practical calculations which were carried out by means of a programmed Wang electronic calculator, it was found most convenient to use $\mathrm{p}K_1^a$ for the butyl and pH for the hexyl copolymer.

Results and Discussion

Potentiometric Titrations. The potentiometric titration behavior of our samples A, B-II, and C is shown in Figure 1. For comparison we have also included the titration curve for a hydrolyzed copolymer of maleic anhydride and methyl vinyl ether (Gantrez An 139, General Aniline and Film Corp). Several features of these results are noteworthy. First, the copolymers exhibit a well-defined equivalence point at $\alpha = 1$, indicating two successive intrinsic ionization constants of different order of magnitude. Second, in the primary dissociation region the curves for the maleic acid copolymers with methyl and ethyl side chains coincide, while increasing deviations from this norm are observed for the copolymers with butyl and hexyl side chains. These deviations are indicative of an abnormally compact state at low α which constitutes

(7) J. Th. G. Overbeek, *Bull. Soc. Chim. Belg.*, **57**, 252 (1948).
(8) A. Katchalsky and J. Gillis, *Rev. Trav. Chim.*, **68**, 879 (1949).
(9) B. H. Zimm and S. A. Rice, *Mol. Phys.*, **3**, 391 (1960).
(10) M. Nagasawa and A. Holtzer, *J. Amer. Chem. Soc.*, **86**, 538 (1964).

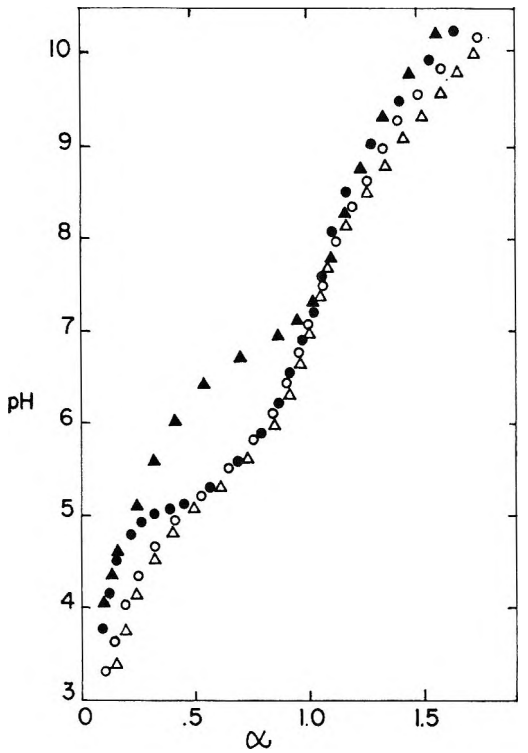

Figure 1. Potentiometric titrations in pure water at 30°: △, methyl vinyl ether–maleic acid copolymer; ○, ethyl copolymer; ●, butyl copolymers; ▲, hexyl copolymer.

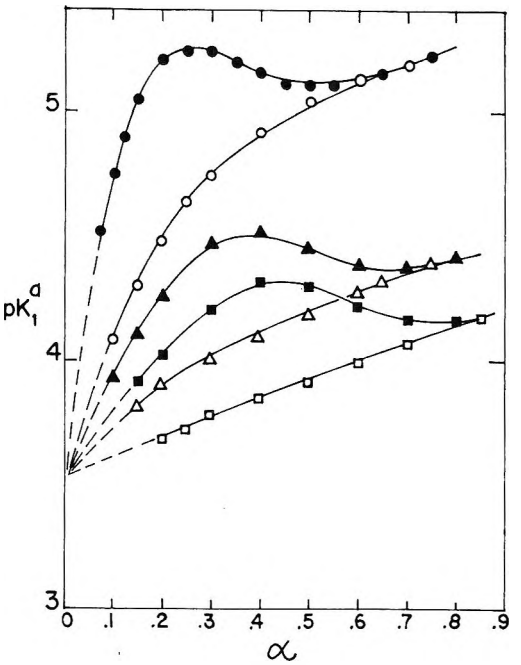

Figure 2. The effect of salt on the titration curves of butyl copolymer (B-II) and ethyl copolymer (A). ● ▲, ■, B-II in 0, 0.04, and 0.10 *M* NaCl; ○, △, □, A in 0, 0.04, and 0.10 *M* NaCl.

the major topic of this paper. Third, at high values of α the curves for the maleic acid copolymers diverge slightly in an apparently systematic fashion. We attribute this effect to minor changes in $\partial G_{ion}/\partial\alpha$ resulting from an increase in chain stiffening with increasing side chain length.

Titration curves for samples B-I, B-II, and B-III were identical. These results indicate that the factors producing the abnormalities in the titration curves do not cause a deviation from the usual insensitivity of polyelectrolyte titration curves to molecular weight.

In the absence of simple electrolyte slight decreases of pK_1^a were observed as the polyacid concentration was raised from 0.010 to 0.025 *N* for both samples A and B-II. However, identical values of ΔG_t° were found for both concentrations, indicating that ΔG_t° is insensitive to interactions between polyelectrolyte molecules.

The effect of electrolyte concentration on the conformational transition is illustrated in Figure 2 where pK_1^a of the butyl copolymer B-II and of the ethyl copolymer A is shown as a function of α in 0, 0.04, and 0.10 *M* NaCl solutions. The major effect of added salt is the shift of the transition to higher values of α. The salt reduces the electrostatic repulsion and therefore a higher electrical charge is needed to overcome the intramolecular attractive forces of the butyl side chains. There appears to be no observable effect of the salt on the value of pK_1^0. Finally, the areas between the butyl and corresponding ethyl copolymer curves are 0.23, 0.20, and 0.22 for 0, 0.04 and 0.10 *M* NaCl, respectively, indicating no significant trend and leading to the conclusion that $-\Delta G_t^\circ$, the free energy of hypercoil stabilization at zero charge, is independent of ionic strength.

While the range of α over which the conformational transition takes place may be seen directly from titration curves in the form shown in Figure 1 or 2, it is convenient for comparison with the viscosity data to calculate a parameter φ_c, defined at each pH in the transition region as

$$\vartheta_c = (\alpha_h - \alpha)/(\alpha_h - \alpha_c) \qquad (5)$$

where α_h and α_c are the values of α of the hypothetical hypercoiled and random coil states at the pH corresponding to the experimental value of α. The α_h *vs.* *p*H curves are obtained by extrapolation of the experimental data for the butyl and hexyl copolymers in the form $\partial G_{ion}/\partial\alpha$ *vs.* pH from the hypercoiled into the transition region; the α_c *vs.* pH curve is assumed to be given by the experimental curve for the ethyl copolymer. The parameter ϑ_c represents the fraction of residues in the random coil state if the following assumptions are valid. First, all acid groups can be considered to belong to either the hypercoiled or the random coil states; second, the titration curves for such groups are identical with those of completely hypercoiled or random coil molecules; third, all residues are in the hypercoiled state at low α. Regardless of the validity of these assumptions on the molecular level, ϑ_c represents a convenient measure of the degree of transition.

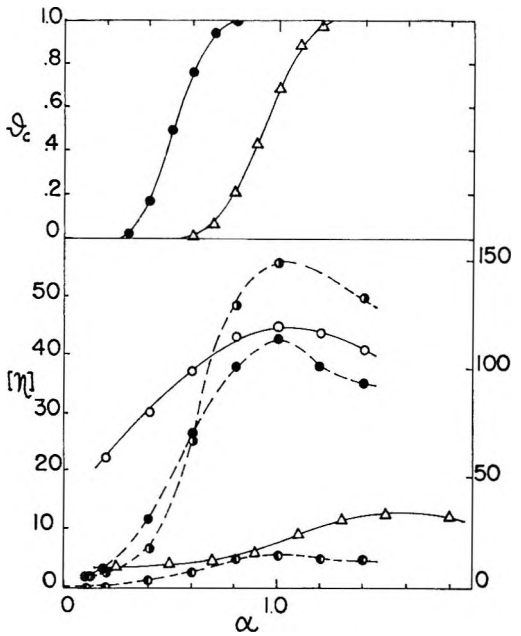

Figure 3. The dependence on the degree of neutralization, α, of: the degree of transition, determined from potentiometric titration, ϑ_c (upper curve); the intrinsic viscosity (lower curve); O, ethyl copolymer; △, hexyl copolymer; ◐, ●, ◑, butyl copolymers B-I, B-II, B-III, respectively. The right-hand scale of the lower curve refers to B-III; all data at 30°, 0.04 *M* NaCl.

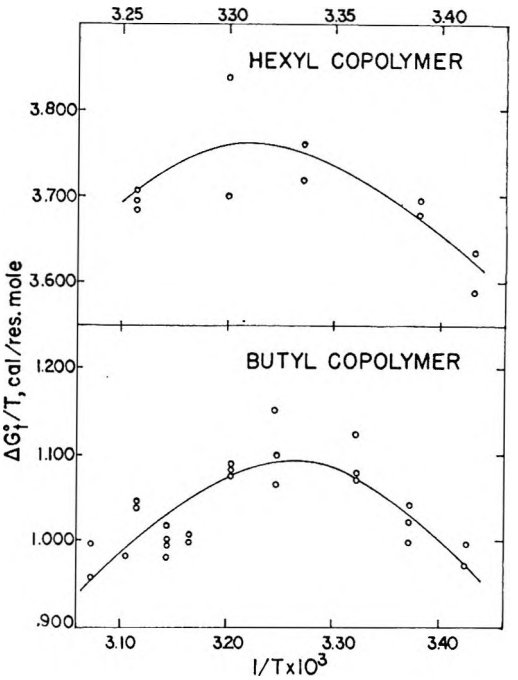

Figure 4. Temperature dependence of the free energy of the conformational transitions of the butyl and hexyl copolymers in pure water.

The dependence of ϑ_c on α for the butyl and hexyl copolymers in 0.04 *M* NaCl is shown in the upper part of Figure 3.

Intrinsic Viscosity. The intrinsic viscosity, expressed in liters per equivalents carboxylate, of copolymers A, B-I, B-II, B-III, and C in 0.04 *M* NaCl solution is presented as a function of the degree of ionization α in the lower part of Figure 3. For convenience in presentation, the data for sample B-III are given on a smaller scale. While the ethyl copolymer shows an increase of $[\eta]$ with α characteristic of normal polyacids, the butyl and hexyl copolymers exhibit exceptionally low values of $[\eta]$ at small α, confirming the high degree of compactness surmised from the titration data. The values of $[\eta]$ of the butyl and hexyl copolymers at $\alpha = 0.1$ were in fact found to be from 25 to 50% of the θ solvent intrinsic viscosities as estimated from measurements of the corresponding unhydrolyzed copolymers in mixtures of cyclohexane and THF containing slightly less cyclohexane than was necessary to induce phase separation. At large enough values of α, all copolymers showed intrinsic viscosities typical of expanded polyelectrolytes. The relatively low value of the hexyl copolymer is presumably due to its lower affinity for water. Similar effects have been reported for alkylpolyvinylpyridinium halides with increasing alkyl content but prior to the polyelectrolyte to polysoap transition.[11] For both the butyl and hexyl copolymers the maximum increase in the intrinsic viscosity is seen to occur over the range of α values in which the potentiometric titration data show the conformational transition.

Thermodynamics of the Conformational Transition. The temperature dependence of ΔG_t°, the free-energy change for the transition from the compact to the hypothetical random coil conformation at zero charge for the butyl and hexyl copolymers, is given in Figure 4 where $\Delta G_t^\circ/T$ is presented as a function of $1/T$. In view of the finding that ΔG_t° is independent of ionic strength, the titration data were obtained in the absence of salt. This procedure was found advantageous because the critical extrapolation to $\alpha = 0$ is made difficult for the hexyl copolymer by its precipitation at low α in the presence of salt. Several titrations were performed at each temperature and the result of each titration is shown as a separate point. The values of ΔG°_t range from 290 to 340 cal/mol residue for the butyl copolymer and from 1060 to 1140 cal/mol of residue for the hexyl copolymer. The data for the butyl copolymer justify a maximum in the curve close to 30°. The data for the hexyl copolymer were also consistent with a maximum in this temperature range. These maxima imply that ΔH_t° and ΔS_t° increase from negative to positive values with increasing temperature. However, the data permit the evaluation of ΔH_t° and ΔS_t° only within very wide margins of error. The results for ΔH_t° for the butyl copolymer B-II are illustrated in Figure 5. The vertical lines

(11) U. P. Strauss, N. L. Gershfeld, and E. H. Crook, *J. Phys. Chem.*, **60**, 577 (1956).

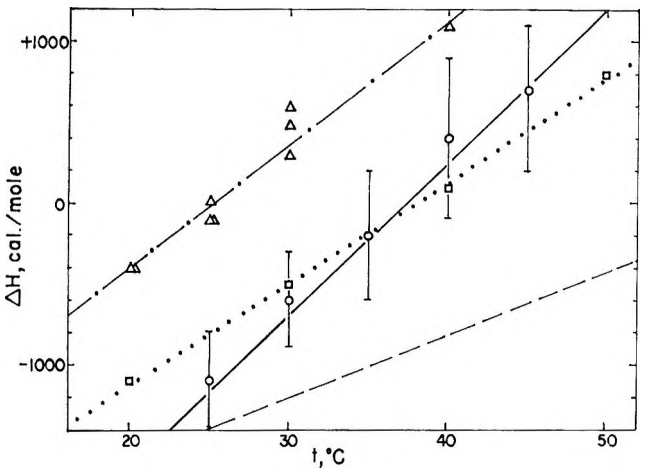

Figure 5. The effect of temperature on: O, $\Delta H_t°$ for the butyl copolymer; △, ΔH of micellization of sodium dodecyl sulfate (ref 12); □, ΔH of solution of butane in water (ref 13); dashed line, ΔH for the formation of hydrophobic bonds between alkyl side chains (ref 14).

through the data points include the range of values consistent with the experimental data. In the same figure we include also literature values of ΔH for two related systems, the micellization of sodium dodecyl sulfate[12] and the water solubility of *n*-butane,[13] as well as the values calculated by Nemethy and Scheraga[14] for the formation of hydrophobic bonds between alkyl side chains of leucine and isoleucine. These examples indicate that the temperature dependence of $\Delta H_t°$, which we have observed, appears to be characteristic of systems involving hydrophobic bonds. Corresponding values of $\Delta S_t°$ for our butyl copolymer B-II range from -2.1 ± 1.5 eu at 25° to $+3.3 \pm 3$ eu at 45°. For our hexyl copolymer we find at 25°, $\Delta H_t° = -2800 \pm 1000$ cal/mol of residue, $\Delta S_t° = -6 \pm 4$ eu; and at 35°, $\Delta H_t° = 1200 \pm 1000$ cal/mol of residue, $\Delta S_t° = -5 \pm 4$ eu.

The free energy for the formation of the uncharged hypercoil from the uncharged random coil results from a number of contributions including the hydrophobic bonding among alkyl side groups and configurational changes of the polymer chain. By taking the difference in the $\Delta G_t°$ values of the butyl and hexyl copolymers we may estimate the contribution of side-chain length to hydrophobic bonding as other contributions may be assumed to cancel. One-half this difference should give the contribution of one methylene group to $\Delta G_t°$. At 25° values of $\Delta G_t°$ are 310 and 1110 cal/mol of residue for the butyl and hexyl copolymers, respectively. Therefore $\Delta G°_{CH_2}$ amounts to 400 cal/mol of residue at this temperature.

It is instructive to compare this figure with related literature data. First, from vaporization and solubility measurements of normal aliphatic hydrocarbons in water at 25°, the free energy of solution has been found to increase by about 900 cal/mol for each methylene group.[15] Second, Nozaki and Tanford have determined from solubility data the free energy of transfer from ethanol to water of several amino acids and found that the leucyl side chain, for example, contributes 2500 ± 200 cal/mol or about 600 cal/mol of methylene group to this process.[16] By comparison with these data, our result indicates that the hydrophobic side chains in our hypercoiled copolymers experience an environment which appears to be not only more polar than hydrocarbon liquid but even more polar than ethanol. Molecular models show that the restraints of the polymer chain prevent efficient contact of the hydrophobic side chains thus exposing a considerable portion of the methylene groups to water. We anticipate an increase in $\Delta G°_{CH_2}$ with the addition of nonpolar solubilizate or with a lengthening of the alkyl side chains.

Acknowledgment. We wish to thank Andrew Schultz of this laboratory for helpful discussions. Expert technical assistance provided by Sylvia Taylor is also gratefully acknowledged.

(12) E. D. Goddard and G. C. Benson, *Can. J. Chem.*, **35**, 986 (1957); B. D. Flockhart, *J. Colloid Sci.*, **16**, 484 (1961); G. Pilcher, *et al.*, *J. Chem. Thermodyn.*, **1**, 381 (1969), as cited by the last.

(13) As calculated by G. Némethy and H. A. Scheraga, *J. Chem. Phys.*, **36**, 3401 (1962), from collected data.

(14) G. Némethy and H. A. Scheraga, *J. Phys. Chem.*, **66**, 1773 (1962).

(15) Calculated in ref 13 for the series methane–butane from collected vapor pressure and solubility data.

(16) Y. Nozaki and C. Tanford, *J. Biol. Chem.*, **238**, 4075 (1963).

NOTES

Energy-Loss Rates of Slow Electrons in Hydrocarbons[1]

by Cornelius E. Klots and P. W. Reinhardt

Health Physics Division, Oak Ridge National Laboratory, Oak Ridge, Tennessee 37830 *(Received March 4, 1970)*

The rate and modes of energy loss by slow electrons in matter are of considerable interest. This is especially true in radiation chemistry where, normally, one's attention is focused on the interactions of more swiftly moving particles. Thus it has been recognized for some time[2] that the ranges of "subexcitation electrons" constitute an important factor in discussions of LET and dose-rate effects. Similarly, initial separation distances of electrons from their positive-charged siblings will modulate the lifetime of charge separation and hence the extent of the ionic chemistry which might intervene.

Measurements of the radiation-induced conductivity of hydrocarbon liquids have revealed several anomalies. The magnitudes of the observed conductivities have implied initial separation distances not easily reconciled with existing information on electron stopping powers.[3] More recent and precise measurements have pointed to differences among isomeric hydrocarbons[4a,b] which again are not simply rationalized. Thus the probability that an ion-pair will survive to contribute to the observed conductivity is believed to be given by $\exp[-\alpha/r_0]$ where α is the Onsager length[5] and r_0 the thermalization length. Conductivity differences then presumably reflect varying thermalization length distributions.

The present experiments were undertaken to obtain information on the stopping powers of low-energy electrons in hydrocarbon vapors. The results are pertinent, of course, insofar as they provide data relevant to range calculations. Of more immediate interest is an intercomparison of the stopping powers of structurally similar hydrocarbons and the light which such a comparison may shed on the origin of the above-mentioned conductivities.

Stopping power measurements at low energies are difficult to perform. The present approach is an oblique one. Consider a swarm of electrons drifting through a gas at pressure P under the influence of an electric field E. The net rate of energy gain and hence, in a steady state, energy loss by the electrons is just $\omega(eE)$ where ω is the average drift velocity. More

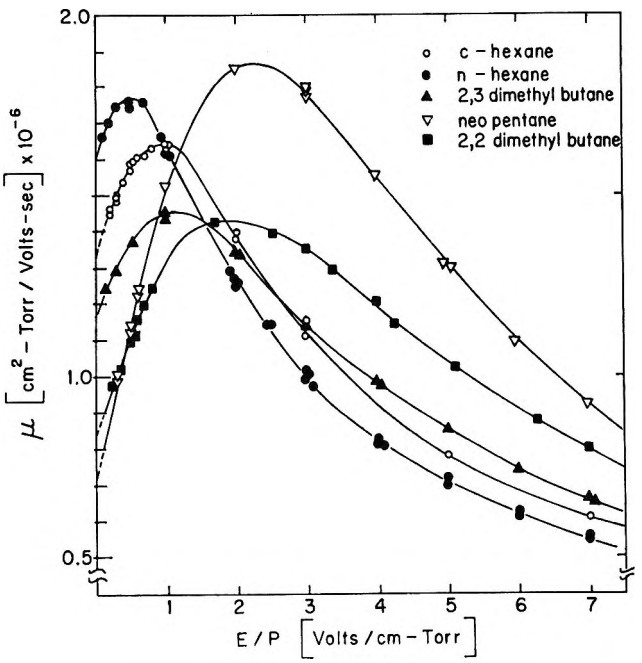

Figure 1. Mobilities of electrons in several hydrocarbon vapors as a function of electric field.

generally, the energy loss rate at a density corresponding to a unit pressure of 1 Torr is just $\omega(eE/P)$. Now the swarm contains a (typically broad) distribution of electron energies. We can, however, obtain a characteristic energy from the ratio $3D_tPe/2\mu$, where D_t is the transverse diffusion coefficient and μ the mobility, given in turn by $\omega/(E/P)$. If the energy distribution within the swarm is approximately Maxwellian, this characteristic energy will provide a measure of the average energy. Hence through the measurement of the transport parameters μ and D_t, one may glean some insight into stopping powers. A more rigorous unfolding of transport data, while surely preferable, is quite laborious and requires, in practice, ancillary information. The simplified analysis used here, as elsewhere,[6] should suffice for the qualitative purposes at hand.

The transport parameters μ and D_l, the longitudinal diffusion coefficients, were measured in an apparatus

(1) Research sponsored by the U. S. Atomic Energy Commission under contract with Union Carbide Corp.

(2) A. H. Samuel and J. L. Magee, *J. Chem. Phys.*, **21**, 1080 (1953).

(3) A. Hummell, A. O. Allen, and F. H. Watson, *ibid.*, **44**, 3431 (1966).

(4) (a) W. F. Schmidt and A. O. Allen, *Science*, **160**, 301 (1968); *J. Chem. Phys.*, **72**, 3730 (1968); (b) P. H. Tewari and G. R. Freeman, *ibid.*, **49**, 4394 (1968); P. H. Tewari and G. R. Freeman, *ibid.*, **51**, 1276 (1969).

(5) L. Onsager, *Phys. Rev.*, **54**, 554 (1938).

(6) T. L. Cottrell and I. C. Walker, *Trans. Faraday Soc.*, **63**, 549 (1967).

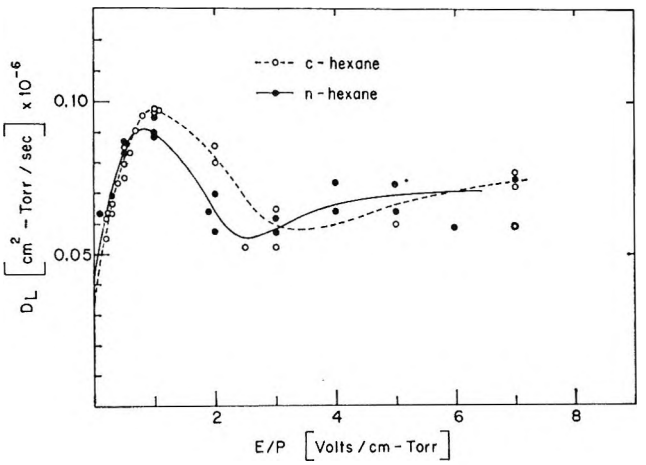

Figure 2. Lateral diffusion coefficients of electrons in *n*-hexane and *c*-hexane vapors.

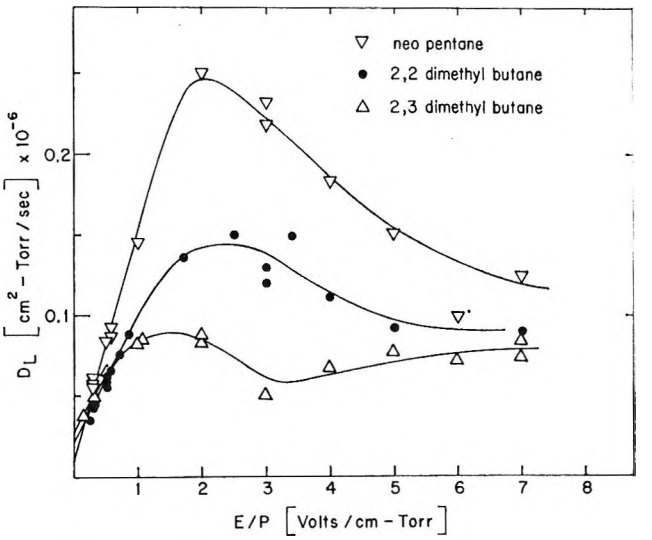

Figure 3. Lateral diffusion coefficients of electrons in the vapors of neopentane, 2,2-dimethylbutane, and 2,3-dimethylbutane.

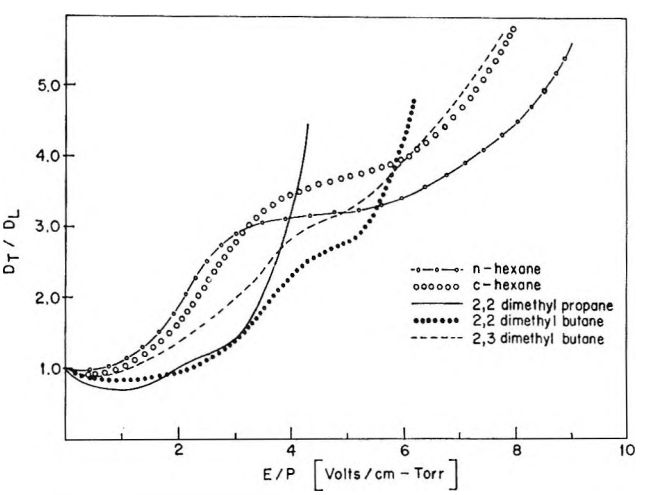

Figure 4. Ratio of transverse to lateral diffusion coefficients from eq 1 and the data of Figure 1.

entirely similar to one described earlier.[7,8] Measurements were made at pressures in the range 4 to 20 Torr and at a temperature of 300°K, corresponding to a molecular density of 3.22×10^{16} [cm³ Torr]$^{-1}$. A sufficient number of checks were made to establish that ω and D_lP were functions only of the ratio (E/P). These hydrocarbon vapors are ideally suited for the Geiger counter used to detect the electrons.

The parameters μ and D_lP obtained for electrons in the several hydrocarbon vapors are presented in Figures 1–3. The precision of the mobility measurement is at least as good as 1%. Diffusion coefficients at large values of the electric field are rather less precise. This scatter results from the finite width of the light source used to generate the electrons and is inherent in the method. It will be noted nevertheless that the several vapors examined yield discernibly different transport parameters.

To obtain characteristic energies the longitudinal diffusion coefficients measured here must be converted to transverse coefficients. This has been effected with eq 1, a relation derived and discussed elsewhere.[9]

$$D_l/D_t = \mathrm{d}(\ln \omega)/\mathrm{d}(\ln E/P) \qquad (1)$$

These correction factors are obtained simply from the present mobility measurements and are illustrated in Figure 4. It will be noted that $D_t/D_l = 1$, both at $(E/P) = 0$ and also where the mobilities of Figure 1 go through a maximum.

Figure 5 presents the stopping rates then obtained as a function of characteristic energy. The rapid change at energies corresponding to vibrational excitation thresholds is noteworthy. To the extent that energy scales can be translated from one phase to another, this would tend to confirm the suggestion that the subvibrational regime is primarily responsible for extending thermalization path lengths.[3,10]

The most striking feature of Figure 5 is the essentially identical pattern obtained for each of the several hydrocarbons. The line through the figure is drawn through the data of the prototype molecules, *n*-hexane and *c*-hexane. It is seen that the implied stopping powers for the branched hydrocarbons are at least as high as those of the prototype molecules. A careful examination of the data at low values of E/P, guided by the limiting Nernst–Einstein relation, shows the near identity of stopping rates to be pervasive. No indication is found of a correlation consistent with the variations in thermalization lengths inferred from the liquid-phase conductivities.

Because of the simplified analysis used here, any structure in the stopping rate functions would be glossed over, and indeed no evidence for such structure is

(7) G. S. Hurst, L. B. O'Kelley, E. B. Wagner, and J. A. Stockdale, *J. Chem. Phys.*, **39**, 1341 (1963).

(8) G. S. Hurst and J. E. Parks, *ibid.*, **45**, 282 (1966).

(9) C. E. Klots and D. R. Nelson, Abstracts, 22nd Gaseous Electronics Conference, Gatlinburg, Tennessee, Oct 1969; *Bull. Amer. Phys. Soc.*, **15**, 424 (1970).

(10) A. Mozumder and J. L. Magee, *J. Chem. Phys.*, **47**, 939 (1967).

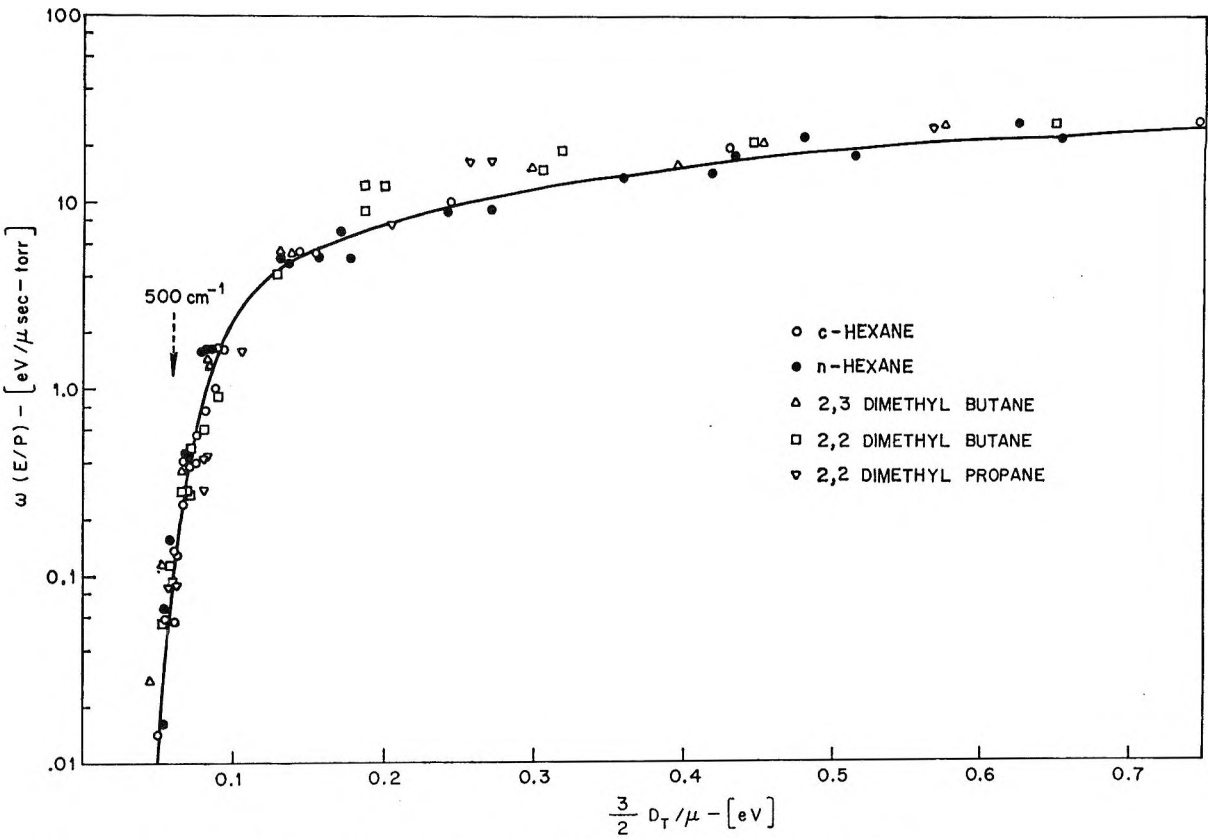

Figure 5. Energy-loss rates in hydrocarbon vapors as a function of characteristic electron energy.

obtained. Similarly, because of our use of a characteristic energy there is necessarily some ambiguity in the energy scale of Figure 5. Our conclusion, however, is self-consistent—when the data for the several hydrocarbons are treated identically, near-identical stopping rates are obtained.

This conclusion is in agreement with earlier suggestions to this effect.[10,11] The variations in the radiation-induced liquid conductivities remain unexplained. In this connection we would point out that the gas-phase mobilities of electrons obtained here, when corrected to the density of the liquids, are similar and approximately 7 cm^2/sec V in magnitude. Recent measurements of the liquid phase mobilities seem also to be approaching this magnitude.[4,12,13] These very large values are of interest in that they imply that electron-scavenging reactions in the liquid are not diffusion controlled. This clarifies the seemingly paradoxical disjunction[14] previously noted between conductivity measurements and susceptibility to geminate ion-pair quenching. But what is most pertinent is that the liquid-phase mobilities no longer cluster around a common value but seem to be rather more sensitive to structural effects than is true in the gaseous state. Again the state of aggregation is implicated as a factor tending to modulate the electrical properties of hydrocarbons.

Schmidt and Allen[4a] have commented on the difficulty in understanding the variations in the radiation-induced conductivities. There is little we can add except to note a semblance of a correlation between these conductivities and the entropies of vaporization of the several hydrocarbons, as obtained from standard vapor pressure data. The significance of any such correlation remains obscure. It seems clear, however, that the conductivity variations are associated with properties of the liquid phase and are not to be understood simply in terms of molecular parameters.

(11) M. Inokuti, R. L. Platzman, and K. Takayanagi, Abstracts, Third International Congress Radiation Research, Cortina D'Ampezzo, Italy, 1966.

(12) R. M. Minday, L. D. Schmidt, and H. T. Davis, *J. Chem. Phys.*, 50, 1473 (1969).

(13) E. C. Conrad and J. Silverman, *ibid.*, 51, 450 (1969).

(14) J. M. Warman and S. J. Rzad, *ibid.*, 52, 485 (1970).

Infrared Evidence for the Association of Vanadium Porphyrins

by F. E. Dickson and L. Petrakis

Gulf Research and Development Company
Pittsburgh, Pennsylvania 15230 *(Received December 18, 1969)*

The important role of various porphyrins in biologically significant systems is well known and extensively

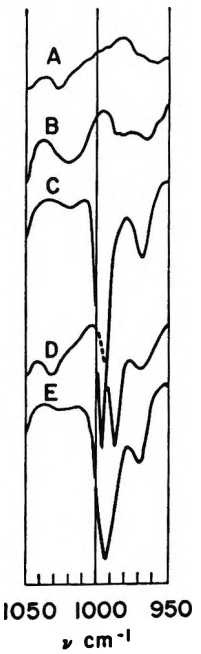

Figure 1. Infrared spectrum of (A) heavy oil solvent, (B) mesoporphyrin IX dimethyl ester, (C) VMP in CS_2 solution, (D) VMP in oil solvent, (E) VMP in KBr pellet; 1050 cm^{-1} to 950 cm^{-1}.

investigated.[1] In addition, porphyrins figure importantly in the structure of petroleum residuals, in general, and the asphaltene portion in particular.[2,3] Dickie and Yen,[3] on the basis of results from several experimental techniques, concluded that asphaltenes were composed basically of unit sheets of pericondensed rings having aliphatic side chains which tend to stack, joined either by actual -C-C- bonds or by some other unspecified form of association, into particles of five or six sheets. The particles associate further into micelles of relatively large size, which account for the high molecular weights observed by colligative measurements, and satisfactorily explain certain anomalous molecular weight measurements.[4] Altgelt,[5] on the other hand, observed that molecular weight measurements by dilute solution vapor pressure osmometry did not support the micelle view in that dissociation in the amount required by such a model could not be noted on dilution in various polar and nonpolar solvents. These experiments suggest that if some kind of molecular association does exist in the asphaltene structure then it must be of such strength as not to be affected by dilution with noninteracting solvents.

Tynan and Yen[6] recently reported the observation of an isotropic $\rightleftharpoons$ anisotropic transition as a function of temperature in the esr spectrum of a natural asphaltene in various solvents. Arrhenius-type calculations based on the assumption that two distinct vanadium(IV) species were represented gave an energy of reaction of 14.3 kcal/mol. Inasmuch as 20–65% of the vanadium(IV) in natural asphaltenes is chelated in porphyrin molecules,[2] it is reasonable to conclude that the results of Tynan and Yen[6] represent a porphyrin-related association. Nonmetalated porphyrin–porphyrin association has been studied, and energies on the order of ~1 kcal/mol have been reported[7,8] through the use of nmr techniques. In addition, the stability of intermolecular complexation in metal porphyrins has been recently observed.[9]

In this paper we are providing direct spectroscopic evidence for the existence of two porphyrin forms through the observation of the vanadyl (V=O) stretching mode in the infrared spectrum of vanadyl mesoporphyrin(IX) dimethyl ester (VMP) in a naturally occurring petroleum environment (Figure 1). This model system should closely represent the environment of porphyrin molecules in petroleum asphaltenes.

Experimental Section

A 100-mg sample of vanadyl mesoporphyrin IX dimethyl ester was prepared according to the method of Erdman and Ramsey[10] using $VOSO_4$ and mesoporphyrin IX dimethyl ester. Although this particular porphyrin is not itself found in natural petroleum, it very closely resembles several naturally occurring species, and its solubility in hydrocarbon solvents makes it extremely useful for study.

The high-viscosity oil solvent used to duplicate a natural environment was a well-characterized oil fraction from a 22% reduced Kuwait residual having a pour point of 40° and average molecular weight of 760. The oil contained ~52% aromatic and ~47% saturate material having less than 1 ppm of vanadium and nickel, 0.03% nitrogen, and 2.8% sulfur.

Variable temperature infrared spectra were obtained on a Perkin-Elmer Model 421 grating spectrometer using an RIIC variable temperature cell having sodium chloride windows and a path length of 0.2 mm. Spectra in CS_2 solution were obtained in a 0.494-mm standard liquid cell.

Results and Discussion

The frequency of the vanadium–oxygen double bond (vanadyl) stretching mode in vanadium complexes

(1) J. E. Folk, "Porphyrins and Metalloporphyrins," Elsevier Publishing Co., New York, N. Y., 1964.

(2) E. W. Baker, T. F. Yen, J. P. Dickie, R. E. Rhodes, and L. F. Clark, *J. Amer. Chem. Soc.*, **89**, 3631 (1967).

(3) J. P. Dickie and T. F. Yen, *Anal. Chem.*, **39**, 1847 (1967).

(4) F. E. Dickson, B. E. Davis, and R. A. Wirkkala, *Anal. Chem.*, **41**, 10, 1335 (1969).

(5) K. H. Altgelt, Preprints, Division of Petroleum Chemistry, American Chemical Society, Washington, D. C., Sept 1968.

(6) E. C. Tynan and T. F. Yen, *Fuel*, **XLVII**, 191 (1969).

(7) R. J. Abraham, P. A. Burbidge, A. H. Jackson, and D. B. MacDonald, *J. Chem. Soc., B*, 620 (1966).

(8) D. A. Doughty and C. W. Dwiggins, Jr., *J. Phys. Chem.*, **73**, 423 (1969).

(9) H. A. O. Hill, A. J. MacFarlane, and R. J. P. Williams, *J. Chem. Soc., A*, 1704 (1969).

(10) J. E. Erdman, V. G. Ramsey, N. W. Kalenda, and W. E. Hanson, *J. Amer. Chem. Soc.*, **78**, 5844 (1956).

has been very well established[11-13] as 985 cm^{-1} ± 50 cm^{-1}. The frequency of the absorption has been shown to vary as a function of the type of coordination and/or interaction with neighboring groups. Garvey and Ragsdale,[14] for example, investigated a series of 21 oxovanadium (IV) complexes with various substituted pyridine-N-oxide ligands and observed a 45 cm^{-1} decrease in frequency (995 cm^{-1}–950 cm^{-1}) on trans–axial coordination.

We have assigned the vanadyl frequency in vanadyl mesoporphyrin IX dimethyl ester to the absorption appearing at 997 cm^{-1} in dilute CS_2 solution (Figure 1C), 986 cm^{-1} in petroleum oil (Figure 1D), and 994 cm^{-1} in a KBr matrix (Figure 1E). Figure 1 also shows that the assigned absorption does not appear either in nonmetalated mesoporphyrin IX dimethyl ester (Figure 1B) or in the oil solvent (Figure 1A).

The 11 cm^{-1} frequency difference observed for the vanadyl mode in CS_2 and in oil suggests some type of coordination or interaction of the V=O in and/or with the oil environment. Alternatively, one might suggest that the apparent shift or appearance of the lower frequency is simply the effect of physical environment (*e.g.*, liquid–solid). However, the frequency for the vanadyl found in solid KBr matrix, 994 cm^{-1}, indicated that factors in addition to the physical environment may be causing the appearance of the lower frequency in the oil. The work of Garvey and Ragsdale[14] would suggest that the observed lowering might be a result of coordination or interaction with some neighboring ligand in the oil.

Previous reports[7,8] have shown that nonmetalated porphyrins (*copro* and *meso*) tend to dimerize in a configuration with the porphyrin rings "stacked" one over the other. Dickie and Yen[3] have proposed that "unit sheets," presumably containing vanadium porphyrins and other heterocycles, in natural asphaltenes also stack with five or six sheets forming a "particle." One might visualize in our system an equilibrium between coordinated and uncoordinated VMP molecules, the coordinated species being bound through the vanadium to a Lewis base site causing the molecules to "stack." The Lewis base sites may be found in various functional groups in the oil environment including other porphyrin molecules, other heterocycles, or possibly the highly aromatic condensed ring systems. If such an equilibrium between coordinated and uncoordinated species exists, then one might expect the intensities of the 986 cm^{-1} (presumably coordinated vanadyl) and 997 cm^{-1} (uncoordinated as observed in CS_2) to vary as a function of temperature.

Such experiments in petroleum oil have shown the gradual appearance of a higher frequency absorption at 1003 cm^{-1}, in addition to the 986 cm^{-1} absorption, as the temperature is increased (Figure 2) and suggest that monitoring the intensity of these two bands as a function of temperature may provide data for a calculation of the energy of reaction, E, for the equilibrium coordinated $\rightleftharpoons$ uncoordinated.

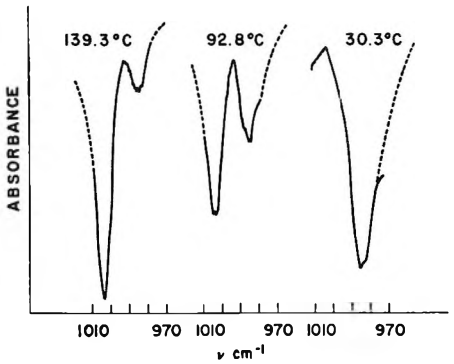

Figure 2. Vanadyl stretching mode of VMP in oil as a function of temperature.

If the usual assumption is made that the integrated area of the infrared absorption, A, is proportional to the concentration, then the equilibrium constant, K, for dissociation may be expressed in terms of the integrated areas representing the two species, and a plot of $\ln A_{1003}/A_{986}$ *vs.* $1/T°K$ would yield the energy of reaction.

The dramatic change of the spectrum of VMP in oil over the temperature range 33.0–139.3° is shown in Figure 2. Qualitatively, one can observe with increasing temperature the complete disappearance of the 986-cm^{-1} absorption and the appearance and subsequent increase in intensity of the 1003 cm^{-1} absorption. The 986-cm^{-1} absorption reappears on return to room temperature, and the ratio A_{1003}/A_{986} is very close to the starting point.

A plot of $\ln (A_{1003}/A_{986})$ *vs.* $1/T°K$ is given in Figure 3 showing a marked temperature dependence. A least-squares analysis of all the points yields an energy of reaction of 11.0 kcal/mol. However, a distinct break in the plot may be observed at ~71° indicating possibly two equilibria. Least-squares analysis of the points below 71° gives an energy of 3.3 kcal/mol while analysis of those above 71° yields 17.4 kcal/mol. These results are entirely consistent with those reported by Tynan and Yen[6] who calculated 14.3 kcal/mol for their suggested equilibrium.

The actual mechanism of the coordination is not entirely clear, but the fact that the coordinated vanadyl frequency (986 cm^{-1}) is not observed either in CS_2 solution nor KBr matrix suggests that the oil medium is definitely involved. An attempt was made to dis-

(11) N. N. Greenwood, "Spectroscopic Properties of Inorganic and Organometallic Compounds," Vol. I, The Chemical Society, London WIVOBN, 1968.

(12) R. J. H. Clark, "The Chemistry of Titanium and Vanadium," Elsevier, Essex, England, 1968.

(13) J. Selbin, L. H. Holmes, Jr., and S. P. McGlynn, *J. Inorg. Nucl. Chem.*, 25, 1359 (1963).

(14) R. G. Garvey and R. O. Ragsdale, *ibid.*, 29, 745 (1967).

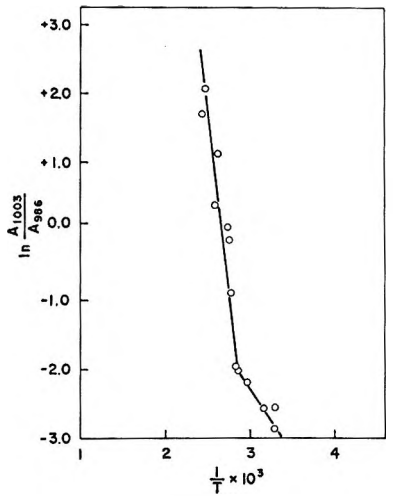

Figure 3. Arrhenius-type plot of the vanadyl stretching modes as a function of temperature.

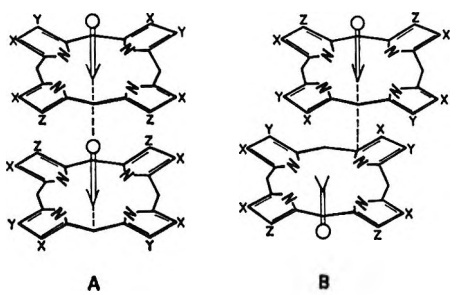

Figure 4. Two of several possible modes of association of VMP: x = CH_3, y = CH_2CH_3, z = $CH_2CH_2COOCH_3$.

solve VMP in a nonaromatic oil without success, indicating the aromatic molecules may play a role in the solution of the porphyrin and perhaps the coordination. This observation along with evidence for two equilibria offers several interesting interpretations. The energy of reaction for the equilibrium below 71°, 3.3 kcal/mol, is in the same order of magnitude as hydrogen bonds and other weak, nonspecific interactions while the more energetic equilibrium represented by 17.4 kcal/mol may be associated with coordination of porphyrin molecules through the vanadium in the vertical direction *via* Lewis base sites. The availability of electrons on oxygen atoms, ring nitrogen atoms, and various π-electron systems offers Lewis base sites for coordination with empty d orbitals of the vanadium. This type of complexing has been observed in other metallo porphyrins[9] and porphyrin-like systems.[14] Tynan and Yen[6] proposed that a similar coordination be considered as a possible interpretation of their esr data.

Several coordinated structures may be visualized including those described in Figure 4. Structure A utilizes the oxygen electrons of another porphyrin ring while B involves coordination with the porphyrin ring nitrogen. Structure B requires a lateral displacement of the rings giving a configuration similar to that proposed by Abraham, *et al.*,[7] for dimerization of coproporphyrins. Steric repulsion of the bulky propionate side chains were suggested as being responsible for the horizontal displacement. A similar interpretation might be invoked in the case of VMP.

The evidence presented supports the conclusion that two distinctly different vanadyl containing species do exist in equilibrium in petroleum oil with an apparent energy of reaction of 17.4 kcal/mol, and in addition, a lower energy equilibrium of ~3.3 kcal/mol suggests a hydrogen bonded or other weakly bonded interaction between porphyrin molecules or porphyrin and solvent molecules. These data lend additional support to current structural theories for asphaltic materials based on associative forces of greater energy than is normally encountered. Also, the energies required in a dissociation process would probably not be observable in solution studies as pursued by Altgelt.[5]

Acknowledgment. The authors wish to express their appreciation to Dr. Earl Baker of Carnegie-Mellon University for several helpful discussions during the course of this research and to Dr. E. L. McGinnis for the metallation of the porphyrin. In addition, the assistance of Mr. W. E. Magison in obtaining the infrared data is also appreciated.

Phosphorus–Proton Spin–Spin Coupling Constants in Acyclic Phosphates

by Masatsune Kainosho

Central Research Laboratories, Ajinomoto Company, Inc., Kawasaki, Japan *(Received September 2, 1969)*

In the previous paper[1] we showed the apparent angular dependence of J_{POCH} similar to the well-known tendency of vicinal proton–proton coupling constants for which theoretical calculations by Karplus[2] have shown the Fermi contact term dominates. Benezra and Ourisson[3] found that an analogous relation to the Karplus curve is operative in case of the vicinal phosphorus–proton coupling constant in P–C–C–H group (J_{PCCH}). Recently a Karplus-like curve has been found for $J_{P^{III}OCH}$ through a complete analysis of the pmr spectrum of 2,7,8-trioxa-1-phosphabicyclo[3.2.1]octane which involves five J_{POCH}'s with different dihedral angles.[4] However, the expected coupling constant (J_{POCH}^{exp}) for trimethylphosphite based on the ϕ–J curve[4] was found to be far different from the observed

(1) M. Kainosho, A. Nakamura, and M. Tsuboi, *Bull. Chem. Soc. Jap.*, **42**, 1713 (1969).

(2) M. Karplus, *J. Chem. Phys.*, **30**, 11 (1949); *J. Amer. Chem. Soc.*, **85**, 2870 (1963).

(3) C. Benezra and G. Ourisson, *Bull. Soc. Chim. Fr.*, 1825 (1966).

(4) M. Kainosho and A. Nakamura, *Tetrahedron*, **25**, 4071 (1969).

one.[5] This discrepancy led us to examine the nature of J_{POCH} in various phosphates and phosphites more precisely.[6] In this note we report that the pmr spectra[7] quinquevalent phosphorus compounds have been examined and suggest that the $J_{P^{V}OCH}$ could be explained approximately by the same mechanisms for vicinal J_{HH}.[2]

small with respect to the changes of J_{POCH}. For this reason one can assume that the π electrons play some role in the coupling mechanism. It is well known that there is much less $d\pi$–$p\pi$ conjugation in the P=S or P=Se than in P=O bond[10] and then the degree of π contribution in J_{POCH} may be considerably different for these three systems. As in I and II there is an appre-

Table I: Pmr Spectral Parameters of Various Acyclic Phosphates

Series	Formula	n[b]	X	En[c]	J_{POCH}, Hz	J_{POCCH}, Hz[d]	$J^{13}_{CH\beta}$, Hz	a^2[f]	δCH_3,[g] ppm	$\Delta\delta CH_3$	δCH_2,[g] ppm	ΔCH_2
	O	0			11.0		148.0	29.60	3.704	...		
I	‖	1			13.7		150.2	30.04	3.866	+0.162		
	$Cl_nP(OCH_3)_{3-n}$	2			17.2		151.7	30.34	4.025	+0.321		
	O	0			8.4	0.85	147.5	29.50	1.276	...	4.024	...
II	‖ β γ	1			9.8[d]	1.20	150.2	30.04	1.362	+0.086	4.232	+0.208
	$Cl_nP(OCH_2CH_3)_{3-n}$	2			11.4	1.45	151.5	30.30	1.466	+0.170	4.421	+0.397
	O		Cl	3.0	13.7							
III[a]	‖		Br	2.8	14.3							
	$XP(OCH_3)_2$		I	2.5	14.9							
IV	$X{=}P(OCH_3)_3$		O	3.5	11.0		148.0	29.60	3.704	...		
			S	2.5	13.4		148.2	29.64	3.690	−0.006		
			Se	2.4	14.2		148.5	29.70	3.688	−0.016		
	β γ		O	3.5	8.4	0.85	147.5	29.50	1.276	...	4.024	...
V	$X{=}P(OCH_2CH_3)_3$		S	2.5	10.0[d]	0.96	147.6	29.52	1.269	−0.007	4.051	+0.027
			Se	2.4	10.1	0.80	148.5	29.70	1.322	+0.046	4.110	+0.086

[a] Except series III (60 MHz; chloroform solution), all compounds were measured at 100 MHz, neat liquids. [b] The number of chlorine atoms substituted on phosphorus. [c] Pauling's electronegativities. [d] Averaged values of the two slightly different couplings caused by the magnetic nonequivalence of methylene protons. [e] Determined directly from the expanded spectra, deviation may be less than 0.02 Hz. [f] Calculated from J^{13}_{CH} by $J^{13}_{CH} = 500a^2$ Hz. [g] Chemical shifts are expressed in ppm from internal TMS.

The parameters of various quinquevalent phosphorus compounds are listed in Table I. Quasilinear relationships between the values of J_{POCH} and the s characters of $C_\beta H$ bonds (a^2) calculated from $J_{C_\beta H}$ are observed for I and II. However, an appreciable difference in the slopes was observed for these two series while the s characters of CH_β *vs.* the number of chlorines (n) showed almost identical slopes for both. One of the probable reasons for the different slopes in a^2–J relations of I and II may be that the actual rotamers do not have exactly the staggered form in II as has been shown in sodium diethylphosphate by the X-ray study.[8] The angle deviations from the ideal *gauche* and *trans* positions may cause the slope of II to differ from that of I.[1] Secondly, the stereospecificity of the chlorine substitution effect on J^g and $J_{POCH}{}^t$ should be considered.[9] For III, J_{CH} values could not be observed with sufficient accuracy, but the electronegativities of the halogens *vs.* J_{POCH} likewise gave a linear plot. This fact suggests that J_{POCH} increases in absolute value on increasing the s-electron density in the coupling route.

Similar relations, the larger s character gives the larger J_{POCH}, have been observed again for IV and V. In these cases changes of the bond characters were rather ciable difference between the slopes of a^2–J_{POCH} relations for IV and V, probably due to similar reasons.

The linear relationship between the number of substituted chlorine atoms and the proton chemical shift, the δH_β, has been reported already by Mavel and Martin[6] for I and II. In addition to these, quasilinear

(5) The expected coupling constant ($J_{POCH}{}^{exp}$) in trimethylphosphite is expressed as $J^{exp} = {}^1/_3J^t + {}^2/_3J^g$, where J^t and J^g represent the P–H coupling constants with dihedral angles of 180 and 60°, respectively. From the ϕ–J curve[4] we can estimate J^t and J^g as 9.3 and 2.5 Hz, respectively. The $J_{POCH}{}^{exp}$ value must be 4.8 Hz, while the observed one is 10.8 Hz.

(6) G. Mavel in "Progress in NMR Spectroscopy," Vol. 1, J. W. Emsley, J. Feeney, and L. H. Sutcliff, Ed., Pergamon Press, Oxford, 1966; and references cited therein.

(7) Pmr spectra were recorded on a Varian HA-100 spectrometer operated at 100 MHz. Samples were neat liquids (III were measured in chloroform solutions) with a small quantity of TMS as the field–frequency controlling signal. The position of resonance line was determined directly with accuracy of 0.1 Hz by a Hewlett-Packard 5512A digital counter; 60-MHz spectra were recorded with a Varian A-60. All samples examined were prepared by the conventional methods unless they were commercially available.

(8) Y. Kyogoku and Y. Iitaka, *Acta. Crystallgr.*, **21**, 49 (1966).

(9) Stereospecificities of the substitution effect on J_{POCH} have been examined using a variety of six-membered cyclic phosphates. The results will be published shortly.

(10) R. F. Hudson, "Structure and Mechanism in Organophosphorus Chemistry," Academic Press, London, 1965.

relations between the s character (a^2) of the $C_\beta H$ bond and δH_β were found. Attention should be directed to the δH_β–a^2 plots for I and II being almost parallel, in contrast to that of J_{POCH}–a^2 (see above). The chemical shifts of methyl protons in II are downfield on substituting the ethoxy groups by chlorines. It may be of interest to point out that these shifts also correlate with J_{POCCH} values. For V, however, such a correlation was not observed, probably due to the same reasons discussed earlier.

Application of Microwave Cavity Perturbation Techniques to a Study of the Kinetics of Reactions in the Liquid Phase

by A. L. Ravimohan

Department of Chemical Engineering, California Institute of Technology, Pasadena, California 91109
(Received March 30, 1970)

Polar liquids are known to have broad absorption bands in the microwave region which arise from orientation of the molecules with increasing electric field E, followed by relaxation to thermal equilibrium as E falls to zero. The absorption is expressed as the loss factor tan δ, and for a dilute solution of a polar solute in a nonpolar solvent it is given[1] by the Debye theory as

$$\tan \delta = \frac{(\epsilon_c + 2)^2}{\epsilon_c} \frac{4\pi\mu^2 cN\nu}{27k_B T\nu_0[1 + (\nu/\nu_0)^2]} \quad (1)$$

where δ = loss angle, ϵ_c = static dielectric constant, μ = dipole moment of solute molecule, c = concentration of solute in moles per cm^3, ν = frequency of radiation, $\nu_0 = 1/2\pi\tau$, where τ = relaxation time of solute in solution, N = Avogadro's number, k_B = Boltzmann constant, and T = absolute temperature of the solution. For a mixture of solutes, tan δ is the sum of the loss factors due to the individual solutes. Jackson and Powles[2] verified eq 1 for solutions of several polar solutes in benzene by measuring resonant frequency shifts and Q factors of cylindrical microwave cavities partially filled with samples of the solution. The proportionality of tan δ to the concentration of dipole c, for constant values of other variables in (1), suggests a convenient method of following the kinetics of certain classes of liquid reactions. Consider a reaction in which the reactants have no dipole moments but the products have appreciable μ's. The time variation of the product concentration, and hence the extent of reaction, can be followed by measuring tan δ (and ϵ_c) of the reaction mixture as a function of time. The method would be fast, accurate, and convenient, as no samples have to be withdrawn for analysis. It is especially suited to the study of the early stages of the reaction, when the use of conventional methods[3] would be difficult. The chief limitations are that one must stay within the bounds of the Debye theory of dilute solutions and of the linearized theory of microwave cavity perturbation.[4] In particular, aqueous reactions are ruled out because of the abnormally high absorption of microwaves by water.

The room temperature (22°) liquid phase bromination of benzene with iodine as catalyst was chosen for the present study. C_6H_6, Br_2, and I_2 have no dipole moments, but C_6H_5Br and HBr have dipole moments of 1.52 and 0.78 D, respectively.[5]

Experimental Technique

The two parameters of a liquid that can be obtained from microwave cavity measurements are the static dielectric constant ϵ_c and the loss factor tan δ. A particular cavity resonance is characterized by the resonant frequency f_0 and the loaded quality factor Q. A liquid placed in a quartz bottle on the axis of the cylindrical cavity introduces a change in both f_0 and Q. As shown by Dunsmuir and Powles[6] and Slater,[4] the first-order perturbation solution takes the form

$$\epsilon_c = 1 + \frac{2(f_0 - f_0')}{f_0\eta} \quad (2)$$

$$\tan \delta = F(R_0, R_1, R_2, \epsilon_b, \epsilon_c)\left(\frac{1}{Q'} - \frac{1}{Q}\right) \quad (3)$$

where η = dimensionless form-factor depending on cavity geometry, R_0 = radius of microwave cavity, R_1 = inner radius of quartz bottle, R_2 = outer radius of quartz bottle, ϵ_b = dielectric constant of bottle material, ϵ_c = dielectric constant of the liquid. When $R_0 \gg R_1$, $R_1 \simeq R_2$, and $\epsilon_b \simeq \epsilon_c$

$$\tan \delta = G(R_0, R_1, R_2, \epsilon_b)\left(\frac{1}{Q'} - \frac{1}{Q}\right)\Big/\epsilon_c = \text{constant}\left(\frac{1}{Q'} - \frac{1}{Q}\right)\Big/\epsilon_c \quad (4)$$

The method used for the measurement of f_0 and Q was a "transmission" method.[7] With the circuit of Figure 1, it is possible to obtain a resonance curve in about 20 sec. A faster sweep may be obtained, if necessary, by using an oscilloscope and high-speed photography. f_0

(1) W. Gordy, *et al.*, "Microwave Spectroscopy," Dover Publications, New York, N. Y., 1966.

(2) W. Jackson and J. G. Powles, *Trans. Faraday Soc.*, **42A**, 101 (1946).

(3) K. J. Laidler, "Chemical Kinetics," McGraw-Hill, New York, N. Y., 1965.

(4) J. C. Slater, "Microwave Electronics," Van Nostrand, Princeton, N. J., 1950.

(5) N. A. Lange, Ed., "Handbook of Chemistry," 9th ed, McGraw-Hill, New York, N. Y., 1956.

(6) R. Dunsmuir and J. G. Powles, *Phil. Mag.*, **37**, 747 (1946).

(7) E. L. Ginzton, "Microwave Measurements," McGraw-Hill, New York, N. Y., 1957.

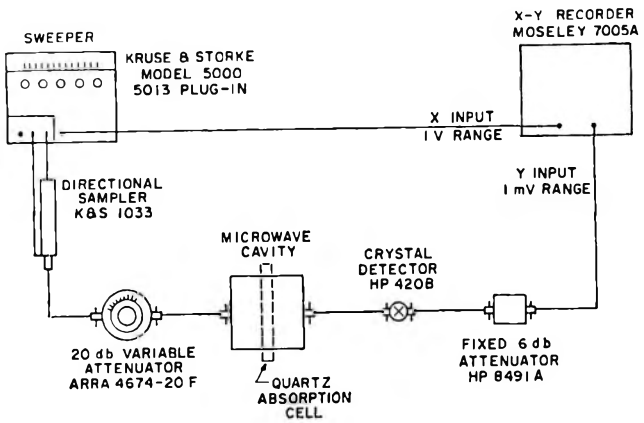

Figure 1. Coaxial circuit for automatic plotting of transmission characteristic of microwave cavity with quartz absorption cell.

and the half-power frequencies f_2 and f_1 are determined directly from the calibrated frequency scale. Now $Q = f_0/(f_2 - f_1)$. The mode of resonance used was TM_{011}, for which η determined empirically from ϵ_c measurements on standard liquids (benzene and *m*-xylene), was found to be 0.01145.

The reaction studied was

$$C_6H_6 + Br_2 \xrightarrow[22°]{I_2} C_6H_5Br + HBr \qquad (5)$$

Since the products are formed in equimolar amounts, a quantity proportional to the common product concentration c can be deduced from (1) and (4) as

$$c = \frac{\text{const}}{(\epsilon_c + 2)^2}\left[\left(\frac{1}{Q_c'} - \frac{\epsilon_c}{\epsilon_{c0}Q_0'}\right) - \frac{1}{Q}\left(1 - \frac{\epsilon_c}{\epsilon_{c0}}\right)\right] \qquad (6)$$

where ϵ_{c0} is the dielectric constant and Q_0' is the quality factor at zero time, and the tan δ of the reaction mixture at zero time has been subtracted out. The reason why Q_0' is not equal to Q is discussed in the next section.

Analytical reagent grade chemicals meeting ACS specifications were used in the work. A known solution of bromine in benzene was prepared and a known weight of iodine dissolved in it. The reaction mixture was poured into the quartz cell which was then closed tightly with a neoprene stopper. Replicated microwave readings were taken at various time intervals, with intermittent shaking of the tube to ensure homogeneity. A test run on the same solution without iodine catalyst revealed that the noncatalytic reaction was negligible under the present conditions. It is believed that the addition reaction is also negligible. Finally, the reaction was stopped after 2.5 hr by pouring the contents into excess KI. Total free halogen was estimated by titration against standard $Na_2S_2O_3$ solution using starch as indicator. This titration provided the means for estimating the constant of eq 6 which is necessary as the microwave absorption data determine only a quantity *proportional* to the product concentration.

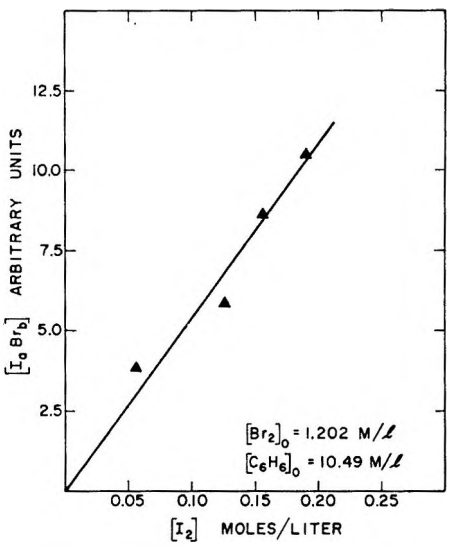

Figure 2. Initial absorption as a function of iodine added.

Discussion of Results

The first noteworthy feature about the results is that there is significant absorption even at zero time, since $Q_0' < Q$. This indicates the instantaneous formation of a species with a dipole moment. A survey of the literature reveals that an intermediate of the type I_aBr_b has been invoked to explain the catalytic action of iodine on the reaction,[8-11] with the most likely form being IBr. Initial absorption data can therefore be used to obtain relative I_aBr_b concentrations. Figure 2 shows a plot of this quantity against moles of added iodine. The approximately linear nature of the plot indicates that $K = [I_aBr_b]^2/[I_2]^a[Br_2]^b$ is very high, a result in accordance with the findings of Price and Arntzen.[10] The high K value means that the I_aBr_b concentration is not affected appreciably by changes in the Br_2 concentration. Hence it is a valid procedure to subtract out the initial reading to get the product concentration, as done in eq 6. If it is assumed that $a = b = 1$, putting $[IBr] = [I_2]/2$ in eq 1, along with Sheka's[12] value of the dipole moment of IBr (1.21 D), yields $\tau = 4 \times 10^{-10}$ sec, which is quite reasonable. If measurements are made at other frequencies, it is possible to get both μ and τ of the intermediate from microwave data, but this was not done here.

The existence of a C_6H_6-I_2 complex with a dipole moment of 0.6 D has been deduced from absorption measurements in the visual range.[13-15] However, no sig-

(8) L. Bruner, *Z. Phys. Chem.*, **41**, 514 (1902).
(9) C. C. Price, *J. Amer. Chem. Soc.*, **58**, 2101 (1936).
(10) C. C. Price and C. E. Arntzen, *ibid.*, **60**, 2835 (1938).
(11) P. W. Robertson, *et al.*, *J. Chem. Soc.*, 933 (1949).
(12) A. L. McClellan, "Tables of Experimental Dipole Moments," W. H. Freeman, San Francisco, Calif., 1963.
(13) H. A. Benesi and J. H. Hildebrand, *J. Amer. Chem. Soc.*, **71**, 2703 (1949).
(14) F. Fairbrother, *Nature*, **160**, 87 (1947).
(15) R. S. Mulliken, *J. Amer. Chem. Soc.*, **72**, 600 (1950).

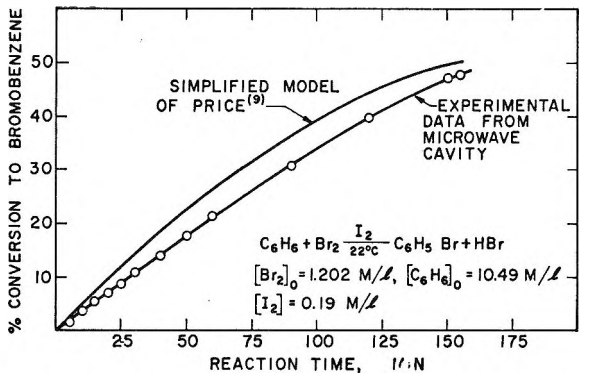

Figure 3. Per cent conversion in substitution reaction as a function of time.

nificant microwave absorption was observed in the present experiments even in saturated solutions of iodine in benzene. This could be either due to the low concentration of the complex or because it has a low ν_0 so that $\nu \ll \nu_0$. Similarily any complex between bromine and benzene was not picked up. In any event, the interpretation of both the initial absorption and kinetic data in the C_6H_6–Br_2–I_2 system was thereby considerably simplified.

Figure 3 shows the conversion in the substitution reaction as a function of time. The order of the reaction with respect to total Br_2, as determined by the method of Powell,[16] is approximately 0.75. This does not agree with Price's[9] value of 1.5, which he derived from some of Bruner's[8] data. The reason for this disagreement is possibly because the model $dx/dt = k[Br_2]^{1.5}[I_2]^{2.5}$ is an oversimplified description of the kinetics of iodine-catalyzed bromosubstitution. In fact, an examination of Bruner's data, *e.g.*, his Table IA reveals that the order with respect to total Br_2 apparently increases with time in the same run. The "order" would thus depend upon which segment of the x–t curve is being considered. The present data fall in a conversion range well below that of (8) for comparable concentrations. Hence there is no real conflict with Bruner's raw data, the only disagreement being with the simplified fits[9,11,17] before. The microwave absorption method was able to illuminate this abnormal behavior as it is ideally suited for measurements at low product concentrations.

Acknowledgment. The author is thankful to Mr. J. M. Yehle for his invaluable assistance in setting up the microwave circuitry and to Professor F. H. Shair for many helpful discussions. This work was supported by the U. S. Atomic Energy Commission under Project Agreement No. 1 under AT(04-3)-767.

(16) R. E. Powell, quoted by A. A. Frost and R. G. Pearson, "Kinetics and Mechanism," Wiley, New York, N. Y., 1961.

(17) "Tables of Chemical Kinetics-Homogeneous Reactions," Circular 510, National Bureau of Standards, Washington, D. C., 1951.

COMMUNICATIONS TO THE EDITOR

The Static Dielectric Permittivities of Solutions of Water in Alcohols

Sir: It is known that the static dielectric permittivities of different alcohols change differently when small amounts of water are added. At room temperature there is an increase in ϵ for methyl, ethyl, *n*-propyl, and isopropyl alcohol,[1,2] while for *t*-butyl and isobutyl alcohol an initial decrease is found on the addition of water.[2,3]

Recently, Lawrence, McDonald, and Stevens[4] published their results of dielectric, viscosity, and nmr measurements on heptanol-1, cyclohexanol, and 3-ethylpentanol-3 mixtures with water. For heptanol-1 (between 5 and 55°) and cyclohexanol (between 25 and 55°) they found an initial decrease of ϵ on the addition of water. For 3-ethylpentanol-3 (between −7.5 and 55°) the dielectric permittivity was found to increase with the water concentration.

In our laboratory we are studying the dielectric behavior of solutions of water in alcohols, and as part of this investigation we have performed dielectric measurements on solutions of water in the same primary and tertiary alcohols and in heptanol-4. Although our temperature range for the primary and secondary alcohols was lower (between −30 and 20°), our results for the static dielectric permittivity are essentially the same as those of Lawrence, *et al.*

Parameters representing the mode and degree of association between alcohol molecules are generally used in the interpretation of the dielectric properties of alcohols. These parameters could also be used in attempts to find the origin of the opposite effects of water

(1) F. X. Hassion and R. H. Cole, *J. Chem. Phys.*, **23**, 1756 (1955).

(2) F. Franks and D. J. G. Ives, *Quart. Rev.*, **20**, 1 (1966).

(3) A. C. Brown and D. J. G. Ives, *J. Chem. Soc.*, 1608 (1962).

(4) A. S. C. Lawrence, M. P. McDonald, and J. V. Stevens, *Trans. Faraday Soc.*, **65**, 3231 (1969).

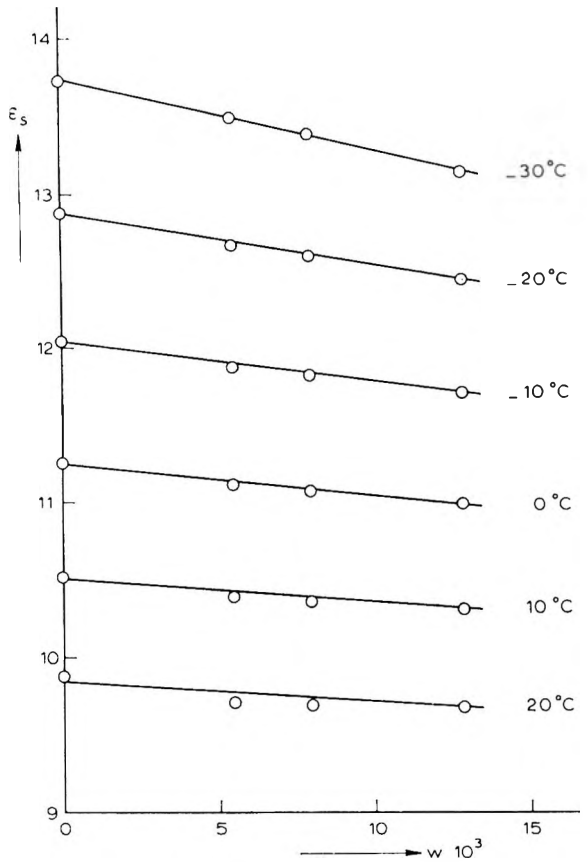

Figure 1. Static dielectric permittivity as a function of the weight fraction of water w for mixture A, a mixture of ethyl alcohol and methylcyclopentane with a hydroxyl group concentration comparable to that of the heptanols.

on the dielectric permittivities of the short-chain alcohols on the one hand and on the primary and secondary long-chain alcohols (and also tertiary butanol) on the other. There is no consensus of opinion on a satisfactory general association model for alcohols, however, and the addition of water only complicates the problem.

Independent of the mode of association assumed, one marked divergence between the short-chain and the long-chain alcohols is the difference in the concentration of the hydroxyl groups. If there were a situation in which molecules of one of the short-chain alcohols (*e.g.*, ethanol) had the same molar concentration as a pure long-chain alcohol (*e.g.*, heptanol), and if such a system showed the same dielectric behavior as the long-chain alcohols (*i.e.*, a negative value of the derivative of the dielectric permittivity with respect to the water concentration), it could at least be concluded that the mode and degree of association in alcohol–water mixtures is highly dependent upon the concentration of the hydroxyl groups of the alcohol. We therefore diluted ethanol with an apolar solvent (methylcyclopentane) until the resulting OH concentration equaled that of a long-chain alcohol and added water to this mixture, and then determined the static dielectric permittivities of these systems.

For such mixtures we indeed found a decrease in the dielectric permittivity when water was added, as Figure 1 clearly shows for a mixture containing 0.425 weight fraction ethanol and 0.575 weight fraction methylcyclopentane, *i.e.*, a mixture with a hydroxyl group concentration comparable to that of the heptanols, hereafter to be referred to as mixture A.

Values for $(\partial\epsilon/\partial w)_{w=0}$ where w is the weight fraction of water are shown in Table I for different samples and different temperatures between −30 and 20°. The results for heptanol-1 are consistent with those of Lawrence, *et al.*, in that the values of $(\partial\epsilon/\partial w)_{w=0}$ are all negative in this temperature range and the absolute value of this derivative decreases with increasing temperature. For heptanol-4, the reversal of the sign of the value of $(\partial\epsilon/\partial w)_{w=0}$ occurs somewhere between 10 and 20°, and for the temperature range considered this quantity varies much more sharply with temperature than for heptanol-1. The values for ethanol are all positive, as could be expected from earlier measurements.[1] In addition to the results for mixture A, we have also tabulated $(\partial\epsilon/\partial w)_{w=0}$ for mixture B, a mixture made up of the same constituents as mixture A but with an OH group concentration comparable to that of the dodecanols (0.27 weight fraction ethanol and 0.73 weight fraction methylcyclopentane).

Table I: Values of $10^4(\partial\epsilon/\partial w)_{w=0}$ Where w Is the Weight Fraction of Water

Temp °C	Heptanol-1	Heptanol-4	Ethanol	Mixture A (42.5% ethanol)	Mixture B (27% ethanol)
20	−0.63	0.17	1.21	−0.15	−0.22
10	−0.62	−0.11	1.16	−0.16	−0.22
0	−0.62	−0.80	1.27	−0.20	−0.37
−10	−0.65	−1.85	1.56	−0.25	−0.55
−20	−0.67	−3.04	1.91	−0.33	−0.75
−30	−0.71	−4.23	2.20	−0.46	−0.94

We conclude that in alcohol–water mixtures the mode and degree of association do depend upon the concentration of hydroxyl groups of the alcohol, but that molecular size and shape also affect the association strongly, as is evident from a comparison of the values of $(\partial\epsilon/\partial w)_{w=0}$ and the variation of these values for heptanol-1, heptanol-4, and mixture A.

CHEMISCHE LABORATORIA
VAN DE RIJKSUNIVERSITEIT,
AFDELING FYSISCHE CHEMIE II,
LEIDEN, THE NETHERLANDS

T. H. TJIA
P. BORDEWIJK
C. J. F. BÖTTCHER

RECEIVED APRIL 13, 1970